Impact of Climate Change on the Water Availability in the Near East and the Upper Jordan River Catchment

Dissertation
zur Erlangung des Doktorgrades
an der Fakultät für Angewandte Informatik
der Universität Augsburg

vorgelegt von

Andreas Heckl
Diplom Geograph

Augsburg, März 2011

Erstgutachter: Prof. Dr. Harald Kunstmann

Zweitgutachter: Prof. Dr. Jucundus Jacobeit

Tag der mündlichen Prüfung: 29. Juli 2011

Contents

List of Abbreviations

AOGCM	Atmosphere-Ocean General Circulation Model
CRU	Climate Research Unit
EM	Eastern Mediterranean
ETP	Potential Evapotranspiration
ETR	Real Evapotranspiration
GCM	General Circulation Model
GPCC	Global Prediction Climatology Centre
IDW	Inverse Distance Weighting
LSM	Land Surface Model
MM5	5th generation Penn State/NCAR Mesoscale Model
NCEP	National Centers for Environmental Prediction
NSE	Nash Sutcliffe Efficiency
RCM	Regional Climate Model
RST	Red Sea Through
SM	Snow Melt
UJC	Upper Jordan River Catchment
WaSiM	Water Balance Simulation Model

List of Figures

List of Tables

I Introduction

I.1 Motivation and Objectives

Freshwater is one of the most important resources for human being. In contrast to many other resources it is renewable through the water cycle. Nevertheless, in comparison to the entire occurrence of water on earth, which is estimated to be 1.39 billion cubic meter, freshwater captures only a small fraction of 2.6 %. The biggest part of it (77 %) is stored in ice masses and in groundwater (22.2 %) and therefore not or only difficult available for human maintenance. Only a very small content of the freshwater is easily accessible from freshwater lakes (0.35 %) and rivers (0.003 %). The source of renewable freshwater, which is precipitation, is controlled by the global atmospheric circulation. The fact that this circulation leads to inhomogeneous distribution of precipitation around the world exacerbates the access to freshwater in many regions worldwide.

Global warming changes the water cycle, particularly the precipitation. The water cycle gets intensified as on the one hand warmer air can capture more moisture. On the other hand the atmosphere gains more latent heat due to higher evaporation rates. This leads to higher atmospheric energy conversions. As a result regionally differing, opposed extremes occur: On the one hand rainfall intensities and the risk of floods are expected to rise, on the other hand droughts may get more frequent and elongated.

The assessment of the future temporal and regional distribution of terrestrial water availability is one of the central scientific challenges of the 21st century (WBGU, 1997). Some regions are more sensitive to climatic change than others. Within these climate-sensitive regions already small changes in the global scale atmospheric boundary conditions causes regional significant impacts.

One of these climate-sensitive regions is the Mediterranean. Due to its pronounced response to global change GIORGI (2006) refers to the Mediterranean as a hot spot. Furthermore, also from the viewpoint of vulnerability big parts of the Mediterranean can be seen as hot spots. Especially the Southern and Eastern Mediterranean (North Africa and Middle East) suffers already of water scarcity. Moreover, most of the countries in this region show high rates on population growth and urbanization, which will add additional stress to the often already overused freshwater resources. The fact that important water resources of the Middle East such as the Nile, the Jordan, and Euphrates

and Tigris, building together the Fertile Crescent, have transboundary basins, gives the challenge of water supply an additional political dimension (AMERY and WOLF, 2000; MEDZINI and WOLF, 2004).

This study focuses on the region of the Jordan River including Israel, Jordan and the Palestinian Authority. The per capita water availability in this region is among the lowest in the world (Israel: 240 m³/year; Jordan: 148 m³/year; Palestinian Authority: 203 m³/year; Source: WORLD RESOURCE INSTITUTE, 2007) and is well below the absolute water scarcity threshold of 500 m³ per capita per year. The Jordan River is the main freshwater system and its water is almost fully utilized by withdrawal from the Lake Kinneret (also Sea of Galilee, Sea of Gennesareth or Lake Tiberias). Thus, the river flow downstream the Lake Kinneret, called the Lower Jordan River, is negligible, while the Upper Jordan River basin feeding the lake Kinneret is of major importance as Israel meets 40 % of its water demand from these sources.

The Upper Jordan River basin benefits from its location in the mountainous and therefore relatively rain-laden region of Hermon, Antilibanon, Golan, and southern Beka'a Valley north of Lake Kinneret. Much of the water is diverted from the Lake Kinneret to the coastal plain and the Negev desert via the Israeli national Water Carrier. These areas in the south are in contrast to the Upper Jordan basin very dry denoting a very sharp climatic transition zone characteristic for the Jordan River region.

According to the FAO (Food and Agriculture Organization of the United Nation) Israel, Jordan and the Palestinian Authority already overuse their renewable water resources (123 %, 115 %, and 179 %, respectively). According to estimates by the GTZ (Gesellschaft für Technische Zusammanarbeit, an international development cooperation organization), water use in the Jordan River region will double by 2040 as a result of population growth (about 2.5 %/a in Israel and 3 %/a in Jordan and the autonomous areas). In this already tense situation reduction of rainfall evoked by global change could aggravate the circumstances considerably.

Therefore, sustainable water management requires scientific sound decisions on future freshwater availability, in particular under global climate change and increasing greenhouse gas emissions.

The objective of the present study is to simulate and analyze the impact of global climate change signals to regional climate conditions in the Eastern Mediterranean and

the water balance of the Upper Jordan River basin. To meet this task, joint regional climate-hydrology simulations based on different green house gas emission scenarios are performed. This includes besides the setup and calibration of the models to the research area, the validation of the performance of the stand alone models as well as the joint modeling system. With the validation model induced uncertainties are to be quantified. The detection of climate change signals with respect to natural climate variability is another central objective within this study. For this purpose numerous observed and simulated meteorological and hydrological variables are tested for trends and their significance. Analysis of the simulation results quantifies possible future changes with variables relevant for water availability like rainfall, evapotranspiration, and discharge. Additionally changes in the risk of droughts are analyzed implementing the EDI (Effective Drought Index).

I.2 The Project GLOWA Jordan River

This thesis is performed within the framework of the project GLOWA Jordan River (www.glowa-jordan-river.de) funded by the BMBF (German Ministry for Educations and Research). It is an international and interdisciplinary research project with the goal to provide scientific support for sustainable water management. The central question of the project is how the benefits from the region's water can be maximized for humans and ecosystems under global change. Results of the regional climate simulations performed within this thesis serve as central input for various impact analysis models of different disciplines like e.g. hydrology, ecology, agriculture, and economy. Therefore, climate simulation data are provided to project partners in Germany, Israel, Jordan and the Palestinian Authority. The results of the joint climate-hydrology simulations in the Upper Jordan River are integrated in WEAP (Water Evaluation and Planning system), which is a software tool that takes an integrated approach to water resources planning. This system is applied within GLOWA Jordan River to identify recent and future water supply and demand of the region.

I.3 Scientific Questions and Innovation

Due to the tense situation on the water resources in the region and the challenge of climate change the following scientific questions have emerged:

- Is high resolution regional climate modeling able to reproduce the sharp transition of climate zones and the spatial and temporal climate variability in the Jordan River Basin?

- Is the hydrological model able to reproduce the complex hydrology of the Upper Jordan River basin?

- What is the expected future climate change in the Eastern Mediterranean and what is its effect on the water availability, especially in the Upper Jordan River region?

- What are the uncertainties of results with respect to 1) the different driving scenarios (i.e. unknown future emissions) and 2) the relation between climate change signal and natural climate variability?

Innovation:

In this thesis, it is the first time that with WaSiM a distributed, mainly physically based hydrological model is implemented in the Upper Jordan River basin. This is a challenging task due to the heterogeneous topography as well as the complex geohydrology and groundwater/surface water interactions. With an implementation of an artificial bypass in combination with WaSiM's 2D-groundwater model a new approach should be inserted to reproduce the typical duality in discharge behavior of karst aquifers, i.e. fast response of highly conductive conduits and delayed drainage of the fractured matrix flow.

Few regional climate simulations exist for the Eastern Mediterranean. However, either these simulations are in a coarse resolution of about 50 x 50 km² and only one scenario run is available not allowing for determination of an uncertainty margin due to different assumptions on future emissions. Or time slice experiments for more scenarios, but only of 30 years are performed. This is the most common period, where it is assumed that natural climate variability is included. However, placing of this period and length of it is more or less arbitrary. Within this period trends can be detected that differ from the general long term trend and may be misinterpreted. In this thesis the first transient high resolution (18 x 18 km²) regional climate simulations for the Eastern Mediterranean are performed for the period 1961 – 2099 including forcing of two scenarios.

II The Study Area

II.1 Climate of the Eastern Mediterranean

The climate of the Eastern Mediterranean as well as the entire Mediterranean area is located in a transitional zone between the influence of mid-latitude and tropical processes. According to the classification of KÖPPEN-GEIGER (1936) the northern part of the Mediterranean region belongs to the warm temperate climate with hot and dry summers (Csa), while the southern part is characterized by a Subtropical Desert Climate (BSh and BWh). Especially for the Jordan River catchment, mainly located in Israel and Jordan steep climatic gradients from north (subhumid to humid mountains) to south (desserts like Negev) and from west (maritime climate at the coast) to east (continental climate) have to be emphasized. Typical for Mediterranean climate are hot and dry summers, mild and wet winters, and short transitional terms that are often overlapped by the two prevailing seasons.

II.1.1 Synoptic Systems

According to ALPERT et al. (2004b) the synoptic systems of the southern parts of Eastern Mediterranean can be classified into six large groups which will be described in the following:

The Cyprus Low

During the winter season extra tropical cyclones pass the Eastern Mediterranean. They are named Cyprus Lows since most of them tend to pass, strengthen or even develop over the region of Cyprus. Cyprus is one of a couple of cyclogenetic regions in the Mediterranean which is due to orographical effects in the lee of the Taurus Mountains in Turkey. Cyprus Lows can develop in that region when upper troughs penetrate the Eastern Mediterranean (ZANGVIL et al., 2003). Usually, the Cyprus Lows start their development in the south-western areas of the Mediterranean Sea, and then migrate to the east. They transport cool air masses of European origin over the warmer Mediterranean. Therefore they get moister and conditionally more unstable. The strong thermal effect is essential in cyclone dynamics over this region (SHAY-EL and ALPERT, 1991). The warm front is relatively inactive since the source of its air masses arises in dry regions of northern Africa or the Arabian Peninsula, whereas the cold front is very active. It is accompanied by strong winds and heavy rain falling from cold convective

clouds and also thunderstorms and hail is common. The Cyprus Lows contribute the vast majority of the rainfall in the southern parts of the Eastern Mediterranean (Turkey, Cyprus, Lebanon, Israel, and sometimes also northeastern Egypt) during the main rainy season (November – March). Their importance to the rainfall in the region was pointed out in many studies (SHARON and KUTIEL, 1986; ALPERT et al., 1990; GOLDREICH, 2004; ZIV et al., 2006). SAARONI et al. (2009) show that the contribution to the rainfall in Israel is higher over the inland areas (around 85%) and slightly lower (77%) along the coastal region. According to them the interannual variations in the number of Cyprus Lows explain over 50% of the variance in the seasonal and annual rainfall. They also point out that the location of the cyclone determines the spatial distribution of rainfall it produces. Cyclones that are located east of Cyprus contribute mainly to rainfall in southern parts of Israel while those located to the west and north of Israel where found to be productive for the north of the country. The annual average occurance of Cyprus Lows is 62 days (ALPERT et al., 2004b), most of them in the cool season (December – March) and their persistence is approximately 3 days on the average (KARAS and ZANGVIL, 1999).

The Persian Trough

The Persian Trough ('summer trough') is a persistant summer weather condition in the southeastern Mediterranean countries as well as in Jordan and Iraq (Alpert et al., 1990). It is a thermal trough that is an extension of the Indian Monsoon low extending from India into the Persian Gulf. Associated with the Azores High it generates the Etesian winds which have in the northern parts of the Eastern Mediterranean northerly directions and are dry. In the southern areas they gained moisture and turn into west and north-westerly winds. They slightly cool the coastal areas, but keep the humidity rather high.

The Red Sea Trough

The Red sea Trough (RST) is a northerly extension of the Sudan Monsoon Low which is a part of a large scale subtropical/equatorial low-pressure thermal system. It is a low pressure system at lower atmospheric levels whose development, intensity and northward extension is usually attributed to topographic and thermal forcing factors over the Red Sea region (KRICHAK et al., 1997). Its northward movement usually is triggered by lee-low effects of the mountains along the coast of Saudi Arabia and an extreme surface heating. The RST is most frequently observed during fall and spring, in some

cases also in winter. Generally the RST is associated with east and south-easterly flows at the lower atmosphere resulting in hot and dry weather conditions over Israel and vicinity. In some cases, the RST is accompanied by an upper trough extending from the north over the Eastern Mediterranean which enhances upward motion and unstable conditions. In that case, called *active RST*, convective storms can develop, occasionally together with heavy showers and thunderstorms, mainly at the eastern and southern parts of Israel (SAARONI et al., 1998).

The Sharav Low

The Sharav Low is a frontal pressure system developing typically in spring in southern Eastern Mediterranean countries like northern Egypt and Israel. It can be created under different circumstances (ALPERT and ZIV, 1989): Often it develops on the lee side of the Atlas Mountains followed by an upper level trough far to the west. Also an upper level trough over the North African coast in conjunction with a surface trough developed in an easterly flow from the Saharan desert can become a Sharav Low. Furthermore, it can be built as a secondary cyclone to a winter cyclone that crosses the Mediterranean Sea. The Sharav Lows travel east along the coast, sometimes moving north through the Eastern Mediterranean into Syria and Turkey. The Sharav Lows are accompanied by extremely dry and hot temperatures and wind speeds that often causes sand storms in the Sahara and the Negev dessert.

The Siberian High

The Siberian High is an extension of the high pressure system centered in northern Asia. It is a thermal high persisting semi permanently during the colder half of the year due to intense cooling of the continental air masses. If the Eastern Mediterranean gets affected by the Siberian High weather conditions are clear, dry and cold with extensive frost.

The Subtropical High

The Subtropical High is associated with the subsidence of the Hadley Cell and covers in summer, when it moves pole wards, the southern parts of the Mediterranean. The subsiding air masses create an inversion that acts as a barrier to vertical convection. Therefore the conditions in summer are very stable and rainfall is almost impossible. The Persian Trough affecting the surface with the Etesian winds in combination with

the subtropical ridge creates a permanent marine inversion in Israel at about 300 to 700 m between the coastal areas and the central mountains. While above this inversion humidity is quite low, the coastal areas are affected by high humidity and air pollution.

II.1.2 Climate Variability and Large Scale Circulations

Many climate features in the Mediterranean, especially precipitation, show a high variability. Since the Mediterranean is affected by both mid-latitude and (sub)tropical systems, Mediterranean climate variability can be explained in a large part by connection to large scale tropical and mid-latitude circulations. Many studies analyzed relationships between monthly and seasonal values of indices and climate variables, mostly precipitation, in the Eastern Mediterranean (i.e. BEN-GAI et al., 1998, 1999; PRICE et al., 1998; ESHEL and FARRELL, 2000; CULLEN et al., 2002; KUTIEL et al., 2002; KRICHAK et al., 2002; KRICHAK and ALPERT, 2005).

An overview to tropical tele-connections to the Mediterranean climate is given in ALPERT et al. (2005), ALPERT et al. (2006), and SEUBERT (2010), to relations between variability in the Mediterranean region and mid-latitudes in TRIGO et al. (2006).

While the North Atlantic Oscillation (NAO) has high influence on the northern and western Mediterranean basin and explains much of the precipitation variability, its influence to the EM is much weaker. CULLEN et al. (2002) showed correlation between NAO and Middle East rainfall and BEN-GAI et al. (2001) found high correlations between the winter mode of the NAO and sea level pressure, but no significant correlations have been found so far between NAO and rainfall in the Eastern Mediterranean. KRICHAK et al. (2005) found that NAO and the East Atlantic / Western Russia (EA/WR) pattern (BRANSTON and LIVEZY, 1987) have a combined effect. According to them, a dry (wet) rainy season occurs in the EM when they are both in a positive (negative) phase. The regional Mediterranean Oscillation (MO, CONTE et al., 1989) explains the largest part of the Mediterranean rainfall variability and is described by opposite pressure and rainfall anomalies between the western and Eastern Mediterranean area. DÜNKELOH and JACOBEIT (2003) mention that MO is not an independent large-scale circulation mode, it rather comprises those parts of the NAO and AO (Arctic Oscillation) being linked with the Mediterranean precipitation variability.

A possible teleconnection between El Nino Southern Oscillation (ENSO) and precipitation in northern Israel was investigated by PRICE et al. (1998). They found significant correlation for the years 1975 – 1995. However, this connection was not found in years before. During ENSO years enhanced contributions of daily torrential rainfall in Italy is shown by ALPERT et al. (2002). The Asian Monsoon influences the climate of the Eastern Mediterranean as well in summer as in winter. In summer the Asian Monsoon is linked to the persistent subsidence in the EM in a closed circulation, which is shown in the isentropic cross section by ZIV et al. (2004). Strengthening (weakening) of the Asian Monsoon enhances (weakens) both dominant dynamic factors in summer, the subsidence and the Etesian winds. This leads to the annual minimum of inter-diurnal temperature variations (SAARONI et al., 2003). For winter rainfall in Israel it was found that extreme seasons are in negative correlation with the rainfall index for the preceding summer Indian Monsoon (ALPERT, 2005).

II.1.3 Recent Climate Trends

Due to its dependence on large scale circulations, like described before in II.1.2, even relatively small modifications of the general circulation (e.g. shifts in the location of mid-latitude storm-tracks) can effect substantial changes in the Mediterranean climate. In fact, the Mediterranean was encountered large scale climatic shifts in the past. An overview to the Mediterranean climate variability over the last centuries is given in LUTERBACHER et al. (2006).

For recent climate trends considering the last century most studies indicate for major parts of the Mediterranean increasing temperatures and decreases in rainfall (XOPLAKI, 2002; JACOBEIT, 2000; GIORGI, 2002). However, the Mediterranean can't be treated as a consistent region. Climate trends can differ considerably across regions, seasonally and temporally. A glance at the EM gives a heterogeneous picture of actual trends.

Mixed rainfall trends were found for the EM, but clearly more stations show decreasing trends in Greece, Turkey, Syria, Lebanon and Israel for the period 1951 – 1990 (XOPLAKI et al., 2004). In spite of decrease in total values in many regions of the Mediterranean, an increase of extreme daily rainfall can be observed (ALPERT et al., 2002). Stations in Israel and Cyprus show trends of increasing heavy rainfall events with a contemporaneous drop in lighter rainfall. However, no significance in these trends can be seen. In contrast to the mainly decreasing rainfall amounts in the EM, a small area

from southern Israel to northern Libya shows some increase in precipitation. This is in accordance with increased positive modes of the Mediterranean Oscillation (JACOBEIT et al., 2004). ALPERT et al. (2004b) show that the frequencies of RST during 1970 – 2000 were doubled from 54 to 108. This could explain on the one hand the general decreasing trend in total rainfall in the EM, on the other hand the increase in heavy rainfall days and the higher rainfall amounts in the south in case of active RST.

Due to the heterogeneous and incomplete picture of recent climate trends in the southern parts of the EM given in the literature, calculations of linear climate trends are made for several stations within Israel in VII.1.

II.2 The Upper Jordan Catchment

II.2.1 Location

The study area is part of the Upper Jordan River Catchment (UJC) (Figure II-1) and is located within the borderland of Israel, Syria and Lebanon. It includes basically the three main tributaries of the UJRC: the Dan, Snir (also Hasbani) and Banias (also Hermon) streams (Figure II-2).

They all emanate from the western and southern slopes of the Mount Hermon, which is with 2814 m asl the highest elevation of Israel and Syria and can be seen as a continuation of the Antilebanon Mountains (Figure II-3).

With an extension of 855 km² the study area is only a small part of the entire Jordan River catchment (18.300 km²), but provides major contingent of the whole discharge.

The Snir stream has a length of 30 km and a surface drainage area of about 600 km² whereas most of it lays in Lebanon. The major gauging station is situated about 20 km downstream from the two main contributing springs Hasbani (in Lebanon) and El Wazzani (in the border area between Lebanon and Israel). To the north and the west the catchment of the Snir is bordered by the watershed to the Litani River.

Figure II-1: Jordan River catchment (source: http://www.glowa-jordan-river.de/Design/html/JRI&II_map.htm)

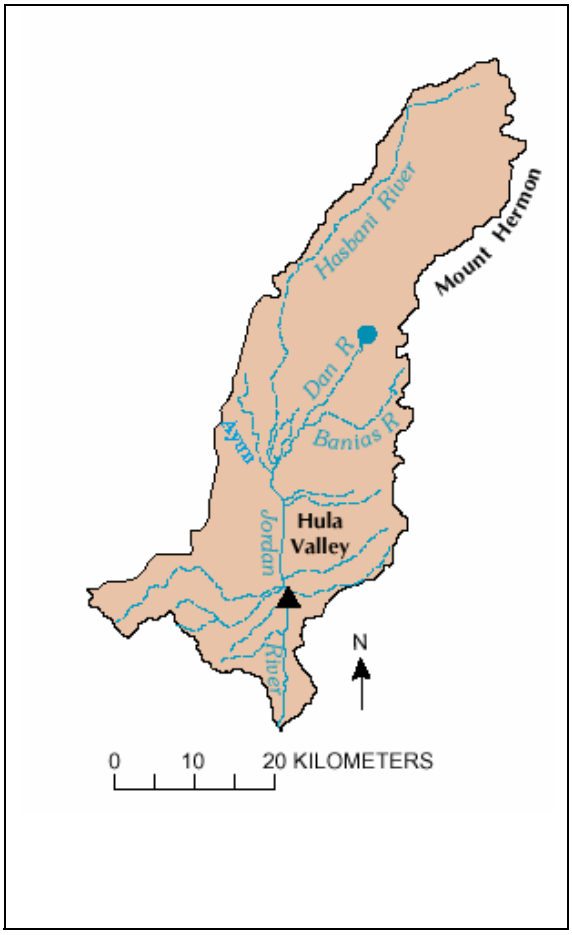

Figure II-2: Upper Jordan catchment (source: http://exact-me.org/overview/p30.htm)

The Banias arises at the foot of the Golan Heights at the homonymous Banias spring. The stream with its surface drainage area of 158 km² and length of 10 km (3 km within Israel) is characterized by a steep gradient having led to the development of deep canyons with a number of waterfalls and rapids. The river is fed besides the Banias spring by the Kezinim spring and by its three intermittent tributaries Sa'ar, Sion, and Guvtah.

The Dan originates in Israel and with its length of 9 km and a surface catchment of 24 km² it is the shortest within the three tributaries, but it has the largest discharge. This is caused by the Dan spring, one of the biggest karstic springs in the Near East. The Dan spring turns into a broad, gushing rivulet flowing southward until it unites with the other two tributaries at the northern part of the Hula valley to the Jordan River at a height of 78 m asl.

Northward after the union of the major tributaries the Ayun, which also belongs to the study area, discharges into the Jordan River draining the Ayun valley in Lebanon situated in the north-west of the Upper Jordan. It has a catchment size of 51 km² and a length of 16 km, whereas half of it resides in Israel.

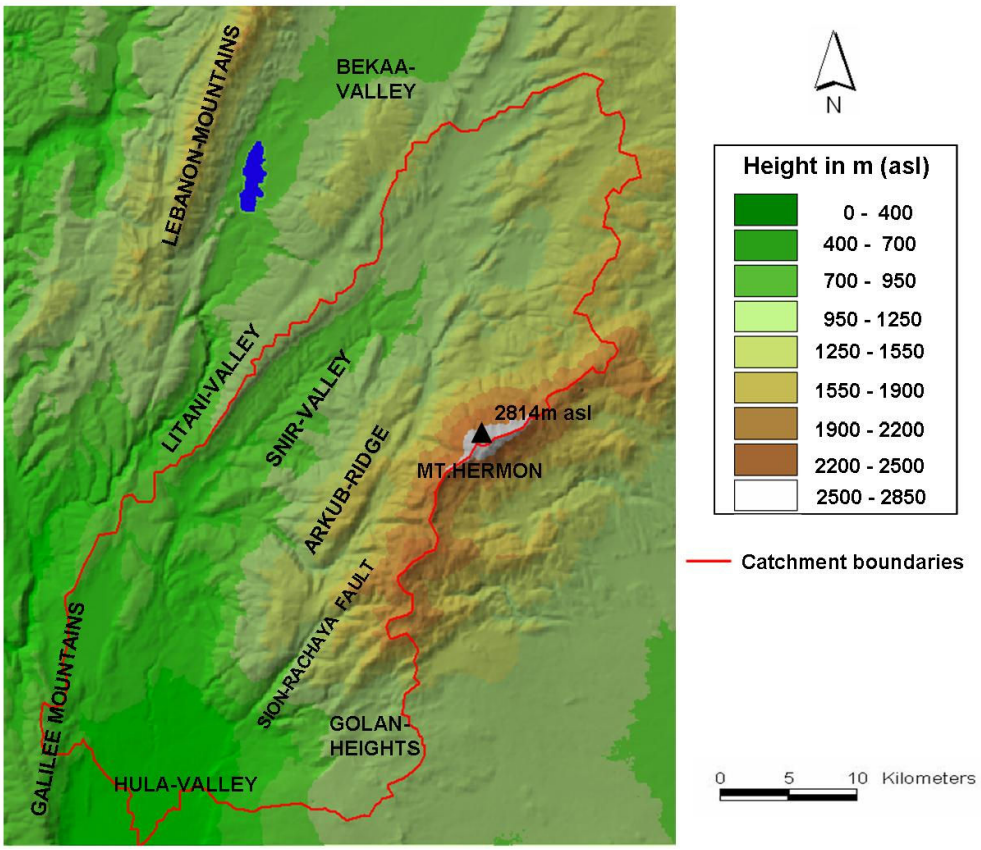

Figure II-3: Topographical overview of the Upper Jordan catchment

II.2.2 Hydrology

The Upper Jordan River catchment is part of the Jordan River network, which additionally comprises other subcatchments like the Yarmouk River, the Zarqua River and the Lower Jordan River. The Upper Jordan River is defined as the northern part of the catchment confined by its outlet into the Lake Kinneret. This study constricts the area to the three major tributaries Dan, Snir, Banias and the Ayun River.

For the hydrology of the Upper Jordan River the hydrogeological conditions are of major importance. The hydrogeology of the Hermon region was first studied by MICHELSON (1975) and GILAD and SCHWARTZ (1978). The composition of the Hermon ridge of predominantly carbonatic rocks caused the development of an extensive karstic sys-

tem. These karstic aquifers serve as a big reservoir allowing perennial large discharges into the Jordan River since a large fraction of the abundant precipitation during winter reaches rapidly into the karstic system before getting evaporated or turned into surface runoff. All three main tributaries of the Upper Jordan Rivers are spring-fed. Most of the springs emerge at the southern and western slopes of the Mount Hermon along the contact between the main faults and the valley fill.

On the main parts of the Mount Hermon and its surroundings in the western and southern parts Jurassic carbonate rocks are exposed building the recharge area for an extensive regional groundwater aquifer with a depth of several hundred meters. The aquifer is interstratified by fissures and cracks causing very high but non-isotropic permeability which is typical for karstic aquifers. On the lower slopes to the west carbonates and sands of Lower Cretaceous and Cenomanian Turonian appear. They equally show high permeability engendered by fissures. SIMPSON and CARMI (1983) assume that hydraulic interconnection between these three aquifers is likely to be considerable. These aquifers feed the springs of the major tributaries. The most important of them are:

Dan-Spring

The Dan-Spring is located at an elevation of 180 m a.s.l. within the Jurassic aquifer (Figure II-4). It is the most yielding spring in the region. The average discharge is $255 \pm 39 \times 10^6$ m³/a (SIMPSON and CARMI, 1983).

Banias-Spring

The Banias (like the river also called Hermon spring) is the biggest spring contributing to the Hermon River at the south-eastern foot of the Hermon (Figure II-4). It is located like the Dan within the Jurassic aquifer. After SIMPSON and CARMI (1983) it discharges on average $70 \pm 22{,}5 \times 10^6$ m³/a.

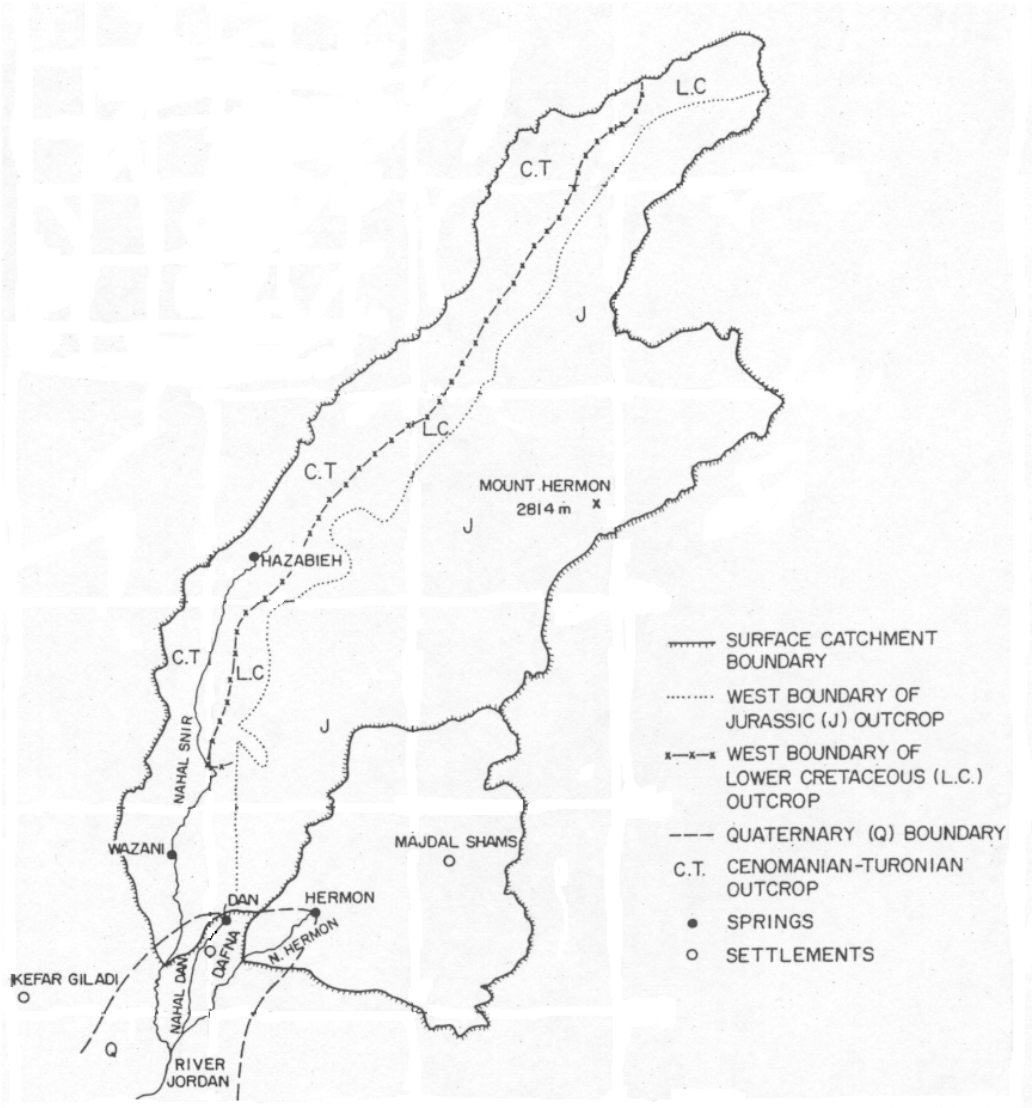

Figure II-4: Aquifers of the sutdy area (modified after SIMPSON and CARMI, 1983)

El Wazani + Hasbani – Spring

El Wazzani and Hasbani are the two major springs of the Snir located in the Hasbani Valley and emerge from the Cenomanian-Turonian aquifer (Figure II-4). Their discharge is $40 – 50 \times 10^6$ m³/a and $25\text{-}30 \times 10^6$ m³/a respectively. The Cenomanian-Turonian layers are only exposed at an area of 40 km², but this is not enough to generate a corresponding discharge in the springs. However, hydrochemical analysis of GUR ET AL. (2003) could show that both springs are also fed by the Jurassic aquifer.

For the description of the discharge characteristics six gauges are available (Table II-1). The location of the gauges can be seen in Figure II-5. The total discharge of the study area is represented at the gauge Yoseph Bridge which is located in the Hula Val-

ley briefly after the union of the big three tributaries Dan, Banias and Snir and the outlet of the Ayun into the Jordan River. Sa'ar is an influent of the Banias.

Table II-1: Gauges of the Upper Jordan Catchment

Gauge	Height [m asl]	Surface drainage [km²]
Banias	400	154,5
Dan	200	20,9
Snir	98	602,6
Ayun	502	35,8
Sa'ar	960	25,5
Yosef-Bridge	75	855,2

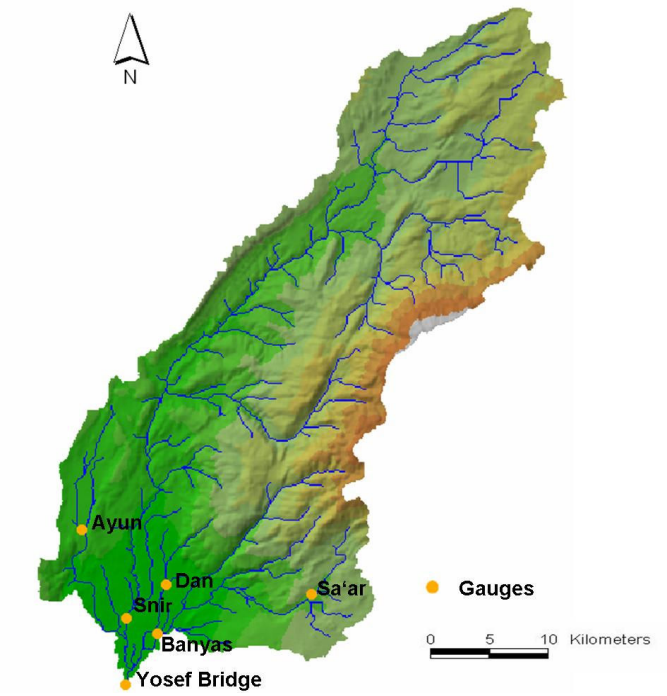

Figure II-5: Location of the discharge gauges in the UJC

The hydrological regime can be described by the hydrological classification numbers (Table II-2) and the discharge coefficients after PARDÉ (1964) generated from the time series of the gauges.

The following hydrological classification numbers are considered:

Table II-2: Hydrological classification numbers of the gauges at the Upper Jordan Catchment

Gauge	Period	AMaF	MHF	MF	MLF	AMiF
Banias	1970 – 2001	38.6 (06.02.1992)	5.5	3.3	2.5	0.7 (06.09.1999)
Dan	1970 – 2001	12.4 (02.08.1993)	8.5	8	7.7	3.2 (19.12.1990)
Snir	1970 – 2001	107 (2.12.1994)	8.2	3.5	2.2	0.5 (22.09.2001)
Jordan	1970 – 2001	126.1 (06.02.1992)	23.4	14.4	10.9	2.8 (01.06.2001)

Values in m³/s; AMaF = Absolute Maximum Flow, MHF = Mean annual High Flow, MF = Mean annual Flow, MLF = Mean annual Low Flow, AMiF = Absolute Minimum Flow

The monthly discharge coefficients are determined by dividing the mean monthly (MF_m) discharge by the mean discharge (MF_a). These values are dimensionless and thus comparable to discharges of different magnitudes.

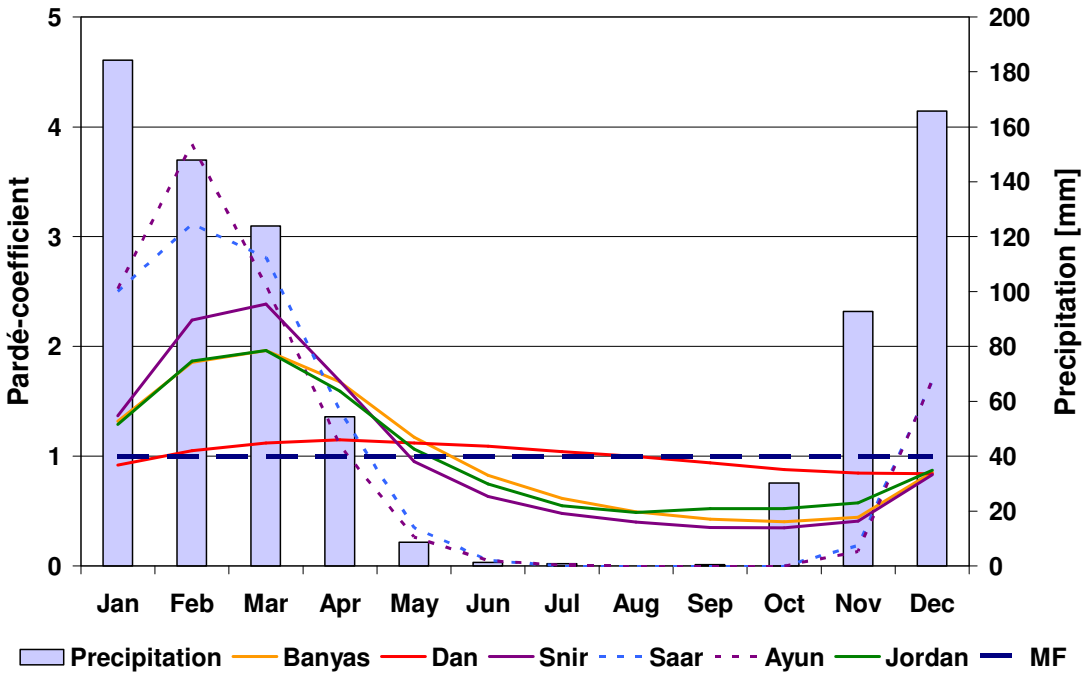

Figure II-6: Monthly Pardé-coefficients of the UJC's subbasins

As it can be seen in Figure II-6, hydrological regimes of the different tributaries vary considerably. However, the streams Dan, Banias and Snir have in common that they can be classified as Mediterranean pluvio-nival systems due to the climate and topographic conditions. Therefore the discharge is governed by rain producing maximum values during the rainy season in winter. As a result of the recharge area sited at high

altitudes they are additionally influenced by snowmelt that continues during spring until early summer generating an attenuated summer low flow.

The Dan has the steadiest hydrological regime with only low fluctuations over the year. Since its surface catchment is negligible it does not directly react on rainfall events. Discharge is solely derived from the spring. Its behaviour indicates the existence of an extended groundwater basin with good storage properties in a karstic environment.

In contrast, the Hermon and Snir show faster reaction on rainfall generating floods in case of extreme rainfall events (see AMaF at Table II-2). Discharge amounts are highest during the rainy season in winter while runoff in summer only originates from the groundwater reservoirs. In comparison to the Banias the Snir evinces a more rain-fed system because of larger amounts of discharge during winter and higher variations throughout the years, while the proportionally higher amounts of discharge during spring and summer indicate for the Banias a more extended groundwater reservoir and snow melt contributions.

Distinct different behavior is given for the Ayun and Sa'ar. They react very fast on rainfall, but their discharge is periodic and limited to the rainy season since they don't have springs and are not connected to aquifers.

In spite of its importance to the water supply in the region only few studies have been made investigating the characteristics as well as the recharge and discharge mechanisms of the Upper Jordan River tributaries.

MICHELSON (1975) detected via hydrograph analysis the existence of an interflow component beside the baseflow for the main tributaries in the Upper Jordan River region.

These findings have been confirmed by the hydrographical and isotopic investigations of SIMPSON and CARMI (1983). They found an interflow component for the Banias and the Snir which is characterized by a very small recession constant. The interflow reservoir is explained by epi-karst conditions which have much greater horizontal than vertical permeability, inhibiting infiltration in preference to subsurface runoff.

GILAD and BONNE (1990) investigated the snowmelt of the Mount Hermon and its contribution to the main sources of the Upper Jordan River. They estimated that the relative contribution of snowfall to the annual water budget for the period 1983 – 1987 was 15 - 182 x 10^6 m³/a, with an average of 50 x 10^6 m³/a. This represents about 12% of the

annual yield and about 30% of the dry weather discharge during late spring and early summer.

GUR et al. (2003) implemented hydrochemical and isotopic analysis for the Dan, Banias and Kezinim springs. They were able to distinguish between conduit and diffusive flow components. While Dan, representing the springs on the western side of the Mount Hermon, is dominated by conduit flow, diffusive water flow is the major source of the Kezinim spring, representing the eastern side. Banias spring instead is governed by both discharge components. The conduit flow indicates a more developed karstic system on the western side of the Hermon range. According to GUR et al. (2003) this is either the result of the tectonic age, or due to its direction facing the rain. They identified for the Dan a large and distant recharge area and a big and stable reservoir, while the recharge area and the reservoir of the Banias is small, nearby and limited.

The most recent work has been done by BRIELMANN (2008). She investigated the recharge and discharge characteristics of the Upper Jordan River applying a combined-method approach that comprises hydrographic techniques, time-series analysis, as well as isotopic and natural geochemical tracers. Similar to GUR et al. (2003) she describes the Kezinim and baseflow of the Banias spring as diffusive matrix flow originating from a regional groundwater system. Additionally, the Banias spring has limited storage capacity and a well developed drainage that responds fast to rain and snowmelt. In contrary, the Dan spring is characterized by an extended, well mixed reservoir where transport occurs in changing portions through both conduit/fissure and matrix flow. Recharge rates of the springs are derived by chloride mass balances and mean residence time estimations and range between 12 to 20% of the mean annual precipitation and 19 to 30%, respectively. She calculates for the subsurface recharge area for the Dan a value of 1324 km² and for the Banias 523 km². However, the quality of these estimations is limited by the uncertainty of the determination of the mean annual precipitation on Mount Hermon. The importance of fast flow components to the entire discharge is emphasized. While there is no surface runoff and interflow in the Dan, hydrograph and natural tracer based analysis show a 46% and 58% amount of these two components for the Banias and the Snir, respectively.

III Climate and Hydrological Modeling: State of the Art

III.1 Emission Scenarios

Emission scenarios are the basis for any investigation of climate change. They are assumptions on future anthropogenic greenhouse gas emissions that impact the climate through radiative forcing and are determined by driving forces like demographic, socio-economic and technical development. Since the future evolution of these driving forces is highly uncertain, scenarios are no predictions or forecasts, but alternative pictures of how the future might unfold.

Most common emission scenarios are those of the SRES (Special Report on Emission Scenarios) prepared by the IPCC (Intergovernmental Panel on Climate Change) (NAKICENOVIC and SWART, 2001). They replaced the IS92 scenarios, which have been developed in 1992 and were used in the Second Assessment Report of the IPCC in 1995. The SRES scenarios were first used in 2001 in the Third Assessment Report (TAR) and also in the newest report AR4 (Fourth Assessment Report) of 2007. The SRES scenarios consist of 40 scenarios which are classified into four scenario families A1, A2, B1 and B2. Probabilities and likelihood are not assigned to the individual scenarios and therefore none of them should be interpreted as more representative or more likely. For climate simulations it is recommended to use more than one scenario family to capture the range of uncertainties associated with driving forces and emissions.

Within this study two scenarios of the families of A2 and B2 are used. Both scenarios represent a more divided world in contrary to the scenarios of A1 and B1, which assume more integration. A2 scenarios are characterized by a world of independently, self-reliant nations with regionally oriented economic development, slower and more fragmented technological changes and continuously increasing population. B2 scenarios are more ecologically friendly and assume intermediate levels of economic development as well as a continuously increasing population, but at a slower rate than A2. Emphasis is given on local rather than global solutions to economic, social and environmental stability.

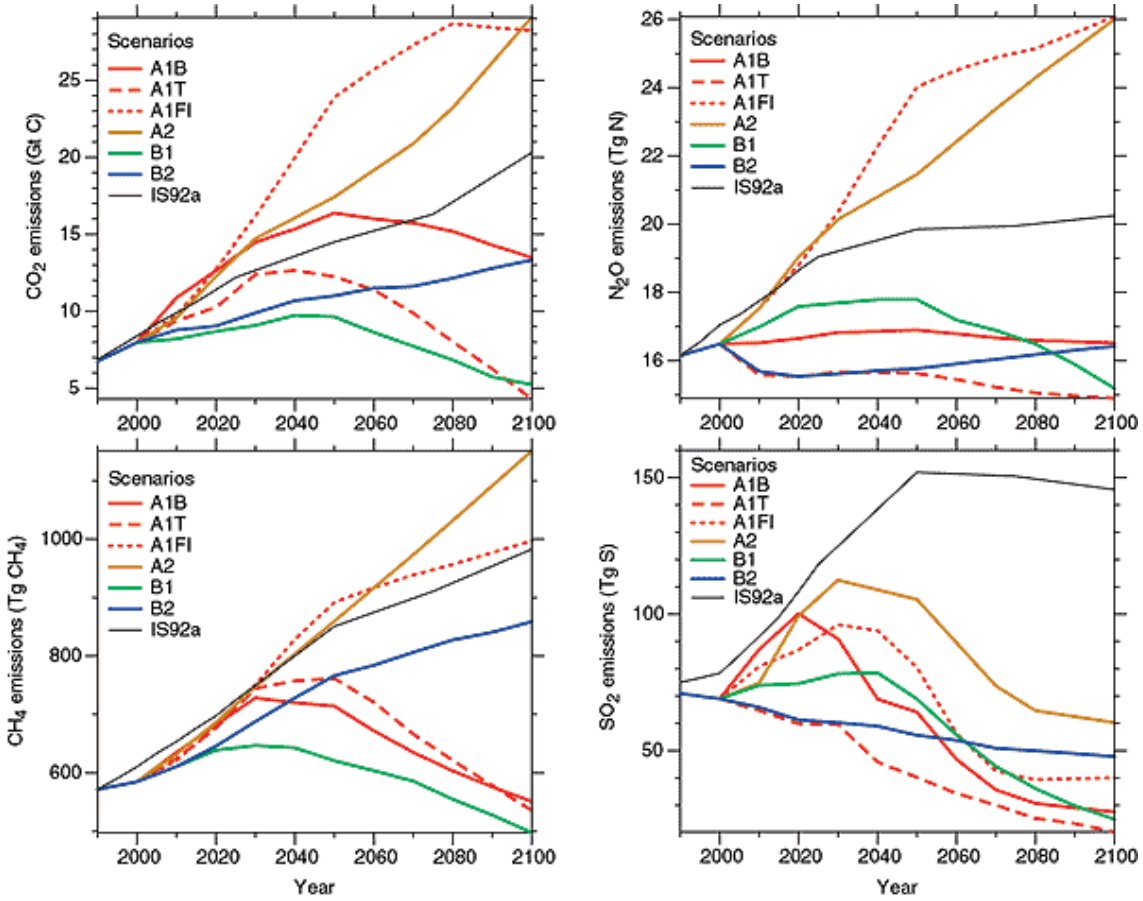

Figure III-1: Anthropogenic emissions of CO_2, N_2O, CH_4, and SO_2 for SRES scenarios (source: http://www.ipcc.ch/ipccreports/tar/vol4/english/099.htm, Jan. 2007)

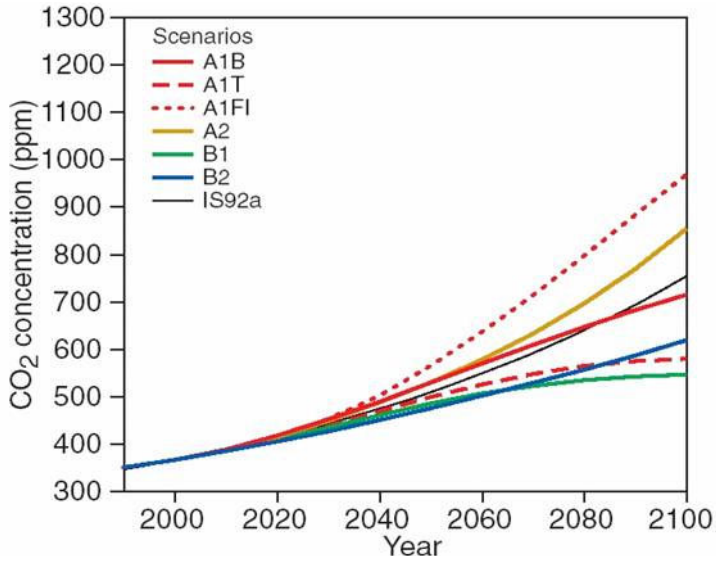

Figure III-2: Atmospheric CO_2 concentrations for SRES scenarios (source: NAKICENOVIC and SWART, 2001)

III.2 Global Climate Modeling

The most common method for investigating the effect of increasing greenhouse gas concentrations in the atmosphere to the global climate is numerical modeling with General Circulation Models (GCMs). While earlier GCMs were purely atmospheric models with parameterized ocean information (AGCM: Atmospheric General Circulation Model), nowadays they are coupled to OGCMs (Ocean General Circulation Models) and are therefore called AOGCM (Atmospheric Ocean General Circulation Model) or CGCM (Coupled General Circulation Model). To assess climate change information for the future, these AOGCMs are run against emissions scenarios like described in III.1. as external forcing.

Performance of GCMs

Many studies have been made to test their ability performing recent or past climate. RANDALL et al. (2007) mention that recent AOGCMs are reproducing observed features of recent climate and past climate changes. For the AR4, the newest report of IPCC in 2007 (IPCC, 2007), a multi model comparison of 21 AOGCMs has been made. In comparison to the previous report there have been ongoing improvements within the different AOGCMs regarding besides resolution, computational methods and parameterizations also the implementation of additional processes (e.g. interactive aerosols). Progress has been made in the simulation of important modes of climate variability. Therefore some AOGCMs can now simulate important aspect of the ENSO, while the reproduction of some other oscillations like the Madden-Julian-Oscillation (MJO) remains unsatisfactory. Progress has also been made in the ability of simulating extreme events. Especially hot and cold spells are well described, while frequency and amount of extreme precipitation events are still underestimated. Improvement has been achieved in the simulation of extratropical cyclones as well as in the reproduction of observed frequency and distribution of tropical cyclones. Nevertheless, some inaccuracies remain like systematic biases in most models for the simulation of the Southern Ocean which results in some uncertainty in transient climate response. Furthermore, the ability to reproduce abrupt climate change is limited in recent AOGCM. Some feedback effects still seem to be insufficient understood. For example, the unexpected high reduction of arctic sea ice in summer 2007 as a result of changed circulation patterns has been considered in none of the AOGCMs used in the AR4 as a possible progress for the near future (ZHANG et al., 2008; STROEVE et al., 2007). However, altogether

there is considerable confidence that AOGCMs provide reasonable quantitative estimates for future climate change, particularly at continental and larger scales. Thereby level of confidence is depending on climate variables (e.g. for temperatures higher than for precipitation) (RANDALL and WOOD, 2007).

Performance of GCM for the Mediterranean

A study for intercomparison of different GCMs with focus on the Mediterranean has been made by GIORGI and LIONELLO (2008) using output from an ensemble of models stored at the Program for Climate Model Diagnosis and Intercomparison (PCMDI) for 1961-1980 compared with CRU land observations. They detected biases in the multimodel mean of 17 GCMs for the region of the Mediterranean as a whole and 6 subregions. They found for temperature a cold bias in the whole Mediterranean for all seasons, while in the Eastern Mediterranean for summer a warm bias was noticed. Precipitation amounts in the Mediterranean are underestimated in all seasons and over most subregions. In contrast, for the Eastern Mediterranean a small overestimation of precipitation in summer and autumn accompanied with an underestimation in winter is observed. Altogether, deviations of GCM simulated rainfall to observations are smallest in the Eastern Mediterranean in comparison to the rest of the Mediterranean. Additionally to the investigation of biases the ability of the GCMs to simulate recent climate trends has been evaluated. Therefore GIORGI and LIONELLO (2008) compared the last 2 decades of the last century (1981-2000) with the previous period 1961-1980. While surface warming of the late 20th century was captured by the ensemble of GCMs very well, in particular its seasonality with maximum in summer and minimum in winter, recent trends of precipitation in the Mediterranean don't agree much with observations based on CRU data. Especially the decreasing winter and spring rainfall amounts are not captured.

Climate Change Projections of GCMs in the Mediterranean

GIORGI and LIONELLO (2008) analyzed multi model projections of the Mediterranean for the A1B scenario and found that precipitation decreases in the whole Mediterranean basin in all seasons and periods. Summer shows greatest decrease with -28% for the period 2081 - 2100 in comparison of 1981- 2000, while decreases for winter of -7%, for spring of -14% and for autumn of -15% are investigated. Throughout the 21 century surface temperatures are steadily increasing with a maximum in summer (+4.6 K) and minimum in winter (3.1K) by comparing the same time periods like for precipitation.

Similar findings are described by CHRISTENSEN and HEWISTON (2007). For the scenario A1B and the GCM ensemble of the AR4 they find for Southern Europe and the Mediterranean a warming of the annual mean in a range of 2.2 – 5.1K for 2080 - 2099 in comparison to 1980 – 1999. For the same period changes in precipitation range GCM dependent from -4 to -27% with reductions in all seasons, whereas percentaged decreases are highest in summer.

III.3 Regional Climate Modeling

GCMs are good tools to predict large scale climate variations at seasonal and interannual scales, but they are usually not successful in reproducing higher order statistics and extreme values. Furthermore, they can not be adapted for impact-oriented applications at regional scale because of their relatively coarse resolution (typically several hundreds kilometers). Since higher resolutions of AOGCMs or global models with variable spatial resolution are still limited by computational power and time demand, methods of regional climate modeling have been introduced. In general, two approaches for downscaling of GCM output can be distinguished: dynamical and statistical downscaling.

III.3.1 Downscaling Methods

Dynamical Downscaling

For dynamical downscaling a Limited Area Model (LAM) like a Regional Climate Model (RCM) gets nested into the GCM. Inside this limited area - the chosen domain - all atmospheric equations for motion, energy and momentum balance are getting solved. The spatial resolution of RCMs usually varies from a few kilometers to several tens of kilometers. RCMs running on resolutions less than 10 km are normally based on the fully non-hydrostatic equations. In spite of the high resolution compared to GCMs, still some sub-gridscale physical processes have to be parameterized. Based on the nesting approach the RCM derives lateral boundary conditions, as well as initial and lower boundary conditions from the GCM. This indicates the dependency of RCM results on the GCM output.

The use of a RCM in higher resolution enables the consideration of forcing like land use and orography at regional scale. Most important mesoscale forcing in the Mediterranean region is associated with the large land-sea contrasts and the complex orogra-

phy, characterized in many coastal regions by steep mountain slopes. Therefore RCMs are able to improve shortcomings of global models like more realistic simulations of Mediterranean cyclones and regional climate phenomena such as heavy rainfall events.

Statistical Downscaling

Another technique the so-called statistical downscaling where statistical methods are used to relate large scale climate variables ("predictors") to regional or local variables ("predictands"). The predictors of a GCM can be fed into a statistical model to estimate the corresponding regional or local climate characteristics. The advantage of these techniques, which have been widely employed in weather forecasting, is that their application needs little computational power compared to dynamical downscaling. A disadvantage from the point of view of simulating climate change is that it can't be secured that recent statistical relations are valid under changed climate conditions (GIORGI ET AL., 2001) since the non stationarity in empirical climate relations is well documented (e.g. RAMAGE, 1983). Different methods have been applied for statistical downscaling including weather typing through classification of circulation patterns, weather generators or transfer functions like linear and nonlinear regression, artificial neural networks, and empirical orthogonal functions (EOF) or canonical correlation analysis (CCA).

III.3.2 Regional Climate Modeling in the Eastern Mediterranean

Although the Mediterranean is considered as one of the hot spots due to climate change (GIORGI, 2006), so far regional climate change projections for the region are relatively sparse. A comprehensive overview of studies for climate change simulations over the Mediterranean is given by ULBRICH et al. (2006).

Several statistical downscaling methods are applied for the Western Mediterranean, especially the Iberian Peninsula, by TRIGO and PALUTIKOV (2001) and GONZÀLEZ-RUOCO et al. (2000). They found small decreases of precipitation for autumn and spring and increases in winter. Considering the whole Mediterranean area, global climate scenarios have been statistically downscaled by HERTIG and JACOBEIT (2008a) for assessments of changes in precipitation and temperature (HERTIG and JACOBEIT, 2008b). They used multiple regression analysis and CCA for downscaling precipitation from seven different AOGCM scenario runs with two different SRES scenarios (A2 and B2).

They found for the period of 2071 – 2100 compared to 1990 – 2019 a shorter wet period with increased precipitation in winter and decreases in the transition seasons for the western and northern regions of the Mediterranean. For the southern and eastern parts they observed mainly negative precipitation changes. Two AOGCM outputs (ECHAM4/OPYC3 and HadCM3) both forced with B2 scenario assumptions have been downscaled with CCA models to assess temperature changes for the 21st century. Results show all over the Mediterranean increasing temperatures for all months and maximum changes of partly more than 4°C by the end of the century.

Many regional climate change projections for Europe using different RCMs have been made within the framework of the PRUDENCE project (CHRISTENSEN et al., 2002), e.g. MACHENHAUER et al. (1998), CHRISTENSEN and CHRISTENSEN (2003), SEMMLER and JACOB (2004). To assess issues of uncertainty, a strategy within this project was chosen to use multiple scenarios (A2 and B2), multiple GCMs (4) as well as multiple RCMs (9) in the same resolution of 50km for mostly the same periods (2071 – 2100 compared to 1961 – 1990). Unfortunately, in most RCM domains only parts of the Mediterranean region are covered, especially the extreme southern and eastern areas are excluded. Only the setup of GIORGI et al. (2004a, 2004b) with the RCM RegCM3 covered the whole Mediterranean. GAO et al. (2006) nested into these experiments a higher resolution domain of 20km to assess more detailed information to future precipitation extremes. They found for the scenario A2 positive future changes in the northern and negative changes in the southern parts of the Mediterranean in winter, while rainfall in the other seasons mostly decreases. For extreme events an increase for the probability of both extreme rainfall and dry spells is detected. Due to the efforts in computer power, recent studies go off time slice experiments and perform transient runs until the end of the 21st century. BOZKURT et al. (2008) downscaled with the RCM RegCM3 ECHAM5 GCM output of SRES scenario A2 in a resolution of 27 x 27 kilometers and found for the Eastern Mediterranean increasing temperatures in all seasons and decreases in precipitation for the southern parts, but slight increases in winter rainfall for the northern region of Turkey along the coastal areas of the Black Sea. KRICHAK et al. (2009) performed a shorter transient climate simulation until the end of the first half of the 21st century for the region of non-boreal East Europe also using RegCM3. As driving input SRES scenario A1B based on the GCM ECHAM5 is used. Their spatial resolution was 50 x 50 km. They found in the early period 2010 – 2035 little change in precipitation over the Jordan River basin, but higher decrease amounts in the later period 2035 – 2060.

III.4 Hydrological Modeling

III.4.1 Model Choice

For this study the demand to a hydrological model is a high degree of transferability to different climate conditions since the aim is mainly the investigation of climate impact on the water cycle. Furthermore, the complex interactions of surface and subsurface runoff components in the UJC should be considered in physically based approaches to gain a better process understanding. Despite the low data availability and the consequent high degree of parameter uncertainty, the mainly physical based distributed hydrological model WaSiM-ETH (SCHULLA and JASPER, 2000) is chosen. It was primarily designed for impact studies of climate or land use change on the terrestrial water balance in complex river basins. But it has been applied for many purposes on a wide range of spatial scales (meters to kilometers) and from event-based to continuous simulations (in temporal resolution of hours to days). It is mainly used in alpine or Middle European catchments, e.g. for climate impact studies by MARX et al. (2008), KUNSTMANN et al. (2004) or JASPER et al. (2004) or for flood forecast by JASPER et al. (2002) and MARX (2007). But it was also successfully applied in semi-arid catchments, e.g. for the Volta Basin in West Africa by WAGNER et al. (2008) and JUNG and KUNSTMANN (2007b)

III.4.2 Hydrological Modeling of the Upper Jordan River

Several models and rainfall-runoff analysis were proposed for the UJC in former studies, but so far no physically based hydrological model has been applied. Various statistical rainfall-runoff correlations relationship connecting directly rainfall in several gauging stations and the streamflow of the Jordan River has been presented by MORIN et al. (1979), the WATERSHED UNIT OF MEKOROT (1991), ROM (1994), and SHENTSIS and BEN TZVI (1994). KESSLER (1999) used a conic linear reservoir for predicting monthly discharge of the Dan spring. Some applications have been partly physically based: A three-reservoir model was presented by BERGER (2001). RIMMER and SALINGER (2006) introduced LASCAM (SIVAPALAN ET AL., 1996) for the UJC, and subsequently developed HYMKE, a daily precipitation-streamflow model for large scale karst basins considering base and surface flow components. The model HYMKE was recently further developed to HYMKE_dual by HARTMANN et al. (2008) introducing a dual permeability approach and making it applicable for climate change scenarios.

III.5 Joint Climate – Hydrology Modeling and Bias-Correction

III.5.1 Approaches

Climate change affects many fields of environment and human life. Therefore more and more scenario outputs from global and regional climate models are used for impact analysis in research fields like hydrology, biology, agronomy and even economy. Typically the coupling to climate models is done off-line and one-way without any feedback to the climate model. In this case, an impact model is fed by the output of the climate simulations. A sophisticated two-way coupling approach, the coupling of climate and chemistry within the model MCCM was presented by FORKEL and KNOCHE (2005), which is based on the RCM MM5.

Although representation of hydrology is included in GCMs and RCMs, they generally do not resolve the hydrological cycle at al level of detail needed for hydrological impact studies, especially at the catchment scale. Typically lacks of sufficient representation of snow storage in mountainous regions and river flow routing routines occur (GRAHAM et al., 2007). Therefore a coupling to hydrological models is required to transfer climate change signals into responses of the hydrological cycle. Several work has been done in joint climate-hydrology modeling over the last years with various strategies using climate simulation output (from GCMs directly, RCMs or statistical downscaled data) and different hydrological models (e.g. WILBY et al., 2000; MIDDELKOOP et al., 2001; MENZEL and BÜRGER, 2002; HAY and CLARK, 2003; KUNSTMANN et al., 2004; LENDERINK et al., 2007; JUNG and KUNSTMANN, 2007b; SAMUELS et al., 2009).

There are different approaches interfacing the transfer between climate and hydrological models. Two main methods can be distinguished: the so called **delta-approach** (referring to HAY et al., 2000) and the **direct forcing approach**. The principle of the delta-approach, which has been used in many hydrological impact studies (e.g. ARNELL, 1998; GELLENS and ROULIN, 1998; MIDDELKOOP et al., 2001) is to compute differences between recent and future climate conditions received from climate simulations (GCM or RCM) and add these changes to observed time-series. In contrast, the climate modeling output is used directly to run the hydrological model at the direct forcing approach. GRAHAM et al. (2007) discussed the advantages and shortcomings of both methods. They mention that using observed climate as baseline is an advantage of the delta method since the capability of the climate model to produce simulations compa-

rable to observed climate is less crucial. It implies also that the variability of the climate does not change as the number of rainy days stays the same and extreme rainfall is modified by the same factor as all other precipitation events. In contrast, the direct forcing approach provides more direct representation of the climate modeling results and thus also more consistency in climate variability. A disadvantage is that this approach is quite sensitive to the quality of the RCM output used as input for hydrological modeling. A problem with the use of RCMs for hydrological purposes is that the simulated variables, especially precipitation, mostly differ systematically from observed values (e.g. FREI et al., 2003). So usually for the direct forcing approach bias correction methods have to be applied.

To identify whether bias corrections are necessary, at first RCM output of recent climate periods has to be compared with observational climate (e.g. reanalysis, observation data). If significant deviations are found, the simulated data have to be transformed by mathematical methods. The same transformation has to be made in the last step also for the future climate. The method of bias correction depends on the purpose of the investigation. If extreme events and their return periods are to be determined, an adjustment on the frequency distribution should be made. If a long term water balance is investigated, the annual cycle of variables like precipitation might be corrected.

Several different bias correction methods exist with different levels of complexity. An overview of principal methods for bias correction is given in DÉQUÉ (2007). A very common and simple method for correcting seasonality is the determination of monthly scaling factors. This technique was for example successful applied by KUNSTMANN et al. (2004) analyzing climate impact on an alpine catchment. More complex methods have been used for example by SHABALOVA et al. (2003) and LENDERINK et al. (2007).

Despite a bias correction is performed, some problems remain for impact modeling. It can be assumed that a static bias correction may not adequately represent future climate changes, such as changes in circulation. Nevertheless, the direct forcing approach combined with some bias corrections will be the preferred approach in the future for impact modeling. With further development of RCMs no (or only little) bias corrections may be necessary.

III.5.2 Joint Climate – Hydrology Modeling in the UJC

In the preceding diploma thesis to this study (HECKL, 2006) first attempts to run the hydrological model WaSiM with downscaled MM5 climate data were made. Climate data of a time slice experiment for the periods 1961 – 1990 and 2070 – 2099 based on the GCM ECHAM4 and the SRES scenario B2 were available in a resolution of 18 x 18 km.

Joint climate – hydrology simulations of this diploma thesis are achieved as a first guess with a very rough approach not including comprehensive validation of the down-scaled climate data and a bias correction.

A similar setup of WaSiM for the UJC like in this thesis was applied according to the used meteorological input data and the spatial data. Springs within the UJC have been considered with constant hydraulic heads, for springs outside the UJC that are likely to be connected to the subsurface UJC, outflow at the catchment boundaries have been defined (see chapter V.2.1). Due to the uncertainties about the subsurface conditions, two calibrations have been done according to two different spatial resolutions and groundwater depths: the one with a grid size of 90 x 90 m and an aquifer depth of 20 m, the other with 450 x 450 m grid size and 100 m aquifer depths. With both approaches it was tried to reproduce the complicated subsurface conditions composed of an extended karst aquifer feeding different springs. The Dan spring as the biggest of these springs contributes as the largest tributary to the Upper Jordan River (see chapter II.2.2). Its subsurface catchment's size exceeds its surface one by far. Due to these conditions in both approaches it was not succeeded to simulate the Dan spring properly. Simulated discharge amounts differed from measurements in magnitude and dynamic considerably, while for the other tributaries good simulation results could be achieved. However, quality of the hydrological simulations of the entire UJC as well as of the joint climate – hydrology simulations suffered from these shortcomings.

The proper reproduction of the karst spring Dan is the crucial point for a successful modeling of the UJC hydrology and water balance. For this reason, in this thesis a new approach is applied simulating the karst aquifer with a combination of the 2-d groundwater model and a bypass from the Snir subbasin to the Dan subbasin within the routing model.

Besides this diploma thesis joint climate – hydrology modeling in the UJC is a research field which is not much focused at so far. The only work is done by SAMUELS et al. (2010). They used the output of the RCM RegCM simulations as input for the hydrological model HYMKE (RIMMER and SALINGER, 2006). RegCM was driven by ECHAM5 with the SRES scenario A1B for the period 1960 – 2060. The spatial resolution of the downscaled data is 50 x 50 km. They performed a bias correction of the precipitation using single grid cells of the RCM output being compared to precipitation stations. With this method they downscaled the RCM output to station level correcting seasonal distribution and intensities of the rainfall. As result they found that the expected changes are nearly insignificant in terms of changing the timing of the discharge. Furthermore, their results suggest an increase in evaporation and a decrease in annual rainfall amounts.

IV The Modeling Approach and Statistical Analysis Methods

Within this study output of NCEP/NCAR reanalysis and of the AOGCM ECHAM4/OPYC is dynamically downscaled with the RCM MM5 to assess regional recent climate and climate change information for the Eastern Mediterranean due to emissions scenario forcing. Additionally, RCM scenario output is used within the hydrological model WaSiM to detect climate change impact on the water balance of the Upper Jordan River.

Within this chapter the applied models are described briefly. Additionally statistical methods used for the analysis of observational data and simulation output are depicted.

IV.1 The Global Climate Model ECHAM4/OPYC3

The AOGCM ECHAM4/OPYC3 is composed of the AGCM ECHAM4 and the OGCM OPYC3. ECHAM4 is based on the global meteorological model ECMWF (*European Centre for Medium Range Weather Forecast*) and was further developed to a GCM at the Max-Planck-Institute for Meteorology and the DKRZ (*Deutsches Klimarechenzentrum*) in HAMburg. ECHAM4 contains, in comparison to the ECMWF model, several changes, mostly in the parameterization, in order to adjust the model for climate simulations. DKRZ (1993) gives a detailed description of ECHAM4 and its parametrization. The OGCM OPYC3 (Coupled Snow, Sea Ice, Mixed Layer and IsoPYCnal Ocean Model) (OBERHUBER, 1993) is coupled quasi-synchronously to ECHAM4. The AOGCM exchanges once a day variables between both model components: While ECHAM4 provides momentum, heat and freshwater to OPYC3, the ocean model returns sea surface temperature (SST) and sea ice variables (RÖCKNER, 1999).

ECHAM4 is a spectral transform model with a resolution of approximately 2.8° longitude/latitude resolution (T42) that uses 19 non-equidistant atmospheric layers in a hybrid-sigma-pressure system. The upper boundary is at a height of 10 hPa (~30km). Prognostic variables are vorticity, divergence, logarithm of surface pressure, temperature, specific humidity and mixing ratio of total cloud water. A semi-implicit time stepping scheme is used together with a weak time filter. The time step for dynamics and physics is 24 minutes. The radiation time step is 2 hours. Both seasonal and diurnal cycles in solar forcing are simulated.

The AOGCM is forced for the time period 1860 to 1989 with observations and from 1990 until 2100 with scenario information of anthropogenic emissions including CO_2, CH_4, N_2O and sulphur dioxide.

IV.2 The NCEP/ NCAR -Reanalysis Data

NCEP/NCAR reanalysis data are used for validation reasons. They are downscaled in the same manner like ECHAM4 and are compared to the control period of the GCM's present climate. The NCEP/NCAR Reanalysis project is a joint product from the National Centers of Environmental Predictions (NCEP) and the National Center of Atmospheric Research (NCAR). It uses a state of the art analysis/forecast system to perform data assimilation using past data from 1948 to the present.

The model used is identical to the operational NCEP global spectral model, except for the horizontal resolution, which is T61 (equivalent to 210km). It uses 28 vertical levels and for data assimilation a 3-dimensional variational (3D-Var) scheme cast in spectral space denoted Spectral Statistical Interpolation (PARRISH and DERBER, 1992). Assimilated data are derived from upper air rawinsondes, satellites, aircraft and oceanic observations as well as land surface reports. More details about the NCAR/NCEP Reanalysis project can be found in KALNAY et al. (1996) and KISTLER et al. (2001).

IV.3 The Regional Climate Model MM5

MM5 (short for 5th generation Penn State/NCAR Mesoscale Model) is a regional model that was developed in cooperation of the Pennsylvania State University (PSU) and NCAR (GRELL ET AL, 1995). It has been designed for use in many different applications in weather forecasting as well as climate projections. Its main characteristics are (i) multi-nest capability, (ii) nonhydrostatic dynamics, (iii) four-dimensional data assimilation capability, (iv) numerous physics options, and (v) portability to a wide range of computer platforms, including OpenMP and MPI systems (DUDHIA et al., 2003). Due to the large number of users MM5 has been applied and validated for many different purposes and different climate conditions all over the world. It has been used, for example, for high resolution simulations in an alpine region of Southern Germany by KUNSTMANN and STADLER (2005) or for climate simulations in West Africa by JUNG and KUNSTMANN (2007a).

In the following a short description of MM5 properties is given. It is mainly based on GRELL et al. (1995) and DUDHIA et al. (2003), where more detailed information on MM5 can be found.

Horizontal Discretization

The horizontal grid of MM5 uses an Arkawana-Lamb B-staggering of velocity variables with respect to the scalars. Scalar variables are defined at the center of the grid square, while the horizontal velocity components are collocated at the corners. This method enables a larger maximum time step.

Vertical Discretization

The vertical discretization in MM5 is realized in a sigma pressure system with respect to the hydrostatic reference pressure p_0. Therefore the pressure levels are height dependent, which makes the vertical sigma pressure coordinate equivalent to terrain following height coordinates (GRELL et al., 2000). While vertical velocity is carried at the full sigma levels, all other variables are defined in the middle of each layer.

Temporal Discretization

For the temporal discretization of temperature, moisture and the slow terms of pressure and momentum a second order leapfrog scheme is used. Since the nonhydrostatic equations are fully compressible, they permit sound waves. These are fast and require a short time step for numerical stability. Therefore, the semi-implicit time splitting scheme after KLEMP and WILHELMSON (1978) is introduced. It treats vertically propagating sound waves implicitly, but horizontally propagating sound waves explicitly and time centered. A horizontal divergence damping technique according to SKAMAROK and KLEMP (1994) is applied, which leads to the short time step being solely dependent on the horizontal and independent of the vertical resolution.

Nonhydrostasy

In mesoscale models, where horizontal resolutions are comparable or greater than the vertical depth of circulation features, the hydrostatic approximation holds and the pressure is completely determined by the overlying air's mass. Due to KALNAY (2003), the hydrostatic assumption does not hold below a resolution of 10km. With higher horizontal resolutions needed for reasonably simulating climate features of the Eastern Medi-

terranean, nonhydrostatic dynamics have to be considered. MM5 uses the fully compressible mass continuity equation. The only term neglected is a diabatic term contributing to the perturbation pressure tendency.

Lateral Boundary Conditions

The model-predicted variables are “relaxed” or “nudged” toward large-scale analysis of the coarser grid (GCM or coarser domain) at the lateral boundaries. The method includes Newtonian and diffusion terms that decreases linearly from the lateral boundaries. Vertical velocity is not nudged. Moisture variables like cloud water, rain water, snow, and ice are considered zero on inflow and zero gradient on outflow.

Nesting

MM5 contains the capability of multiple nesting with up to nine domains running at the same time and interacting. Nesting means that a domain with higher resolution is put inside the coarser one and getting from it input via the boundaries like the coarse domain from the GCM. Beside this 1-way nesting approach, additionally feedback to the coarser domain can be given over the nest interior in the 2-way nesting approach. The nesting ratio for spatial and temporal resolution between two domains is always 3:1 when using 2-way nesting.

IV.4 The Hydrological Model WaSiM

The hydrological model WaSiM (Water Flow and Balance Simulation Model) (SCHULLA and JASPER, 2007), developed at the Swiss Federal Institute of Technology (ETH), is a deterministic, fully distributed modular model. It uses mainly physically based algorithms for the description of vertical water fluxes and groundwater, whereas for lateral runoff aggregation lumped approaches are implemented. The model can be used in two different versions differing in the way the unsaturated zone is simulated. The first version models the soil water balance and runoff generation by applying a modified variable saturated area approach quite similar to the TOPMODEL after BEVEN and KIRKBY (1979) in a conceptual manner. The second version, which is used in this study, uses the Richards-equation for describing the water flow within the saturated zone. In this version additionally a coupling to a 2D-groundwater model is possible.

In the following a short description of the hydrological model WaSiM and its modules is given mainly based on SCHULLA (1997) and SCHULLA and JASPER (2007), where more detailed information can be found.

Preprocessing

Together with the model WaSiM the preprocessing tool TANALYS (Topographical ANALYSis) is delivered, where input data like exposition, slope, flow net structure, flow directions, flow times, and subcatchment boundaries are derived from the DEM (Digital Elevation Model).

Interpolation of the Meteorological Input Data

Hydrological simulations with the approaches described in this chapter need as driving meteorological input time series on precipitation, temperature, relative humidity, wind speed, and global radiation or sunshine duration. With simpler approaches also fewer variables are sufficient, but precipitation and temperature are essential. Usually these variables are available as station data and have to be interpolated to the predefined regular grid. In WaSiM different methods for interpolation are available: These are among others:

- Altitude-dependent regression: This method considers the fact that in mountainous catchments some meteorological variables, e.g. temperature and wind speed, have a stronger vertical than horizontal dependence.

- Inverse Distance Weighting (IDW): This interpolation method considers all available station within a specified search radius. The interpolation result on a special grid point is the sum of all contributing stations weighted according to their distance to the interpolated point.

- Combination: A combination of IDW and altitude-dependent regression is possible for variables with horizontal and altitude dependency. The weight of each method can be specified as a percentage.

Potential and Real Evapotranspiration

Potential evapotranspiration is calculated using the approach after Penman-Monteith (MONTEITH, 1975; BRUTSAERT, 1982). This method takes the most important plant

properties into account like stomata resistance, root density distribution, root depth, Leaf Area Index (LAI), effective vegetation height and vegetation coverage. The development of plant properties during an annual cycle can be considered. The real evapotranspiration is calculated in two steps: First, potential evaporation is reduced by the amount of water in the interception storage. A further reduction of potential evapotranspiration is done in a second step dependent on the actual suction of soil under consideration of soil and plant physiological properties.

Snow Model

Snow accumulation and snow melt is performed after ANDERSON (1973) and BRAUN (1985), a method that is developed for daily time steps. For snow accumulation the type of precipitation is estimated for each grid cell using the interpolated air temperature during the event. Both kinds of precipitation are taken within a transition range.

Snow melt is calculated only at air temperature above a specific threshold temperature. In case of precipitation > 2 mm/d, snow melt is composed of radiation melt, melt from sensible heat, from latent heat, and from energy import from precipitation. Beside the meteorological variables temperature, precipitation and wind, temperature and wind dependent melt factors are accounted for. At time steps without precipitation snow melt is calculated by using a season dependent radiation melt factor.

Interception

Interception is simulated using a simple bucket approach. The capacity depends on LAI, vegetation coverage degree and maximum height of water at the leaf surface. Interception is calculated after the snow model in order to be able to store melt water next to rain water. The extraction of water out of the interception storage by evaporation is assumed to be at a potential rate. If the interception storage is filled, further precipitation or snow will be put directly to the soil model for infiltration or building surface runoff.

Infiltration and Generation of Surface Runoff

Calculation of infiltration is integrated in the soil model. When using the Richards equation approach, infiltration is considered when calculating the uppermost soil layer. Surface runoff will be created, if precipitation intensities are larger than the actual hydraulic conductivity of the soil.

Unsaturated Zone

The one dimensional vertical fluxes in the unsaturated zone are calculated using the Richards-equation (RICHARDS, 1931) solved in a spatially and temporally discretized form for each grid cell allowing the modeling of vertical moisture profiles, flux profiles and consideration of percolation, as well as capillary rise. The dependence of the suction head and the hydraulic conductivity on soil moisture content is parameterized according to VAN GENUCHTEN (1976). Saturated hydraulic conductivity decreases (dependent on soil texture) with depth according to a recession constant:

This enables generation of interflow within the different soil layers, which depends on drainable water content, hydraulic conductivity and gradient. Groundwater recharge is defined as the remaining vertically percolating water. The groundwater table is defined as the first saturated soil layer.

Groundwater Model

A horizontally two-dimensional groundwater flow model is dynamically coupled to the unsaturated zone. The uppermost aquifer is assumed to be unconfined, whereas aquifers below can either be confined or unconfined. The calculation of the lateral fluxes is based on the continuity equation and Darcy's law. Infiltration from rivers into groundwater and exfiltration from groundwater into the rivers (which is the base flow), is calculated using the hydraulic gradient and the colmation (in- and exfiltration resistance) at the river bed.

Runoff Accumulation

The discharge generated at each grid cell is given to the subcatchment outlet with a temporal retardation. The fastest runoff component, the direct runoff, is routed to the subbasin outlet using a subdivision of the basin into flow time zones. For considering retention, a single linear storage approach is applied in the last flow time zone.

The generated interflow is averaged over the subbasin and adjacent also put into a single linear storage. The surface runoff and the interflow are then superimposed with the base flow to the total runoff of the subbasin.

Discharge Routing

The further way of the runoff in the riverbed below the subbasin, where runoff has been generated before, is described by a discharge routing. Discharge routing is performed by a cinematic wave approach using different flow velocities for different water levels in the channel. Flow velocities and flow times are calculated using the equation after Manning-Strickler. The required parameters for this calculation like slope, hydraulic radius, and roughness are derived within TANALYS using DEM and information on average discharge. After the translation of the wave, a single linear storage is applied accounting for diffusion and retention. The discharge routing subroutine allows considering external inflows as well as artificial or natural abstractions. Furthermore, a combination of an abstraction of the one subbasin and an inflow in another subbasin, called bypass, is possible.

IV.5 Model Coupling

The coupling of the RCM MM5 and the hydrological model WaSiM is realized off-line in a one-way approach by passing results from the RCM as input to the hydrological model (see Figure IV-1).

For the combined climate-hydrology simulations an interface, which has been developed at IMK-IFU and successfully applied at different regions (e.g. KUNSTMANN et al., 2004 or JUNG and KUNSTMANN, 2007b), is used. Within this interface, each grid point of the MM5 model grid represents one input station (further referred to as virtual station). Between these virtual stations the input variables are interpolated in WaSiM to the grid of the distributed hydrological model.

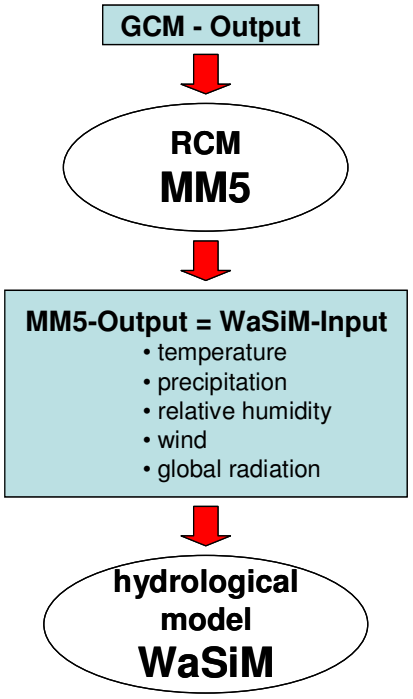

Figure IV-1: Coupling scheme for using climate simulation output in hydrological modeling

The input data required in WaSiM (precipitation, temperature, wind, global radiation, and relative humidity) are generated from the MM5 output as follows:

- Precipitation: The simulated gridscale precipitation and subgridscale precipitation is summed up to the total precipitation amount.

- Temperature: The MM5-output of temperature at 2 m above surface is used directly.

- Wind: The wind velocity w is calculated using the wind vectors components u and v at 10 m above surface with:

- Global radiation: In WaSiM global radiation is defined as direct and diffuse shortwave radiation. Therefore, the simulated short wave radiation of MM5 is used as global radiation.

- Relative humidity: For the calculation of the relative humidity h_r the MM5-output of temperature T [K], surface pressure P_a [hPa] and mixing ratio w_v [kg/kg] is used after JACOBSON (2005).

The created variables are averaged (in case of precipitation summed up) over the number of MM5 output time steps to build one WaSiM input time step.

IV.6 Technical Realization

Regional Climate Modeling

MM5 originally is a regional weather forecast model. To apply the model for climate simulations several adaptations are needed that are described briefly within this chapter. Dynamical downscaling of ECHAM4 output is done in several steps that are visualized in Figure IV-2. The procedure includes besides the downscaling simulation itself several pre-processing steps that are described briefly in the following (based on DUDHIA et al., 2003. All programs are automated in batch jobs based on c-shell scripts allowing for continuous performance of simulations. The pre-processing differs slightly from the original procedure to enable use of ECHAM4 as GCM input.

The first pre-processing program is TERRAIN, where the mesoscale design configuration is defined (size and location of the domains). Elevation and land use are horizontally interpolated onto the chosen domains. Furthermore, additional fields such as soil types, vegetation fraction, and annual deep soil temperature are generated for the land-surface model (LSM).

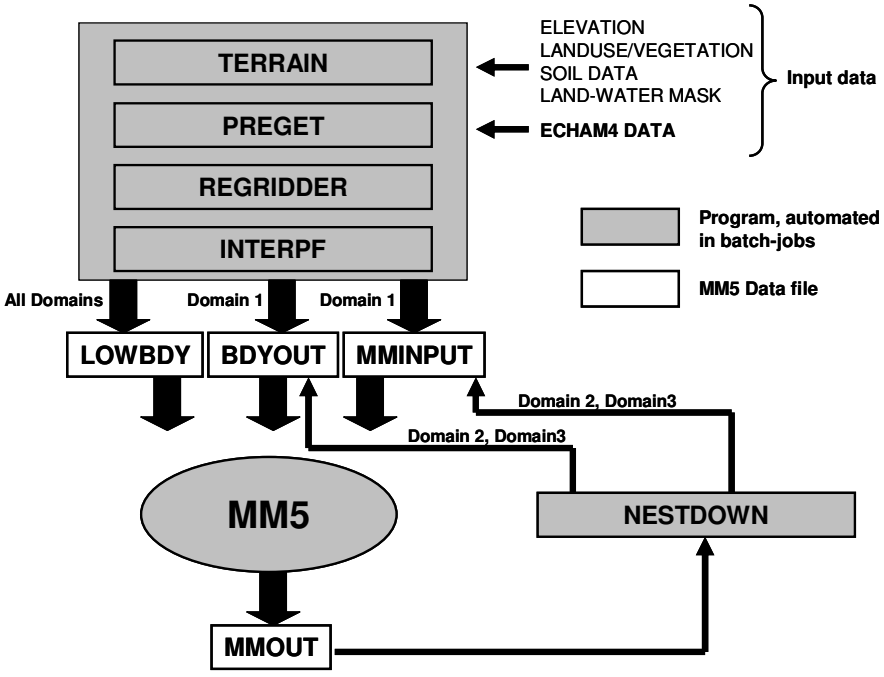

Figure IV-2: MM5 workflow (modified after JUNG, 2006)

To read the ECHAM4 input data the original program PREGRID is substituted for the program PREGET developed at IMK-IFU. This programs process gridded, pressure-level meteorological fields from ECHAM4 and puts the data in an intermediate format. The program REGRIDDER takes the intermediate format and output file from TERRAIN and creates fiels containing 3-dimensional meteorological fields of wind, temperature, relative humidity, geopotential height, and 2-dimensional fields like sea-level pressure and sea-surface temperature. The data of REGRIDDER are then interpolated to the MM5 fields in INTERPF. The output of this program serves as input for the first domain in MM5. It includes 3 files on monthly basis, namely MMINPUT containing initial conditions, LOWBDY and BDYOUT comprising lower and boundary fields, respectively. The pre-processing program NESTDOWN interpolates the output of a coarser MM5 grid to input data of the next domain with finer resolution producing the same MM5 input files like INTERPF. For climate simulations domain 2 and domain 3 derive only BDYOUT and MMINPUT from the coarser domain with NESTDOWN. LOWBDY originates directly from the ECHAM4 output (via PREGET, REGRIDDER, and INTERPF) allowing for consideration of variable SST conditions, which is not implemented in NESTDOWN.

ECHAM4 data are delivered on monthly basis, so no continuous simulations are technically feasible. However, for long-term climate simulations it is important that slowly developing variables are not influenced by a new initialization at the beginning every month. Therefore, soil moisture and soil temperature for all 4 soil layers as the most important slowly responding variables are handed over from the end of the preceding month as initial conditions. This is done by modifying the MMINPUT file. In this way feedback mechanisms between atmosphere and soil are enabled to develop.

Another modification for the use of MM5 with ECHAM4 input data has to be considered: While within MM5 a regular counting of days within a year (365, 366 in case of a leap year) is included, in ECHAM4 every year consists of 360 days and 12 equidistant months each with 30 days. To overcome this problem these 5 (or in case of a leap year 6) missing days are cut out. This is done equally distributed over the year including March 1st (for leap years), May 1st, July 1st, August 1st, October 1st, and December 1st.

Dynamical downscaling is a time demanding method requiring large resources of computational power and storage. For these climate simulations a Linux cluster consisting of 74 nodes with 4 Opteron processors each working with distributed memory is avail-

able. Parallelization of the nodes is realized with MPI over InfiniBand allowing for fast communication between the nodes. MM5 is compiled with PGI compiler pgi 6.2 64-bit.

Table IV-1: Time and CPU demand of each domain for the simulation of 1 month

Domain	Number of CPUs	Time [min]
Domain 1	24	17
Domain 2	32	65
Domain 3	32	165

For the first domain 24 CPUs are used, 32 CPUs for the domains 2 and 3. The time demand dependent on the used CPUs for 1 month is shown in Table VII-1. When all simulated years of downscaled ECHAM4 and NCEP and the used CPUs are summarized 181.374 CPU x h are required. This means that one single CPU would need 7557.25 days or 20.69 years to perform these climate simulations.

Hydrological Modeling

The hydrological simulations are performed on the same Linux cluster. In contrast to MM5, WaSiM is not used in a parallel MPI-mode, but simulated on a single CPU. The huge number of CPUs enabled the performance of a large number of parallel calibration runs. C-shell scripts enable fast modification of parameters and optimized calibration procedure.

IV.7 Statistical Analysis Methods

In this chapter statistical methods used for analysis of observational data and simulation results are described briefly. These are on the one hand methods for calculating the significance of a detected climate change signal, on the other hand the EDI (Effective Drought Index), an index describing the risk of droughts.

IV.7.1 Testing Significance of Change Signals

Due to the transient climate simulations from 1961 to 2099 two approaches to investigate climate change signals of several climatic and hydrological variables can be applied: On the one hand time slices (typically 30 years) of present and future climate can be compared, on the other hand long year time series (e.g. 1961 – 2050 or 1961 - 2099) can be analyzed. Climate change signals are superimposed by natural variabil-

ity. To test whether a climate change signal exceeds the natural variability two methods are applied. In case of time slice analysis a signal to noise ratio is calculated. In case of time series analysis the significance of climate change signals is tested by trend analysis after Mann-Kendall.

Signal to Noise Ratio

The signal to noise ratio (SN) is defined as

$$SN = \frac{\left|\overline{X_{future}} - \overline{X_{present}}\right|}{\sigma_{X\ present}} \qquad \text{IV-1}$$

where $\overline{X_{present}}$ and $\overline{X_{futuret}}$ are the seasonal or annual mean of a certain variable *X* for the present and the future time slice, respectively. $\sigma_{Xpresent}$ is the standard deviation of this variable for the present time slice. If SN > 1, a change signal is detected, as the inter-annual variability (noise) of the present-day time slice, represented by the standard deviation, is exceeded.

Mann-Kendall Trend Test

This test is applicable to the detection of a monotonic trend of a time series with no seasonal or other cycle. It can be used for detecting annual climate trends (e.g. NEUMANN et al., 2006). The Mann-Kendall test is adaptive in cases when the data values x_i of a time series can be assumed to obey the model

$$x_i = f(t_i) + \varepsilon_i\,, \qquad \text{IV-2}$$

where *f(t)* is a continuous monotonic increasing or decreasing function of time and the residuals ε_i can be assumed to belong to the same distribution with zero mean. Therefore, it is assumed that the variance of the distribution is constant in time.

The null hypothesis H_0 states no trend, i.e. the observations x_i are randomly ordered in time. It is tested against the alternative hypothesis H_1, where there exists an increasing or decreasing monotonic trend.

The Mann-Kendall test statistic S is calculated using the formula

$$S = \sum_{k=1}^{n-1} \sum_{j=k+1}^{n} \operatorname{sgn}\left(x_j - x_k\right), \qquad \text{IV-3}$$

Where x_j and x_k are the annual values in years j and k, $j>k$, respectively, and

$$\operatorname{sgn}(x_j - x_k) = \begin{cases} 1 & if\ x_j - x_k > 0 \\ 0 & if\ x_j - x_k = 0 \\ -1 & if\ x_j - x_k < 0 \end{cases} \qquad \text{IV-4}$$

If n is at least 10 the normal approximation is used. In that case the variance of S is calculated like in formula ….which takes into account possible ties (i.e. equal values).

$$VAR(S) = \frac{1}{18}\left[n(n-1)(2n+5) - \sum_{p=1}^{q} t_p\left(t_p - 1\right)\left(2t_p + 5\right) \right] \qquad \text{IV-5}$$

In formula IV-5 q is the number of tied groups and t_p is the number of data values in the p^{th} group.

The values of S and $VAR(S)$ are then used to calculate the test statistic Z as follows:

$$Z = \begin{cases} \dfrac{S-1}{\sqrt{VAR(S)}} & if\ S > 0 \\ 0 & if\ S = 0 \\ \dfrac{S+1}{\sqrt{VAR(S)}} & if\ S < 0 \end{cases} \qquad \text{IV-6}$$

A positive (negative) value of Z indicates an upward (downward) trend. The statistic Z has a normal distribution. For testing as well upward as downward trends a two-tailed test is performed at different levels of significance a. H_0 is rejected if the absolute value of Z is greater than $Z_{1-\alpha/2}$, where $Z_{1-\alpha/2}$ is obtained from the standard normal cumulative distribution tables. For calculation of the Mann-Kendall test the software template after SALMI et al. (2002) is used, which calculates automatically 4 different significance levels of α = 0.001, 0.01, 0.05, and 0.1.

Additionally to the Mann-Kendall test the Sen's nonparametric method is used to estimate the true slope of an existing trend as change per year (SALMI et al., 2002). The

Sen's method can be used when the trend can be assumed to be linear, which means that *f(t)* in formula IV-2 is equal to

$$f(t) = Qt + b \qquad \text{IV-7}$$

Where *Q* is the slope and *b* is a constant.

To get the slope estimate in formula IV-7 first the slopes of all data value pairs have to be calculated

$$Q_i = \frac{x_j - x_k}{j - k} \qquad \text{IV-8}$$

where *j>k*.

If *n* values exist x_j in the time series there are *N=n(n-1)/2* slope estimates Q_i. The Sen's estimator of slope is the median of these *N* values of Q_i. The *N* values of Q_i are ranked from the smallest to the largest and the Sen's estimator is

$Q = Q_{[(N+1)/2]}$, if *N* is odd or $Q=1/2(Q_{[N/2]}+Q_{[(N+2)/2]})$, if *N* is even. IV-9

IV.7.2 Drought Index EDI

Due to NOAA (National Oceanic and Atmospheric Administration of the United Stattes, http://www.nws.noaa.gov/om/brochures/climate/Drought.pdf) a drought is a normal, recurrent feature of climate that occurs in all climate zones. It is a temporary aberration from normal climate conditions, thus the characteristics of a drought vary significantly between regions and climate zones. It differs from aridity, which is a permanent feature of a climate region, where low precipitation is the norm, e.g. in a desert. Several conceptual definitions of a drought exist (e. g. PALMER, 1965 or BERAN and RODIER, 1985), describing a drought as an extended period, where deficiency in water supply occurs in relation to long term conditions.

Due to the disciplinary perspectives usually three main types of droughts are defined: meteorological, agricultural, and hydrological drought. A meteorological drought is brought about when an extended period of below average precipitation or relation between precipitation and evapotranspiration occurs. A meteorological drought usually precedes the other types of droughts. An agricultural drought occurs when a deficiency

in water supply inhibits an average agricultural production of economic plants. A hydrological drought is defined, when water reserves of different sources such as aquifers, rivers, lakes, and reservoirs undermatch the statistical average.

As these conceptional definitions of droughts do not allow for quantifying questions like severity and length of droughts, operational definitions of droughts like drought indices have to be introduced.

In this thesis a drought is defined as a period with negative values of the EDI (Effective Drought Index). As this indicates a precipitation deficiency this index describes meteorological droughts.

The EDI is an objective drought index developed by BYUN and WILHITE (1999) and is calculated on basis of daily precipitation height values. It uses an approach of Effective Precipitation (EP) representing the summed value of daily precipitation with a time-dependent reduction function and therefore the daily depletion of water resources. The EP is calculated after

$$EP_j = \sum_{n=1}^{i} \left[\left(\sum_{m=1}^{n} P_m \right) \Big/ n \right], \qquad \text{IV-10}$$

where *j* is the index of a current day and *i* is the duration over which the sum is calculated. In this case EP amount is calculated for the period of 1 year ($i = 360$ for ECHAM4 data). P_m is the precipitation *m-1* days before the current day.

On basis of the values of EP MEP and DEP can be calculated. MEP (Mean Effective Precipitation) is the long year climatological mean of EP for each calendar day and illustrates the climatological mean of stored water quantity. DEP is the deviation of EP from the MEP.

With the values of daily DEP the precipitation needed for a return to normal conditions (PRN) can be calculated. PRN represents the amount of precipitation required to recover the accumulated deficit. It is calculated after

$$PRN_j = \frac{DEP_j}{\sum_{N=1}^{j}(1/N)}, \qquad \text{IV-11}$$

where *j* is actual duration over which DEP values have been calculated.

Finally, the EDI is calculated as the standardized value of PRN:

$$EDI_j = \frac{PRN_j}{STDV(PRN_j)}, \qquad \text{IV-12}$$

where STDV (PRN_j) is the standard deviation of each day's PRN.

Positive EDI values indicate more than average humid conditions, negative dry conditions. A drought is defined as a period of time in which EDI values are negative. Values of EDI < -1 denote moderate droughts, while EDI < -2 describe severe droughts. Based on the EDI duration and intensities of droughts can be calculated. Duration of a drought is defined as number of days, in which negative values occur, while the integral of the absolute values of the EDI within a drought is an indicator for intensity (Figure IV-3).

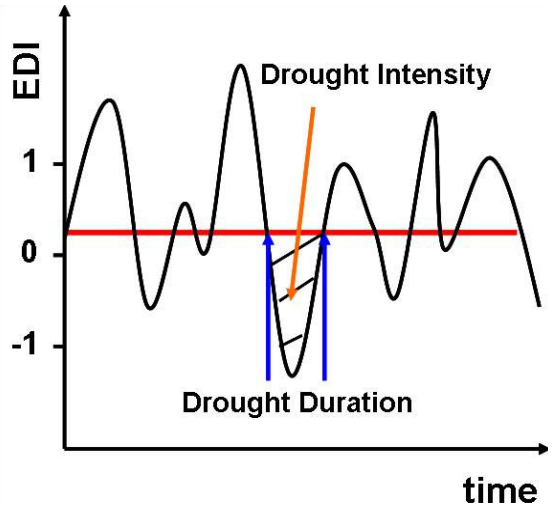

Figure IV-3: Definition of drought duration and intensity based on EDI (modified after LAUX et al., 2009)

To analyze whether regional climate change impacts also the risk and severity of drought events, the Effective Drought Index (EDI) is calculated for the time slices of the control run and of the near and far future based on the two emission scenarios A2 and B2.

V Setup and Calibration

In this chapter the setup and parameterization of the RCM MM5 is described (chapter V.1). Hereupon the setup and the calibration procedure of the hydrological model WaSiM is introduced (chapter V.2). Finally the adjustments for the joint climate-hydrology simulations are presented in chapter V.3.

V.1 MM5

V.1.1 Domain Setup and Discretization

Domain Setting

Domain settings are a controversial discussed problem. Some researchers suggest (e.g. JONES et al., 1995) that the circulation of the RCM should not differ significantly from that of the GCM. Others (e.g. WANG et al., 2004) recommend that for RCM large domains should be used to allow modifications of the atmospheric circulation by the RCM at spatial scales which are not well represented by the GCM.

As the climate of the Mediterranean is conditioned by its position in the transition zone between the midlatitude westerlies and the subtropical high pressure belt, many of its characteristics and variability is associated with upper air circulation (e.g. JACOBEIT, 1987, in TRIGO et al., 1999). However, the unique weather features of the region are also highly influenced by the complex topography steering air flow and the almost enclosed Mediterranean Sea representing an important source of energy and moisture for cyclone development. Many of the cyclones in the region originate over the sea itself or are reinforeced by it. The most important regions of cyclogenesis in the Mediterranean have been analyzed by TRIGO et al. (1999) and TRIGO et al. (2002). In many of these regions topography plays an important role, especially lee effects of mountains like the Alps for the Genua Lows or the Taurus for the Cyprus Lows. Therefore, topography in higher resolution of a RCM might have effects on the circulation and therefore on climate features.

To see, whether the extension of the domain has significant effects on the climate of the Eastern Mediterranean, in particular on precipitation amounts in the Jordan River Catchment as the most important variable for this study, two different domain sizes are tested. In these experiments MM5 is forced with ECHAM4 for the control period 1961 –

1989 in a resolution of 54 km. The smaller domain contains only the Eastern Mediterranean including southern Italy as the uppermost north-western extension (Figure V-1 left), whereas the bigger domain protrudes widely the entire Mediterranean including all important mountainous regions influencing cyclogenesis like the Alps and the Atlas Mountains (

Figure V-1 right).

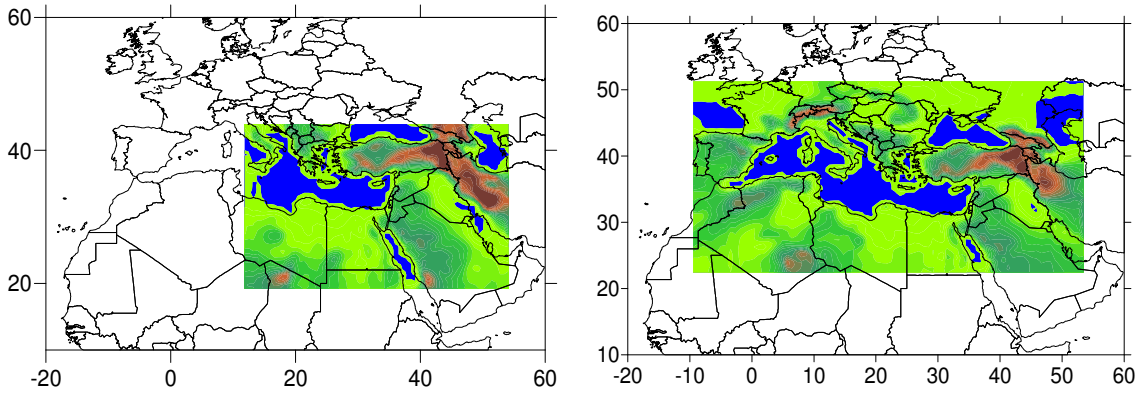

Figure V-1: Topography of the two different domains including eastern Mediterranean (left) and the entire Mediterranean (right) in 54 x 54 km resolution

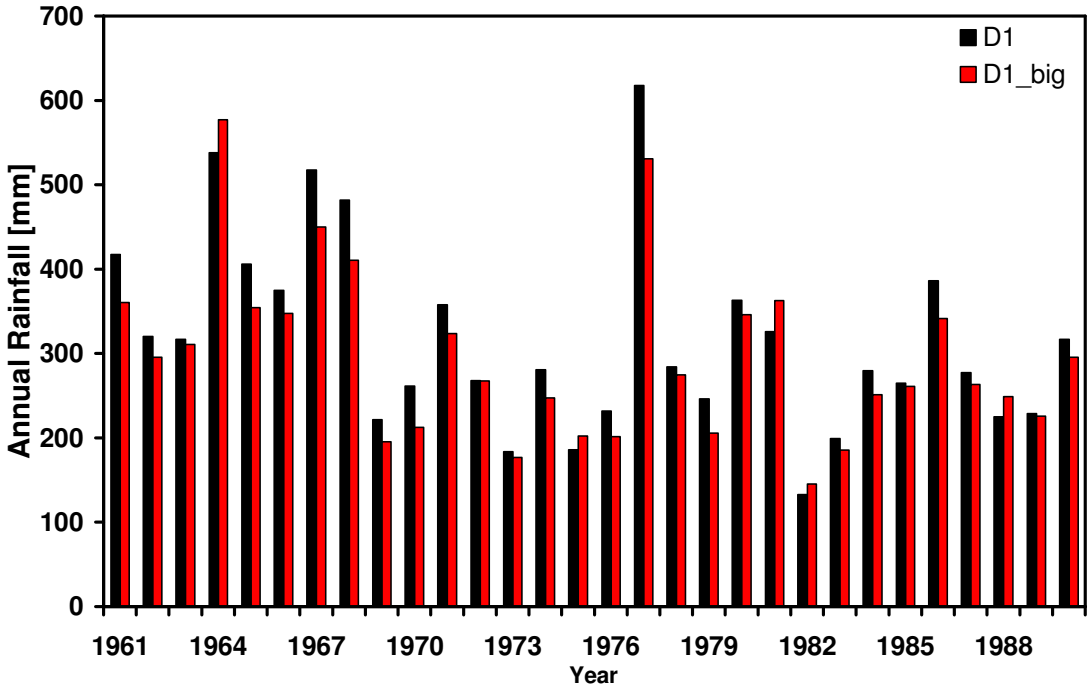

Figure V-2: Comparison of annual precipitation in the UJC for the smaller (black) and the bigger (red) domain size

The effects on the amounts of annual rainfall in the UJC are shown in Figure V-2. A tendency towards higher precipitation within the smaller domain can be seen, but in some years also the bigger domain delivers more rainfall. Over the whole period the difference between the different domain sizes is < 7 %. In some studies that investigated cyclones in the Mediterranean much coarser resolutions of ECMWF (European Center of Medium-Range Weather Forecast) Reanalysis data are used, like ALPERT et al. (1990) analyzing data in 2.5° x 2.5° resolution or TRIGO et al. (2002) in 1.125 x 1.125° resolution. This evidence that all typical Mediterranean cyclones are already created within the GCM and therefore no climatologically important circulation has to be created within the RCM. Differences in the results of both domain size experiments are most probably due to lateral boundary effects, but don't show significance.

Therefore and for reasons of computational time demand, the smaller domain size is chosen for further climate simulations.

Nesting

For the climate simulations 3 model domains were chosen in a 1-way nesting approach (Figure V-3).

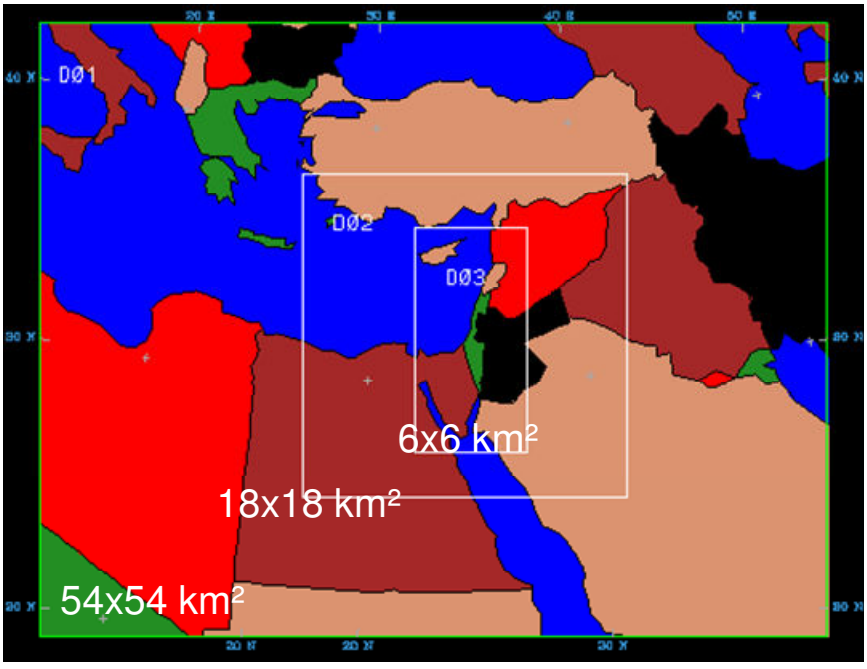

Figure V-3: Domain setup with 3 domains in 54, 18 and 6 km side length of a grid point

Discretization

The horizontal resolution of the 3 domains is 54 x 54 km² for the first domain (D1), 18 x 18 km² for the second domain (D2) and 6 x 6 km² for the third domain (D3). This yields due to their particular extension the simulation of 3200 (D1), 6241 (D2) and 13366 (D3) grid points. For vertical discretization 25 layers were chosen up to the model top level of 30 mbar, which approximates 17 km. The temporal discretization reaches from 150 s for D1, over 45 s for D2 up to 20 s in D3.

V.1.2 Parameterization

Radiation

Radiation schemes represent radiative effects in the atmosphere and at the surface. The applied cloud-radiation scheme provides long wave and short wave interactions due to clear sky and modeled clouds. Additionally an upper boundary condition, developed by KLEMP and DURRAN (1983) and BOUGEAULT (1983), is included. It allows wave energy to pass through unreflected (GRELL et al., 1995).

Planetary Boundary Layer (PBL)

Planetary Boundary Layer schemes represent sub-grid vertical fluxes due to turbulence. In this study Hong-Pan PBL scheme (HONG and PAN, 1996) is used, which is based on a nonlocal boundary layer vertical diffusion scheme of TROEN and MAHRT (1986).

Explicit Moisture Scheme

Explicit moisture or microphysics schemes describe the treatment of cloud and precipitation processes on the resolved scale. The microphysical processes influencing precipitation formation and conversion processes between the different phases of water are parameterized with the Reisner-Graupel scheme. The scheme is activated as soon as saturation at a grid point is reached. It is based on the Reisner mixed phase scheme (REISNER et al., 1998) and includes additionally to the calculation of cloud water, cloud ice, rain water, snow, super cooled water, melting of snow also graupel and ice particle number concentration.

Sub-Gridscale Precipitation

Sub-gridscale precipitation schemes, often referred to as cumulus parameterization, enable generation of precipitation before gridscale saturation is reached. It allows accounting for sub-gridscale processes, as well as grid-scale instability associated with a saturated conditionally unstable atmosphere. In the applied Grell scheme (GRELL and KUO, 1991) single updraft and downdraft properties are included. Along the cloud edges no entrainment and detrainment are considered. Therefore, only at the top and the bottoms of the circulations mixture between clouds and the surrounding air occurs. No cloud water is produced; condensate falls out immediately as rain or snow. The amount of convection is related to the destabilization rate of the environment by a closure scheme. Therein quasi-equilibrium between destabilization by the large scale environment and stabilization by convection is assumed.

Land Surface Scheme

Land surface schemes represent effects of land and water surfaces. Mesoscale structures within the planetary boundary layer are strongly influenced by topography, soil moisture and vegetation. Soil has the property as a memory of past climate conditions. Thus, the implementation of a sophisticated Land Surface Model (LSM) is a central precondition for a regional meteorological model to be used for climate purposes. Since the introduction of the Oregon State University Land Surface Model (OSU-LSM) into MM5 in version 3 it can be operated as a regional climate model. The OSU-LSM is a fully developed 1-dimensional SVAT (Soil Vegetation Atmosphere Transfer) Model. It uses 4 soil layers with a thickness of 10, 30, 60 and 100 cm, respectively from the ground surface to the bottom. The total soil depth is 2 m, with the root zone located in the upper 1 m of soil. The lower 1 m of soil acts like a reservoir with gravity drainage at the bottom. The depths of the different plant roots can be specified as a function of vegetation type. Soil temperature is derived solving the diffusion equation, including heat capacity and thermal conductivity as a function of soil moisture. Soil temperature at the lower boundary is defined as the annual mean and assumed to be found at 3 m. Hydraulic conductivity and diffusivity are functions of soil moisture. Maximum soil moisture and soil temperature both depend heavily on soil texture. Interception, evaporation from soil surface, direct runoff, interflow, and vertical, gravitational soil water fluxes are considered.

V.2 WaSiM

V.2.1 Setup

Meteorological Data Input

Hydrological simulations with the approaches described in chapter IV.4 need as driving meteorological input time series of different variables. The used variables and their interpolation approach are described in the following:

- Precipitation [mm]: height dependent regression (50%) + IDW (50%)
- Air temperature [mm]: height dependent regression (70%) + IDW (30%)
- Wind speed [m/s]: IDW
- Relative humidity [1/1]: IDW
- Global radiation [W_{24h}/m^2]: IDW

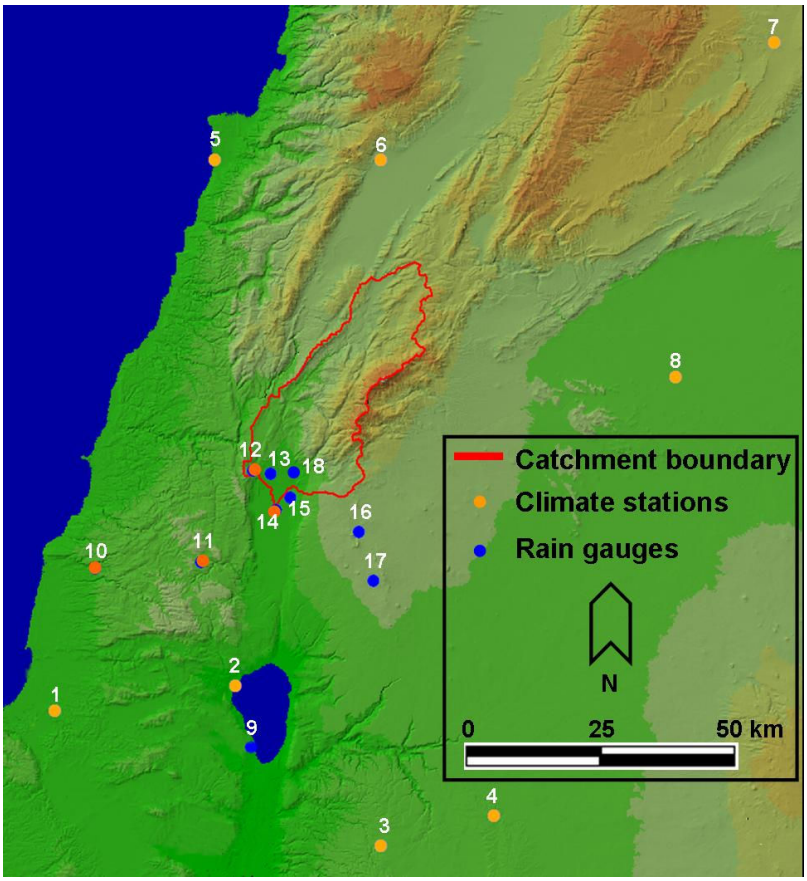

Figure V-4: Climate stations overview

For hydrological simulations of the UJC the climate stations and precipitation gages listed in Table V-1 and shown in Figure V-4 are used. The available station data are from different sources. Some of them are obtained from the NCDC (National Climate Data Center) of NOAA (National Oceanic and Atmospheric Administration), others are provided by the KLL (Kinneret Limnological Laboratory). It can be seen that only three precipitation stations, one temperature station, but no climate station with all variables are directly within the UJC available. Therefore, information has to be taken from outside of the research area and interpolated over it. In some cases, especially for climate stations, distances to the UJC are quite large (see Figure V-4).

All stations are in daily resolution, therefore 24h has been chosen as time step for the hydrological model.

Table V-1: Meteorological stations

Number	Station	Source	Height [m asl]	Precipitation	Temperature	Wind speed	Relative Humidity	Global radiation
1	Haifa	NCDC	8		X	X	X	
2	Ginosar	KLL	-170	X	X	X	X	X
3	Irbit	NCDC	619		X	X	X	
4	Daraa	NCDC	543		X	X	X	
5	Beirut	NCDC	19		X	X	X	
6	Houche al Oumara	NCDC	920		X	X	X	
7	Nabk	NCDC	1333		X	X	X	
8	Damascus	NCDC	605		X	X	X	
9	Kineret	KLL	-170	X				
10	Eilon	KLL	300	X	X			
11	Yiron	KLL	690	X	X			
12	Kefar Giladi	KLL	340	X	X			
13	Mayan Barukh	KLL	240	X				
14	Kefar Blum	KLL	75	X	X			
15	Kefar Szold	KLL	170	X				
16	Golan Exp Station	KLL	940	X				
17	Allone Bashan	KLL	960	X				
18	Dan	KLL	?	X				

Discharge Data

River discharge data give good integrated information of the corresponding basins and are therefore the most applied data for calibration of a hydrological model. Thus, in this study calibration is based mainly on the comparison of observed and simulated discharge. For the simulation of the UJC six discharge gauges that are described in II.2.2 are available.

Since measured data are always a source of uncertainties, the discharge data have to be checked before they can be used for calibration purposes.

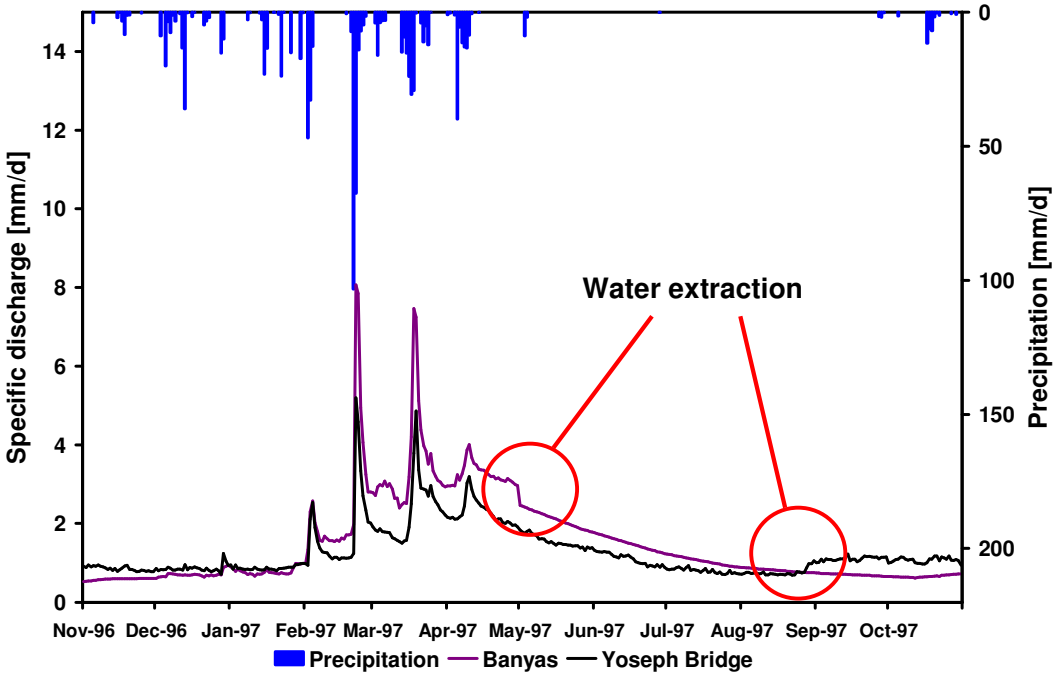

Figure V-5: Rainfall and discharge at the gauges Banyas and Yoseph Bridge for the hydrological year 1997

When looking at the hydrographs of the available gauges, Banyas and Yoseph Bridge show conspicuous characteristics. While the hydrograph of Yoseph Bridge increases already before the beginning of the rainy season, the hydrograph of the Banyas decreases abruptly at the beginning of the summer as it can be seen in Figure V-5 showing precipitation and discharge of the Banyas and the Jordan at Yoseph Bridge for the hydrological year 1997. In both cases this is due to water consumption. Measuring errors can be excluded since the same or similar phenomena of the annual cycle exist also in other hydrological years. Unfortunately, the amount of the consumption is unknown. This has to be considered when estimating the model performance using the measured discharge at these gauges, especially for the dry summer season where consumption is assumed to be at maximum.

Geographical Data

The distributed hydrological model needs a number of spatial information. The most important data for WaSiM are the Digital Elevation Model (DEM), landuse and soil

properties information. Spatial data are handled within the model in grid format. Appropriately to the temporal resolution of 24h a spatial resolution of 450 m was chosen. Both, temporal and spatial resolution must have a corresponding resolution to avoid numerical inaccuracies, e.g. when water movements cross more than one grid cell during one time step.

DEM

The DEM is needed at different parts of the model. On the one hand it is used directly, e.g. for the interpolation of meteorological data with a height dependent regression or in the groundwater model. On the other hand it is the input for the preprocessing tool TANALYS, where a number of further spatial input data are deduced from the DEM.

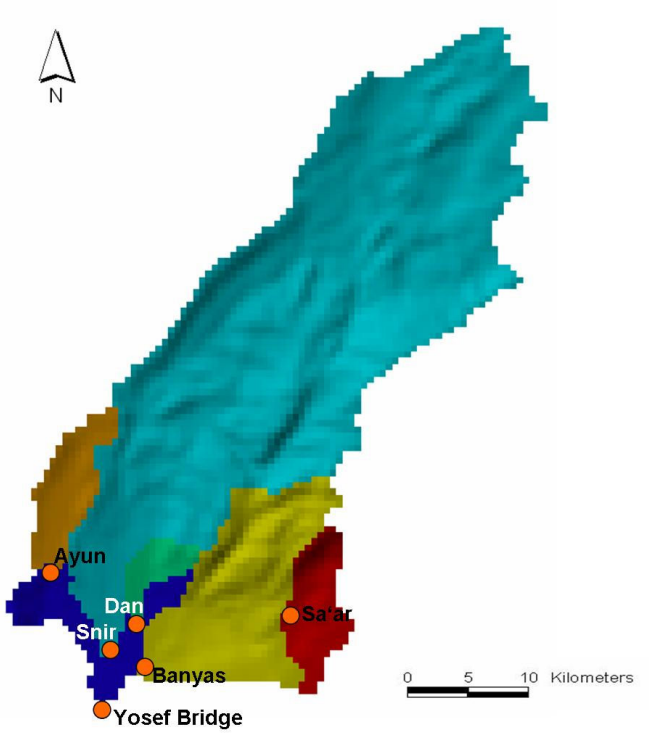

Figure V-6: Subbasins of the UJC and the corresponding gauges derived by TANALS

The DEM used for the UJC is derived from the SRTM (Shuttle Radar Topography Mission, www2.jpl.nasa.gov/srtm), where in 2000 the earth was scanned on near global scale from 56°S – 60°N in order to obtain a high-resolution digital elevation database (FARR et al., 2007). The data are freely available and have a spatial resolution of 90 m. To derive the resolution of 450 m the SRTM data are averaged by arithmetic mean.

Together with additional information of location of the gauges (described in II.2.2 and shown in Figure II-5) and the mean discharge, the DEM is used in TANALYS. The derived data are i.e. the subbasins according to the gauges (Figure V-6) or the river network (Figure 0-1 in the Appendix), and the flow time grid of the routing model (Figure 0-2 in the Appendix).

Soil Texture

WaSiM needs spatial information on soil types. From the literature (SCHEFFER and SCHACHTSCHABEL, 1998 and BAUMGARTNER and LIEBSCHER, 1990) the dominating soil types are chosen for each soil type. Two sources of soil maps are available: For the Israeli part of the UJC the soil map of Israel (DAN et al., 1977) is available in a resolution of 1:500.000. For the rest of the area the digital soils map of the FAO (Digital Soil Map of the World and Derived Soil Properties, CD-ROM, Version 3.5, 1996) with a very coarse resolution of 1: 5.000.000 has to be taken.

In Table 0-1 the different soil types and the assigned soil textures can be seen, while Figure 0-3 shows the derived map of the soil textures for the UJC (in the Appendix).

Land Use

As for the soil textures, two sources have to be applied for the land use information. For the Israeli part land use data are derived from the KLL, while for the rest of the area MODIS data are used. These are remote sensing data, which are recorded by the instrument MODIS (Moderate Resolution Imaging Spectroradiometer). It is located at the satellite TERRA (EOS AM-1) and is composed of a 36-channel spectrometer with a resolution of 250 – 1000 m (depending on spectral range). Since the deduced land use classes of MODIS as well as those from Israel do not do not concur completely with those used in WaSiM, assignments have to be made (Table 0-2). The resulting land use map for the UJC can be seen in Figure 0-4 (in the Appendix).

Groundwater Data

For the use of the groundwater model a number of spatial distributed parameters are needed. These are amongst others:

- Aquifer thickness (aq) [m]
- Saturated horizontal conductivity in x-direction (k_x) [m/s]

- Saturated horizontal conductivity in y-direction (k_y) [m/s]
- Constant head boundary (bh) [m a.s.l.]
- Boundary fluxes (bq) [m/s]

Within the groundwater model the consideration of boundary conditions is implemented. These are on the one hand hydraulic heads describing the upper boundaries of the groundwater, on the other hand lateral fluxes at the catchment's boundaries describing the lateral boundaries.

Within this model setup hydraulic heads are set at locations where it is known that the groundwater table shows little fluctuations and is almost stable all over the year. This is the case in the study area for the springs. Therefore, hydraulic heads are set for all springs within the UJC. The height of the hydraulic heads is assumed to match the ground level and is derived from the DEM at the corresponding locations. The location of the springs is derived from GUR et al. (2003) and can be seen in Figure V-7.

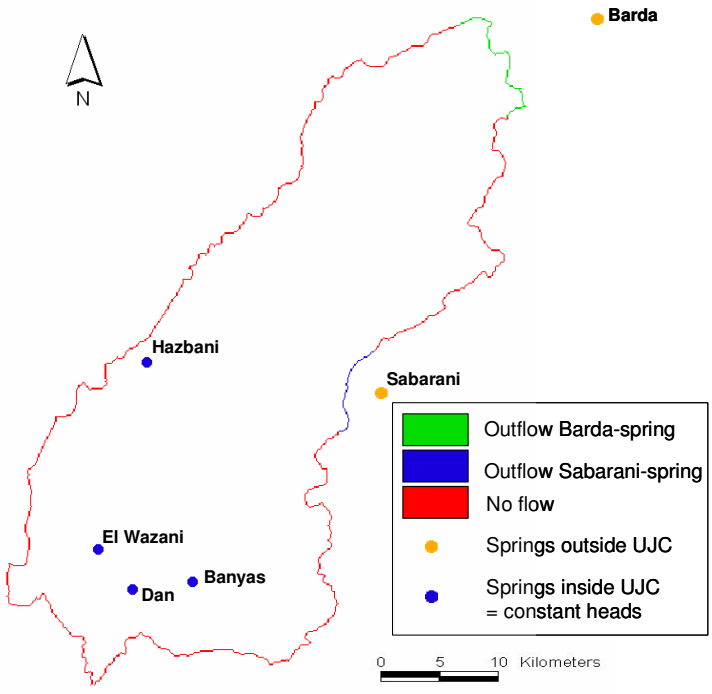

Figure V-7: Boundary conditions for the groundwater model

Other boundary conditions can be set at the lateral boundaries of the catchment. Both, inflows and outflows can be considered. They are described for every considered boundary grid point in m/s vertical to the grid point surface as a constant value, whereas inflow has a positive sign, outflows a negative one.

For the study area no concrete data about in- and outflows are available. Nevertheless, it is known that the regional Jurassic aquifer extends the surface catchment of the Upper Jordan. Therefore there is a loss of groundwater within the study area. Easterly and north-easterly of the UJC there are two springs resided, which are located at the boarders of the exposed Jurassic layers of the Mount Hermon and thus still belong to the Jurassic aquifer. Due to their location at the dry eastern slope of the Hermon, large parts of their delivery arises in the western parts and hence in the UJC. From GUR et al. (2003) and RIMMER and SALINGER (2006) the location and the average annual delivery of the springs are derived. From this information the lateral outflows for the groundwater model is calculated. Since no information on annual fluctuations of the spring discharge can be found in the literature, constant values are chosen. For the outflow to the east to the Sabarani-spring, which has a delivery of about 25 – 50 x 10^6 m^3/a, 15 grid points get an outflow of -1.7 x 10^{-7} m/s. The northeastern outflow to the Barda-spring, which discharges about 50 – 100 x 10^6 m^3/a, is considered by setting an outflow of -1.7 x10^{-7} m/s at 30 grid points (see Figure V-7).

Like described in II.2.2, the study area has an extended regional aquifer with a depth of several hundred meters. It is built within the Jurassic carbonate rocks and has therefore a karstic character.

The main characteristics of an aquifer are described by its storage capacity and its conductivity (DYCK and PESCHCKE, 1995). Just in these properties a karstic aquifer differs from a porous one explicitly. While porous aquifers are characterized by slow and homogenous flow, fissured and karstic aquifers show fast movements in the underground. Fissured aquifers have accelerated fluxes through so called preferential flow paths, whereas the flow velocities in karstic aquifers through caves and conduits can reach order of magnitudes like surface rivers.

Since the groundwater model of WaSiM is designed for porous aquifers, the mentioned parameters like aq, k_x and k_y have to be interpreted as effective parameters approximating the karstic environment. The groundwater model is not able to simulate the varying and higher flow rates of the karst conduits, but it is possible to reproduce the continuous flow rates of the fissured rock matrix.

To compensate the higher flow velocities of the matrix flow in comparison to porous material, the aquifer thickness is set to a strong reduced extension of 20 m using 40 layers of 50 cm thickness for solving the discretized Richard's equation.

Implementation of Bypass

For the most parts the setup described so far corresponds to the setup of the preceding diploma thesis (see chapter III.5.2). A difference appears in the usage of the groundwater model: While in the diploma thesis it was tried to describe the karst properties including fast and low flow, in this setup it is restricted to the simulation of the slow matrix flow.

However, accompanied with the modified application of the groundwater model with the implementation of a bypass, a completely new approach is installed.

The background for this approach is shortly explained in the following:

The extension of the aquifer feeding the Dan spring is much bigger than its surface catchment size. In contrast, the Snir River is mainly fed by the relatively small springs El Wazani and Hazbani, which emerge within the quite small-area Cenomanian-Turonian aquifer and have only little inflow from the big Jurassic aquifer (see II.2.2). With over 600 km² the Snir subbasin has the biggest part of the UJC and it is mainly built by the exposed Jurassic carbonate rocks forming the recharge area for the extensive karstic aquifer. Therefore, the source of the Dan spring's discharge is located mainly within the surface catchment of the Snir.

Hence, with a conventional approach of the hydrological model WaSiM on the one hand the discharge of the Snir is overestimated (see Figure V-9). On the other hand the Dan spring's discharge is underrated by far. Moreover, the trend of the hydrograph cannot be captured at all. Observations of the Dan spring show a maximum of discharge in May, three month after the rainiest months January and February. Afterwards, the discharge diminishes until January. The delay of the discharge to the rainfall indicates the good development and large extension of the karstic aquifer feeding the Dan spring. In contrast, the simulated discharge reacts on the rainfall amounts with maximum in the rainy winter season (see Figure V-10).

As mentioned before, the 2d-groundwater model is not able to deliver the magnitude and the dynamic of baseflow at the Dan generated at main parts of the Snir's surface catchment. The transport of the other discharge components interflow and surface runoff from one subbasin to another is not possible, as they are simulated subbasin-wise. The only alternative for the transport of water from the Snir to the Dan basin beside the

groundwater flow is the definition of an artificial bypass within the routing model. The situation is illustrated in Figure V-8: The arrows represent the water fluxes and their thickness the amount of transported water. While the amount of baseflow is small, the arrows of the surface runoff and the interflow are thicker, but they are interrupted pointing up that no transport between subbasins is considered. Only the method of a bypass in the routing model allows for overcrossing of bigger water amounts into another subbasin.

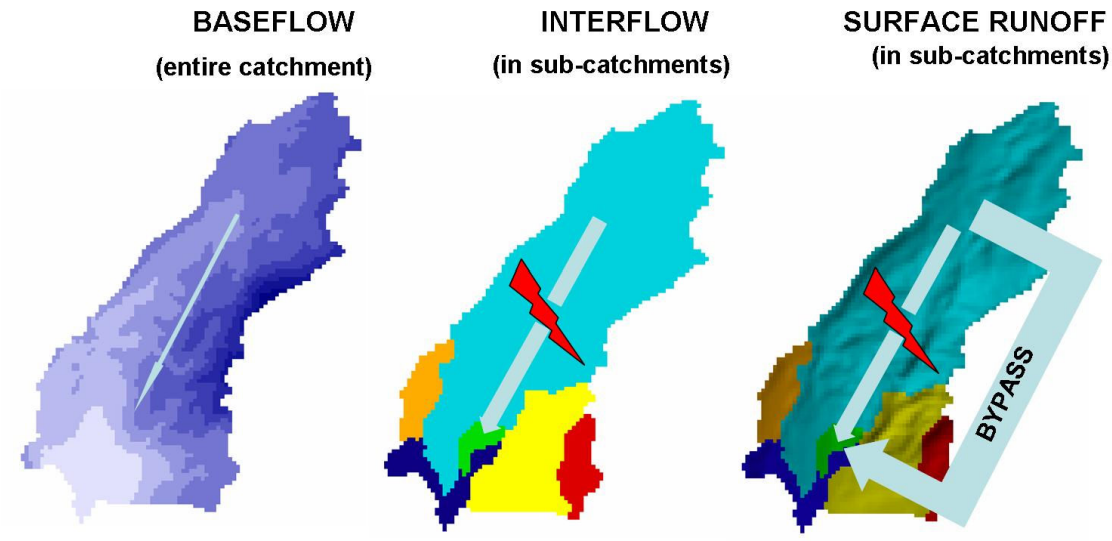

Figure V-8: Water fluxes of the discharge components and the implemented bypass

The bypassed water consists of river discharge composed of surface runoff, interflow and baseflow, while the discharge of the Dan spring mainly consists of baseflow. In this case the use of the bypass within the routing model is necessary, since it does not represent typical groundwater flow, but a karstic aquifer. Water from a karstic aquifer differs from baseflow of a porous aquifer in the time needed for infiltration and percolation. The fast components of karstic behavior can be represented by the surface runoff and the interflow built within the Snir basin. Moreover, by calibrating the routing parameters of the bypass (see chapter V.2.2) the delayed discharge at the spring after the rainy season can be reproduced. Therefore, the bypassed water to the Dan out of the routed discharge represents more real conditions than the baseflow by itself could do.

In this way, the biggest challenge in modeling groundwater flow in karst aquifers, the duality of its discharge behavior, i.e. rapid response of highly conductive karst conduits

and delayed drainage of the low-permeability fractured matrix after recharge events (SAUTER et al., 2006) can be met.

V.2.2 Calibration

Calibration Period

The calibration period for a hydrological model should be chosen in a way that all typical meteorological and hydrological phenomena (wet and dry season, high and low water periods, as well as accumulation and depletion of the snow layer) are considered. Only in this way it can be responded to these phenomena during calibration, and transferability to other simulation periods is enabled. Unfortunately, in most cases longer calibration periods are hampered by a lack of data availability. In this study especially meteorological data input is limited. Although discharge data are available for 1970 – 2001 for most of the stations, only the hydrological years 1996 – 1999 can be used for simulations with the full set of climate input data. Therefore, the hydrological year 1997 serves as calibration period, while 1996 is used as spin up for the groundwater table and other storages like e.g. soil moisture and snow layer. For validation the hydrological years 1998 and 1999 are used, while the period 1996 - 1997 in turn is applied as spin up time.

Parameter Estimation Technique

Hydrological models are getting more and more complex and often the number of parameters rises. Therefore, also the calibration of these models is getting more extensive. In general it cannot be assumed that there exists one perfect parameter set that can be determined by a calibration of a hydrological model. This can only happen theoretically if a model and data input are assumed to be perfect (BASTIDAS et al., 2002). In reality always a number of 'best-fit' parameter sets may exist that produce similar results. This phenomenon is called 'equifinality' (BEVEN, 1989). A general overview of the parameter estimation problem is given in SINGH and FREVERT (2002).

In general two different approaches for parameter estimation can be distinguished. These are on the one hand automatic calibration techniques on the other hand the trial-and-error method.

With automatic calibration techniques the process of parameter estimation can be automated and optimized. For hydrological models a number of different methods have

been applied. Some examples are the Generalized Likelihood Uncertainty Estimation (GLUE), the Marcov Chain Monte Carlo method (MCMC), the Bayesian Recursive Estimation (BaRE) or the Shuffled Complex Evolution algorithm (SCE-U). The Parameter Estimation Tool PEST, which uses a gradient based nonlinear parameter estimation algorithm after Gauss-Marquardt-Levenberg, has been applied for parameter estimation of WaSiM by KUNSTMANN et al. (2005).

The trial-and-error approach describes all methods, where parameters are manipulated manually and subsequently the results of the model simulations are compared to observations. The comparison can be done directly or under consideration of defined performance criteria. This process is executed iteratively untill a satisfying optimized parameterization is found.

In this study the trial-and-error method is used for parameter estimation. On the one hand this method is more time demanding than an automatic calibration technique. On the other hand it seems more promising since observation data for discharge are of limited applicability for use in an automated calibration method as described in V.2.1. An automatic calibration would try to fit the simulated discharge to the observed one which would cause underestimation of runoff generation in periods, where the hydrograph is biased by consumption. Since the quantity of consumption is unknown, no optimal parameter set can be found with these methods.

Performance Criteria

For the mathematical quantification of model performance based on observations a number of different criteria are introduced for hydrological modeling. A comparison of several of these efficiency criteria is given e.g. by KRAUSE ET AL. (2005). One of the most used performance criterion in hydrological modeling is the Nash Sutcliffe Efficiency (NSE), which is also used in this study. The NSE is defined as

$$NSE = 1 - \frac{\sum_i \left(Q_{sim,i} - Q_{obs,i}\right)^2}{\sum_i \left(Q_{obs,i} - \overline{Q_{obs,i}}\right)^2} \qquad \text{V-1}$$

with: i time step

Q_{sim} simulated discharge [mm or m³/s]

Q_{obs} observed discharge [mm or m³/s]

The range of NSE values is [-∞…1], while performance is best the closer NSE approximates to 1. When applying NSE it is assumed that the values are normal distributed. However, usually runoff data do not fulfill this theoretical requirement. Therefore, flood peaks in the hydrograph are overestimated. To overcome this gap the NSE is additionally calculated with the logarithm of the runoff values (further referred to as NSE_{log} in contrast to NSE_{lin}). The logarithm approximates the runoff data more to a Gaussian distribution and therefore the entire flow spectrum of discharge and also low flows are considered.

Additionally the coefficient of determination R^2 is calculated.

Another performance criterion for the hydrological simulations can be how good the water balance equation adds up. Main components of the water balance are precipitation (*P*), evapotranspiration (*ET*) and discharge (*Q*) resulting in a general water balance equation:

$$P = ET + Q + \Delta S, \qquad \text{V-2}$$

where ΔS respects change in storage within soil or bedrocks. In long terms of many years this component should be minimized. Therefore this criterion is only used for the analysis of long term simulations (see chapter VI.5)

Calibrated Parameters

In the hydrological model WaSiM those parameters have to be calibrated which have a wide range of possible values, which are difficult to measure, or which describe predominantly empirical processes (SCHULLA, 1997).

The following parameters of different parts of the model are calibrated:

Table V-2: Calibrated parameters of WaSiM

Groundwater model:	
k_x	saturated lateral hydraulic conductivity in x-direction
k_y	saturated lateral hydraulic conductivity in y-direction
Soil model:	
k_d	recession constant for direct runoff
k_i	recession constant for interflow
d_r	drainage density [m^{-1}]
k_{rec}	recession constant for hydraulic conductivity with depth [-]
Snow model:	
$T_{r/s}$	temperature, at which 50% of precipitation are falling as snow [°C]
T_{trans}	½ of the temperature –transition range from snow to rain [K]
T_0	threshold temperature for beginning with snow melt [°C]
c_1	temperature dependent melt factor [mm*(°C*d)$^{-1}$]
c_2	wind dependent melt factor [mm*(°C*m/s*d)$^{-1}$]
Routing Model:	
Q_{min}	Minimal discharge for starting bypass [mm/t]
Q_{max}	Maximal bypassed discharge [mm/t]
BP_{rel}	Amount of bypassed water [%]
L	Length of the routing channel [m]
AE	basin area [km²]
k	storage coefficient for the single linear reservoir considering retention in a channel

Groundwater Model

Within the groundwater model only the parameters k_x and k_y are calibrated. The 2-dimensional lateral groundwater flow between two grid points linearly depends on these two parameters. By calibration of these parameters the dry discharge within the summer season, which is mainly composed of baseflow, can be fitted. Therefore, as performance criteria not only the NSE (especially the NSE_{log}) is accounted for, but also the visual checking of the discharge in the dry season. As a constraint again the consumption in the gauges of the Banias and the Yoseph Bridge have to be considered.

By dividing the saturated lateral conductivities in two directions x and y, the consideration of anisotropies is included. Since no information about potential anisotropies within the aquifer is available, it is assumed that behavior of lateral conductivities is homogenous ($k_x = k_y$).

Saturated conductivities show in reality a wide range of values. Even by determining the conductivities of soil samples within the micro scale in laboratories, in the literature different values for the same soil type can be found. In addition in the described approach (see chapter V.2.1), the groundwater model does not represent porous media, but the fissured rock matrix of a karst system. Due to this approach and the missing measurements of physical subsurface properties, the calibration of the parameters k_x and k_y is not done on the basis of the soil types, but on the basis of each subbasin. Calibration of these parameters for the subbasins of Dan and Snir is done in combination with the parameters of the bypass in the routing model.

Soil Model

The parameters of the soil model k_d, k_i and d_r are calibrated for each subbasin. Only the parameter k_{rec} depends on soil types. With this parameter the decrease of the saturated hydraulic conductivity with depth can be described after.

$$k_{s,z} = k_s \cdot k_{rec}{}^{z} \qquad \text{(V-3)}$$

with $k_{s,z}$ saturated hydraulic conductivity within depth z [m/s]
k_s saturated hydraulic conductivity at the soil surface [m/s]
k_{rec} recession constant [-]
z depth [m]

Because of its dependence on the soil type, k_{rec} can only be calibrated unsatisfactorily: Since the spatial distribution of subbasins and soil types differ, a value of k_{rec} for one soil type can have melioration in the result of one subbasin, while within another subbasin an aggravation of the simulations is evoked. Therefore, the calibration of k_{rec} has always to be a compromise.

In case of k_{rec} is <1, interflow is generated. The strength of the interflow depends on the parameter drainage density d_r. It describes the river density within a grid cell as well as the difference between the horizontal and the vertical hydraulic conductivity. It is an effective parameter which linearly affects the amount of interflow after:

$$q_{ifl} = k_s(\Theta_m) \cdot \Delta z \cdot d_r \cdot \tan\beta \qquad \text{(V-4)}$$

with k_s saturated hydraulic conductivity [m/s]
Θ_m water content in the actual soil layer m [-]

d_r scaling parameter used to consider river density as well as effects like a anisotropy of $k_{s,horizontal}$ to $k_{s,vertical}$ [m^{-1}]

β local slope angle

Further calibrated parameters of the soil model are k_d and k_i. These are the recession constants of the single linear storage for surface runoff (k_d) and interflow (k_i).

Within this single linear storage the runoff component Q_i at time i is calculated by the runoff component Q_{i-1} at time $i-1$, the time step Δt and the recession constant k.

$$Q_i = Q_{i-1} \cdot e^{-\frac{\Delta t}{k}} \qquad \text{(V-5)}$$

with Q_i runoff component at time i [mm]

Q_{i-1} runoff component at time i-1 [mm]

Δt time step [h]

k recession constant [h]

Snow Model

Although the investigated area is located in the south-eastern parts of the Mediterranean and hot desserts are only a few hundreds of kilometers away, snow in the higher regions plays an important role for the discharge of the UJC (see II.2.2). Therefore also the snow model has to be implemented and calibrated. The parameters of the snow model are divided into two parts. The first part is responsible for snow accumulation. These parameters are $T_{r/s}$ and T_{trans}. The other part of parameters, T_0, c_1, and c_2 affect the snow melt. The parameters of the snow model are related to the entire UJC and are not divided into the subcatchments. Only the subbasins of the Banias, the Snir and the Sa'ar are affected by snowfall. For the calibration of the snow accumulation and the snowmelt as performance criteria not only the NSE and the hydrographs are used, but also the temporal development of the snow storage within the respective subbasins is considered.

Routing Model

Within the routing description the abstraction of discharge of the Snir is parameterized by three parameters: A minimum value of discharge for the start of the abstraction (Q_{min}), the percentage of the abstracted water (BP_{rel}) and the maximum value of abstracted water (Q_{max}).

The minimum value Q_{min} is set to 0, as the abstraction should work at any amount of discharge. The maximum value Q_{max} is set bigger than the maximum simulated discharge of the Snir to enable that always the same percentage of the discharged water is led into the abstraction. The percentage of the abstracted water is calibrated with the goal that with the implemented bypass both tributaries simulate the right magnitude of discharge during the calibration period. At least this parameter is set to 75%.

In Figure V-9 a comparison of simulated discharge with and without implementation of the bypass to observed discharge is shown for the Snir. The simulation without bypass overestimates as well the peak flows as the discharge during the dry period. In contrast, with the implemented bypass the model is able to fit both, peak flows and low flow periods.

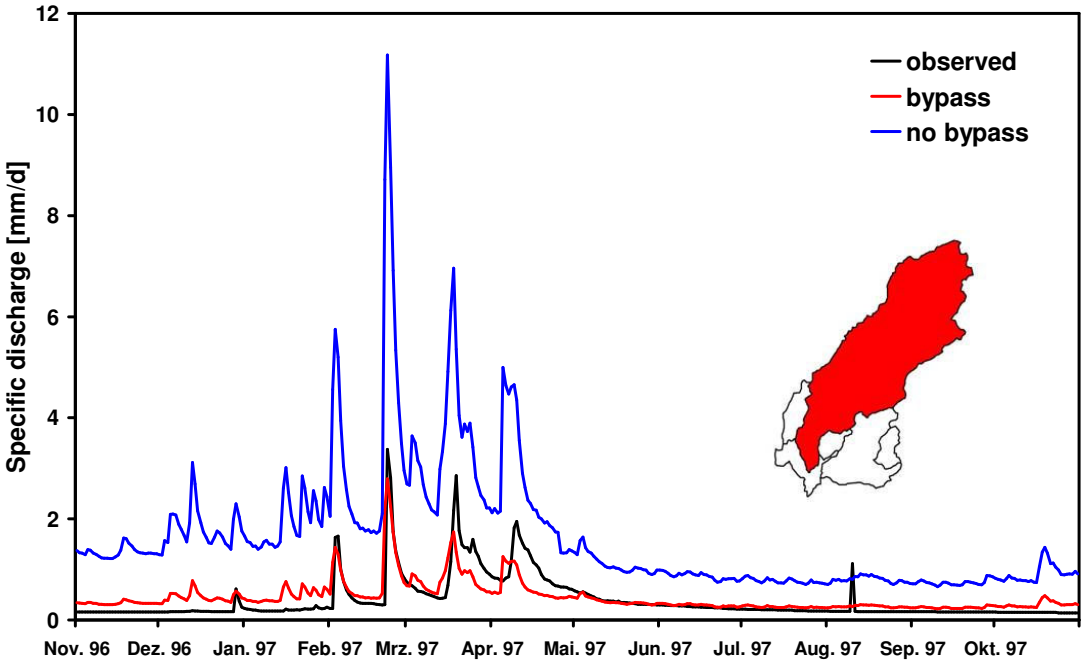

Figure V-9: Simulation results for the Snir with and without bypass in comparison to observed discharge

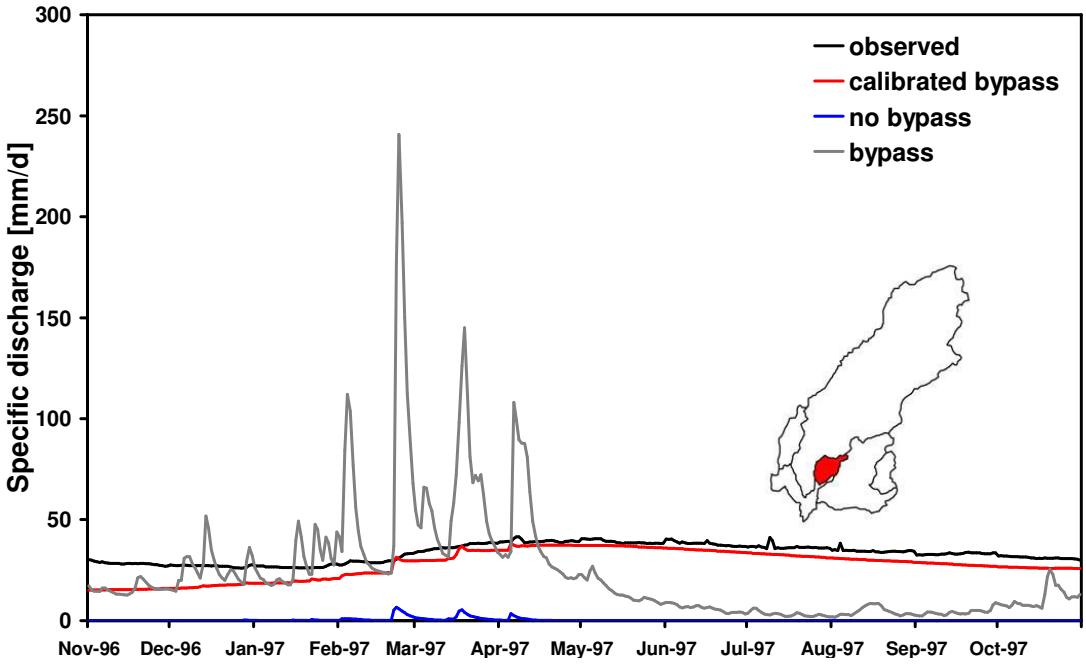

Figure V-10: Simulation results for Dan with and without bypass as well as with calibrated bypass in comparison with observed discharge

Figure V-10 illustrates the simulation results for the Dan. The simulation without bypass is done with a physically plausible parameterization for porous aquifers. In this case the massive underestimation of discharge stands out. With the implementation of the bypass the volume of discharged water during the simulated hydrological year is met, but the course of the hydrograph not at all. The applied routing parameters of the bypass are taken from the Snir basin.

Therefore, an additional calibration of the bypass has to be done. Calibrated parameters are:

- *L*: Length of the routing channel [m]
- *AE*: basin area [km²]
- *k* storage coefficient for the single linear reservoir considering retention in a channel

In this case these parameters do not represent a channel, but the characteristics of a karstic aquifer: length of flow paths through the fissures and channels, the spatial extension of the aquifer as well as its storage and retention capacities.

With the calibrated bypass parameters the Dan can be simulated in a more reasonable manner: The peaks of the hydrograph are cut and the long term retention to the rainy

period is met. The underestimation until March (Figure V-10) is due to the long spin up time needed for the large extension of the aquifer. The spin up of one hydrological year is not enough to turn into a realistic level.

Calibration Results

Calibration of the hydrological model and estimation of the obtained performance is mainly achieved by the comparison of simulated to observed discharge. For this purpose for each subcatchment the NSE in its linear and logarithmic form as well as the R^2 is computed. Additionally a visual analysis is done by examination of the discharges of the calibration period.

In Table V-3 the NSE values of all subbasins for the calibration period of the hydrological year 1997 are given. Figure V-11 to Figure V-17 show the corresponding simulated and observed hydrographs. For the gauge at Yoseph Bridge additionally two specifications of the routing module are considered. It is possible to run the routing module for each subbasin either with observed or with simulated discharge at the inlet of the subbasin's channel. For calibration reason it is better to use observed discharge (routing 2) in order to avoid error propagation. Since in this study the model should not only be calibrated to reproduce observations, but also has to be driven successfully with climate simulation data as input, its performance for the routing with simulated discharge (routing 1) has to be controlled as well. This is done only for the Jordan River at the gauge Yoseph Bridge, as it gains its discharge beside its own small basin from all other sub catchments and is representing the discharge of the entire UJC.

Table V-3: Nash Sutcliffe Efficiencies for the calibration period

gauge	Banyas	Dan	Saar	Snir	Ayun	**Yoseph Bridge** routing 2*)	**Yoseph Bridge** routing 1*)
NSE_{lin}	0.44	0.12	0.69	0.19	0.12	0.94	0.51
NSE_{log}	0.52	0.34	0.69	0.43	0.15	0.84	0.48
R^2	0.75	0.91	0.82	0.64	0.75	0.94	0.75

*) routing 2: with observed discharge; routing 1: with simulated discharge

The mainly high values of the NSE in Table V-3 attest to satisfying simulation results. The hydrographs show an overall good reproduction of the peaks as well as the dry discharge.

The start and the end of the discharge at the episodic running rivers Sa'ar (Figure V-13) and Ayun (Figure V-15) is well captured, but the peaks of the Sa'ar are underestimated.

While the peaks at the gauge Banyas (Figure V-11) are slightly overestimated, the curve of the simulated dry discharge is below the observed one despite the previous described water consumption. This appears due to the fact that the surface catchment of the Banias River is smaller than its subsurface catchment since it is also connected to the regional karstic aquifer like the Dan spring (II.2.2). Total amounts of discharged water are much smaller in comparison to the Dan, an additional implementation of a bypass like between the Snir and the Dan is renounced.

The discharge at the Dan is underestimated until March (Figure V-12), thereafter the level and the continuum is in good agreement with the observations. The underestimation is due to the long spin up time needed for simulating the retention of the karstic aquifer via the implemented bypass.

By comparing the simulated versus the observed discharge at the gauge Yoseph Bridge (Figure V-16) the consumption during summer is conspicuous. This affects also the NSE_{log} representing also the low flows, which is lower than the NSE_{lin} (Table V-3).

Figure V-17 shows the simulated discharge at the Yoseph Bridge based on routing with simulated discharge from the other basins. In comparison to the simulations with the routing method using observational data (Figure V-16) both hydrographs are in good agreement. This good result of the simulations without observed discharge as input for the routing model is an essential prerequisite for the use of the hydrological model with simulated climate data for future times.

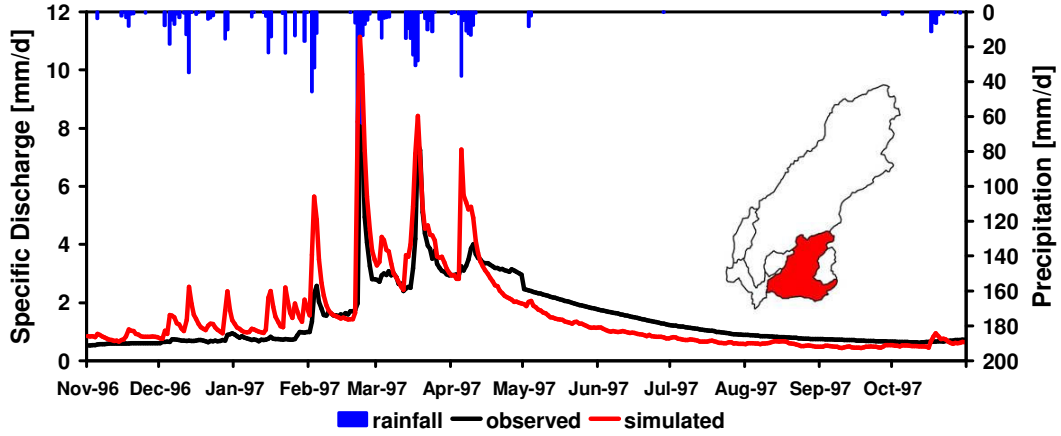

Figure V-11: Comparison of observed and simulated discharge at gauge Banyas and precipitation

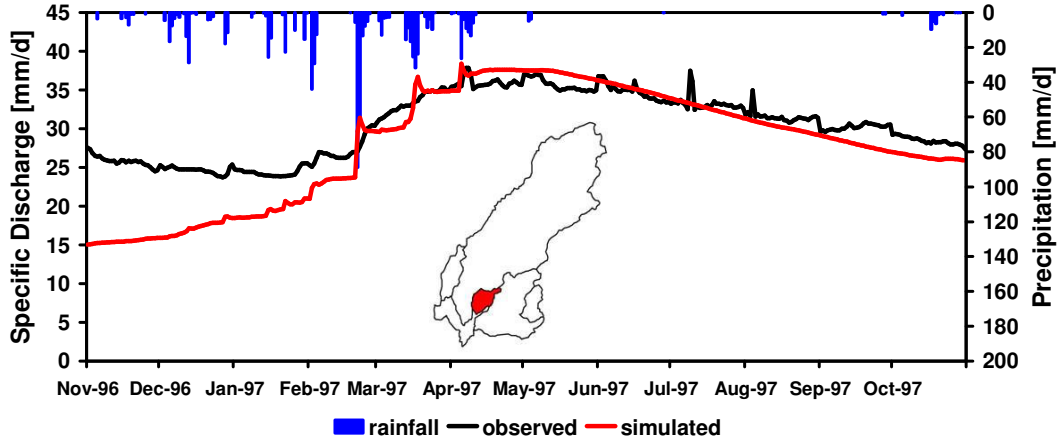

Figure V-12: Comparison of observed and simulated discharge at gauge Dan and precipitation

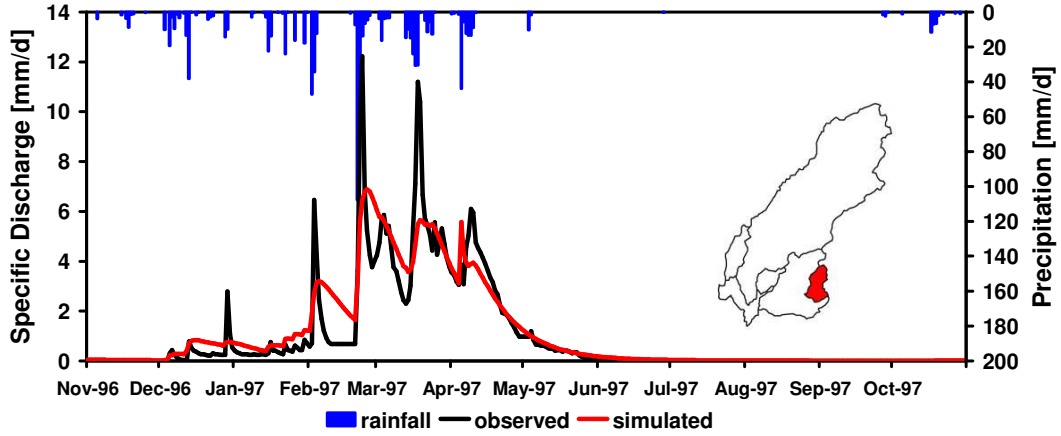

Figure V-13: Comparison of observed and simulated discharge at gauge Sa'ar and precipitation

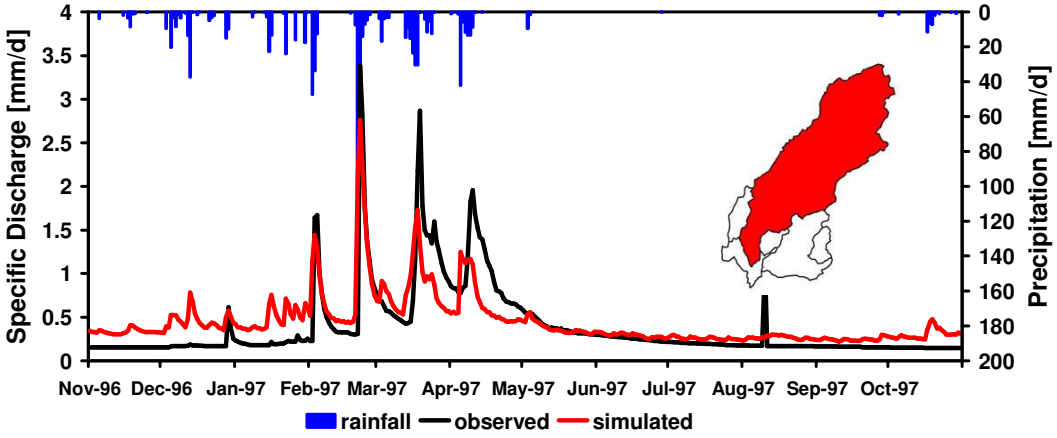

Figure V-14: Comparison of observed and simulated discharge at gauge Snir and precipitation

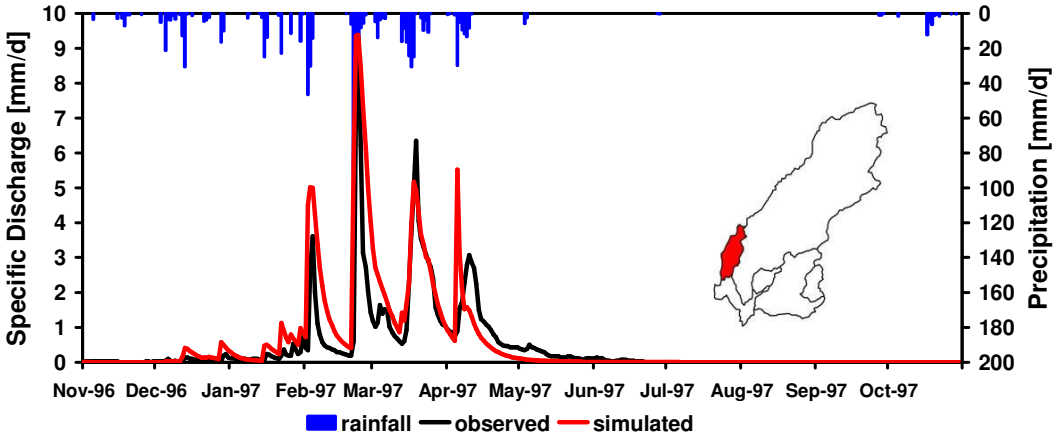

Figure V-15: Comparison of observed and simulated discharge at gauge Ayun and precipitation

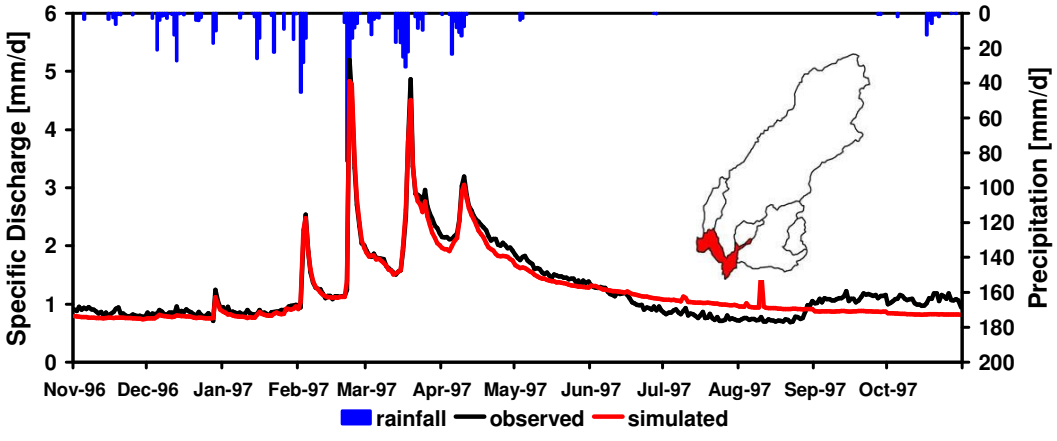

Figure V-16: Comparison of observed and simulated discharge of the Jordan River at gauge Yoseph Bridge (routing with observed discharge) and precipitation

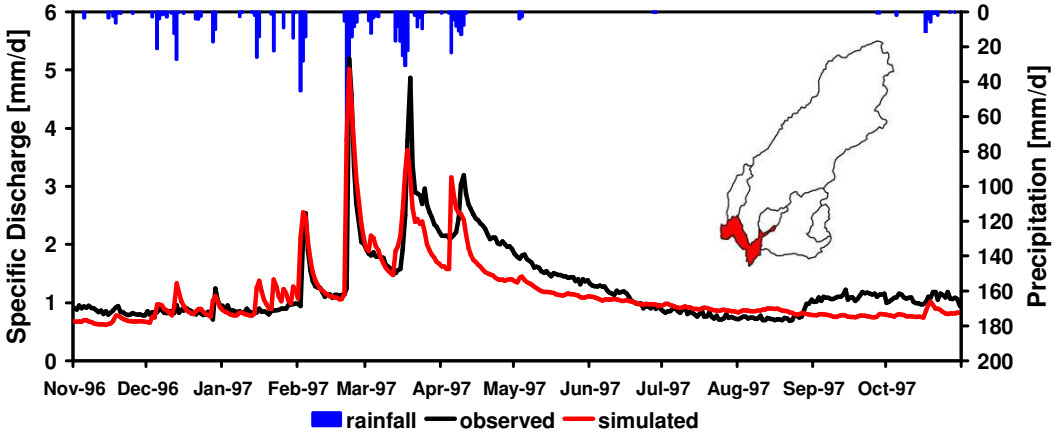

Figure V-17: Comparison of observed and simulated discharge of the Jordan River at gauge Yoseph Bridge (routing with simulated discharge) and precipitation

Besides the discharge as indicator for estimating the simulation performance other important components of the water balance have to be considered.

The temporal distributions of potential and real evapotranspiration for the hydrological year 1997 in dependence of the temperature are shown in Figure V-18 and Figure V-19, respectively. As it can be expected, rates of potential evapotranspiration are strongly depended on the available energy in the form of temperature with maximum in summer (Figure V-18). In contrast, real evapotranspiration rates do not follow the temperature graph. Maximum of real evaporation is during April and May when high temperatures are accompanied with high water availability. Evapotranspiration amounts decrease during the rainy period because of lower temperatures and in summer due to reduced water availability (Figure V-19). The hydrological model calculates for the hydrological year 1997 a potential evaporation of about 1200 mm, while the amount of real evapotranspiration is about 450 mm, which is > 50 % of the precipitation (880 mm) within that timeframe.

The available water amount for evapotranspiration depends also on soil moisture. The soil moisture averaged over the UJC is shown in Figure V-20. It is differed between the upper layers of the rooted zone and the entire unsaturated zone. Soil moisture in the upper rooted layers reacts fast on precipitation in the winter period and decreases strongly during the hot and dry summer. The unsaturated zone as a whole does not dry out as much as the rooted zone in summer, during the rainy period soil moisture increases with delay to rainfall events due to the percolation process.

Another important component of the water balance in the UJC is the snow storage. Since no data on snow amounts and snow depths are available it is a difficult factor for calibration. It is accounted for that snow accumulation and snow melt are in reasonable magnitude and development during a hydrological year. In Figure V-21 can be seen, that snow accumulation starts in January and snow melt ends in May. It is conspicuous that major accumulation events occur when high amounts of precipitation are accompanied with low temperatures. The temporal development seems to represent realistic conditions as similar information can be found in the literature (e.g. GILAD and BONNE, 1990).

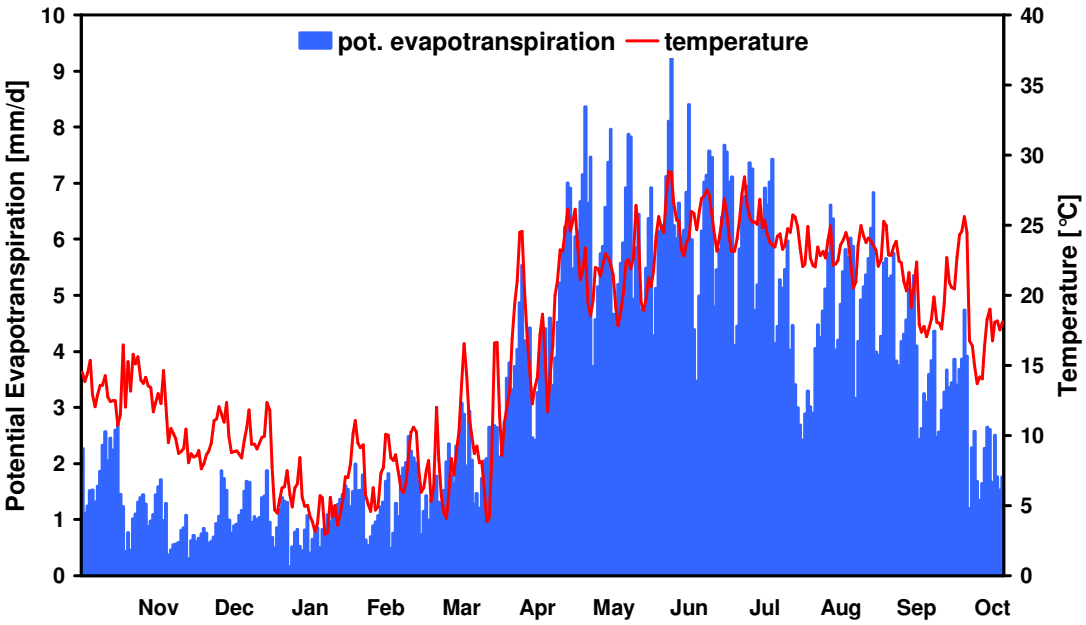

Figure V-18: Temporal distribution of the potential evapotranspiration in dependence of the temperature

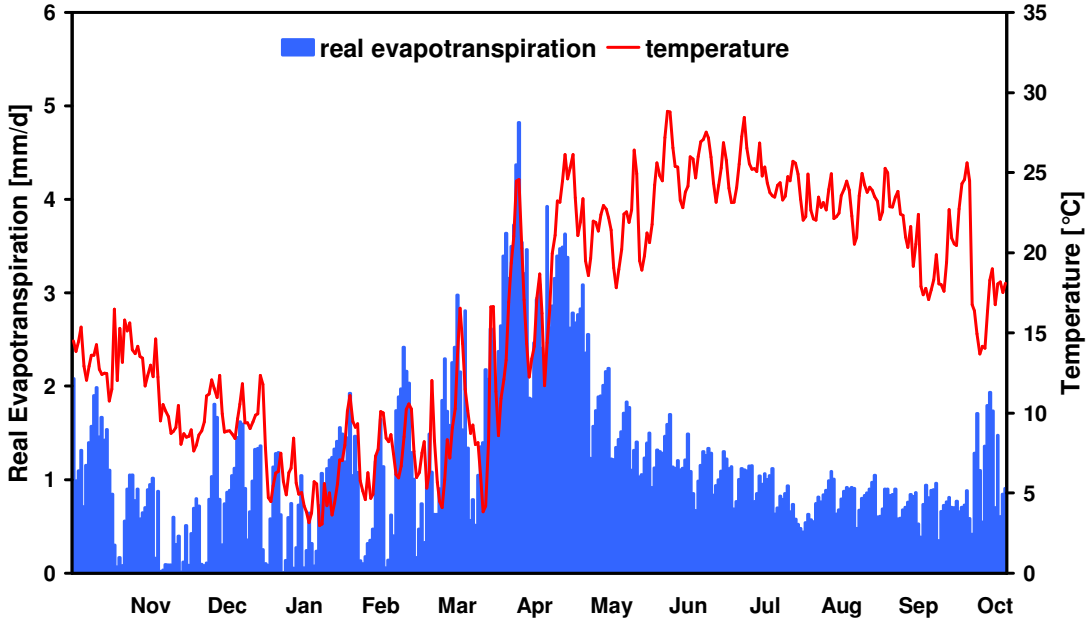

Figure V-19: Temporal distribution of the real evapotranspiration in dependence of the temperature

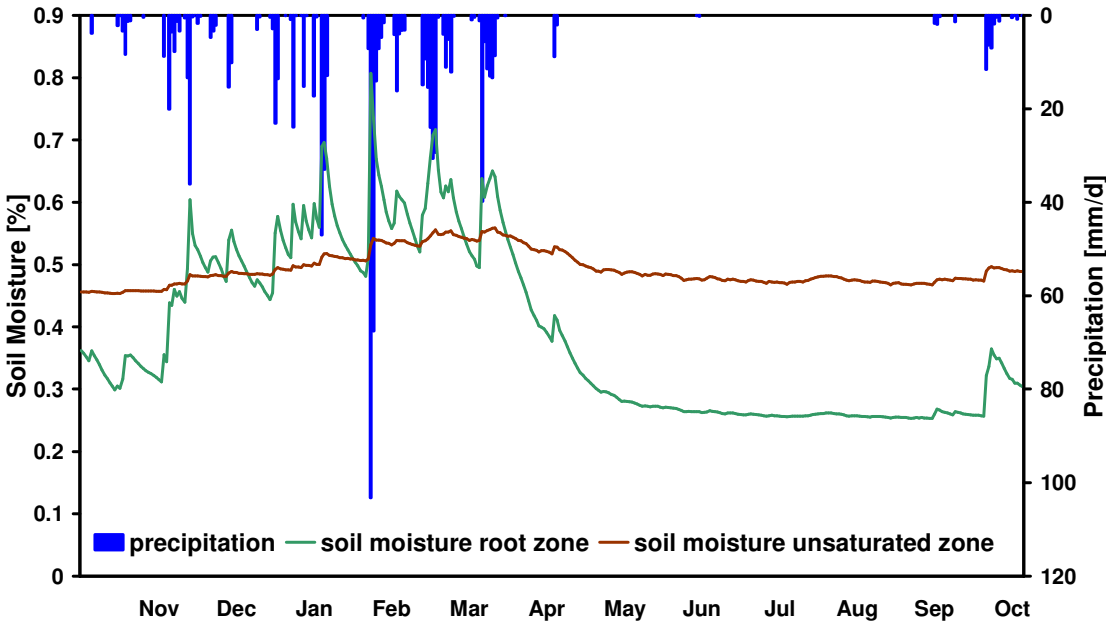

Figure V-20: Temporal distribution of the soil moisture in the root zone and the unsaturated zone

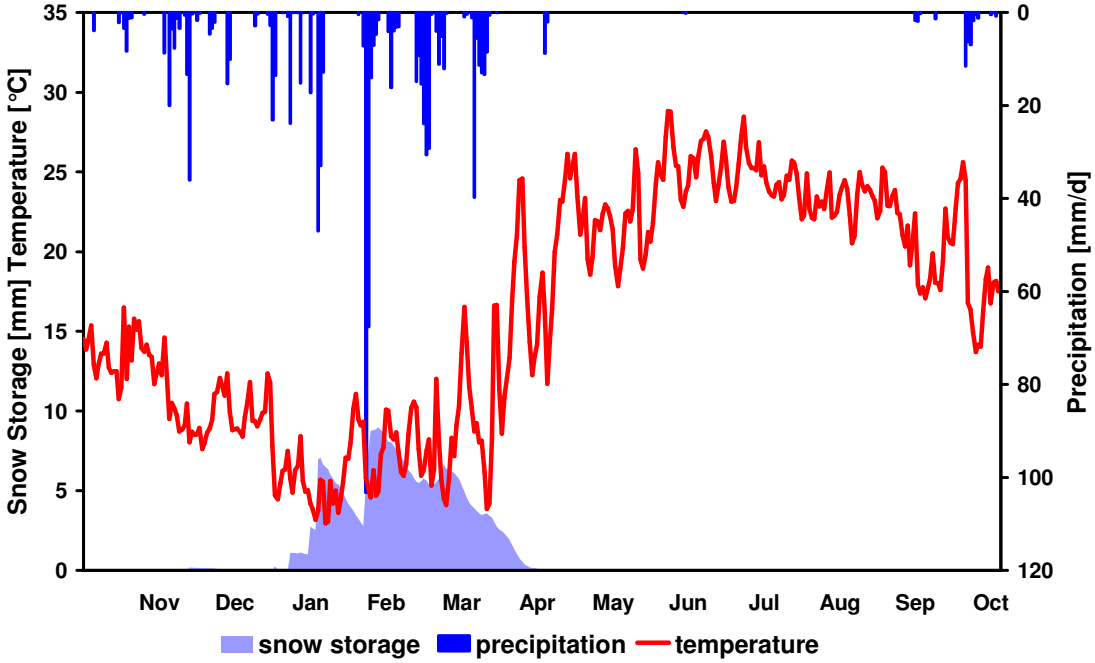

Figure V-21: Temporal distribution of the snow storage in dependence of the temperature and precipitation

V.2.3 Discussion of the Bypass-Approach

In general conceptions, a duality in the hydrodynamic is assigned to karst aquifers. Karst aquifers are composed of a porous or fissured matrix and a system of conduits. While the matrix represents the storage of the aquifer and has low permeability, the conduit system crucially contributes to the drainage of the system due to its high permeability and regional interconnections. However, the conduits contribute only little to the storage as their volumetric content to the karst aquifer is low (e.g. ATKINSON, 1977; FORD and WILLIAMS, 1989, or KIRLAY, 2002).

The modeling of the extreme heterogeneity and duality of the hydraulic parameters is a big challenge. Several approaches exist to reproduce the typical behavior of karst aquifers. An overview of these approaches is given in SAUTER et al. (2006). They mention that porous medium models like the implemented one in WaSiM are not able to reproduce the typical discharge behavior of a karst aquifer. In discrete fracture network models (like e.g. DERSHOWITZ et al., 2004) or hybrid models composed of continuum and discrete fracture network models (e.g. LIEDL et al., 2003), the structure of the karst aquifer is reconstructed in detail and therefore the hydraulic behavior can be reproduced quite well. However, these models have high requirements on field data which mostly

can not be provided. Less data requirement is needed for so called double-/ or multi-continuum models, where at the same time characteristics of porous matrix and conduits can be simulated without the knowledge of their position and geometry. This approach was first applied by TEUTSCH (1988).

A similar approach is followed in this thesis: At the same time matrix and conduit flow should be simulated by the combination of the 2D-groundwater model and the bypass implemented into the routing model. In this way the duality of the karstic discharge behavior, i.e. rapid response of highly conductive karst conduits and delayed drainage of the low-permeability fractured matrix after recharge events can be met. Like described in chapter V.2.1, the fast recharge events through the conduits into the aquifer are represented by the surface runoff and interflow built within the Snir basin and diverted into the bypass to the Dan basin. The slow matrix flow is represented by both, the groundwater model and the routing parameterization of the bypass.

This approach is not able to reproduce the physical structure of the karst aquifer in the UJC like in discrete fracture network or hybrid models. Furthermore, important karst processes have to be neglected or replaced by conceptual approaches. Replaced processes are e.g. the conduit flow characteristics that are represented by the surface runoff and interflow components of the bypass. In more physically based approaches hydraulic processes like laminar flow within tubes and hydraulic parameters like diameter, slope and conductivity of the conduits would be respected. Another replaced process is the flow within the epikarst. The concept of the epikarst was introduced by MANGIN (1975). It develops close to the surface due to higher solution activity because of water entering from the soil with higher carbon dioxide concentrations. It is regarded to act as a temporary storage and distribution system for infiltrating water into the karst system. The progression of the mechanism with first temporary storage and low permeability and adjacent high flow rates within conduits can not be explicitly simulated. However, the comparatively low flow velocities within the epikarst are represented by the interflow.

In summary, the applied approach for modeling the karst aquifer of the UJC enables the successful simulation of the discharge in all sub basins. The conception of the bypass does not disturb the water balance, as only the way the discharge reaches the basin outlet is manipulated. Other components like evapotranspiration snow storage

are not affected. Therefore, the feasibility for the application of the model for climate impact analysis on water balance in the UJC is enabled.

V.3 Model Coupling

With help of the coupling routine described in IV.5 it is possible to run the hydrological model WaSiM besides with station data also with simulated climate data. For the joint climate-hydrology simulations, MM5 output of the second domain with horizontal resolution of 18 x 18 km² based on ECHAM4/OPYC3 as driving GCM is used. It is renounced to use data from domain 1 with 54 x 54 km² resolution since the first domain is too coarse for the relatively small investigation area of the UJC with its topographically very heterogeneous properties. The output of the third domain with the finest resolution of 6 x 6 km² is not used as instead of transient runs only short time slices of 15 years (1961 – 1975 and 2085 – 2099) are performed.

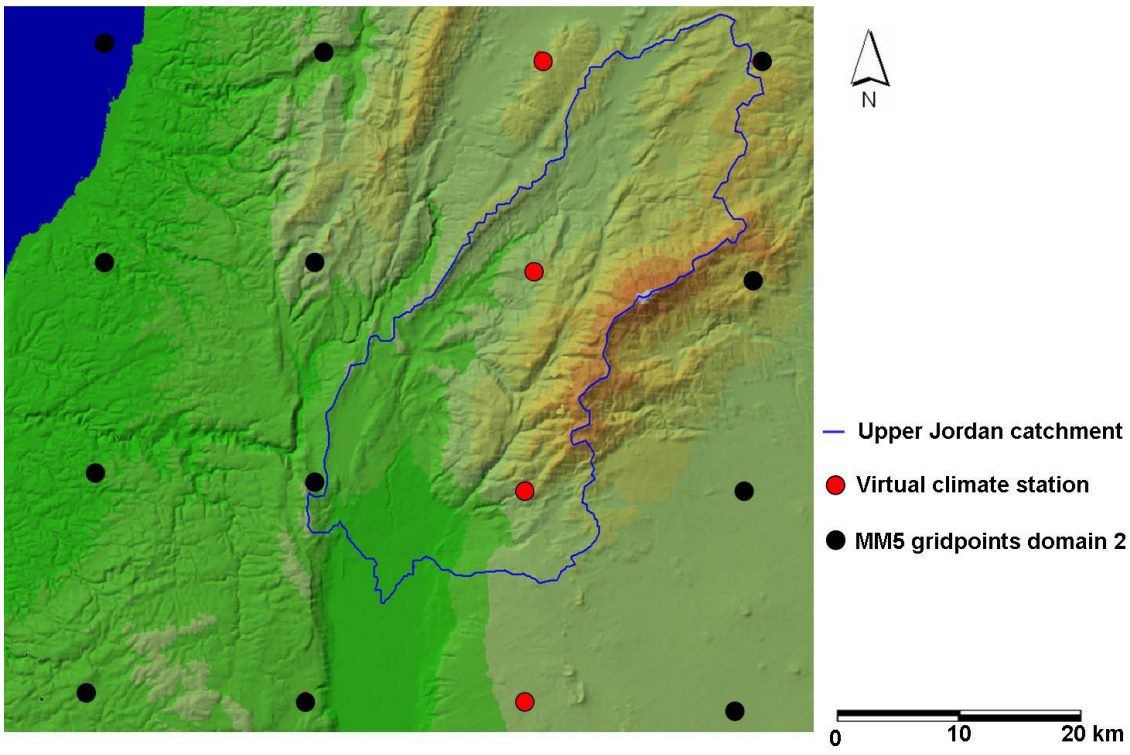

Figure V-22: Location of virtual climate stations derived from domain 2 (18 x 18 km²) resolution

Since the UJC has only an extension of about 850 km² it is reasonable not to apply the entire output of the domain 2 as input for WaSiM, but to choose some grid points inside or next to the investigation area. At least only 4 grid points are chosen for the joint climate –hydrology simulations. Their position can be taken from Figure V-22 (red points).

These stations have elevations of 739, 1033, 1204, and 1232 m asl (from south to north). With a simulated precipitation of the ECHAM4 control run of 532, 602, 688, and 715 mm/a they represent well the height dependency of the precipitation in the UJC. The grid points east to them are higher, but show less annual precipitation. Thus, an interpolation would cause a wrong rainfall distribution over the basin. Therefore, only these 4 grid points are chosen as virtual stations.

These virtual stations with a distance of 18 km to their direct neighbor are interpolated to the 450 x 450 m² grid of WaSiM. To be comparable with the calibration runs based on station data the same interpolation methods are used (see V.2.1). In that way the height dependence of precipitation and temperature can be incorporated as the compared to WaSiM still relatively coarse resolution of the domain cannot consider the height dependence satisfactorily.

The output time step of MM5 is set to 1 h. Therefore, the input variables needed for WaSiM have to be averaged (in case of precipitation summed up) to the time step of the hydrological model of 24 h.

VI Validation

Before statements about future climate trends and their possible impacts can be made, the reliability of the used models and data must be proved. In this chapter the validation of the GCM output (VI.1), the downscaled MM5 output (VI.2), the hydrological model (VI.4) and the joint climate-hydrology simulations (VI.5) is described. Furthermore the bias correction of the downscaled precipitation is delineated (VI.3).

VI.1 GCM Output Analysis

One of the most crucial factors on the validity of predictions about future climate change is the ability of a model to reproduce current climate conditions. In this study the period of 1961 – 1989 serves as reference representing current climate. A period of about 30 years is a common time span where it is assumed that most interannual variabilities are considered. One possibility of validation is the comparison of the model output to gridded observational data. The most important climate variables, where usually numerous observation data are available, are temperature and precipitation.

First the surface temperature of ECHAM4/OPYC3 (resolution 2.8° x 2.8°) is compared to gridded observational temperature of the Climate Research Unit (CRU) in a resolution of 0.5° x 0.5° (CRU CL 1.0, NEW et al., 1999) for the period 1961 – 1990 (see Figure VI-1).

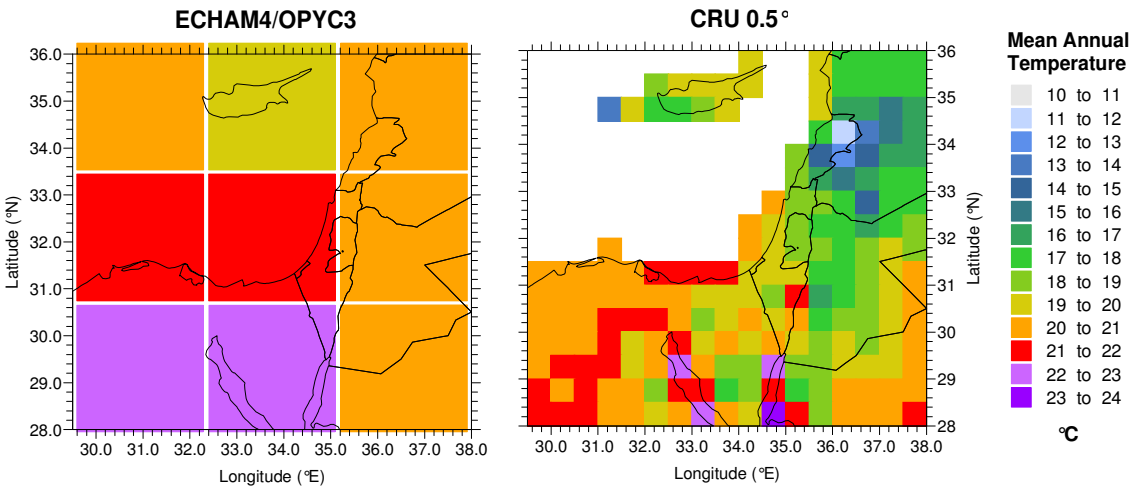

Figure VI-1: Comparison of temperature of ECHAM4 output and CRU gridded observation

It is difficult to compare regional area means in different grid resolutions. The rough approximation especially of the coastlines causes in many cases relevant deviations.

However, a general slight overestimation of about 1 – 2 K for the annual mean temperature can be seen in ECHAM4 compared to the observations. The spatial distribution of temperatures with increasing values in the south-western parts turns out to be reliable. No conclusions can be made on the grid points over sea, since CRU data are limited to land observations.

The annual mean precipitation of ECHAM4 is compared to the CRU data in 0.5° x 0.5° resolution as well as to gridded observations of GPCC (Global Prediction Climatology Centre) in 2.5° x 2.5° resolution (SCHNEIDER et al., 2008). The simulated data and the GPCC data are in good agreement for the considered region of the Eastern Mediterranean. The grid point including Cypress is overestimated in the simulated data, while the grid point directly to the east is clearly underestimated. Also the central grid point and the grid point next to it to the west show an overestimation. Again, direct comparison is difficult as grid points of GPCC are smaller and shifted to southwest.

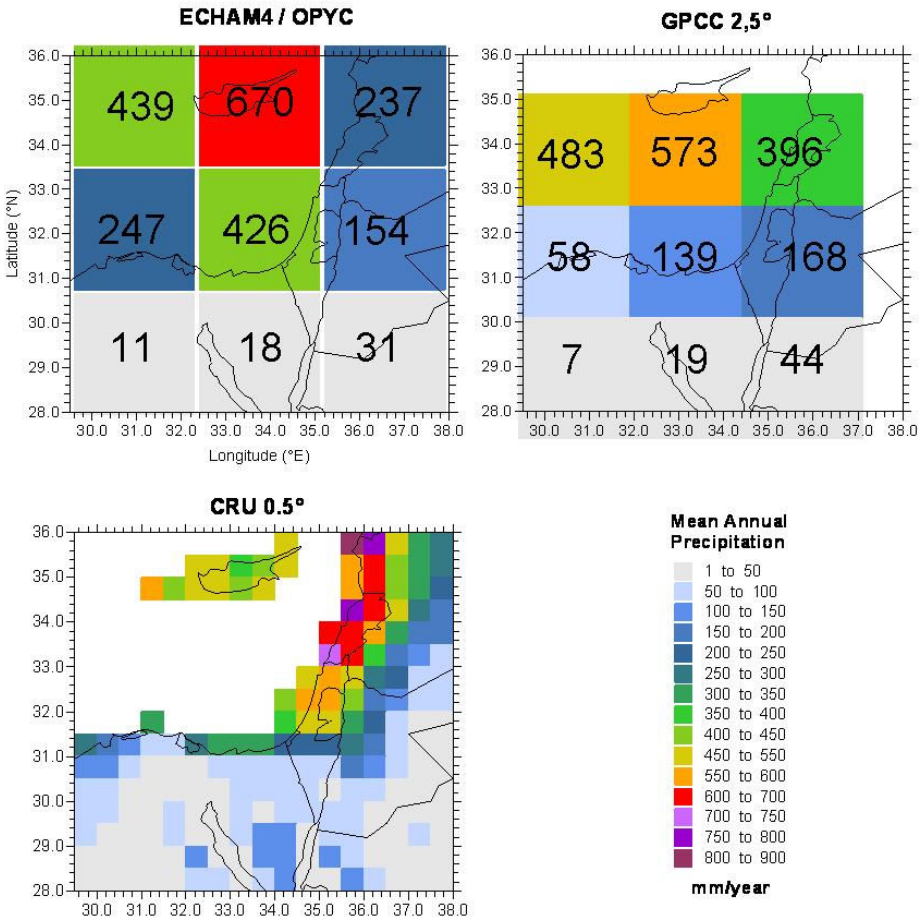

Figure VI-2: Comparison of mean annual precipitation of ECHAM4 to gridded GPCC and CRU observations

Additionally it makes in the model a big difference in simulated rainfall amounts whether a grid point is defined as land or sea. This also causes deviations at coastlines and can explain inaccuracies e.g. at the central grid point with the Egyptian coast north of Sinai. Rainfall at the coast is higher than in the inland as it can be seen in the CRU data, while the grid point averages over a steep climatic gradient. Averaged over the Eastern Mediterranean the rainfall amounts of the model accord well with the observations with an overestimation of 6.7 % compared to the GPCC data.

Another possibility for validation of climate model output is the analysis of the synoptic systems instead of comparing averaged meteorological fields of variables like precipitation and temperature. A comparison of ECHAM4/OPYC3 with NCEP reanalysis based on the objectively classified synoptic systems' approach after ALPERT et al. (2004b) is done by OSETINSKY and ALPERT (2004) for the Eastern Mediterranean. The classified synoptic systems of the EM are described in II.1.1.

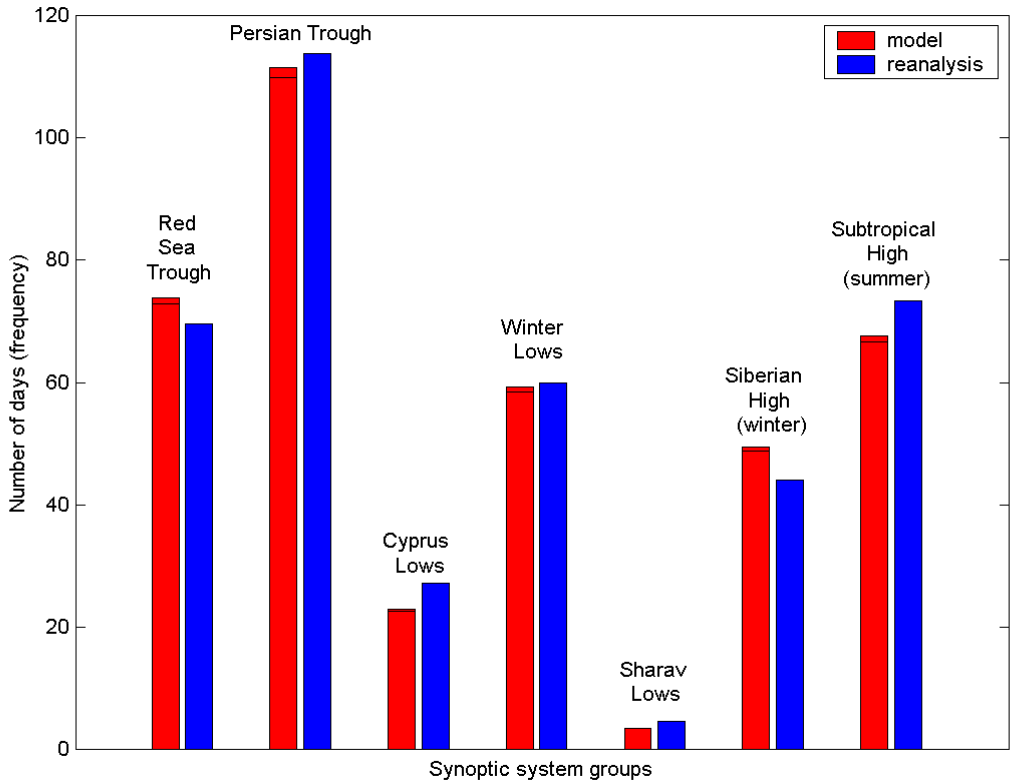

Figure VI-3: Average annual frequencies of EM synoptic systems groups in comparison of ECHAM4/OPYC3 (red) and NCEP reanalysis (blue) for the period 1950 – 2000 (source: OSETINSKY and ALPERT, 2004)

They found that averaging over 1950 – 2000 the ECHAM4/OPYC3 model predicts the annual frequencies for each synoptic system quite similar to the NCEP reanalysis data (see Figure VI-3).

VI.2 Analysis of Downscaled MM5 Output

After the examination of the ECHAM4/OPYC3 GCM data the output of the regional climate model MM5 is validated. Mainly the output of the domain 2 with a horizontal resolution of 18 x 18 km² is analyzed as it is comparable to the CRU data with 10 min resolution (CRU TS 1.2, MITCHELL et al., 2004; MITCHELL and JONES, 2005) and as the joint simulations are conducted with this domain results (V.3).

As described in IV.2 not only climate simulations of the AOGCM ECHAM4/OPYC3 are getting downscaled, but also reanalysis data of NCEP. When performing climate simulations, numerous sources of uncertainties have to be considered. Besides e.g. the uncertainty of the data quality, each model itself is a source of uncertainty. In case of regional or climate models this is due to imperfect knowledge or representation of physical processes, limitations due to numerical approximations of the physical equations and assumptions or simplifications included in the physics parameterization schemes.

To identify possible uncertainties or biases arising from the RCM MM5, NCEP reanalysis data are downscaled with the same setup of MM5 like the ECHAM4/OPYC3 output and compared to each other and additionally to observed climate.

NCEP reanalysis data are downscaled to a horizontal resolution of 18 x 18 km² for a 19 – year period of 1961 – 1979. Therefore, comparison with the control run of the climate model is done for this period, while the CRU data represent the 30 – year time slice1961 – 1990. Figure VI-4 shows annual mean temperature of the Jordan River region simulated with MM5 and based on AOGCM and reanalysis data in a resolution of 18 x 18 km² in comparison of gridded observational data of CRU in a resolution of 10 minutes. The simulation results of both, ECHAM4/OPYC3 and NCEP reanalysis are very similar in their spatial distribution of mean temperatures. They are in good agreement with the observations, but tend to underestimate the temperatures in the southwestern parts and within the Jordan Graben. The underestimation within the graben may partly be explained by the higher resolution of the observations, which allows for better representation of the topographically induced temperature gradient. Altogether it

can be assumed that MM5 in the applied parameterization causes a small cold bias, especially since it is shown in chapter VI.1 that ECHAM4/OPYC3 tends to overestimate temperatures.

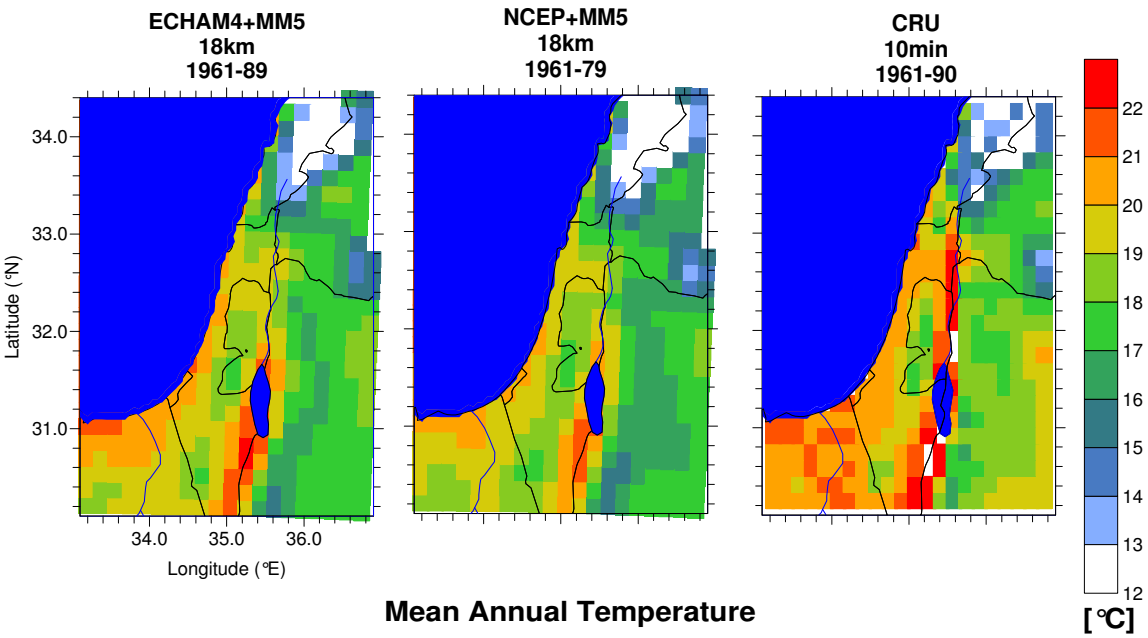

Figure VI-4: Comparison of annual mean temperature of downscaled ECHAM4/OPYC3 and NCEP reanalysis data (resolution 18 x 18 km²) to gridded climate data of CRU (resolution 10 min)

One of the scientific challenges of this study is to test the ability of the RCM MM5 to reproduce the steep climatic gradient within the Jordan River region described in chapter II.1. For that purpose four sub areas along the Jordan River are built representing climatic change from the sub-humid conditions in the north (sub area A) to the arid conditions in the south (sub area D). Their location can be seen in Figure VI-5.

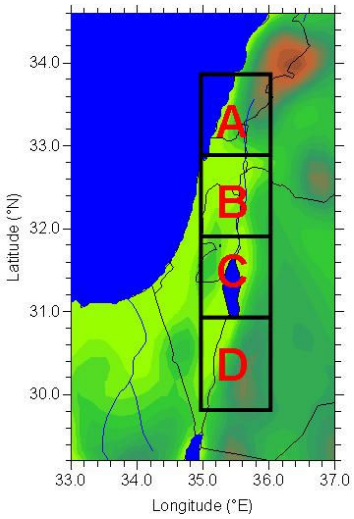

Figure VI-5: Location of the four sub areas representing the steep climate gradient from north to south along the Jordan River

Until now only annual means of climate variables are analyzed. In the following also monthly values for the sub areas are considered. In that way it can be evaluated, whether besides annual also seasonal means can be simulated and whether deviations from observations differ regionally.

Figure VI-6 shows the monthly and annual mean temperatures of downscaled ECHAM4/OPY3 and NCEP reanalysis data of domain 2 compared to observed climate data of CRU for the regions A to D.

The main findings are:

- Although there is a general tendency to a cold bias induced by MM5, there is no general bias in temperature over the Jordan River region: While temperatures in the sub area A are overestimated, in the very southern region D an underestimation can be seen.

- Since the overestimation in the sub area A can be seen in the downscaled GCM data as well as in the reanalysis data, it can be concluded that this is caused by the RCM MM5.

- An underestimation of the months October November, and December occurs for all sub areas besides A in the downscaled GCM and reanalysis data and is hence assumed to be generated by MM5.

- No general seasonal bias can be seen over the regions induced by the driving AOGCM. Only one month (May) shows an overestimation in all sub areas.

In summary the regionalized climate data are in good agreement with the downscaled reanalysis data and the observed climate. Thus it can be concluded

- that MM5 in the resolution of 18 x 18 km² is able to reproduce satisfactorily the regional distribution of temperatures as well for annual as for monthly means and

- that the control period of the climate simulations represent sufficiently well the observed temperatures.

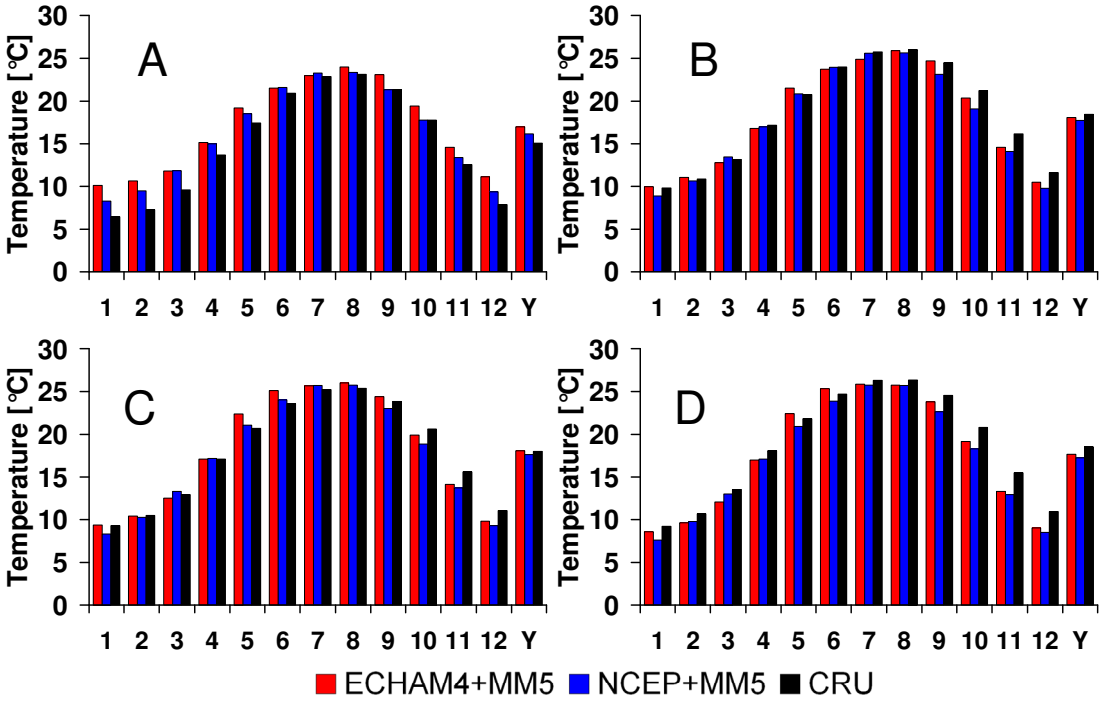

Figure VI-6: Comparison of annual and monthly mean temperatures of downscaled ECHAM4/OPYC3 and NCEP reanalysis data (resolution 18 x 18 km²) to gridded climate data of CRU (resolution 10 min), Regions A – D

In Figure VI-7 the annual mean precipitation of downscaled ECHAM4/OPYC3 and NCEP reanalysis is compared to gridded observations of CRU and additionally to observed rain gauges, which are interpolated to the grid of the domain 2 with a resolution of 18 x 18 km². The used interpolation method is external drift kriging (AHMED and DE MARSILY, 1987) using the DEM as external drift allowing for consideration of topographically induced gradients. About 50 stations which are averaged over the period

1961 – 1990 are used for the interpolation. It is assumed that this quantity of stations is higher than the number of stations that was available for the CRU data. Thus, it should even better represent the distribution of rainfall. As it can be seen in Figure VI-7 both datasets are in very good agreement. Compared to these two datasets the climate simulations based on ECHAM4/OPYC3 show little underestimation in the West Bank and the adjacent parts of Israel in the West. In the other regions the annual rainfall amounts are met very well. The same underestimation can be seen in the downscaled reanalysis data. Additionally there occurs a severe underestimation of rainfall amounts in the northern parts of Israel and the Lebanon. In this case the reanalysis data cannot be used for validation of the climate simulations. Validation of simulated rainfall has to concentrate on observed data.

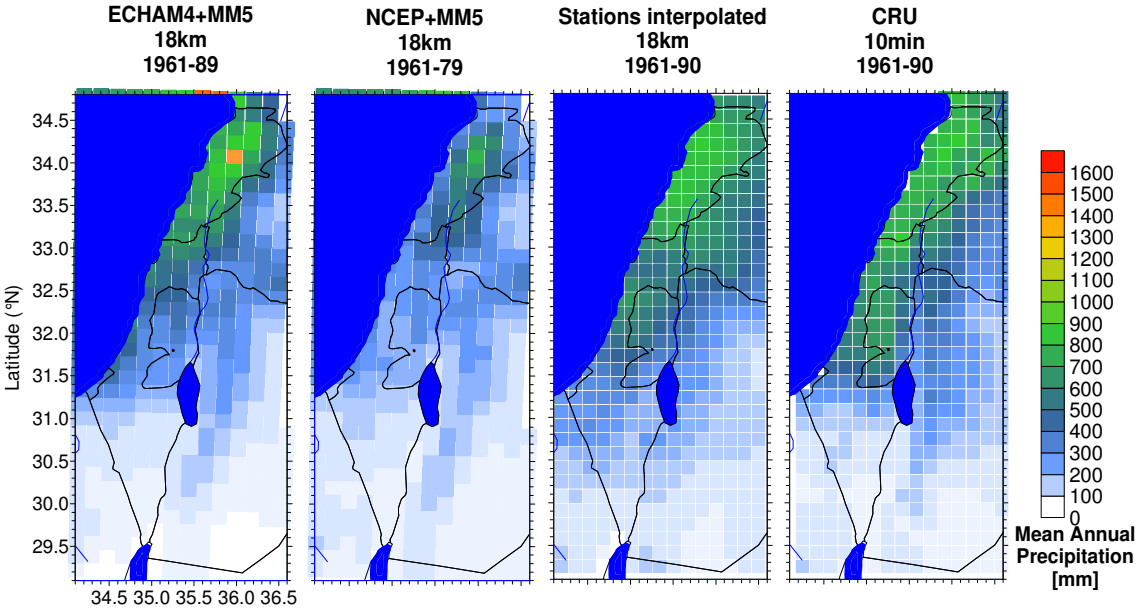

Figure VI-7: Comparison of mean annual precipitation of downscaled ECHAM4/OPYC3 and NCEP reanalysis data (resolution 18 x 18 km²) to gridded climate data of CRU (resolution 10 min) and interpolated station data (resolution 18 x 18 km²)

The monthly means of precipitation in the regions A – D are shown in Figure VI-8. While the annual means are met very well like described before, the monthly distribution shows a clear seasonal bias: The maximum of precipitation is shifted to November, while the measurements show the maximum in December and January. Rainfall in October shows an overestimation in the simulations, while precipitation in spring turns out being too low. The downscaled climate and reanalysis data show rainfall during summer, although the region is almost completely dry during this season. This precipitation

is built within MM5 and is due to limitations in the model's precipitation parameterization. However, simulated amounts are negligible.

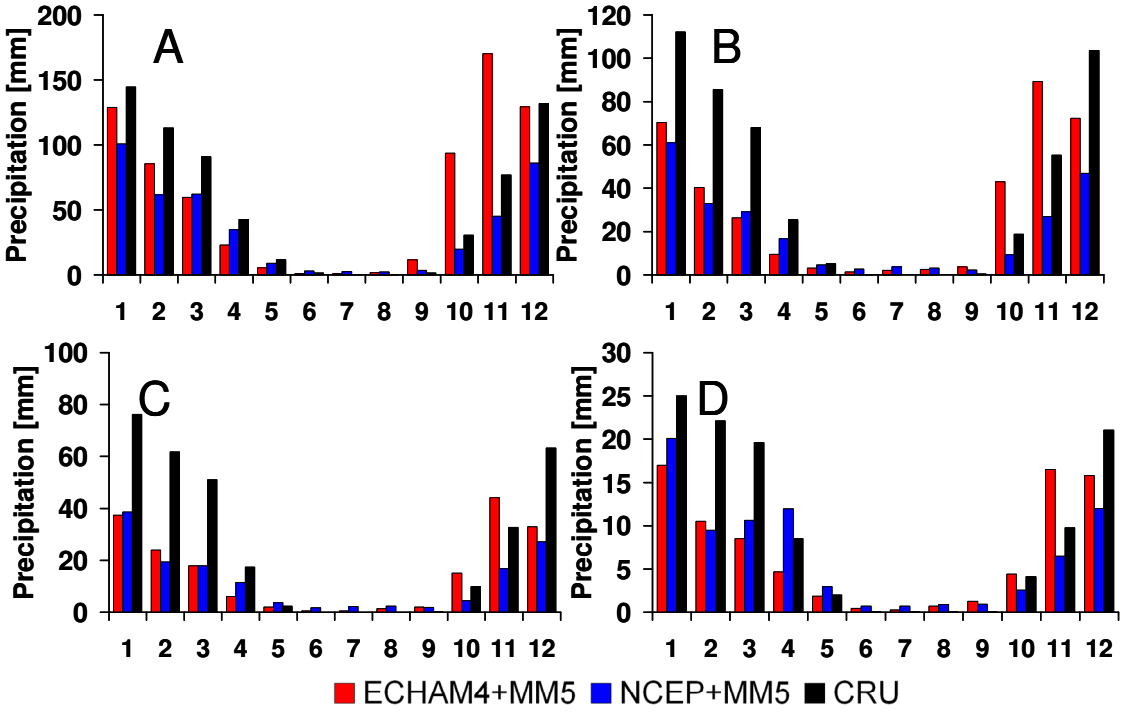

Figure VI-8: Comparison of annual and monthly mean precipitation of downscaled ECHAM4/OPYC3 and NCEP reanalysis data (resolution 18 x 18 km²) to gridded climate data of CRU (resolution 10 min), Regions A – D

The same bias can be seen when comparing precipitation amounts between station values and simulated values using the nearest gird point to the station. While the annual amounts are met quite well with a slight tendency to underestimation (Figure VI-9), the precipitation in winter and autumn are overestimated (Figure VI-10 and Figure VI-11).

This seasonal bias is seen in all sub areas and does not occur in the reanalysis data. The downscaled reanalysis output almost consequently underestimate rainfall amounts, but show the correct seasonal distribution. The bias stems therefore from the driving data, namely the ECHAM4/OPYC3 data. This assumption is certified when considering Table VI-1, where the monthly contribution to mean annual rainfall for the Jordan River region (averaged over the 4 sub areas A – D) is listed. The interpolated stations are in good agreement with the CRU data and the downscaled reanalysis data

are very close to them. In contrast, the downscaled ECHAM4/OPYC3 data exhibit the same seasonal bias like the original ECHAM4/OPYC3 output.

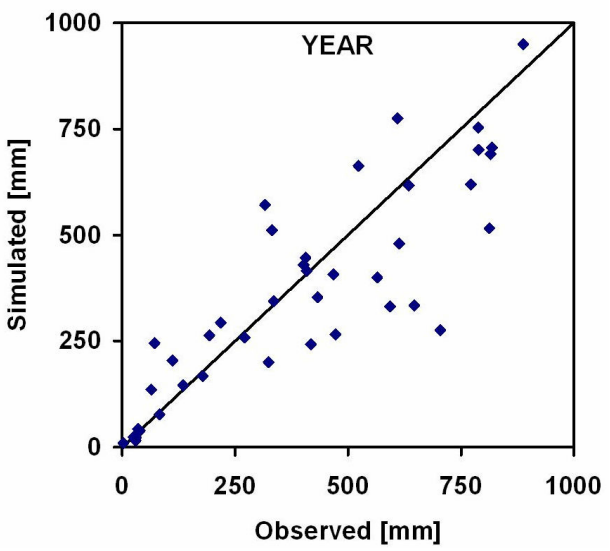

Figure VI-9: Mean annual precipitation, observed station values compared to ECHAM4+MM5 simulations (grid point nearest to station, 18 x 18 km² resolution)

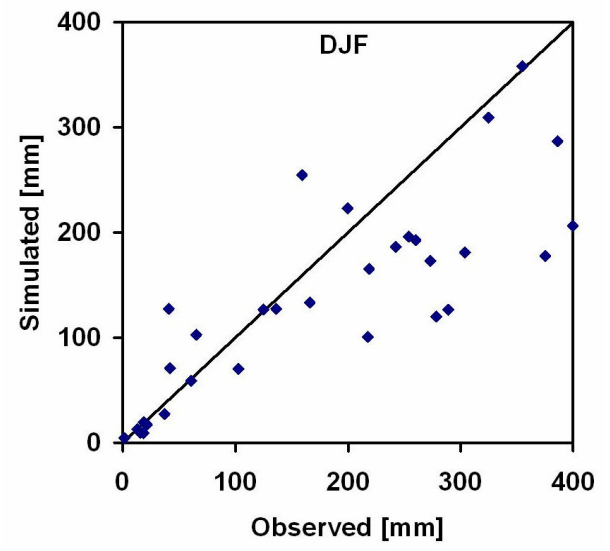

Figure VI-10: Mean winter precipitation, observed station values compared to ECHAM4+MM5 simulations (grid point nearest to station, 18 x 18 km² resolution)

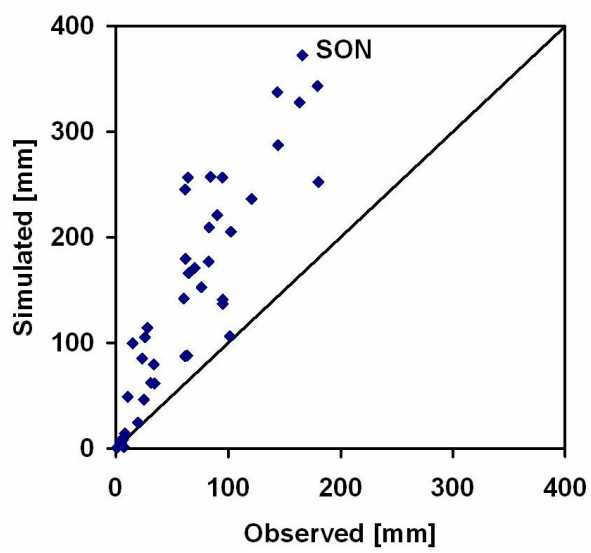

Figure VI-11: Mean autumn precipitation, observed station values compared to ECHAM4+MM5 simulations (grid point nearest to station, 18 x 18 km² resolution)

Table VI-1: Monthly contribution to mean annual precipitation [%] in the Jordan River region

	Monthly contribution to mean annual precipitation [%]											
	Jan	**Feb**	**Mar**	**Apr**	**May**	**Jun**	**Jul**	**Aug**	**Sep**	**Oct**	**Nov**	**Dec**
STATIONS	23.9	18.3	14	5.1	0.9	0.1	0	0.1	0.3	4.9	11.7	21.2
CRU	23.1	18.7	15.5	6.3	1.4	0.1	0	0	0.1	3.9	10.7	20.3
NCEP+MM5 18x18km	25.2	13.4	13.1	9.5	2.6	1	1.2	1.1	1.1	3.7	10.3	18.3
ECHAM4+MM5 18x18km	19.6	12.2	8.9	3.7	1.3	0.4	0.3	0.7	1.3	9.6	23.2	18.8
Original ECHAM4	18.1	11.9	7.3	2.2	1.1	0.7	1.5	2.6	2.6	10.5	22.5	19.1

This seasonal bias turns out to be serious, especially when it is intended to use the climate simulations for impact studies in hydrology. The application of these precipitation data would inevitably lead to a seasonally shifted simulation of runoff. The seasonality of evapotranspiration would be incorrect, as with a rainfall maximum in the autumn higher amounts would be evapotranspirated due to higher temperature in this season. In the case of the UJC it is even more problematic, since the correct simulation of snow accumulation and snow melt as an important factor in this region for the water balance would be hampered. The highest precipitation rates wouldn't be accompanied with the lowest temperatures when the rainfall maximum is shifted to the warmer autumn, which would lead to a considerable lower snow accumulation.

Thus a correction of the seasonal bias has to be done before the results of the regional climate simulations based on ECHAM4/OPYC3 can be used for joint climate-hydrology simulations in the UJC. The bias correction and its approach are described in VI.3.

When analyzing the ability of the RCM MM5 to simulate rainfall correctly in its spatial and temporal distribution also the effect of different resolutions has to be considered. In coarse resolutions land-sea-effects and orographically induced rainfall gradients cannot be considered satisfactorily. This is the main reason why RCMs are introduced for further refinement of GCM simulation results. In this study the ECHAM4/OPYC3 data are dynamically downscaled with the RCM MM5 into three domains with different resolutions using the nesting approach (V.1.1).

In Figure VI-12 simulated mean annual precipitation is shown for all three domains and additionally compared to station data. Because of better lucidity less stations than for the comparison in Figure VI-9 to Figure VI-11, or for the interpolation of station data (Figure VI-7) are used. Because of storage and CPU time constraints for domain 3 instead of transient simulations only time slice experiments of 15 years are conducted. Thus, the comparison of simulated rainfall is limited to the period 1961 – 1975, while the observations represent the mean of 1961 – 1990.

It can be seen that in domain 1 with the coarse resolution of 54 x 54 km² the rainfall is predominantly underestimated, while in domain 2 with 18 x 18 km² resolution the station values (illustrated as colored circles) are met better. The underestimation in the region of the West Bank and the region west to it was already mentioned before. This underestimation is not seen any more in domain3 with the highest resolution of 6 x 6 km². Thus it can be concluded that the finer resolution ameliorates in most cases the quality of simulated precipitation. Nevertheless, it must be emphasized that higher model resolution does not mandatory mean an enhancement of the simulation results (e.g. MARX, 2007). When looking in the northern parts of domain 3 in Figure VI-12 an overestimation and therefore pejoration compared to domain 2 can be noticed. This is the region with high mountains in Lebanon where the air masses are forced to ascend causing high precipitation amounts. The grid size of 6 x 6 km resolution is a critical resolution where the model starts to be able to simulate convective cells explicitely without cumulus parameterization. However, in this study also for the domain 3 the cumulus parameterization is used.

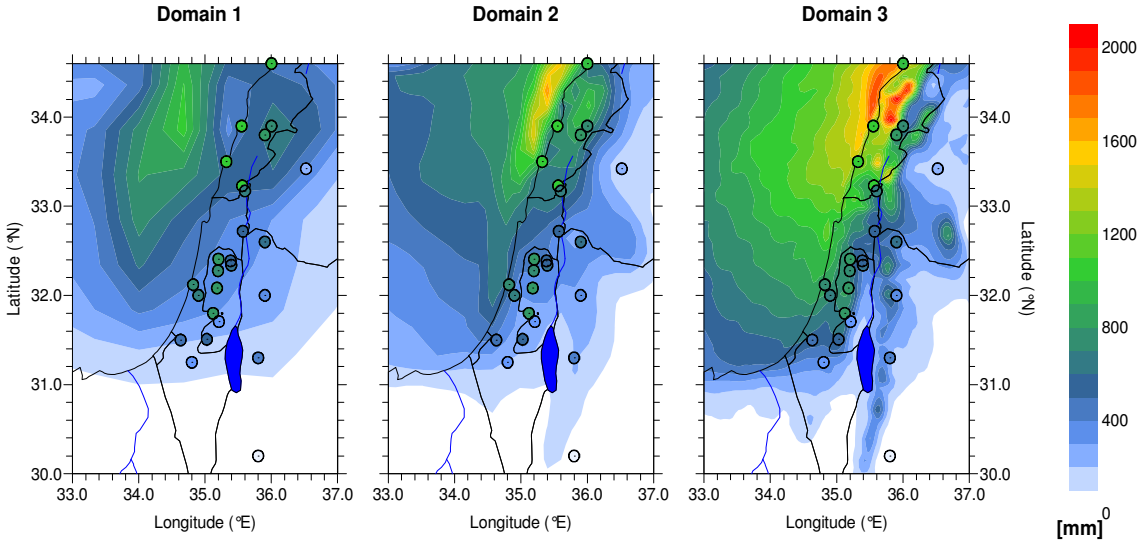

Figure VI-12: Comparison of observed (colored circles) and simulated mean annual precipitation at different resolutions of MM5 for the period 1961 – 1975

In summary the potential of high-resolution simulations with domain 3 could be shown for the available time slices. Furthermore, it can be concluded that the resolution of domain 2 allows for sufficient consideration of topographical effects in MM5.

VI.3 Bias Correction

As the results of the validation of the downscaled rainfall based on ECHAM4/OPYC3 for the control period show (see chapter VI.2), the bias has to be corrected when it should be used for impact studies on water balance in the UJC.

Like described in III.5 numerous different approaches for bias corrections of climate data exist. Since the bias in precipitation found here is a seasonal bias in form of a shift of the rainy season, the determination of monthly scaling factors is an appropriate method. The used approach is described in the following:

Each grid point with the coordinates *i* and *j* of the downscaled precipitation fields in domain 2 is corrected at every time step *t* with a monthly scaling factor *k*. Since the hydrological simulations are done in a 1-day time step, also the joint climate-hydrology simulations are done in this temporal resolution (*t = 1day*). The scaling factors *k* for each month are obtained by calculating the ratio of simulated and observed mean precipitation. As observation data the interpolated station data are used (see chapter VI.2 and Figure VI-7). They have in comparison to the gridded observation data of CRU on

the one hand the advantage that they are assumed to be more representative due to the available number of rain gauges. On the other hand they have the advantage that they are interpolated to the same grid as the modeled data and thus directly comparable.

Therefore, the scaling factor *k* is calculated e.g. for January (following KUNSTMANN et al., 2004):

$$k_{January}(i,j) = \frac{\frac{1}{30}\sum_{year=1961}^{1990}\sum_{day=1}^{31} observations_{year,January,day}(i,j)}{\frac{1}{29}\sum_{year=1961}^{1989}\sum_{day=1}^{30} simulations_{ControlPeriod,year,January,day}(i,j)} \qquad \text{VI-1}$$

The period of the simulations is restricted to 29 years, as the control run of ECHAM4 is 1961 – 1989. With the help of the scaling factors precipitation at each grid point is transformed e.g. for January:

$$simulation_{Control\ Period}(t,i,j)' = simulation_{Control\ Period}(t,i,j) \times k_{January}(i,j) \qquad \text{VI-2}$$

The same scaling factors that are obtained for the control period representing current climate are used to correct the results of future climate simulations:

$$simulation_{Future\ C\lim ate}(t,i,j)' = simulation_{Future\ C\lim ate}(t,i,j) \times k_{January}(i,j) \qquad \text{VI-3}$$

For the remaining months the correction is performed accordingly. The same bias correction method is applied for the downscaled NCEP reanalysis using the available period of 1961 – 1979.

Applying this correction method for precipitation with the goal of joint climate-hydrology simulations to detect climate change impact on water balance some constraints have to be considered after KUNSTMANN et al. (2004):

- While the number of precipitation events of the MM5 output remains unchanged, the intensity of each event is adjusted such that the overall average monthly sum agrees with the observed average monthly values.

- Precipitation is adjusted according to a spatially (i.e. at every grid point) different climatological factor averaged over a period of 30 years. Within each month, each

precipitation event at a given grid point is adjusted with the same factor *k*. It is not secured, that in future climate conditions these factors are endured (e.g. changing tracks of rain producing cyclones).

- While the precipitation is scaled, all other meteorological fields that are passed from MM5 to WaSiM (temperature, wind, humidity, and radiation) remain unchanged. This implies that the precipitation fields are not necessarily consistent with the other meteorological fields.

VI.4 Validation of WaSiM

The best fit parameterization of the calibration period (hydrological year 1997) is validated by running the model for another time period.

Due to the limitations in climate data availability described in V.2.2 two validation runs are performed. The first one is done with the full set of available climate input data for the hydrological years 1998 and 1999, while the hydrological years 1996 and 1997 are used as spin up time for the groundwater table and storages like soil moisture.

In a second validation run the period 1970 – 1999 is simulated. For this period only a reduced set of climate input data is available with 7 precipitation stations (stations numbers 9 – 15, see Figure V-4) and 4 temperature stations (station numbers 10, 11, 12, 14). As for wind, global radiation ad relative humidity no data are obtainable, monthly mean values of the years 1995 – 1999 are used. It is assumed that monthly means for these variables are sufficient as they are less sensitive compared to precipitation and temperature. To test whether this approach is applicable, a simulation run with this reduced set of climate input data is compared to the validation run with the complete climate input data.

Results of the Validation Run with Full Climate Data Input

Table VI-2: Nash Sutcliffe Efficiencies and R^2 for the calibration and validation periods

Period	gauge	Banyas	Dan	Saar	Snir	Ayun	Yoseph Bridge routing 2*)	Yoseph Bridge routing 1*)
Calibration (1997)	**NSE_{lin}**	0.44	0.12	0.69	0.19	0.12	0.94	0.51
	NSE_{log}	0.52	0.34	0.69	0.43	0.15	0.84	0.48
	R^2	0.75	0.91	0.82	0.64	0.75	0.94	0.75
Validation (1998-1999)	**NSE_{lin}**	0.56	0.78	0.45	0.26	0.37	0.89	0.61
	NSE_{log}	0.1	0.84	0.69	0.11	0.1	0.69	0.57
	R^2	0.68	0.86	0.53	0.28	0.5	0.93	0.63

*) routing 2: with observed discharge; routing 1: with simulated discharge

Table VI-2 shows the NSE_{lin}, NSE_{log} and R^2 values reached for the validation period in comparison to the calibration. For the validation period a comparable performance like for calibration can be reached. The simulated discharges in comparison to observations are given in Figure VI-13 to Figure VI-19.

The hydrological year 1999 is very dry. It is important to determine the ability of the found model's parameterization to simulate these conditions very well. Especially the gauge Dan, which is calibrated with an artificial bypass, is able to reproduce the decline in discharge. The very high NSE values for the validation period are evidence for the good parameterization of the bypass representing the extended karstic aquifer. While the lower NSE values during the calibration period are due to the long spin up time of the bypass, for the validation, where a 2-year spin up time is possible, simulated discharges agree very well with observations in both, quantity and dynamics (Figure VI-14).

The Dan is the most important tributary to the Jordan River. Thus a good performance of the Dan enables good results for the runoff simulation of the Upper Jordan represented at the Yoseph Bridge. Especially when examining the simulations with routing based on simulated discharge (routing 1, Figure VI-19) the better results in comparison to the calibration period have to be emphasized. This is the crucial precondition for the use of WaSiM in a joint climate-hydrology model environment with simulated climate data input. The little weaker performance at the Yoseph Bridge with routing based on observed discharges (Figure VI-18) can be explained by the comparatively to the precipitation and discharge amounts high withdrawal of water out of the river.

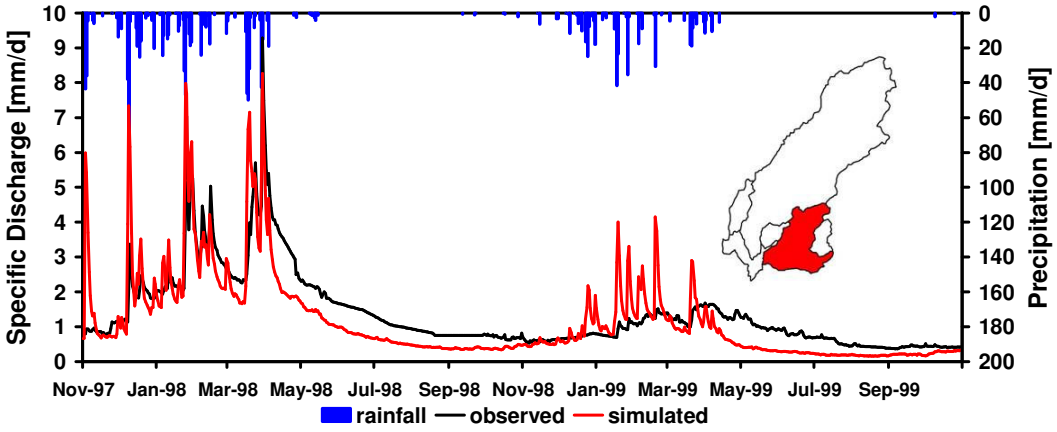

Figure VI-13: Comparison of observed and simulated discharge at gauge Banyas and precipitation for the validation period

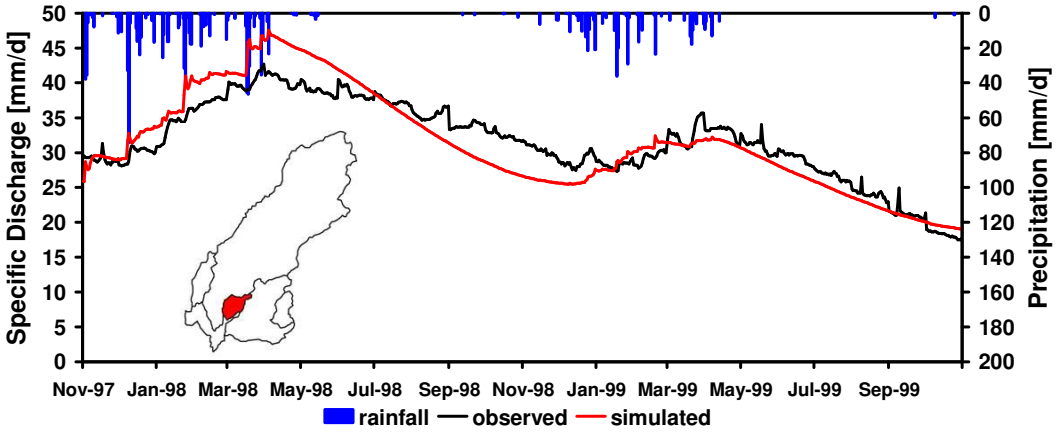

Figure VI-14: Comparison of observed and simulated discharge at gauge Dan and precipitation for the validation period

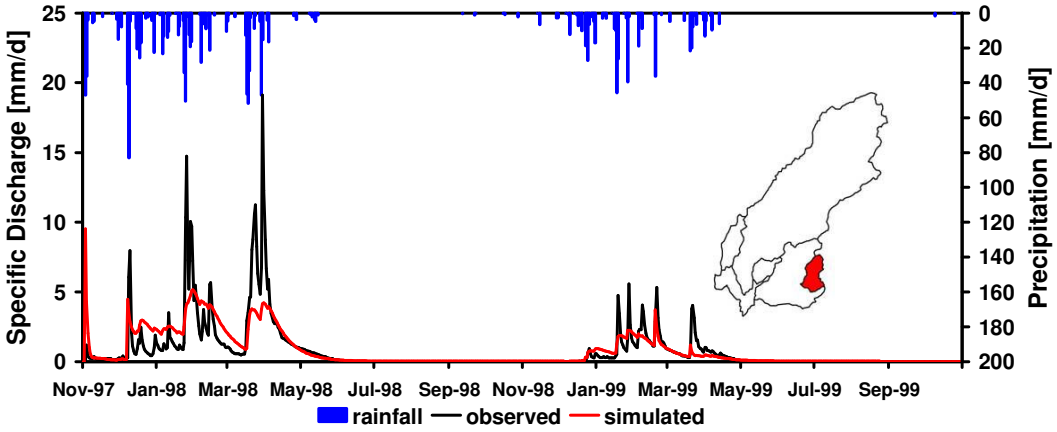

Figure VI-15: Comparison of observed and simulated discharge at gauge Sa'ar and precipitation for the validation period

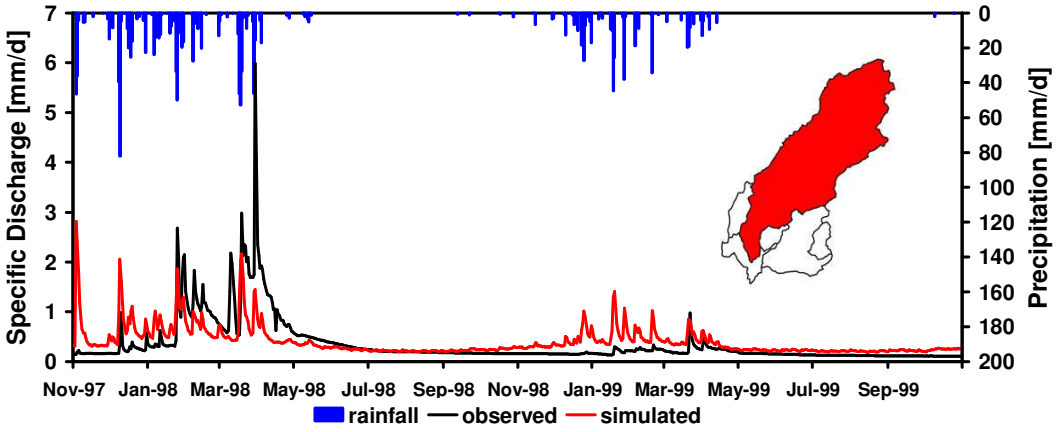

Figure VI-16: Comparison of observed and simulated discharge at gauge Snir and precipitation for the validation period

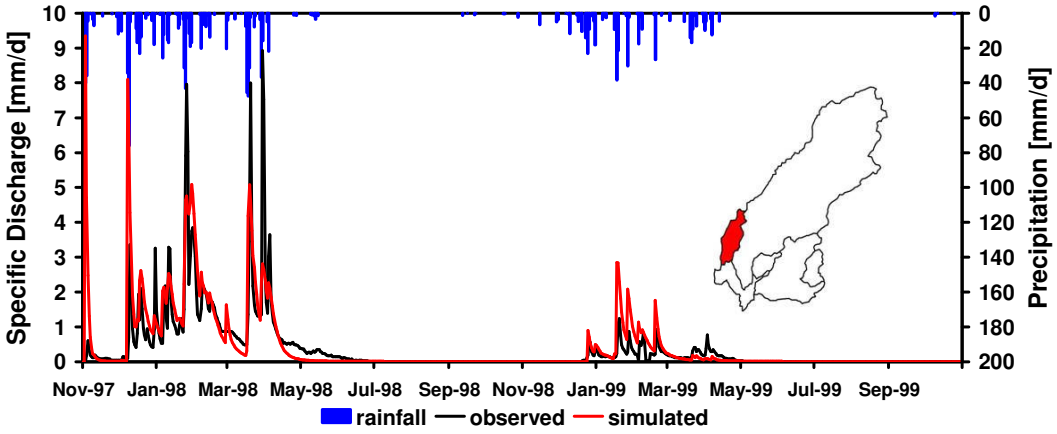

Figure VI-17: Comparison of observed and simulated discharge at gauge Ayun and precipitation for the validation period

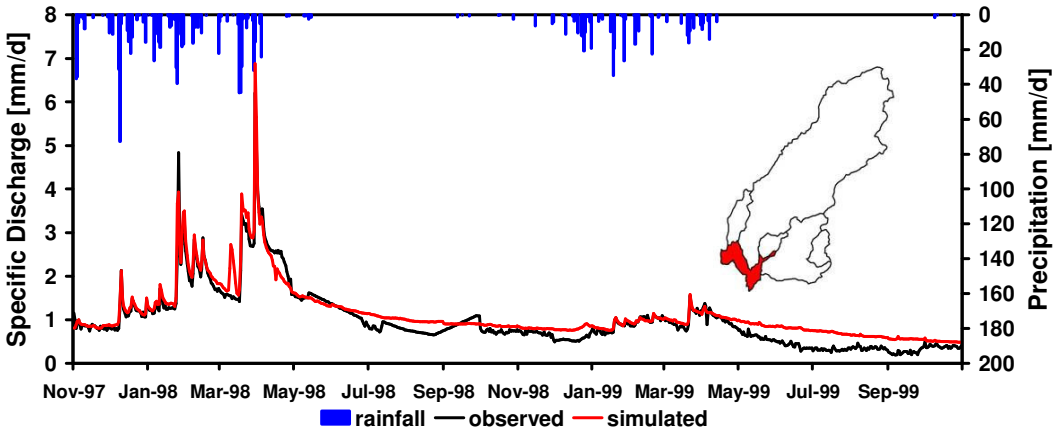

Figure VI-18: Comparison of observed and simulated discharge of the Jordan River at gauge Yoseph Bridge (routing with observed discharge) and precipitation for the validation period

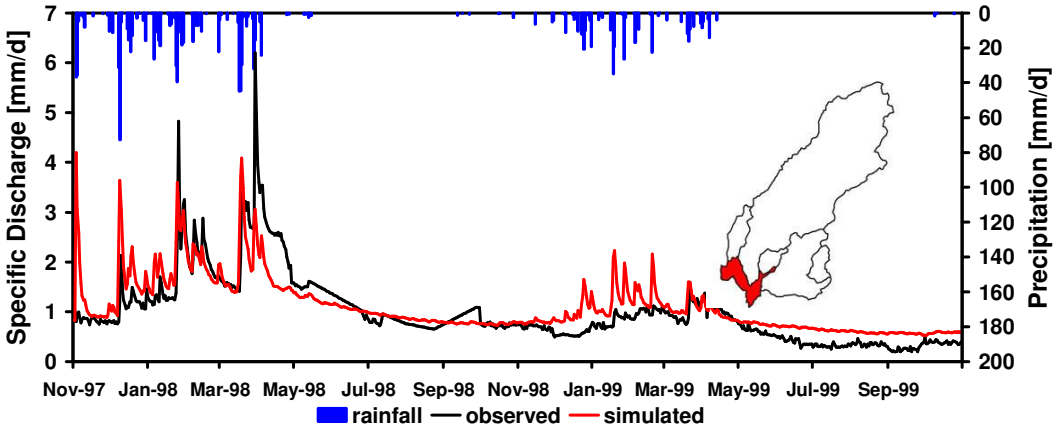

Figure VI-19: Comparison of observed and simulated discharge of the Jordan River at gauge Yoseph Bridge (routing with simulated discharge) and precipitation for the validation period

Comparison of Reduced Climate Data Input with Full Climate Data Input

Before long term simulations based on a reduced number of climate stations and monthly means for the input variables wind, global radiation and humidity are performed, this approach is tested by simulating the same period like for the validation with the full data input. It is obvious that an interpolation based on IDW and height dependent linear regression with a different number of stations produces altered spatial patterns. To gain comparable spatial means in the UJC (Figure VI-20) a correction factor for temperature of 0.94 and for precipitation of 0.89 has to be used. However, when comparing the spatial distribution of these variables within the UJC differences can be seen: While for precipitation the lesser number of stations causes a more pronounced differentiation due to the height, for temperature the opposite occurs (Figure VI-21). Therefore, temperatures in higher altitudes are warmer in the simulation with the reduced input. As a result, evapotranspiration is increased as in the more humid higher regions more energy is available (Figure VI-20). Another effect is that with this plus in temperature snow accumulation is hampered and almost no storage is simulated in comparison to the simulations with the full data input (Figure VI-22).

However, apart from these limitations the results are very close to the simulations with the full climate input which can be seen from the quite similar NSE and R^2 values in Table VI-3. Therefore, the approach with the reduced number of station data for precipitation and temperature and the use of monthly means for the other climate variables is considered as applicable.

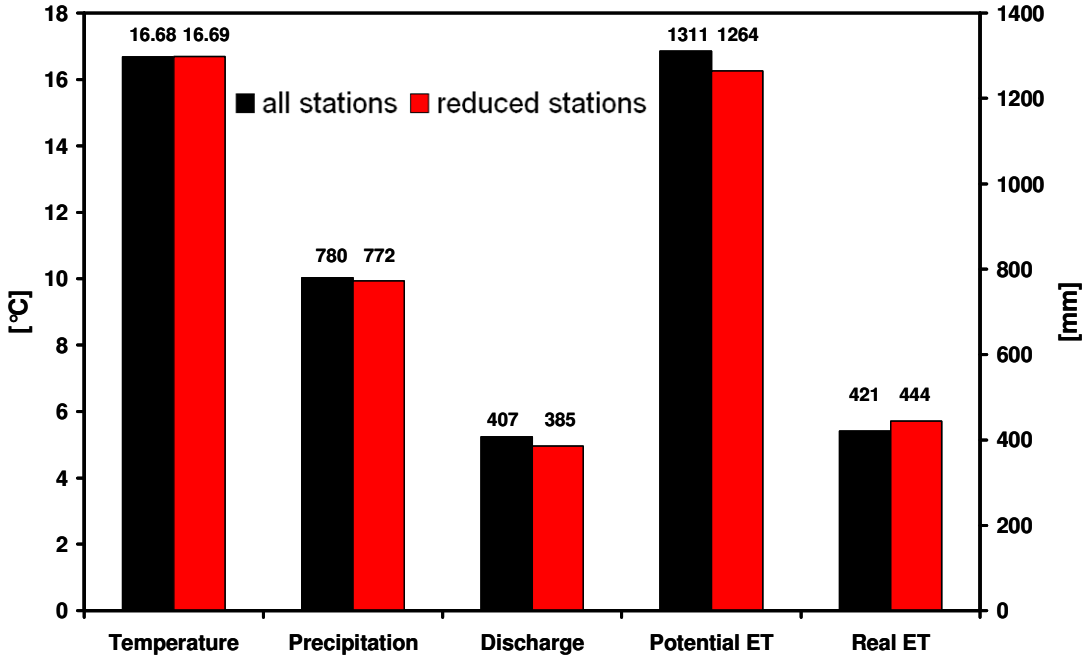

Figure VI-20: Comparison of the simulation results for the full and the reduced climate data input (annual means, hydrological years 1998 - 1999)

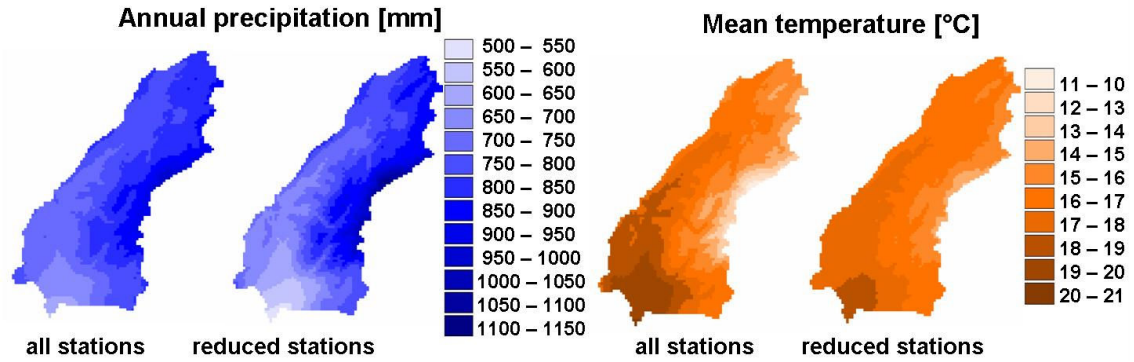

Figure VI-21: Comparison for annual precipitation and mean temperature of the full and the reduced climate data input

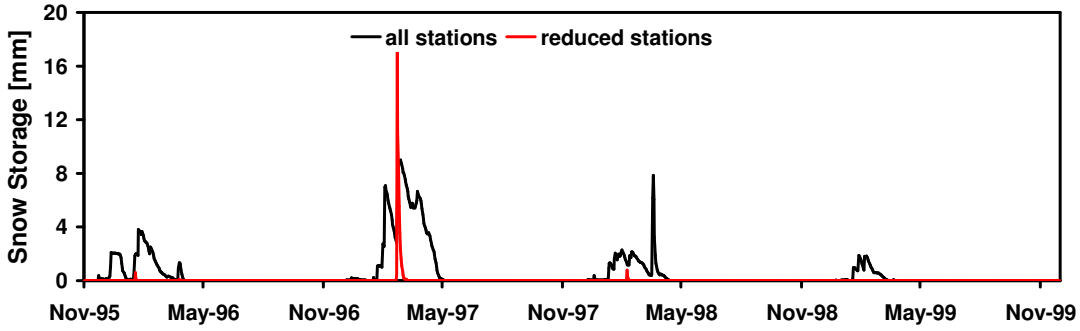

Figure VI-22: Comparison of the simulation of the snow storage with the full and the reduced climate data input

Table VI-3: Nash Sutcliffe Efficiencies and R^2 for the simulation of 1998 – 1999 with the full and the reduced climate data input

	gauge:	Banyas	Dan	Saar	Snir	Ayun	Yoseph Bridge
all stations	**NSE_{lin}**	0.56	0.78	0.45	0.26	0.37	0.89
	NSE_{log}	0.1	0.84	0.69	0.11	0.1	0.69
	R^2	0.68	0.86	0.53	0.28	0.5	0.93
reduced stations	**NSE_{lin}**	0.47	0.78	0.42	0.24	0.40	0.89
	NSE_{log}	0.08	0.82	0.41	0.12	0.18	0.69
	R^2	0.63	0.86	0.45	0.26	0.41	0.93

Results of the Long Term Validation Run with Reduced Climate Data Input

The simulated discharge of the long term validations of the UJC represented by the gauge Yoseph Bridge is in very good agreement to observations (Figure VI-23). Performance criteria of NSE_{lin} = 0,62, NSE_{log} = 0,56, and R^2 = 0,54 (routing with simulated discharge) are comparatively good results taking into account the restrictions in data availability described in V.2.2. The comparison of the observed and simulated hydrograph in Figure VI-23 shows that the high runoff events mostly can not be captured while summer discharge is overestimated. However, real discharge in summer is difficult to estimate as observed runoff is biased by withdrawal out of the river.

The long term validation run is analyzed in detail together with validation of the joint climate hydrology simulations based on downscaled ECHAM4 control run and downscaled NCEP reanalysis with bias corrected precipitation in VI.5.

As the main result of this validation run it has to be emphasized that the hydrological model with the bypass-approach remains stable in long-term model runs and is therefore applicable to climate simulations.

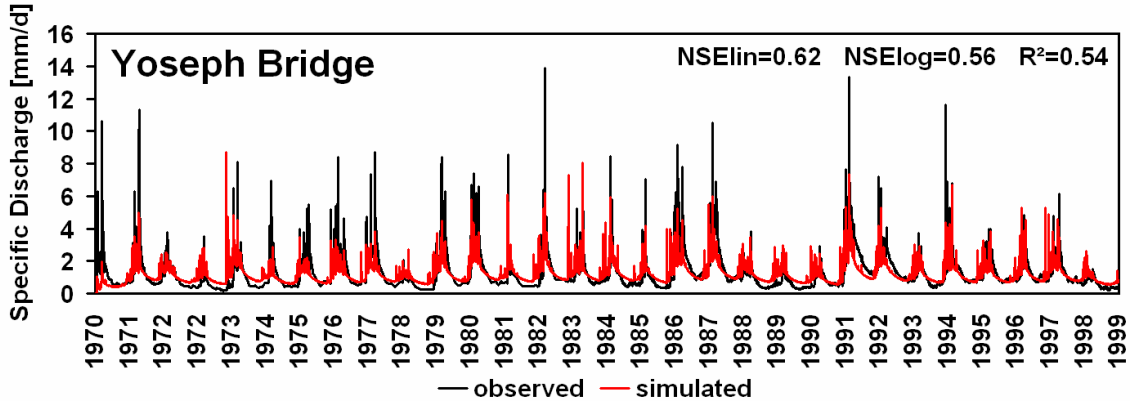

Figure VI-23: Comparison of observed and simulated discharge of the Jordan River at gauge Yoseph Bridge (routing with simulated discharge) for the period 1970 - 1999

VI.5 Analysis of Joint Modeling System

Validation of the joint modeling system (see chapters IV.5 and V.3) is done by analyzing simulation results based on downscaled (18 x 18 km resolution) ECHAM4 control period 1961 – 1989 and NCEP reanalysis (period 1961 - 1979) using bias corrected precipitation (see chapter VI.3) in comparison to observations and the long term validation run based on station data (see chapter VI.4), further on referred to as “reference simulated” in contrast to direct observations (“reference observed”). In this analysis only discharge data are direct observations. All other variables that are based on station data (like precipitation) are denoted as simulated reference as they are modified with in the hydrologicqal model, e.g by interpolation. Especially the water balance components precipitation, discharge, and evapotranspiration are evaluated.

The bias in the temporal distribution of the annual precipitation has been corrected (see chapter VI.3) in a way that monthly mean rainfall amounts are consistent with the interpolated stations data (“simulated”) as it is shown in Figure VI-24.

Besides the temporal distribution of the rainfall also the spatial distribution is of importance. The station distribution between the rain gauges (see Figure V-4) and the virtual stations adapted from the MM5 grid (see Figure V-22) is very dissimilar. The influence of the number and location of station data on the results of an interpolation of precipita-

tion has already been mentioned in VI.4. Therefore, it has to be analyzed whether interpolated precipitation fields of the downscaled climate simulations are comparable to those of interpolated rain gauges for the control period.

In Figure VI-25 the interpolated mean monthly precipitation of the rainy period October – April is displayed for the ECHAM4 control run and NCEP reanalysis (both uncorrected and bias corrected) in comparison to the station data. Conspicuous is the overestimation of the uncorrected control run in October and November as well as the severe underestimation of uncorrected NCEP for most months. In contrast, the bias corrected data are very close to the station data in the spatial pattern. The reason for the good agreement is partly evoked by the interpolation method applied in WaSiM with 50 % IDW and 50 % height dependent regression allowing for considering height gradients in rainfall partly independent from the location of station's location.

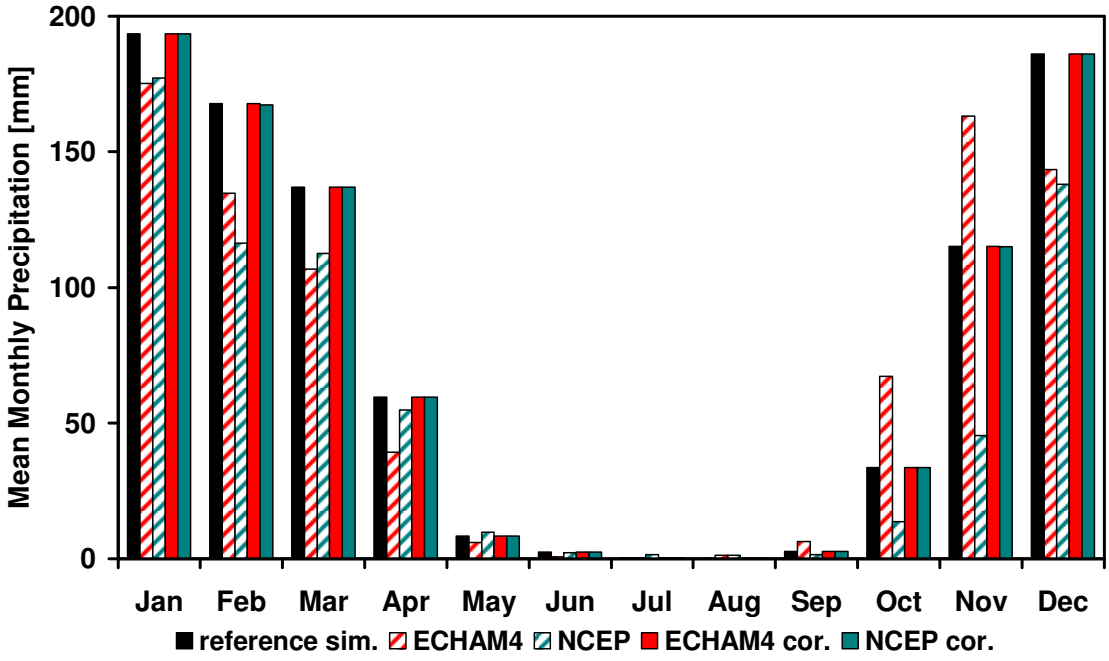

Figure VI-24: Mean monthly precipitation for station data (1961 - 90), original and bias corrected NCEP (1961 - 79) and ECHAM4 RCM output (1961 - 89), interpolated to the UJC

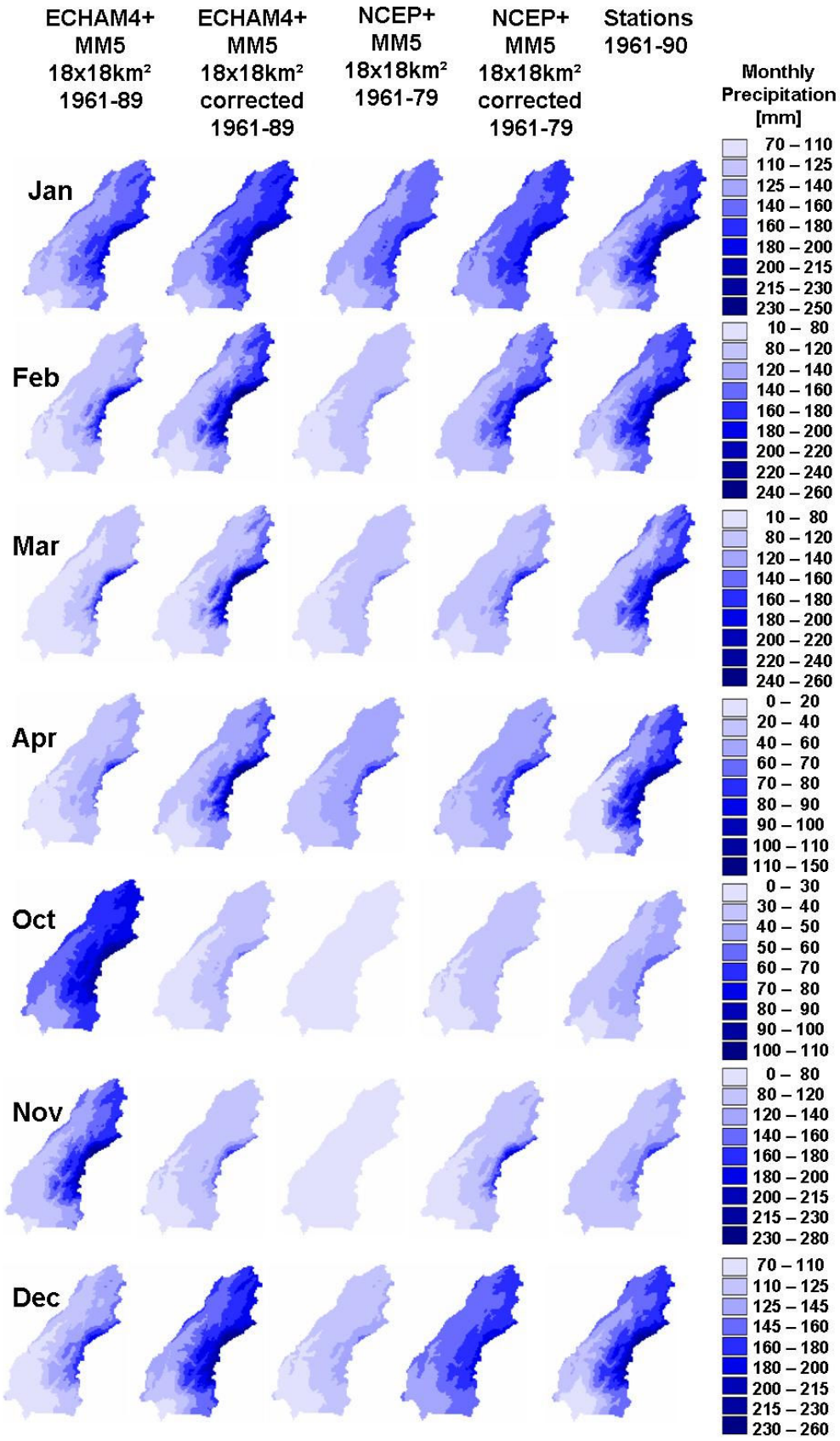

Figure VI-25: Monthly long time mean precipitation in the UJC

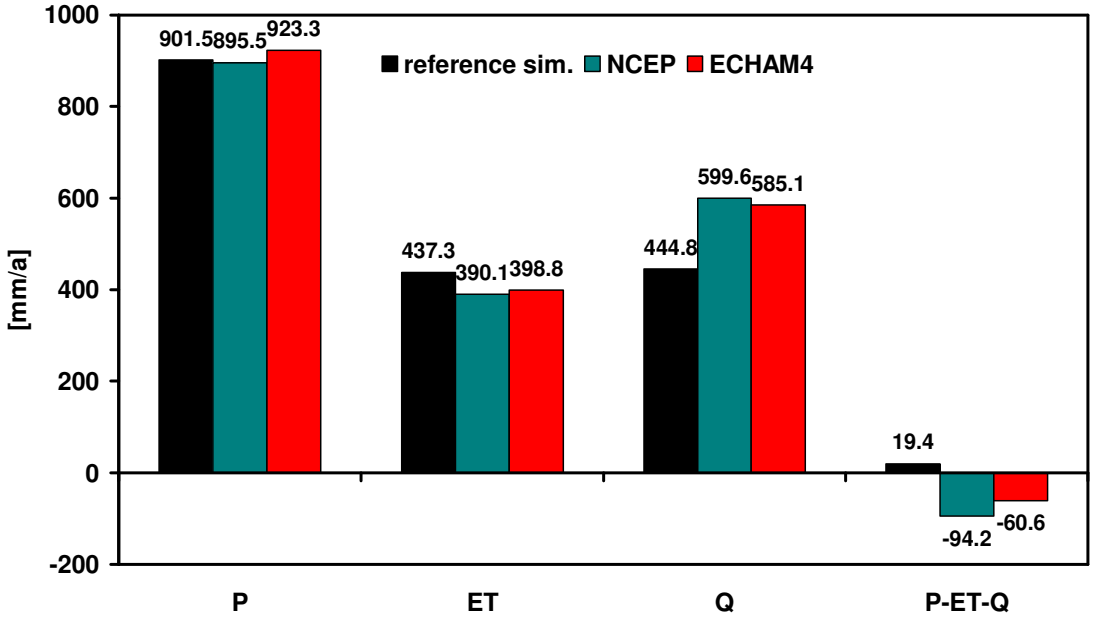

Figure VI-26: Water balance of long term simulations (reference simulated 1970-99, NCEP 1961-79, ECHAM4 control period 1961-89)

For the comparison of yearly precipitation amounts in the UJC, the control run and the reanalysis are with a mean of 931.9 mm/a and 895.5 mm/a very close to the observations of 901.5 mm/a (Figure VI-26). Without the bias correction the annual mean rainfall for the control run would be still very similar to the station data (843.9 mm/a), while the reanalysis underestimates considerably (665.0 mm/a). A comparable annual precipitation value of 958 mm for the UJC was calculated by RIMMER et al. (2006). They also found a nearly linear function between elevation and precipitation in the region that was already mentioned before by other researchers (e.g. GUR et al., 2003). In that way they calculated the rainfall for the entire UJC by a function including elevation dependency based on 4 rainfall stations at different elevation levels ranging from -100 – 960 m asl.. However, it is not clear whether the calculated value applies for the 10–year period 1991 - 2000 or for a longer period.

Analysis of rainfall intensities (Figure VI-27 and Figure VI-28) shows for the reanalysis data and the control run an underestimation in the extreme events >100 mm/d accompanied with an overestimation of the less extreme events with 40 - 80 mm/d. This is due to the nature of RCM data where one grid cell represents a spatial mean, while station data can capture very local extremes. This divergence declines with higher resolutions. The used resolution of 18 x18 km² is already capable of reproducing rainfall intensities quite well, but uncertainties in the very extreme events remain.

Within the 30-year period (1970 – 1999) the gauge at Yoseph Bridge shows an annual mean discharge rate of 444.7 mm/a, while the simulated discharge for the same period is with a value of 444.8 mm/a almost the same. However, it has to be emphasized that the simulated value is underestimated as the observed values are depleted by consumptions. The joint modeling system simulates values of 599.6 mm/a and 585.1 mm/a for the ECHAM4 control period and the NCEP reanalysis, respectively. The lateral outflow defined as lateral boundary condition in WaSiM (see chapter V.2.1), which accounts for 55 mm/a is not included in these numbers of simulated discharge. This overestimation becomes apparent looking at hydrographs of long term mean discharge for a hydrological year (Figure VI-29). It also can be seen in a shift in discharge frequencies (Figure VI-30 and Figure VI-31) to higher amounts than the observations and the station based simulations, especially at low discharge intensities. The overestimation of winter discharge may not fully be explained by consumption and has to be ascribed to shortcomings of the modeling system. Another indication to some inaccuracies is that the water balance equation is not solved properly in the control run and the reanalysis, where more water evaporates or turns into runoff than is put into the system as rainfall. One reason for the overestimation in the discharge can be ascribed to the hydraulic heads that are set at the locations of springs as upper boundary conditions (see chapter V.2.1). When at these locations the groundwater table drops, the model puts artificially as much water into this grid cell to keep the groundwater level constant.

Validation of the simulated discharge is not only done by analyzing the entire runoff, but also by considering runoff components separately. One possibility is the examination of the ratio of surface and subsurface components. BRIELMANN (2008) found by investigations to runoff generation processes based on hydrographic long-term data and natural tracer analysis of storm runoff events a subsurface discharge component at the Banias of 54 % and at the Snir 42 %. This is especially for the Snir in very good agreement to the simulation results shown in Table VI-4.

Table VI-4: Subsurface discharge components for Banias and Snir

River	BRIELMANN (2008)	Reference simulated	NCEP+MM5	ECHAM4+MM5 control run
Banias	54%	58%	60%	61%
Snir	42%	45%	42%	41%

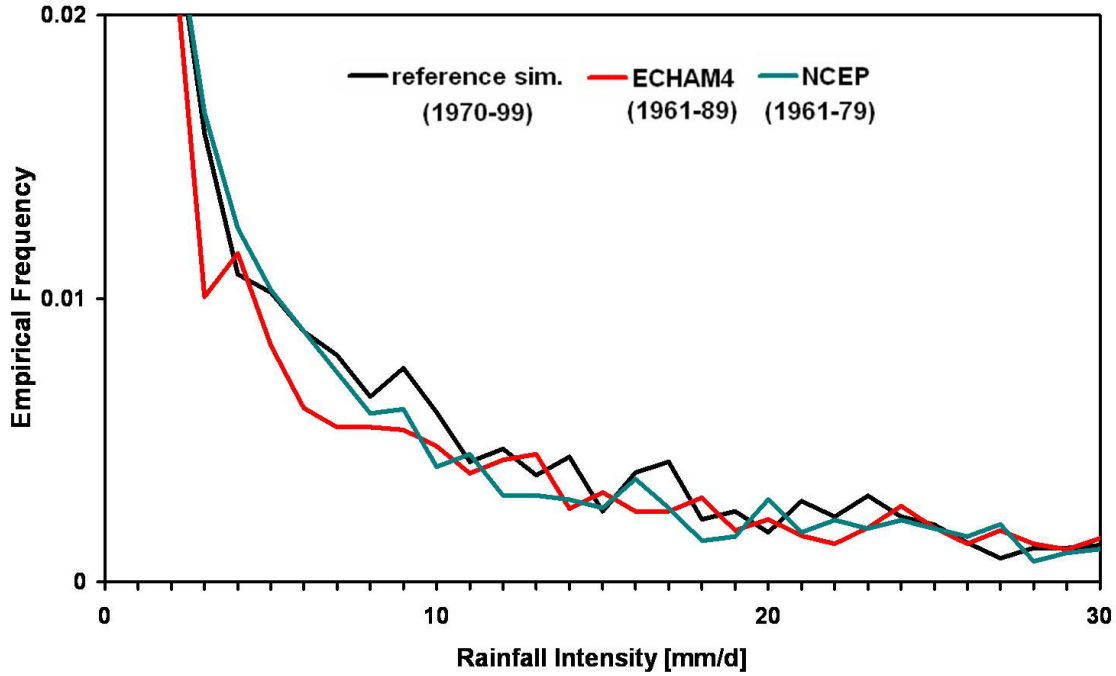

Figure VI-27: Normalized empirical frequencies of daily rainfall intensities 1 - 30 mm (class width 1 mm)

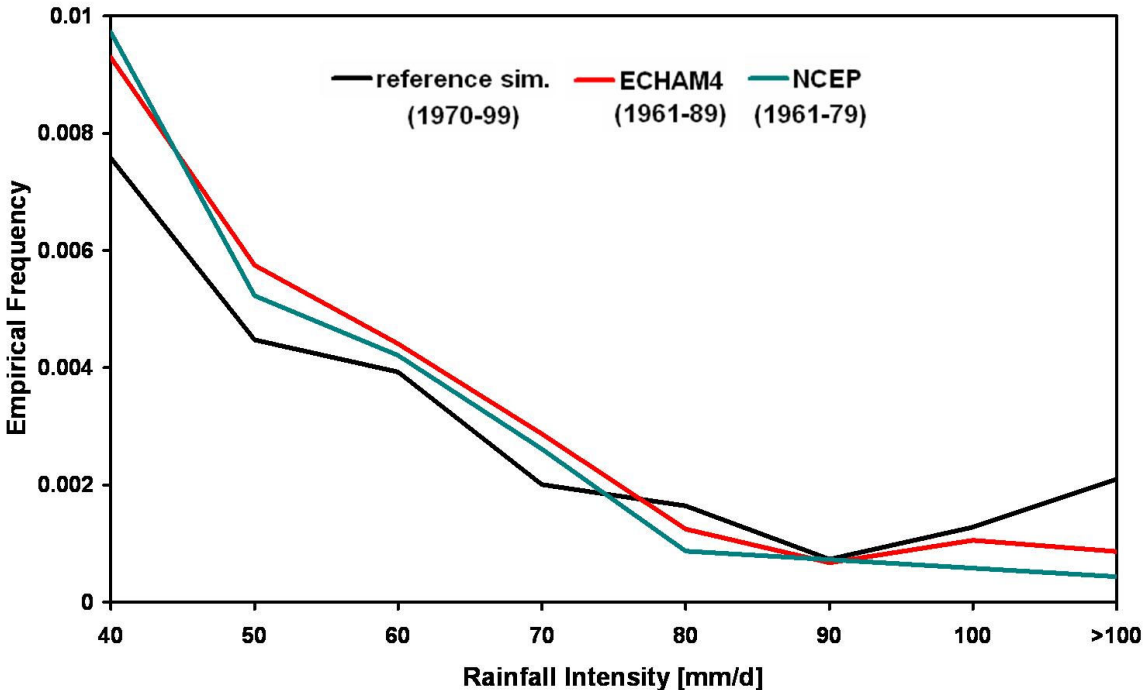

Figure VI-28: Normalized empirical frequencies of daily rainfall intensities > 30 mm (class width 10 mm)

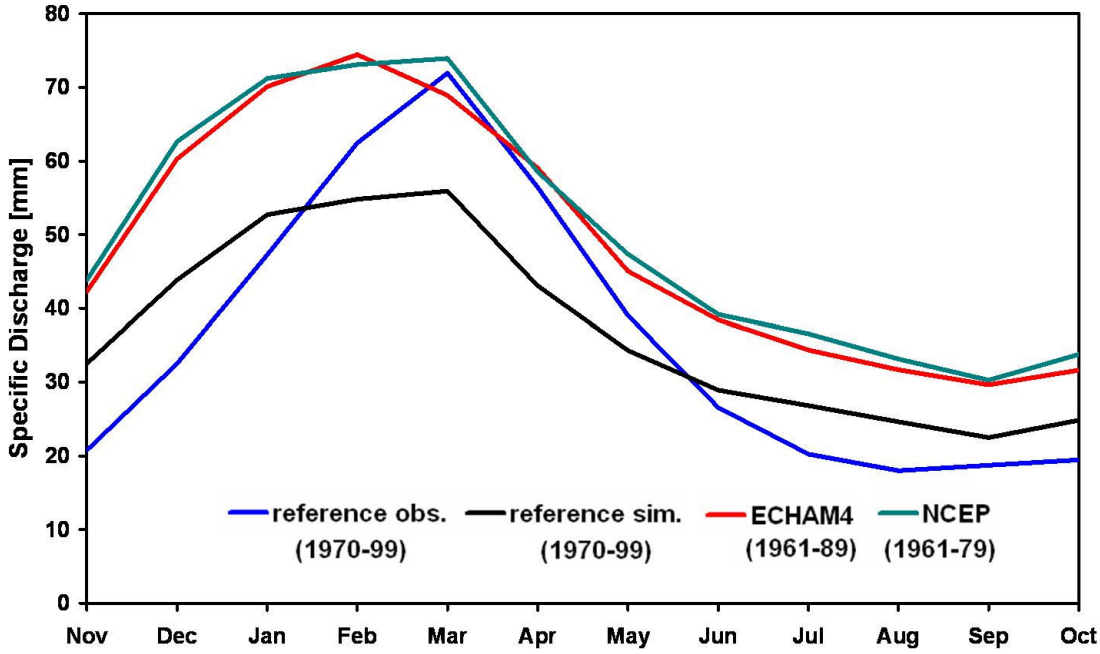

Figure VI-29: Monthly mean discharge in the UJC (at gauge Yoseph Bridge)

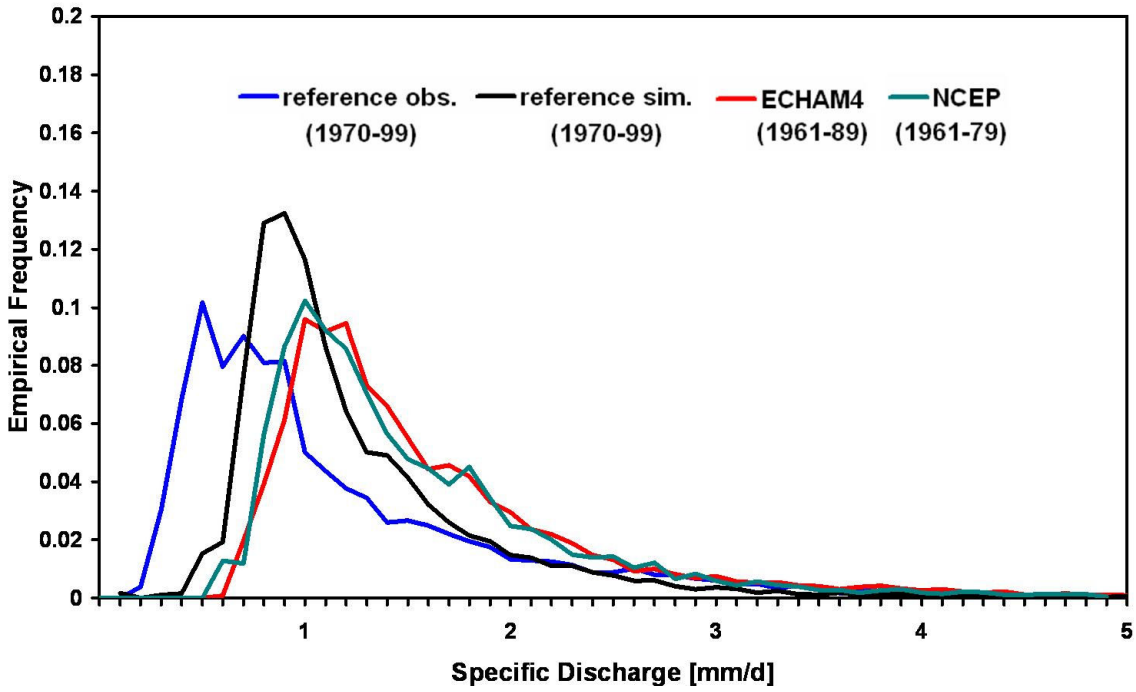

Figure VI-30: Normalized empirical frequencies of daily specific discharge 0 – 5 mm/d in the UJC (at gauge Yoseph Bridge, class width 0.1 mm/d)

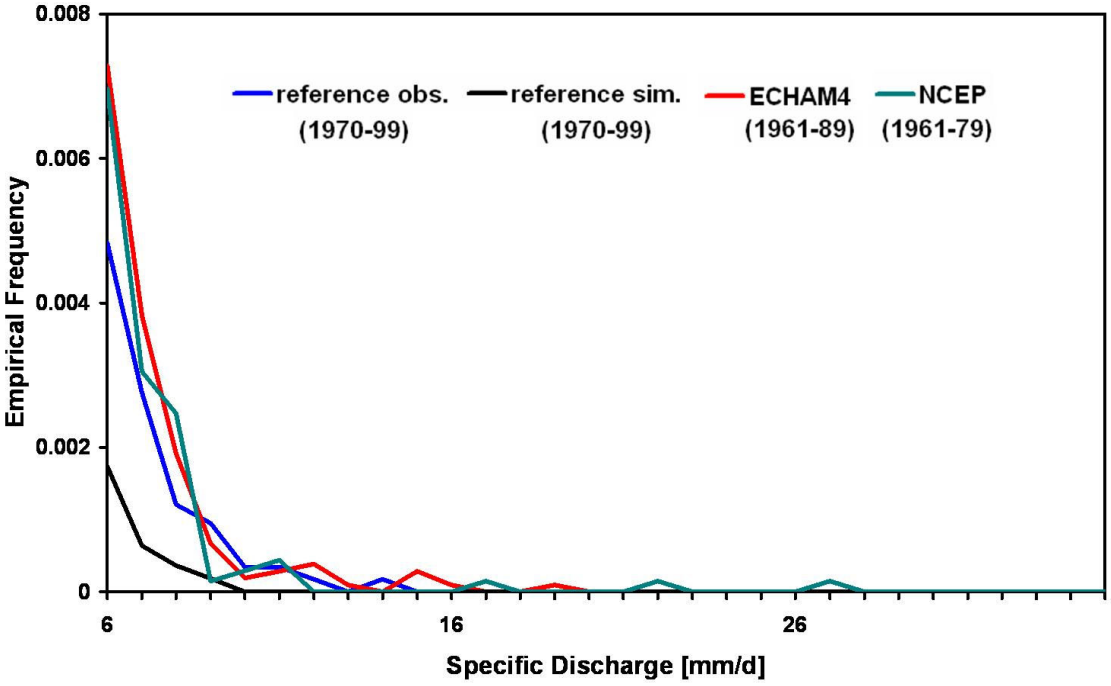

Figure VI-31: Normalized empirical frequencies of daily specific discharge >5 mm/d in the UJC (at gauge Yoseph Bridge, class width 1 mm/d)

The validation of evapotranspiration is difficult as no measurements are available. Simulated mean annual values of evapotranspiration are 437.3 mm for the station based simulations, 398.8 mm for the control run and 390.1 mm for the reanalysis (Figure VI-26), monthly mean values are illustrated in Figure VI-32. The higher value of the station based simulation can be explained by the higher temperatures (see monthly mean temperatures in Figure VI-33 and frequencies of daily temperatures in Figure VI-34). Again, the estimation of the real mean temperature over the UJC is difficult to estimate. On the one hand a little cold bias produced by MM5 within the control run and the reanalysis can be found as described in VI.2. On the other hand the interpolation of the station data produces very likely overestimation of temperatures in higher altitudes (see chapter IV.4). Extreme extrapolations have to be done as the highest station is located at 690 m asl.

Calculations for evaporation have been done by RIMMER et al. (2008). They were based on three long term (1970 - 2000) pan A evaporation measurements (PONCE, 1989). They estimated the total potential evapotranspiration in the UJC of about 1000 - 1200 mm. This fits well to the calculations in WaSiM of about 1200 mm for the control run, the station based simulations as well as for the reanalysis. The calculated real evaporation in the model HYMKE is with 226 mm well below the simulations with

WaSiM. However, this is a calibrated value to fit the mass balance, while in WaSiM with Penman-Monteith a more physically based approach is used.

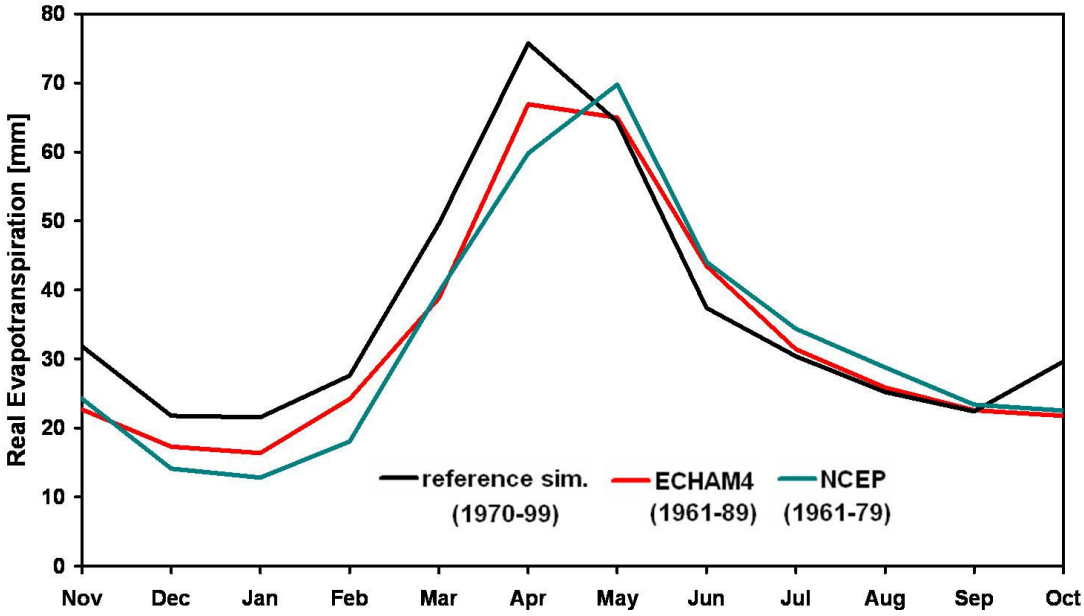

Figure VI-32: Monthly mean evapotranspiration in the UJC

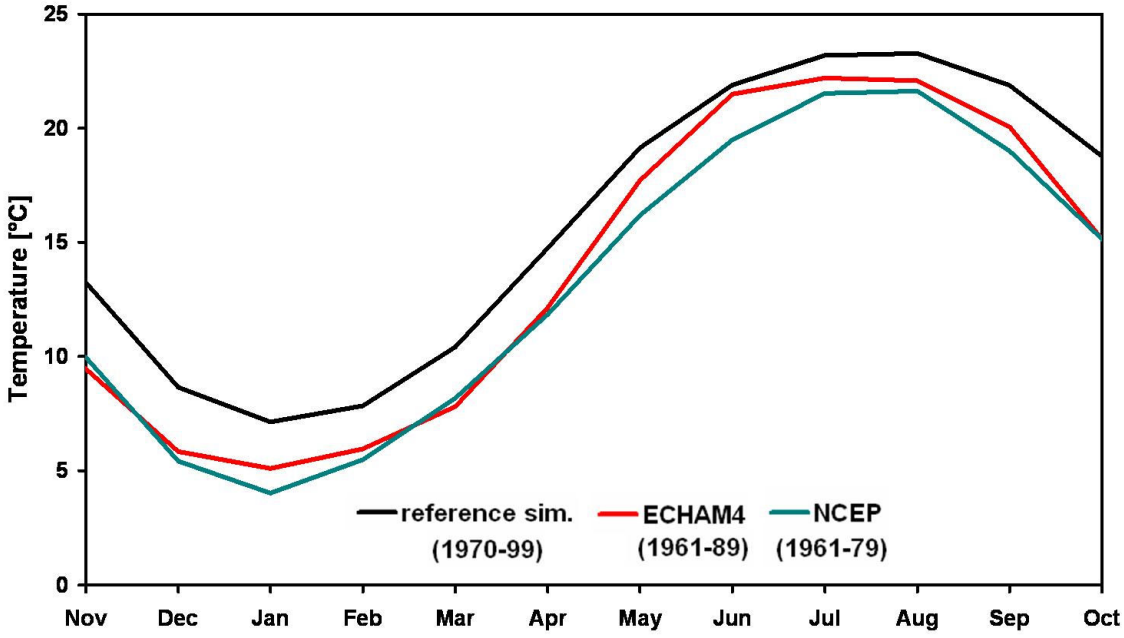

Figure VI-33: Monthly mean temperature in the UJC

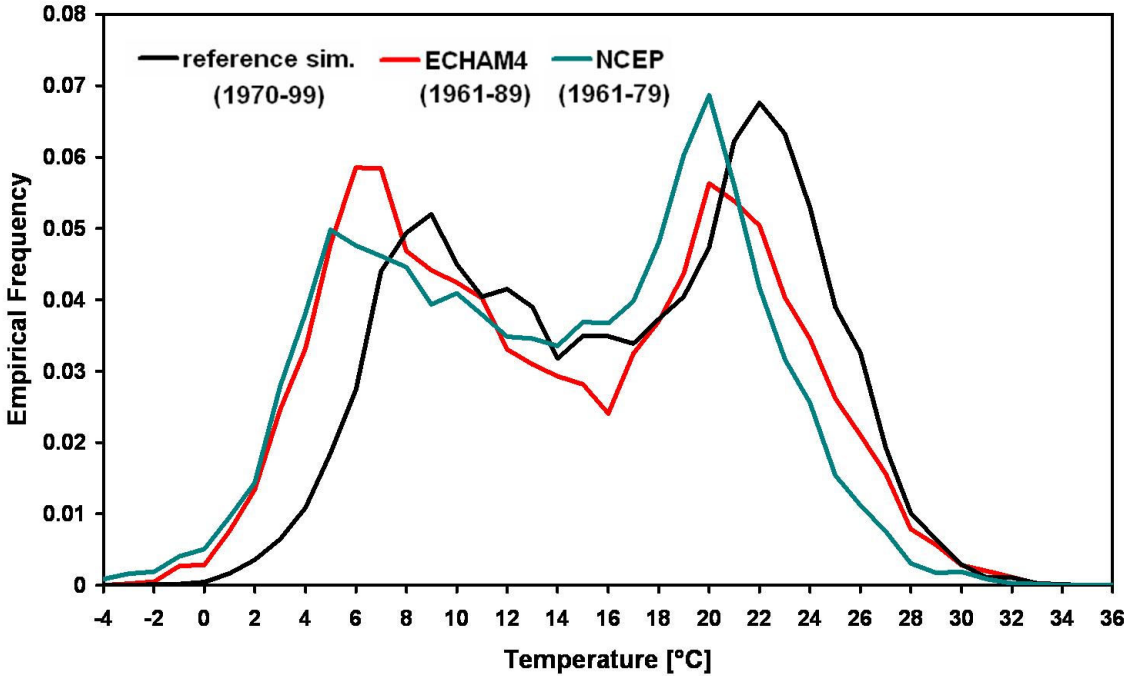

Figure VI-34: Normalized empirical frequencies of daily temperatures

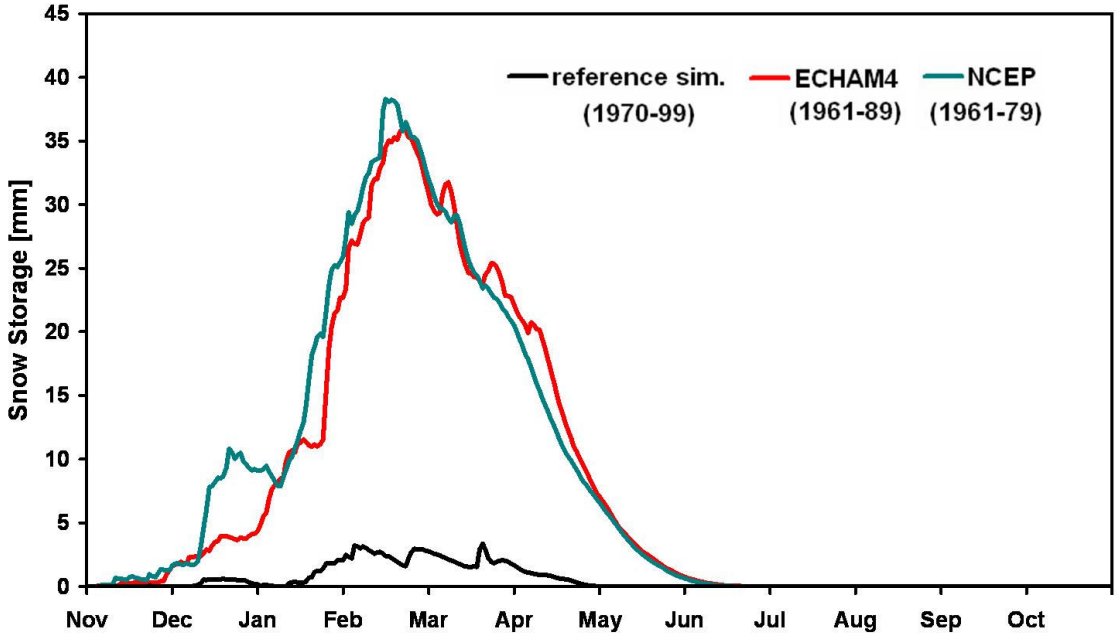

Figure VI-35: Mean snow storage

The uncertain estimation of temperatures in higher elevations effects the simulation of the snow storage. It is very likely that the station based simulations underestimate the snow storage while the control run of ECHAM4 and the NCEP reanalysis overestimate due to the cold bias. Again reanalysis and the control run show very similar results.

In summary it can be said, that the joint climate-hydrology simulations show reasonable results allowing in a next step for estimations for future changes based on scenario forcing. Some differences between the results based on simulated climate data input (ECHAM4 and NCEP) and based on station data input accompanied by the similarity between the ECHAM4 and NCEP results remain. This means that the different characteristics between MM5 output (spatial mean) and station data (punctual information) accompanied with the different interpolation over the UJC due to height and location of the (virtual) stations generate more uncertainties than the difference between the driving forces NCEP and ECHAM4.

VI.6 Discussion of Uncertainties

When using models, which are representing only a simplified abstract view of the complex reality, uncertainties have to be considered. The situation is getting even more complex when they are implemented trying to make projections to an unknown future.

Within the present study a chain of succeeding models is applied using simulation results of the preceding model. This implicates numerous sources of uncertainties, which will be discussed in the following.

Some of the uncertainties are tried to be minimized in case of the used models in this study. In other cases, when model output from other sources is implemented, no influence is exerted on the results.

Observations

The quality of a model can only be as good as their input data. Therefore, the first discussed source of uncertainties is observational data. It is caused by measurement errors and sparseness of stations. When station data should be used in a distributed model or compared to model output, interpolation of the station data is needed. This introduces another source of uncertainty, especially when station intensity is low.

In this study observational data are used for validation of the global and regional climate model. In case of the hydrological model numerous observations are implemented for setup, calibration and validation.

For the calibration and the validation WaSiM is driven by meteorological station data. The most crucial input variable for hydrological modeling is precipitation. For the UJC

11 rainfall gages in daily resolution are available (see Table V-1 and Figure V-4). Solely 3 of them are located inside the UJC, another 2 at least directly adjacent to the watershed of the UJC. The rest of them are up to 30 km away from the research area. The bigger the distance of the stations to the investigated area, the more worsened is the ability of an interpolation to reproduce the realistic precipitation pattern. Rainfall in the UJC is predominantly cyclonal. The tracks of the cyclones are prevailing from west to the east accompanied with orographical precipitation effects upwind of the Hermon ridge. An interpolation method has to be chosen that is able to reproduce these effects on height dependence of rainfall amounts. However, the 5 stations inside or next to the UJC do not fully represent the range of elevations in the basin from 80 to 2814 m asl. The highest station is Allone Bashan with 940 m asl. Therefore, rainfall amounts have to be extrapolated. The absence of rain gages at higher regions and the top of the Mount Hermon is the biggest deficit in the metrological equipment of the region. Within the project GLOWA Jordan River this problem was recognized and two climate stations have been installed at 2082 m asl and about 1600 m asl. Due to recording interruptions, measurements are too short to derive more exact gradients. The implemented interpolation method with 50 % IDW and 50 % height dependent regression for precipitation data is assessed to be the most appropriate approach considering the available gauges and their location within and around the investigation area. However, it is most likely that maximum precipitation is not reached at the top of Mount Hermon, as it is produced by the interpolation, but some hundreds of meters below (personal communication Hydrological Service Israel). In contrast to the uncertainties due to the unknown precipitation pattern in higher regions the low density of stations is less problematic. In general this implicates that small scale precipitation events are not considered or are transferred to other regions by interpolation. In the case of the UJC cyclonal precipitation have more large scale character and their intensities differ predominantly by orographical effects. Small scale convective events like in summer of the mid-latitudes are rare due to the persistent inversion in the region and their effect to the discharge behavior negligible.

Besides precipitation temperature, relative humidity, wind and global radiation is needed as driving input of WaSiM. For this study 8 climate stations are available, only one of them delivers global radiation. In contrast to the rain gages these stations are with 20 – 80 km even more distant to the UJC. This allocation of climate stations is considered to be problematic due to the steep climatic gradients of the region. Temperature is after the rainfall the most important climate variable since it controls impor-

tant components of the water balance like evapotranspiration, snow accumulation, and snow melt. Temperature has also the clearest correlation to elevation of all required climate variables. Therefore, with the interpolation method of 50 % IDW and 50 % height dependent regression it is tried to overcome the uncertainties introduced by the wide spread allocation of gauging stations.

Especially for temperature the time step of 24 hours is another weak point. Though the hydrological model simulates day and night temperatures, inaccuracies can be evoked in the snow simulations at temperatures ranging about the threshold temperatures for snowfall and snowmelt.

The available recording periods of the climate stations are yet another source effecting possible uncertainties in hydrological modeling. While for precipitation long time records of more than 30 years are available for numerous stations, other climate variables are very limited. Therefore, it is only possible to utilize the hydrological years 1996 – 1999 for calibration and validation. Although during this period all typical meteorological and hydrological phenomena (wet and dry season, high and low water periods, as well as accumulation and depletion of the snow layer, and with 1999 an extremely dry year) are considered, even longer calibration and validation periods would sustain verification of the model's parameterization and performance.

Besides the meteorological input data various hydrological data are considered. For testing the model's performance observations of discharge gages are used. With 6 gages within the UJC the investigation area is well equipped. The discharge data are for long term records without noteworthy breaks available and represent well the characteristics of the UJC: The gauges at Ayun and Sa'ar stand for periodic discharge limited to rain events during the rainy season. In contrast, the gage at the Dan is solely spring fed representing the characteristics of the karst aquifer. In addition there are the two gages at Banias and Snir, which are as well spring fed as reacting directly to rainfall events. Constraints in their quality have to be mentioned according to unknown consumption; especially at the gages Banias and Yoseph Bridge (see chapter V.2.1. and Figure V-5). This hampers the appraisement of the overestimation found in the joint climate-hydrology simulations (see chapter VI.5 and Figure VI-29).

In contrast to the well equipped discharge gages there is a lack in the availability on information about the subsurface conditions. This turns out as the biggest weak point for the modeling of the water balance in the UJC. The region is characterized by the

extensive karstic aquifer. However, its spatial extension and depth is unknown. Additionally, there are no groundwater level observations available. Solely information about springs within the UJC can be implemented as hydraulic heads. Conclusions about the dynamic of the aquifer can be drawn from the Dan spring, which is gaged. Springs outside the UJC indicate subsurface outflow of the region. The parameterization of the unsaturated zone is complicated by missing information on soil properties and geological conditions as the used soil maps are very coarse and no information on spells is available.

Similar is the situation for modeling the snow. There is no data on snow depth at different elevation or snow lines on Mount Hermon available. This hampers the calibration of the snow model.

Validation of the global and regional model output is done by comparison of gridded station data. The quality of these gridded datasets strongly depends on the number and spatial distribution of station observations. E.g., the interpolation of precipitation data to the grid of domain 2 (see Figure VI-7), which is also used for the bias correction of the downscaled rainfall by MM5, is in good agreement to the CRU data in 10' resolution. As both data sets are very similar, it is assumed that the amounts and the pattern of rainfall of the Jordan River region are representative and reasonable.

Emission Scenarios

Emission scenarios are the first link of the chain of models used for climate projections and thus their first source of uncertainty. This is simply due to the unknown future development of demography, technologies, and socio-economics, and the subsequent emissions of greenhouse gases and aerosols. The conversion of the scenario's assumptions to atmospheric concentrations and effects on radiative forcing are an additional source of uncertainty (GIORGI et al., 2001). In principle the IPCC scenarios are to be treated as equally probable. With the selection of the scenarios A2 and B2 as a more optimistic and a more pessimistic one it is tried to cover a wide range of possible future developments.

Global Climate Model

At global climate models internal uncertainties are found. The quality of an AOGCM stands out due to their ability to reproduce all important atmospheric and oceanic proc-

esses. The challenges of global climate modeling consist of the chaotic nature of the atmospheric processes, the variety of processes that are involved in long term simulations. These are atmospheric, oceanic as well as land surface related processes. Furthermore, natural and anthropogenic processes have to be considered (BENGTSSON, 2003). Due to their coarse resolution not all processes can be simulated physically based and have to be parameterized. Therefore, uncertainties within AOGCMs can mainly be traced back to resolution and parameterization inaccuracies. Several studies, e.g. by GIORGI AND FRANCISCO (2000), showed that the dominant source of uncertainty when examining GCMs on a regional scale is found in inter-model variability more than in inter-scenario or internal model variability. An example that the reproduction of realistic climate conditions by a global model is a difficult task can be given in this study: Although in reanalysis data like the used one of NCEP observations are implemented, this does not imperatively mean that the simulations correspond well with observations. In this case underestimation of precipitation in the Jordan River region is that high, that the dataset cannot be utilized for validation of climate simulation.

For the AOGCM ECHAM4/OPYC3 that is used in this study a little warm bias is found for the Jordan River region. Furthermore, the validation of the precipitation shows a bias in the seasonality which is that severe that a bias correction has to be performed for further use of the data in hydrology.

Regional Climate Model

Like for global climate models, intrinsic uncertainties exist also in regional climate models. That is due to deficient knowledge or representation of physical processes, limitations due to numerical approximations of physical equations, as well as assumptions or simplifications of parameterization schemes. Differing from global models there are additional uncertainties concerning limited area models consisting of the spatial resolution or the domain choice (KOTLARSKI et al., 2005).

The validation of the regional climate simulations (see chapter VI.2) shows that via error propagation the seasonal bias in precipitation is also found in the MM5 results. Analysis of the temperature displays a small cold bias produced by MM5 compensating the warm bias of ECHAM4 a little. The influence of the domain choice is tested in chapter V.1.1, but turns out in this case as insignificant. In contrast, the domain size has big influence on the amount and distribution of precipitation. The higher the resolution the better the orographical effects, that are crucial in this region, can be reproduced.

The most promising approach for the uncertainty analysis of regional climate change projections is the evaluation of multi-model ensembles. Ensemble runs mean the use either of different models or of one model with different parameterizations, initial conditions, lateral and lower boundary conditions, or resolutions. For a complete uncertainty analysis of regional climate changes projections at least two different emissions scenarios, two different global climate models and two different regional climate models should be considered. Therefore, the decision was made to perform high resolution (18 x 18 km²) eregional climate model runs based on two extreme scenarios for hydrological impact analysis. Within the GLOWA Jordan River project a full evaluation of uncertainties can be done as additionally to this work the RCM RegCM2 and the scenario A1B based on the GCMs ECHAM5 and HadCM3 are used.

Hydrological Model

As the goal of hydrological modeling in this study is the investigation of climate impact to the water cycle the demand to the hydrological model is a high degree of transferability to different climate conditions. Furthermore, the complex interactions of surface and subsurface runoff components in the UJC should be considered to gain a better process understanding. Therefore, with WaSiM a mainly physically based hydrological model is chosen.

The internal uncertainties of every model approach that has been mentioned already for the global and regional climate models hold also for the hydrological model.

The model is built for porous aquifers, while the UJC is characterized by karstic conditions. The karst aquifer is represented by the combination of the 2D-groundwater model and the implementation of an artificial bypass in the routing model (see chapter V.2.2). Therefore, subsurface processes can not be described physically based. However, this is also the case for the runoff generation of the direct runoff and the interflow which use lumped approaches, either. This does not hamper the model's transferability to changed climate conditions as processes that are of more importance like evapotranspiration and snow dynamics are not afflicted by the modifications implemented for discharge generation.

The transmission of climate data from the regional climate model to the hydrological model adds additional uncertainty by the interpolation of the meteorological fields of the RCM to the finer grid of WaSiM. With the chosen interpolation method of 50% IDW and

50% height dependent regression differences between the observational data input and the RCM output in the precipitation pattern is minimized. However, the important role of the interpolation method for a distributed model was already mentioned in the chapters VI.4 and IV.5. It was shown that the altered combination of station data changed the temperature distribution in a manner that considerable consequences in the modeling of other variables like snow occurred. Outstanding is the detection that more uncertainties are generated by the difference between measured and simulated climate data accompanied with the different interpolation over the UJC due to height and location of the (virtual) stations than by the difference between the driving forces NCEP and ECHAM4.

Neglected Impacts on Regional Climate

A last source of uncertainty that will be discussed here are processes that are neglected in the models.

First there has to be mentioned the missing consideration of dust. Dust forced cooling/warming of the atmosphere varies as the dust layer ascends or descends. Insufficient knowledge about three-dimensional knowledge about three-dimensional distribution of dust may cause significant errors in the determination of its effect on climate and global warming prediction. In the climate models aerosols are implemented, but no special dust model like the dust prediction approach by ALPERT et al. (2004a) is considered. The Eastern Mediterranean is regularly affected by Saharan dust that is transported by southern winds, especially by Sharav Lows in spring and early summer. It is assumed that Saharan dust has considerable influence on the climate conditions of the research area at local and regional scales.

Another neglected process is land use change. The global impact on land use changes by altering the greenhouse gas concentrations in the atmosphere is considered in the emission scenarios. in the regional climate and hydrological modeling it is not implemented. Land use changes can have significant impact on the atmosphere through feedback mechanisms (e.g. albedo) and on hydrological behavior (e.g. infiltration) on local and regional scale. In case of the UJC the influence on land use changes in the future is assumed to be insignificant as the major part of the region is very mountainous and consists of grassland with poorly developed soils. Therefore, it is not of interest for further agriculture or settlement.

In addition to this chapter, where uncertainties are more qualitatively discussed, in chapter VII.3.3 the uncertainties of the model chain in comparison to the climate change signal are illustrated in a quantitative manner.

VII Climate Change and Impact Analysis

On the basis of the validation (chapter VI) the ability of the modeling approach to simulate properly the regional climate and terrestrial hydrology of the UJC is shown and the model induced uncertainties are discussed. Thus, it can be used for analysis of future climate change analysis. With the consideration of two different IPCC emissions scenarios (A2 and B2) the investigation of another source of uncertainties is enabled, namely the uncertainty of unknown future anthropogenic greenhouse gas emissions.

In this chapter the impact of increasing greenhouse gas concentrations based on two extreme scenarios and the resulting global climate change to regional climate and water balance in the Eastern Mediterranean and in particular in the Upper Jordan River is investigated.

First numerous station data within the research area are tested for recent climate trends (chapter VII.1). Afterwards the results of the regional climate simulations are analyzed (chapter VII.2) and subsequently the findings of the joint regional climate-hydrology simulations within the UJC (chapter VII.3). Finally, the results are discussed in chapter VII.4.

Since simulations are performed transient from 1961 to 2099 two approaches to investigate climate change signals of several climatic and hydrological variables can be applied: On the one hand time slices of present and future climate can be compared. The most common time span in climate research is 30 years assuming that within this period natural variability is included and a representative mean climate is displayed. In this study present climate is represented by the control period 1961 – 1989, which has been validated to its ability to reproduce real climate conditions in chapter VI. For future climate two time slices are chosen from 2021 – 2050 and from 2070 – 2099, further on referred to as near and far future, respectively. Another possibility offered by transient simulation is the analysis of long year time series.

Climate change signals are superimposed by natural climate variability. They are defined as deviations from mean climate exceeding natural variability. The variability of climatic and hydrological variables is considered within the analysis by calculating the standard deviation and the variations coefficient (ratio between standard deviation and mean). The significance of climate change signals is tested in case of time slice analy-

sis by a signal to noise ratio, in case of time series analysis by trend analysis after Mann-Kendall (for the description of the methods see chapter IV.7).

VII.1 Observed Regional Climate Change

Due to the heterogeneous picture on climate trends given in the literature (see chapter II.1.3), besides the analysis of the regional climate simulations some additional trend tests on different climate variables are performed for station data. For this purpose 15 climate stations within Israel have been chosen (Figure VII-1), where data are available for the same time period of 46 years for the years 1958 – 2003. Their spatial distribution represents well the small scale climate regions of the area with more humid conditions in the mountainous north and very dry climate in the very south, as well as more maritime climate at the coast in contrast to the continental conditions in the eastern parts. Tested variables are precipitation, as well as mean, minimum and maximum temperature for annual and seasonal values.

Table VII-1 and Table VII-2 show for each variable beside the change per 10 years and the significance of the trend additionally the mean values, the standard deviation and the coefficient of variation CV, which is defined as the ratio of the standard deviation to the mean.

Mean findings are:

- Three of the 15 investigated stations show negative trends in precipitation. But significance can only be found in spring at the station Quiyat Anavim and in autumn at station Beer Sheva. This fits well to the findings of FREIWAN and KADIOGLU (2008), who also could not find much significance in precipitation trends.

- In all stations a slightly increase in mean temperatures can be seen and at most stations these trends are significant.

- Especially for summer and autumn, mean temperature increasing trends are significant, while increasing mean spring temperature are insignificant and winter mean temperatures are unchanged.

- Like for the mean temperatures significant increasing trends in maximum temperatures are concentrated on summer and autumn.

- The main role in increase of temperature play the minimum temperatures, which are significant at yearly values for almost every station. Again changes are distinct especially in summer and autumn, while increases in spring are less and in winter not significant.

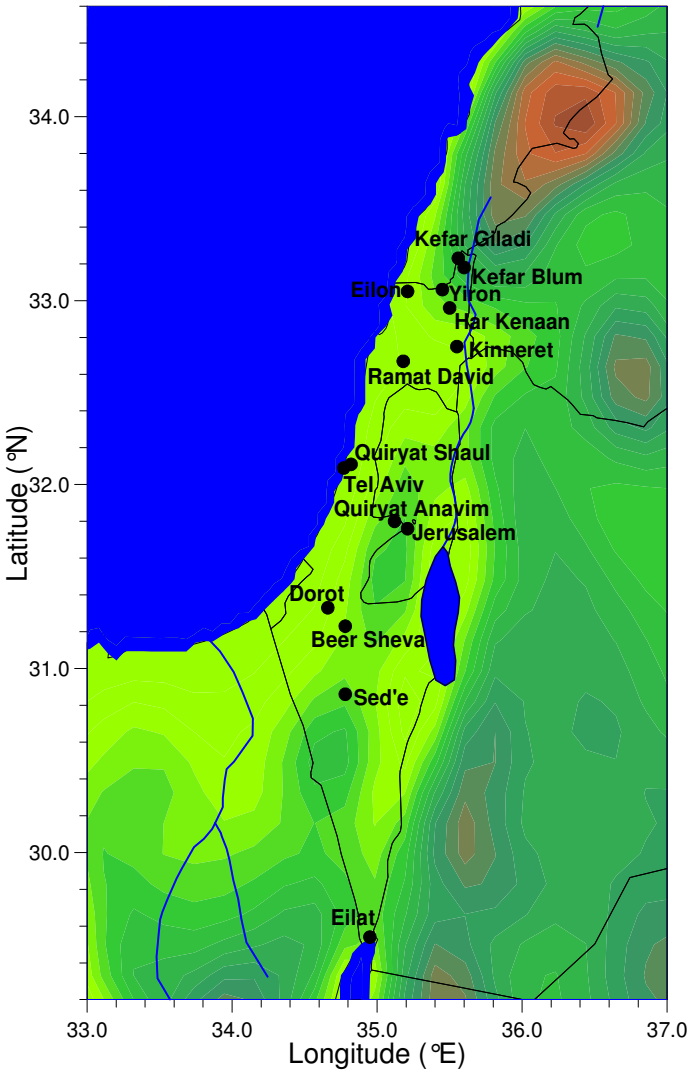

Figure VII-1: Climate stations for trend analysis

Table VII-1: Trend statistics for observations of precipitation and mean temperature

Precipitation

Station	YEAR					MAM					JJA					SON					DJF				
	MEAN [mm]	STDEV [mm]	CV [%]	CHANGE [mm/10y]	*)	MEAN [mm]	STDEV [mm]	CV [%]	CHANGE [mm/10y]	*)	MEAN [mm]	STDEV [mm]	CV [%]	CHANGE [mm/10y]	*)	MEAN [mm]	STDEV [mm]	CV [%]	CHANGE [mm/10y]	*)	MEAN [mm]	STDEV [mm]	CV [%]	CHANGE [mm/10y]	*)
Har Kenaan	698,7	159	22,8	8,6		139,9	61,6	44	-0,8							108,6	71,5	65,8	7,9		449,1	136,8	30,5	-6,8	
Tel Aviv	518,6	171,6	33,1	2,5		73,6	40,7	55,3	5,3							101,5	83,3	82,1	-6,8		343,2	135,8	39,6	-5,9	
Jerusalem	538,1	168,1	31,2	14,7		120,7	60,1	49,8	2,7							72	57	79,2	0,3		345,2	134,5	39	6,5	
Elat	27,2	17,9	65,8	-2,4		6,9	8,5	123,2	-0,3							6,2	9	145,2	0		14,1	15,8	112,1	-0,4	
Eilon	801,5	180,4	22,5	30,9		144,1	62,2	43,2	5,6							143,8	79,4	55,2	8,4		511,7	153,3	30	11,4	
Yiron	770,4	191,7	24,9	6,6		171,5	86,4	50,4	-4,4							122,2	69,4	56,8	10,4		475,9	143,6	30,2	-12,2	
Kefar Galad	787,9	205,5	26,1	6		176,7	82,7	46,8	1							123,6	70,2	56,8	7,6		485,6	162,1	33,4	0,2	
Kefar Blum	528,7	128,7	24,3	9,6		112,9	48,1	42,6	-1,9							86	52,6	61,2	5,9		328,8	107,4	32,7	-0,9	
Kinneret	399,9	117,5	29,4	-11,5		84,2	37,4	44,4	-4,8							61,7	44,7	72,4	-1,1		253,8	91,6	36,1	-3,6	
Qiryant-Shaul	566,8	182,6	32,2	10,4		88,9	39,8	44,8	6,8	+						111,9	93,9	83,9	-6,4		365,6	141,4	38,7	11,7	
Qiryant-Anav	692,7	209,4	30,2	23,5		145,9	63,5	43,5	4,9							97,9	76,5	78,1	6		448,7	169,3	37,7	8,5	
Dorot	367	142,8	38,9	24,3		60,9	37,9	62,2	1,9							61,6	53,7	87,2	1,1		244,3	110,9	45,4	9,9	
Sede	110,2	52,3	47,5	4		26,9	20,3	75,5	1,7							16,2	18,1	111,7	-1,5		67,1	42,1	62,7	2,6	
Ramat-David	525,6	127	24,2	-1,1		96,6	42,6	44,1	-2,3							82,5	60,6	73,5	3,4		346	110,9	32,1	-12,1	
Beer-Sheva	200,4	77,5	38,7	1,8		43	27,5	64	1,9							27,1	26,5	97,8	-4,2	*	130,3	61,7	47,4	1	

Temperature, mean

Station	YEAR					MAM					JJA					SON					DJF				
	MEAN [°C]	STDEV [K]	CV [%]	CHANGE [K/10y]	*)	MEAN [°C]	STDEV [K]	CV [%]	CHANGE [K/10y]	*)	MEAN [°C]	STDEV [K]	CV [%]	CHANGE [K/10y]	*)	MEAN [°C]	STDEV [K]	CV [%]	CHANGE [K/10y]	*)	MEAN [°C]	STDEV [K]	CV [%]	CHANGE [K/10y]	*)
Har Kenaan	16,4	0,7	4,3	0,2		15	1	6,7	0,2		23,8	0,9	3,8	0,2		18,7	0,9	4,8	0,1		7,9	1	12,7	0	
Tel Aviv	20,1	0,5	2,5	0,2	*	18,4	0,7	3,8	0,1		25,4	0,5	2	0,2	***	22,5	0,7	3,1	0,2	***	14,2	0,7	4,9	0,1	
Jerusalem	17,6	0,7	4	0,2	+	16,6	0,9	5,4	0,1		23,7	0,8	3,4	0,2	+	19,9	0,9	4,5	0,2	*	10,1	1,1	10,9	-0,1	
Elat	24,9	0,6	2,4	0,2	*	24,3	0,7	2,9	0,1		32,3	0,6	1,9	0,2	*	26,5	0,8	3	0,2	*	16,3	0,9	5,5	0	
Eilon	18,4	0,7	3,8	0,2		17	1	5,9	0,2		25,8	0,9	3,5	0,2		20,7	0,9	4,3	0,1		9,9	1	10,1	0	
Yiron	17,4	0,7	4	0,2		16	1	6,3	0,2		24,8	0,9	3,6	0,2		19,7	0,9	4,6	0,1		8,9	1	11,2	0	
Kefar Galad	18,4	0,7	3,8	0,2		17	1	5,9	0,2		25,8	0,9	3,5	0,2		20,7	0,9	4,3	0,1		9,9	1	10,1	0	
Kefar Blum	18,9	0,7	3,7	0,2		17,5	1	5,7	0,2		26,3	0,9	3,4	0,2		21,2	0,9	4,2	0,1		10,4	1	9,6	0	
Kinneret	18,4	0,6	3,3	0,1		17	0,9	5,3	0,1		25,6	0,7	2,7	0,2	+	20,7	0,8	3,9	0,1		10,2	0,9	8,8	-0,1	
Qiryant-Shaul	18,9	0,6	3,2	0,2	*	17,5	0,8	4,6	0,1		24,6	0,6	2,4	0,2	***	21,2	0,8	3,8	0,3	***	12,2	0,9	7,4	0	
Qiryant-Anav	18,6	0,7	3,8	0,2	+	17,6	0,9	5,1	0,1		24,7	0,8	3,2	0,2	+	20,9	0,9	4,3	0,2	*	11,1	1,1	9,9	-0,1	
Dorot	21,6	0,6	2,8	0,1	*	20,8	0,9	4,3	0,1		28	0,6	2,1	0,2	*	23,5	0,8	3,4	0,3	***	13,9	0,9	6,5	0	
Sede	19,4	0,6	3,1	0,1	*	18,6	0,9	4,8	0,1		25,8	0,6	2,3	0,2	*	21,3	0,8	3,8	0,3	***	11,7	0,9	7,7	0	
Ramat-David	20,4	0,5	2,5	0,1		18,9	0,8	4,2	0,1		27,3	0,5	1,8	0		22,6	0,7	3,1	0,1		12,5	0,8	6,4	0	
Beer-Sheva	20,6	0,6	2,9	0,1	*	19,8	0,9	4,5	0,1		27	0,6	2,2	0,2	*	22,5	0,8	3,6	0,3	***	12,9	0,9	7	0	

***) trends at significance levels α = 0.001: ***, α = 0.01: **, α = 0.05: *, α = 0.1: +**

Table VII-2: Trend statistics for observations of maximum and minimum temperature

Temperature, min																							
Station	YEAR					MAM					JJA					SON					DJF			
	MEAN [°C]	STDEV [K]	CV [%]	CHANGE [K/10y]	*)	MEAN [°C]	STDEV [K]	CV [%]	CHANGE [K/10y]	*)	MEAN [°C]	STDEV [K]	CV [%]	CHANGE [K/10y]	*)	MEAN [°C]	STDEV [K]	CV [%]	CHANGE [K/10y]	*)	MEAN [°C]	STDEV [K]	CV [%]	CHANGE [K/10y]	*)
Har Kenaan	12,1	0,6	5	0,2	*	10,4	0,9	8,7	0,2		18,1	0,8	4,4	0,2	***	14,4	0,8	5,6	0,1		5,2	0,9	17,3	0,1	
Tel Aviv	16,2	0,6	3,7	0,2	***	14,2	0,8	5,6	0,1		22	0,6	2,7	0,2	****	18,3	0,9	4,9	0,3	****	10,1	0,8	7,9	0,1	
Jerusalem	13,5	0,6	4,4	0,1	+	12,3	0,9	7,3	0,1		18,8	0,7	3,7	0,1		15,8	0,8	5,1	0,2	+	7,2	0,9	12,5	-0,1	
Elat	18,5	0,6	3,2	0,1		17,7	0,7	4	0		25,2	0,7	2,8	0,2	*	20,3	0,9	4,4	0,2		10,6	0,8	7,5	0	
Eilon	14,1	0,6	4,3	0,2	*	12,4	0,9	7,3	0,2		20,1	0,8	4	0,2	**	16,4	0,8	4,9	0,1		7,2	0,9	12,5	0,1	
Yiron	13,1	0,6	4,6	0,2	*	11,4	0,9	7,9	0,2		19,1	0,8	4,2	0,2	**	15,4	0,8	5,2	0,1		6,2	0,9	14,5	0,1	
Kefar Galad	14,1	0,6	4,3	0,2	*	12,4	0,9	7,3	0,2		20,1	0,8	4	0,2	**	16,4	0,8	4,9	0,1		7,2	0,9	12,5	0,1	
Kefar Blum	14,6	0,6	4,1	0,2	*	12,9	0,9	7	0,2		20,6	0,8	3,9	0,2	**	16,9	0,8	4,7	0,1		7,7	0,9	11,7	0,1	
Kinneret	12,6	0,5	4	0,3	****	10,7	0,8	7,5	0,2	***	19,1	0,7	3,7	0,3	****	14,6	0,7	4,8	0,3	***	5,8	0,8	13,8	0,1	
Qiryant-Shaut	14,9	0,6	4	0,2	***	13,3	0,8	6	0,1		20,4	0,6	2,9	0,2	***	17,1	0,8	4,7	0,3	***	8,7	0,8	9,2	0,1	
Qiryant-Anav	14,5	0,6	4,1	0,1	+	13,3	0,9	6,8	0,1		19,8	0,7	3,5	0,1		16,8	0,8	4,8	0,2	+	8,2	0,9	11	-0,1	
Dorot	14	0,6	4,3	0,3	****	12,6	0,8	6,3	0,2	+	19,6	0,8	4,1	0,4	****	15,7	0,9	5,7	0,4	****	7,9	0,8	10,1	0	
Sede	11,8	0,6	5,1	0,3	****	10,4	0,8	7,7	0,2	+	17,4	0,8	4,6	0,4	****	13,5	0,9	6,7	0,4	****	5,7	0,8	14	0	
Ramat-David	13,1	0,6	4,6	0,3	****	10,9	0,7	6,4	0,3	****	20	0,7	3,5	0,4	****	14,8	0,8	5,4	0,3	****	6,5	0,8	12,3	0,1	
Beer-Sheva	13	0,6	4,6	0,3	****	11,6	0,8	6,9	0,2	+	18,6	0,8	4,3	0,4	****	14,7	0,9	6,1	0,4	****	6,9	0,8	11,6	0	

Temperature, max																							
Station	YEAR					MAM					JJA					SON					DJF			
	MEAN [°C]	STDEV [K]	CV [%]	CHANGE [K/10y]	*)	MEAN [°C]	STDEV [K]	CV [%]	CHANGE [K/10y]	*)	MEAN [°C]	STDEV [K]	CV [%]	CHANGE [K/10y]	*)	MEAN [°C]	STDEV [K]	CV [%]	CHANGE [K/10y]	*)	MEAN [°C]	STDEV [K]	CV [%]	CHANGE [K/10y]	*)
Har Kenaan	24,1	0,5	2,1	0,1		19,5	1,2	6,2	0,1		29,3	1	3,4	0,1		22,9	1	4,4	0,1		10,5	1,1	10,5	-0,1	
Tel Aviv	21,6	0,7	3,2	0,2		22,5	0,8	3,6	0		28,8	0,5	1,7	0,1	+	26,5	0,7	2,6	0,2	***	18,3	0,7	3,8	0	
Jerusalem	31,3	0,6	1,9	0,2	*	20,9	1	4,8	0,1		28,5	0,8	2,8	0,2	*	23,9	0,9	3,8	0,3	*	12,9	1,2	9,3	-0,1	
Elat	22,6	0,8	3,5	0,1		30,9	0,8	2,6	0,1		39,4	0,6	1,5	0,2	***	32,5	0,8	2,5	0,3	***	22,1	0,9	4,1	0	
Eilon	21,6	0,8	3,7	0,1		21,5	1,2	5,6	0,1		31,3	1	3,2	0,1		24,9	1	4	0,1		12,5	1,1	8,8	-0,1	
Yiron	22,6	0,8	3,5	0,1		20,5	1,2	5,9	0,1		30,3	1	3,3	0,1		23,9	1	4,2	0,1		11,5	1,1	9,6	-0,1	
Kefar Galad	23,1	0,8	3,5	0,1		21,5	1,2	5,6	0,1		31,3	1	3,2	0,1		24,9	1	4	0,1		12,5	1,1	8,8	-0,1	
Kefar Blum	23,3	0,7	3	0,1		22	1,2	5,5	0,1		31,8	1	3,1	0,1		25,4	1	3,9	0,1		13	1,1	8,5	-0,1	
Kinneret	22,8	0,6	2,6	0,1	*	22,2	1,1	5	0,1		30,8	0,8	2,6	0,1		25,8	0,9	3,5	0,2		14,2	1,1	7,7	-0,1	
Qiryant-Shaut	22,6	0,7	3,1	0,2		21,7	0,9	4,1	0,1		28,6	0,6	2,1	0,2	*	25,2	0,8	3,2	0,2	*	15,6	0,9	5,8	0	
Qiryant-Anav	27,1	0,6	2,2	0,2	+	21,9	1	4,6	0,1		29,5	0,8	2,7	0,2	*	24,9	0,9	3,6	0,3	*	13,9	1,2	8,6	-0,1	
Dorot	24,9	0,6	2,4	0,2	+	26,6	1	3,8	0,2		33,9	0,7	2,1	0,2	*	29,1	0,9	3,1	0,3	***	18,8	1,2	6,4	-0,1	
Sede	26	0,6	2,3	0,1		24,4	1	4,1	0,2		31,7	0,7	2,2	0,2	*	26,9	0,9	3,3	0,3	***	16,6	1,2	7,2	-0,1	
Ramat-David	26,1	0,6	2,3	0,2	+	24,9	1,1	4,4	0,1		32,3	0,7	2,2	0		28,7	0,8	2,8	0,2		17,9	1,1	6,1	0	
Beer-Sheva	20,6	0,6	2,9	0,1	*	25,6	1	3,9	0,2		32,9	0,7	2,1	0,2	*	28,1	0,9	3,2	0,3	***	17,8	1,2	6,7	-0,1	

) trends at significance levels α = 0.001: *, α = 0.01: **, α = 0.05: *, α = 0.1: +

VII.2 Expected Future Regional Climate Change

Analysis of the RCM simulations is limited to the output of the domain 2 with a horizontal resolution of 18 x 18 km². This is due to the fact that simulations in higher resolution of 6 x 6 km² are limited to time slices of 15 years (1961 – 1975 and 2085 – 2099). Thus they are too short to represent mean climate without natural fluctuations. Furthermore, validation is mainly based on this resolution and detected future climate change signals are therefore more comprehensible.

Analysis concentrates on temperature and precipitation as these variables have been validated before (see chapter VI.2).

Temperature

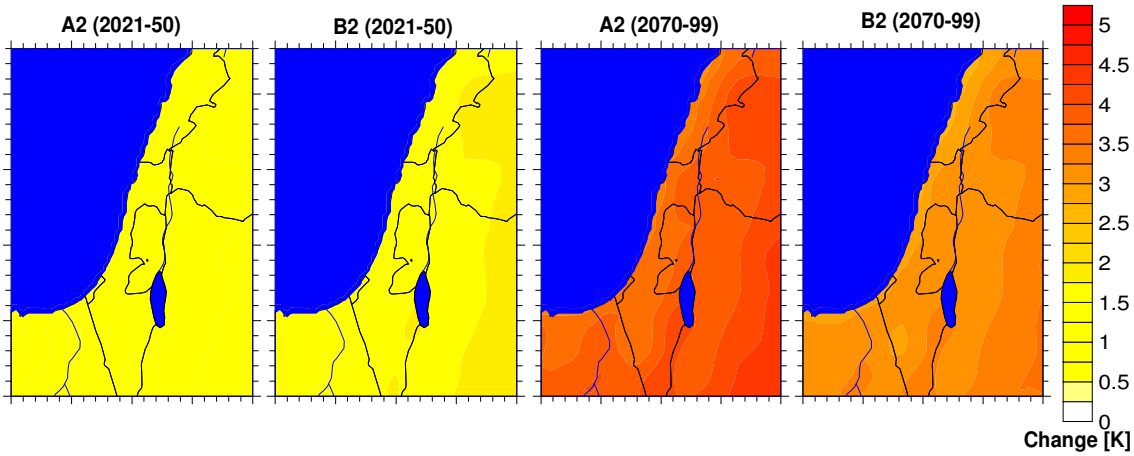

Figure VII-2: Mean temperature change of the scenarios A2 and B2 for the near and far future in comparison to the control period (1961 - 89)

Figure VII-2 shows the change of mean temperature for the Eastern Mediterranean for the near and far future in dependence of the emission scenario. For the near future changes are very homogenous over the considered area. Differences between the scenarios are very low. The increase of annual mean temperatures varies scenario and region depended between 1.3 and 1.7 K. In the far future increase in temperature is significantly higher for scenario A2 (about 3.8 K) than for B2 (about 3 K). Again no big differences within the region appear. When considering the four sub regions A to D from north to south (compare Figure VI-5) a little higher change is found in the southern parts (Table VII-3). Seasonal changes are for all sub regions, for all seasons and both scenarios positive (Figure VII-3). Temperature increases are higher in summer and autumn than in winter and spring. For the near future seasonal changes are compara-

ble between the scenarios like for annual values. The only exception is winter, where increase in scenario A2 is considerably lower (0.5 – 0.7 K) than in scenario B2 (1.6 – 1.7 K). In the far future positive temperature change signals of A2 exceed B2 in any season and sub region.

Table VII-3: Seasonal and annual temperature mean [°C], change [K], and signal to noise ratio [-] of the sub regions A – D for near and far future

	SCENARIO	A2					B2				
REGION		MAM	JJA	SON	DJF	YEAR	MAM	JJA	SON	DJF	YEAR
A	MEAN 1961-89	15.4	22.8	19	10.6	17	15.4	22.8	19	10.6	17
	MEAN 2021-50	16.6	24.4	20.9	11.3	18.3	16.7	24.8	20.7	11.9	18.5
	MEAN 2070-99	18.1	27	23.2	13.6	20.5	17.7	26.2	22.3	13	19.8
	ΔT 2021-50	1.2	1.6	1.9	0.7	1.3	1.3	2	1.7	1.3	1.6
	ΔT 2070-99	2.7	4.2	4.2	2.9	3.5	2.4	3.4	3.3	2.4	2.8
	SN 2021-50	1.66	2.1	2.12	0.92	3.01	1.77	2.67	1.93	1.7	3.53
	SN 2070-99	3.64	5.58	4.7	3.93	7.85	3.2	4.53	3.66	3.19	6.4
B	MEAN 1961-89	17	24.8	19.9	10.5	18.1	17	24.8	19.9	10.5	18.1
	MEAN 2021-50	18.3	26.6	22	11.1	19.5	18.3	27	21.8	11.7	19.7
	MEAN 2070-99	19.8	29.4	24.6	13.4	21.8	19.5	28.5	23.6	12.9	21.1
	ΔT 2021-50	1.3	1.7	2.1	0.6	1.4	1.3	2.1	2	1.2	1.6
	ΔT 2070-99	2.7	4.6	4.7	2.9	3.7	2.5	3.7	3.7	2.4	3.1
	SN 2021-50	1.64	2.13	2.17	0.65	3.01	1.68	2.58	2.02	1.36	3.48
	SN 2070-99	3.52	5.62	4.9	3.25	7.91	3.19	4.52	3.84	2.63	6.47
C	MEAN 1961-89	17.3	25.6	19.5	9.9	18.1	17.3	25.6	19.5	9.9	18.1
	MEAN 2021-50	18.6	27.3	21.6	10.4	19.5	18.7	27.7	21.5	11.2	19.7
	MEAN 2070-99	20.2	30.4	24.3	12.9	21.9	19.9	29.3	23.3	12.3	21.2
	ΔT 2021-50	1.3	1.8	2.1	0.6	1.4	1.4	2.1	2	1.3	1.7
	ΔT 2070-99	2.9	4.8	4.8	3	3.9	2.6	3.7	3.8	2.5	3.2
	SN 2021-50	1.53	2.37	2.15	0.55	2.98	1.57	2.8	2.01	1.24	3.46
	SN 2070-99	3.28	6.46	4.9	2.95	8	2.98	5.06	3.86	2.39	6.51
D	MEAN 1961-89	17.1	25.7	18.7	9.1	17.7	17.1	25.7	18.7	9.1	17.7
	MEAN 2021-50	18.5	27.5	20.9	9.6	19.1	18.5	27.8	20.8	10.3	19.4
	MEAN 2070-99	20.1	30.7	23.7	12.2	21.7	19.8	29.5	22.7	11.6	20.9
	ΔT 2021-50	1.4	1.8	2.2	0.5	1.5	1.4	2.1	2	1.3	1.7
	ΔT 2070-99	2.9	5	4.9	3.1	4	2.7	3.9	3.9	2.5	3.2
	SN 2021-50	1.5	2.7	2.14	0.46	3.04	1.53	3.11	2.01	1.12	3.52
	SN 2070-99	3.28	7.4	4.89	2.72	8.28	2.97	5.69	3.88	2.2	6.71

Mean temperatures do not show high variability as it can be seen from the annual time series in Figure VII-4. Therefore, analysis of the signal to noise ratio shows almost solely positive values indicating significant positive changes in temperature. Unique exception is the winter in the near future for scenario A2 (Table VII-3).

Analysis of mean temperature's time series (

Table VII-5) indicates steadily rising mean, minimum, and maximum temperatures with very low variability (variations coefficient ranging from 2.8 to 7.7 %) and an increase of 0.21 – 0.34 K / 10 years. All changes are highly significant.

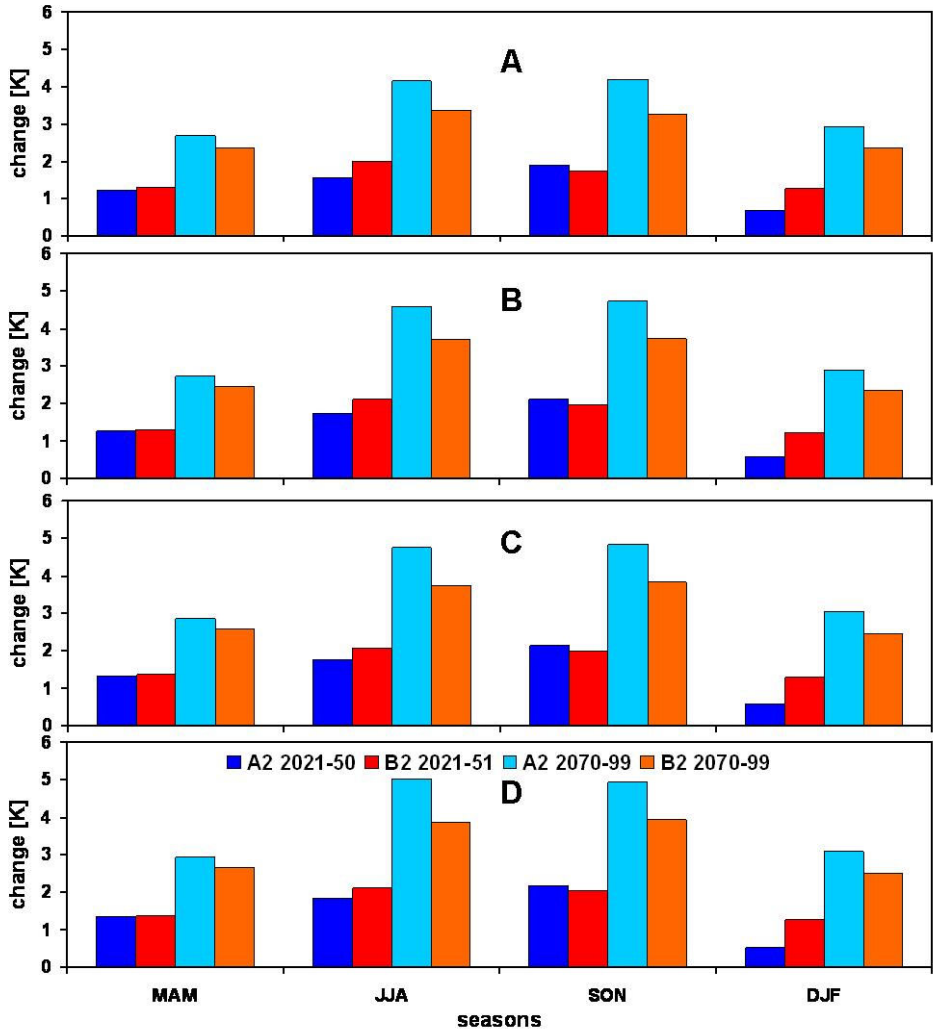

Figure VII-3: Seasonal changes in temperature for the scenarios A2 and B2 in the near and far future in comparison to the control period (1961 - 89)

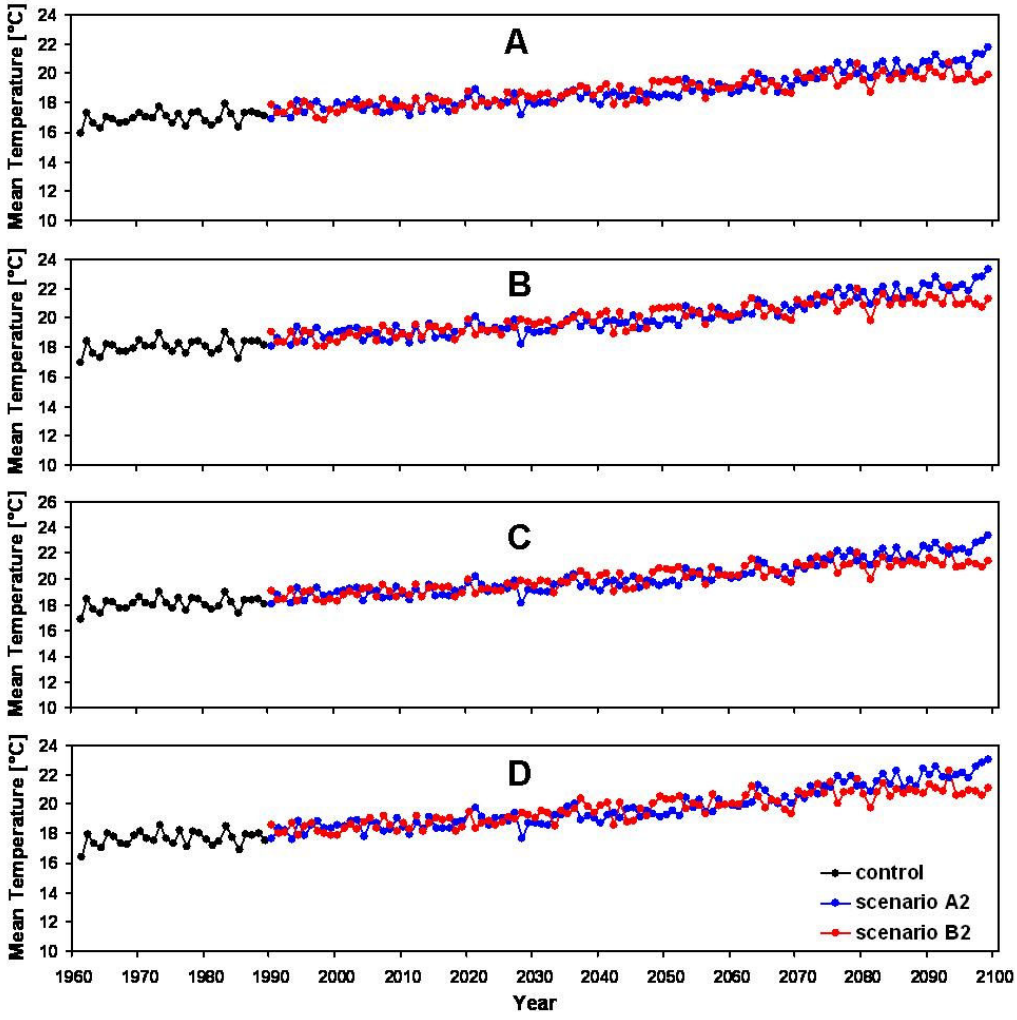

Figure VII-4: Time series of annual mean temperatures for control run and the scenarios A2 and B2

Changes in temperatures can be summarized as follows:

- Changes in temperatures are throughout positive over all seasons and regions.
- Already warmer seasons (summer and autumn) and regions (in the south, sub region D) receive higher increases.
- As well signal to noise ratio as linear trend tests highlight the significance of changing signals.
- Differences between scenarios are marginal in the near future, but become eminent in the far future with higher changes in scenario A2.

Precipitation

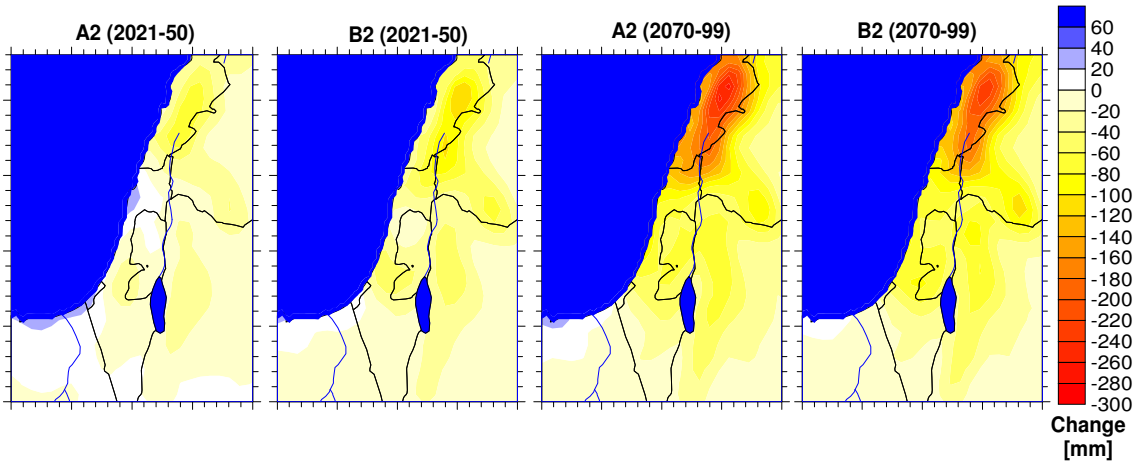

Figure VII-5: Mean annual precipitation change (absolute) of the scenarios A2 and B2 for the near and far future in comparison to the control period (1961 - 89)

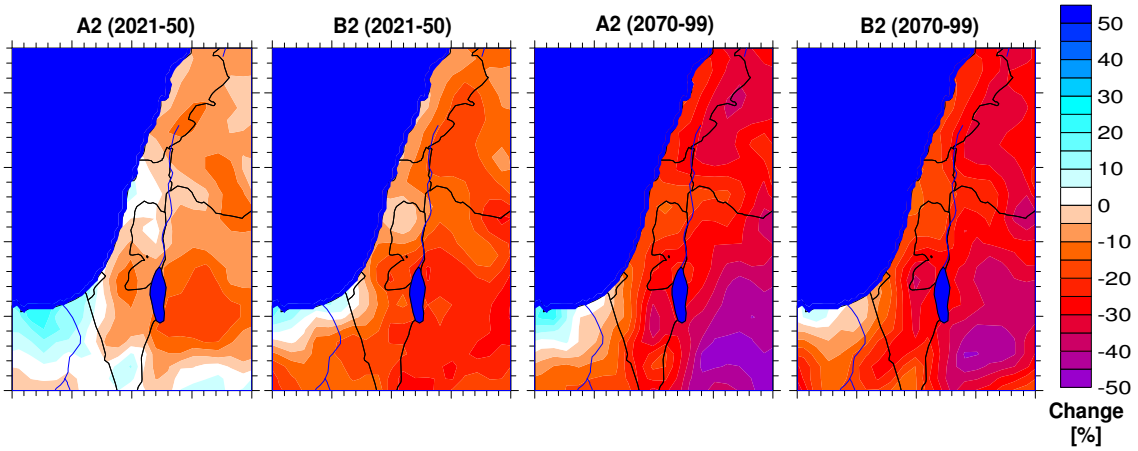

Figure VII-6: Mean annual precipitation change (relative) of the scenarios A2 and B2 for the near and far future in comparison to the control period (1961 - 89)

Within the investigated area regional and temporal variability of precipitation is much higher in comparison to temperature. Due to the steep climatic gradient described before, precipitation decreases significantly from north to south. Contemporaneously the variability increases, as it is shown with the standard deviation and the variations coefficient of mean annual precipitation in the regions A to D in Table VII-4. Analysis of the simulated future scenarios show that variability of rainfall stays very high in the near and far future with variations coefficients of about 27 % in the north (sub region A) to more than 45 % in the south (sub region D). In the time series of annual precipitation

(Figure VII-7) extreme wet years can be seen also in the future. However, they become less frequent, while dry years occur more frequently.

In the near future in most parts of the region precipitation amounts decrease, whereas decreases are higher in scenario B2 than in A2 (Figure VII-5 and Figure VII-6). Exceptions are parts in the south and southwest at the Egyptian coast, where increases of up to 20 % appear. However, absolute values are small (Figure VII-5).

In the far future decreases in precipitation are higher than in the near future. Highest absolute negative changes are found in the northern parts, particularly in the region of Lebanon, whereas the highest relative decrease resides in the central and southern parts of Jordan. Like for the near future increasing precipitation occurs at the Egyptian coast. In the far future changes (positive and negative) are more pronounced in scenario A2 than in B2.

Table VII-4: Mean, standard deviation (STDV), variations coefficient (CV), change, and signal to noise ratio (SN) of precipitation for the subregions A – D for the near and far future

	SCENARIO:	A2				B2			
PERIOD	REGION:	A	B	C	D	A	B	C	D
1961 - 1989	MEAN [mm]	710.8	363.7	184.1	82	710.8	363.7	184.1	82
	STDV [mm]	190.6	134.3	75.4	40.1	190.6	134.3	75.4	40.1
	CV [%]	26.8	36.9	41	48.9	26.8	36.9	41	48.9
2021 - 2050	MEAN [mm]	683.9	361	165.7	74.7	658.1	330.1	149.4	64
	STDV [mm]	187.4	116.3	59.5	33.9	192.3	104.7	44.2	24.3
	CV [%]	27.4	32.2	35.9	45.4	29.2	31.7	29.6	38
	Δ abs [mm]	-26.9	-2.7	-18.4	-7.3	-52.7	-33.6	-34.7	-18
	Δ rel [%]	-3.8	-0.7	-10	-8.9	-7.4	-9.2	-18.8	-22
	SN [-]	0.14	0.02	0.24	0.18	0.28	0.25	0.46	0.45
2070 - 2099	MEAN [mm]	531	289.8	130.5	53.4	569.9	293.2	129.1	54.5
	STDV [mm]	147.5	91.4	36.7	18	158.4	105.6	53.5	24.2
	CV [%]	27.8	31.5	28.1	33.7	27.8	36	41.4	44.4
	Δ abs [mm]	-180	-73.9	-53.6	-28.6	-141	-70.5	-55	-27.5
	Δ rel [%]	-25.3	-20.3	-29.1	-34.9	-19.8	-19.4	-29.9	-33.5
	SN [-]	0.94	0.55	0.71	0.71	0.74	0.52	0.73	0.69

Although changes in the far future within the sub regions A – D are of very high amounts (20 – 35 %), no significance is found when analyzing the time slices with the SN ratio. However, a decreasing trend appears to be traceable examining the time series of annual precipitation amounts in Figure VII-7. Here the advantage of transient simulations compared to time slice experiments becomes apparent. Due to its high

variability significant signals in precipitation decrease remain hidden, while a trend analysis of a long year time series bares significant trends (Table VII-5): While for the near future only in the sub regions C and D decreasing trends with small significance are seen in scenario B2, trends in the far future are significant for both scenarios and in all sub regions.

If simulation results are not averaged to sub regions, but analyzed in their original resolution of 18 x 18 km grid cells, the SN ratio exceeds 1 in the far future at several places in the northern parts of the considered region of the Eastern Mediterranean, while no significant changes due to the SN ratio can be found in the near future (Figure VII-8).

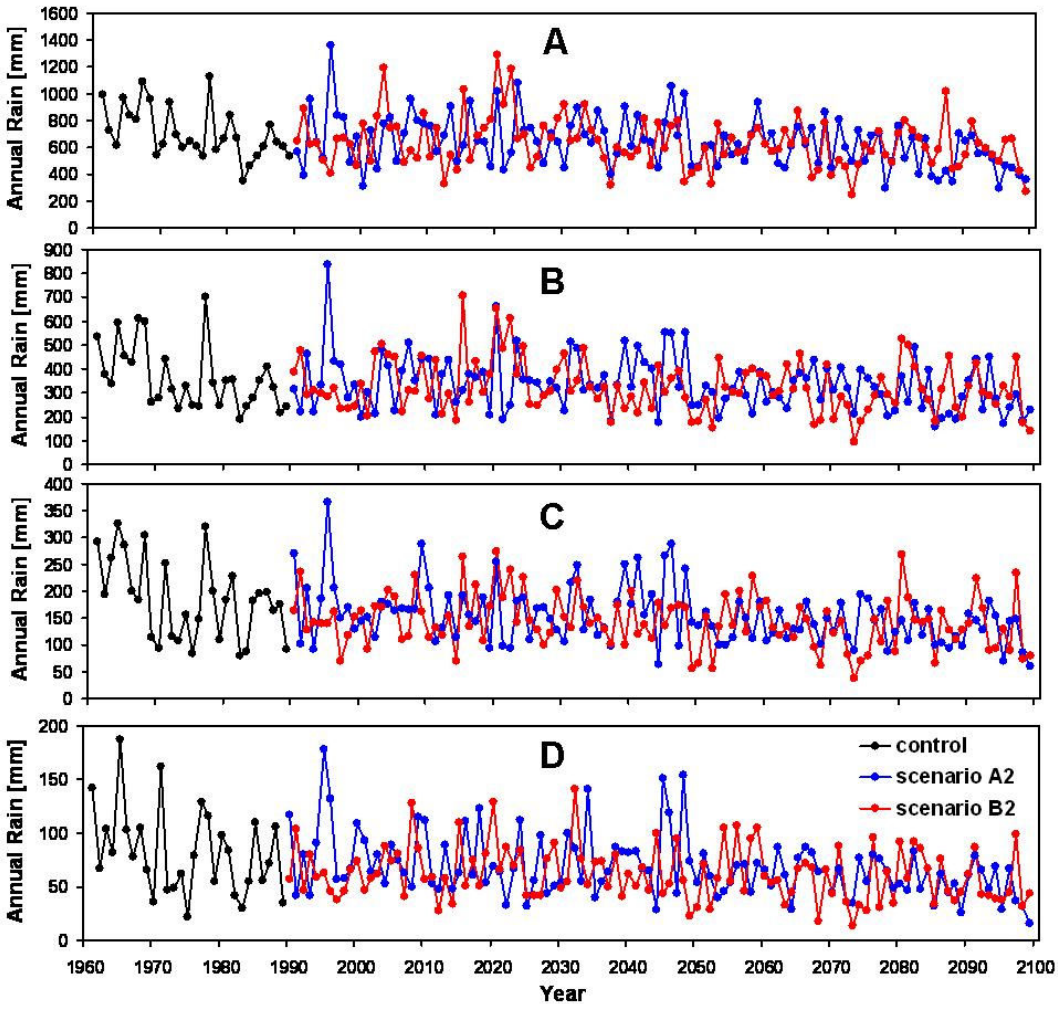

Figure VII-7: Time series of annual precipitation for control run and the scenarios A2 and B2

Table VII-5: Future trends in precipitation and temperature

Precipitation																
Scenario	A2					B2					A2				B2				
Period	1961 - 2050					1961 - 2050					1961 - 2099				1961 - 2099				
Area	MEAN [mm]	STDEV [mm]	CV [%]	CHANGE [mm/10y]	*)	MEAN [mm]	STDEV [mm]	CV [%]	CHANGE [mm/10y]	*)	MEAN [mm]	STDEV [mm]	CV [%]	CHANGE [mm/10y]	*)	MEAN [mm]	STDEV [mm]	CV [%]	CHANGE [mm/10y]	*)
A	699,6	197,6	28,2	-7,4		681,7	199,7	29,3	-12,6		653,9	192	29,4	-15,5	****	648,6	189	29,1	-11,4	***
B	364,3	128,7	35,3	-0,2		348,6	121,9	35	-6,8		341,3	118,6	34,7	-6,1	**	333,5	116,1	34,8	-5,2	*
C	174,2	64,8	37,2	-2,9		162,6	59,3	36,5	-5,5	*	159,4	59,2	37,1	-4,6	****	152,7	57,7	37,8	-4,4	****
D	79	35,2	44,6	-1,2		70,9	31,2	44	-2,3	*	71,3	31,9	44,7	-2,3	****	66,3	29,7	44,8	-1,8	***
Temperature, mean																				
Scenario	A2					B2					A2				B2					
Period	1961 - 2050					1961 - 2050					1961 - 2099				1961 - 2099					
Area	MEAN [°C]	STDEV [K]	CV [%]	CHANGE [K/10y]	*)	MEAN [°C]	STDEV [K]	CV [%]	CHANGE [K/10y]	*)	MEAN [°C]	STDEV [K]	CV [%]	CHANGE [K/10y]	*)	MEAN [°C]	STDEV [K]	CV [%]	CHANGE [K/10y]	*)
A	17,7	0,7	4	0,21	****	17,8	0,8	4,5	0,27	****	18,5	1,3	7	0,3	****	18,4	1,1	6	0,25	****
B	18,8	0,7	3,7	0,23	****	18,9	0,8	4,2	0,28	****	19,7	1,4	7,1	0,32	****	19,6	1,2	6,1	0,27	****
C	18,8	0,7	3,7	0,23	****	18,9	0,8	4,2	0,28	****	19,7	1,5	7,6	0,33	****	19,6	1,2	6,1	0,28	****
D	18,4	0,8	4,3	0,23	****	18,5	0,9	4,9	0,28	****	19,4	1,5	7,7	0,34	****	19,2	1,3	6,8	0,29	****
Temperature, min																				
Scenario	A2					B2					A2				B2					
Period	1961 - 2050					1961 - 2050					1961 - 2099				1961 - 2099					
Area	MEAN [°C]	STDEV [K]	CV [%]	CHANGE [K/10y]	*)	MEAN [°C]	STDEV [K]	CV [%]	CHANGE [K/10y]	*)	MEAN [°C]	STDEV [K]	CV [%]	CHANGE [K/10y]	*)	MEAN [°C]	STDEV [K]	CV [%]	CHANGE [K/10y]	*)
A	13,6	0,7	5,1	0,22	****	13,7	0,8	5,8	0,26	****	14,4	1,3	9	0,3	****	14,3	1,1	7,7	0,26	****
B	12,7	0,8	6,3	0,24	****	12,7	0,8	6,3	0,28	****	13,5	1,4	10,4	0,33	****	13,4	1,2	9	0,29	****
C	12	0,7	5,8	0,23	****	12	0,8	6,7	0,28	****	12,8	1,4	10,9	0,33	****	12,7	1,2	9,4	0,28	****
D	10,7	0,8	7,5	0,24	****	10,7	0,8	7,5	0,28	****	11,6	1,5	12,9	0,34	****	11,5	1,3	11,3	0,29	****
Temperature, max																				
Scenario	A2					B2					A2				B2					
Period	1961 - 2050					1961 - 2050					1961 - 2099				1961 - 2099					
Area	MEAN [°C]	STDEV [K]	CV [%]	CHANGE [K/10y]	*)	MEAN [°C]	STDEV [K]	CV [%]	CHANGE [K/10y]	*)	MEAN [°C]	STDEV [K]	CV [%]	CHANGE [K/10y]	*)	MEAN [°C]	STDEV [K]	CV [%]	CHANGE [K/10y]	*)
A	22,5	0,8	3,6	0,23	****	22,6	0,9	4	0,29	****	23,3	1,4	6	0,32	****	23,3	1,2	5,2	0,27	****
B	26,8	0,9	3,4	0,23	****	27	1	3,7	0,29	****	27,7	1,5	5,4	0,35	****	27,7	1,3	4,7	0,28	****
C	27,5	0,9	3,3	0,23	****	27,7	1	3,6	0,3	****	28,5	1,6	5,6	0,36	****	28,5	1,4	4,9	0,3	****
D	28,1	0,8	2,8	0,23	****	28,2	1	3,5	0,3	****	29	1,6	5,5	0,36	****	29	1,3	4,5	0,3	****

*) trends at significance levels $\alpha = 0.001$: ****, $\alpha = 0.01$: ***, $\alpha = 0.05$: *, $\alpha = 0.1$: +

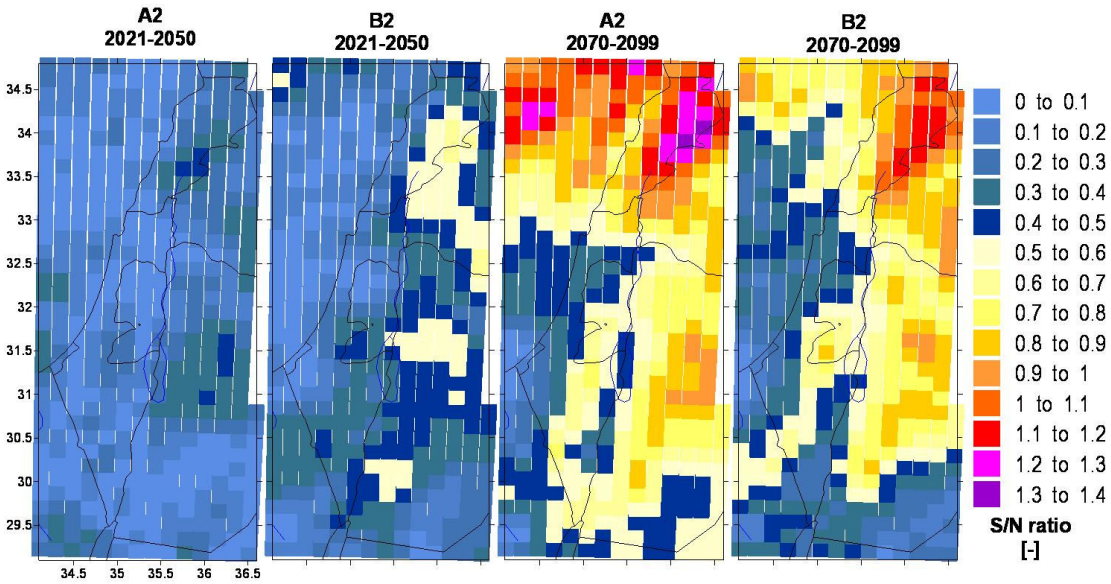

Figure VII-8: Signal to noise ratio of precipitation for the near and far future in relation to the control period (1961 - 89)

Drought Analysis

To analyze whether regional climate change impacts also the risk and severity of drought events, the Effective Drought Index (EDI, see chapter IV.7.2) is calculated for the time slices of the control run, and of the near and far future based on the two emission scenarios A2 and B2.

The calculation of the EDI is based on the Mean Effective Precipitation (MEP). Differences of the MEP between the regions A to D are illustrated in Figure VII-9 for the control period. Accordingly to the already described steep climatic gradient the MEP drops from north to south considerably. In the near future the decrease in MEP in all regions is higher for scenario B2 than for scenario A2 (Figure VII-10). In the sub areas A and B the MEP of the near future remains almost unchanged for scenario A2. In the far future decrease of MEP for scenario A2 is higher than for B2 and in general higher than for the near future. For all sub areas negative changes of the MEP are most extreme during the months February to April. Highest decrease in MEP is found in sub area D.

The occurrence of extreme dry conditions (EDI = -2) increases in sub area A for the scenario A2 in the near and the far future, while for the scenario B2 no changes can be seen. In the regions C and D an increase in variability for the near and the far future

can be seen. As well the frequency of extreme wet (EDI > 4) as of extreme dry events (EDI < -2) rises considerably.

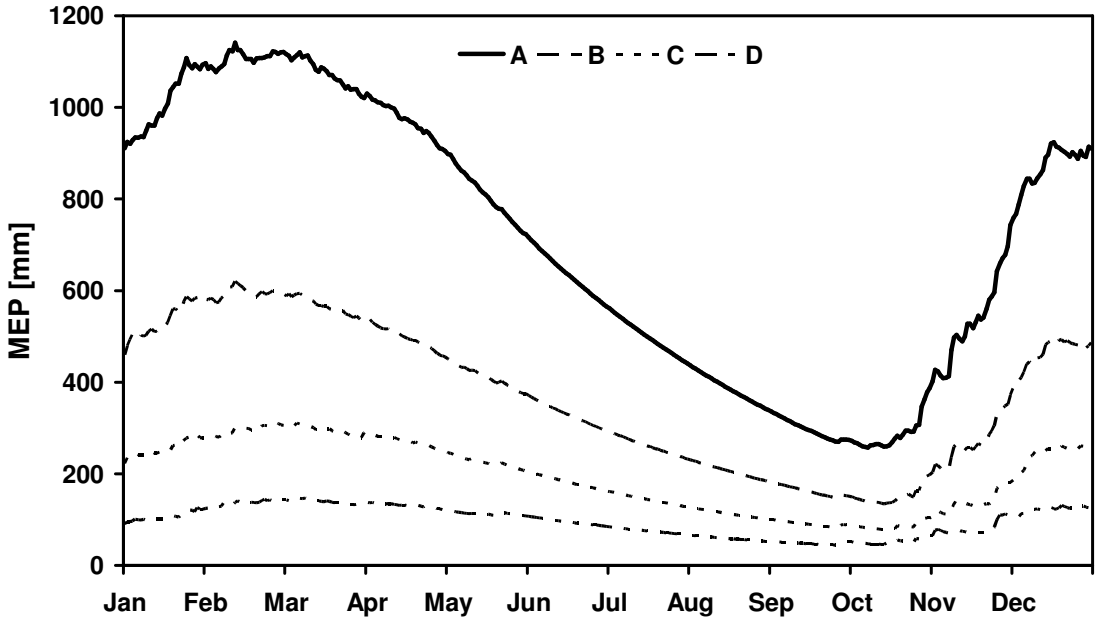

Figure VII-9: MEP (Mean Effective Precipitation) of the control run (1961 - 89) for the sub regions from North (A) to South (D)

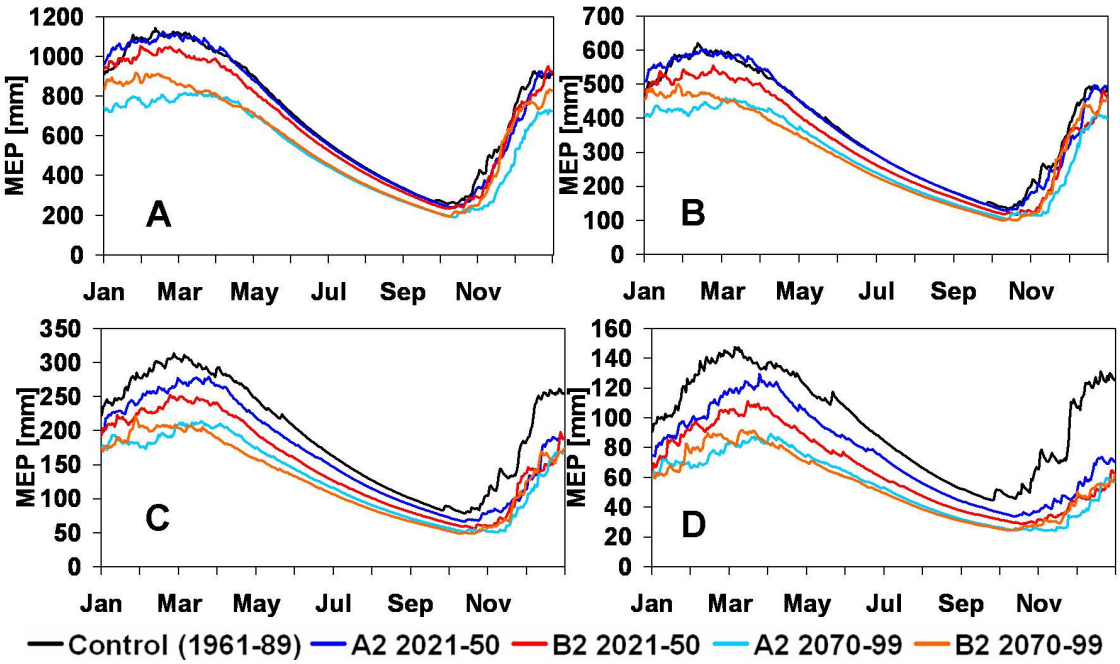

Figure VII-10: MEP (Mean Effective Precipitation) for the regions A – D

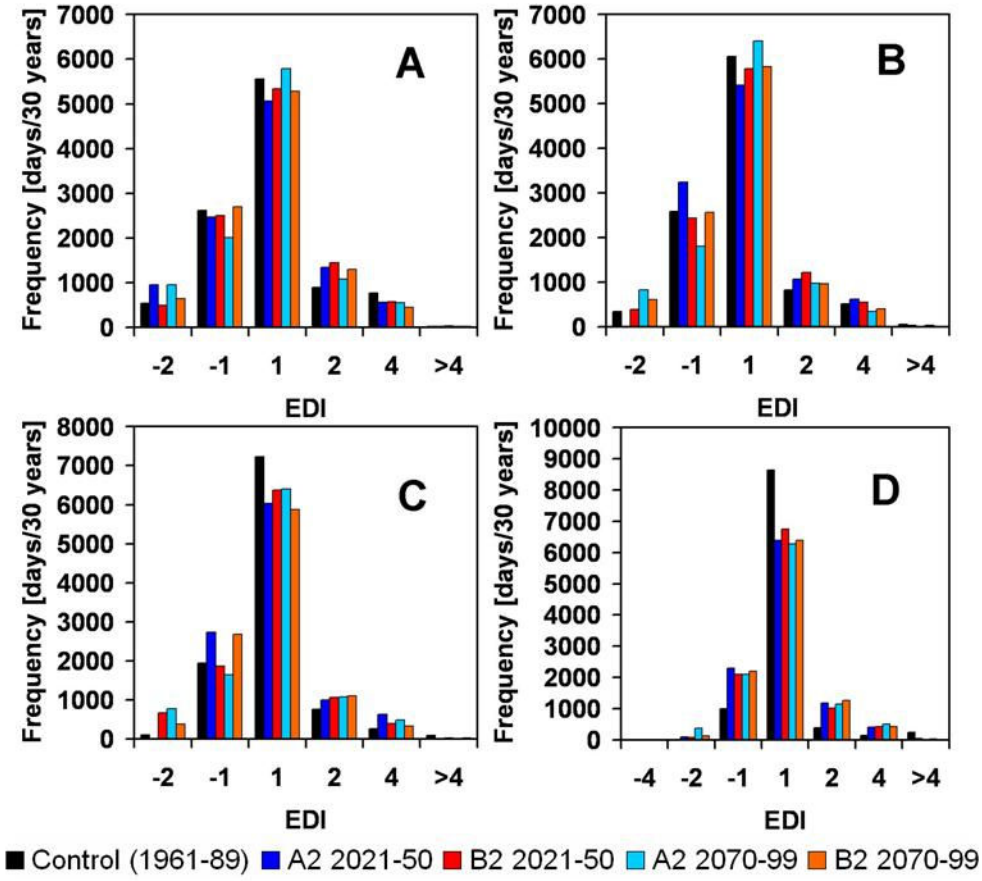

Figure VII-11: EDI frequencies for the regions A – D

The relation between drought duration and drought intensity is shown in Figure V-12. Drought intensity is defined as the cumulated EDI (addition of absolute values of EDI during a drought period). The relation between drought duration and drought intensity differs between the sub areas. While drought duration is longer in the south (sub area D) than in the north (sub area A), drought intensities are higher in sub area A and lower in sub area D. For the future, no significant changes in drought duration can be found. However, drought intensity tends to increase for both scenarios as well in the near as in the far future, especially in the sub areas C and D.

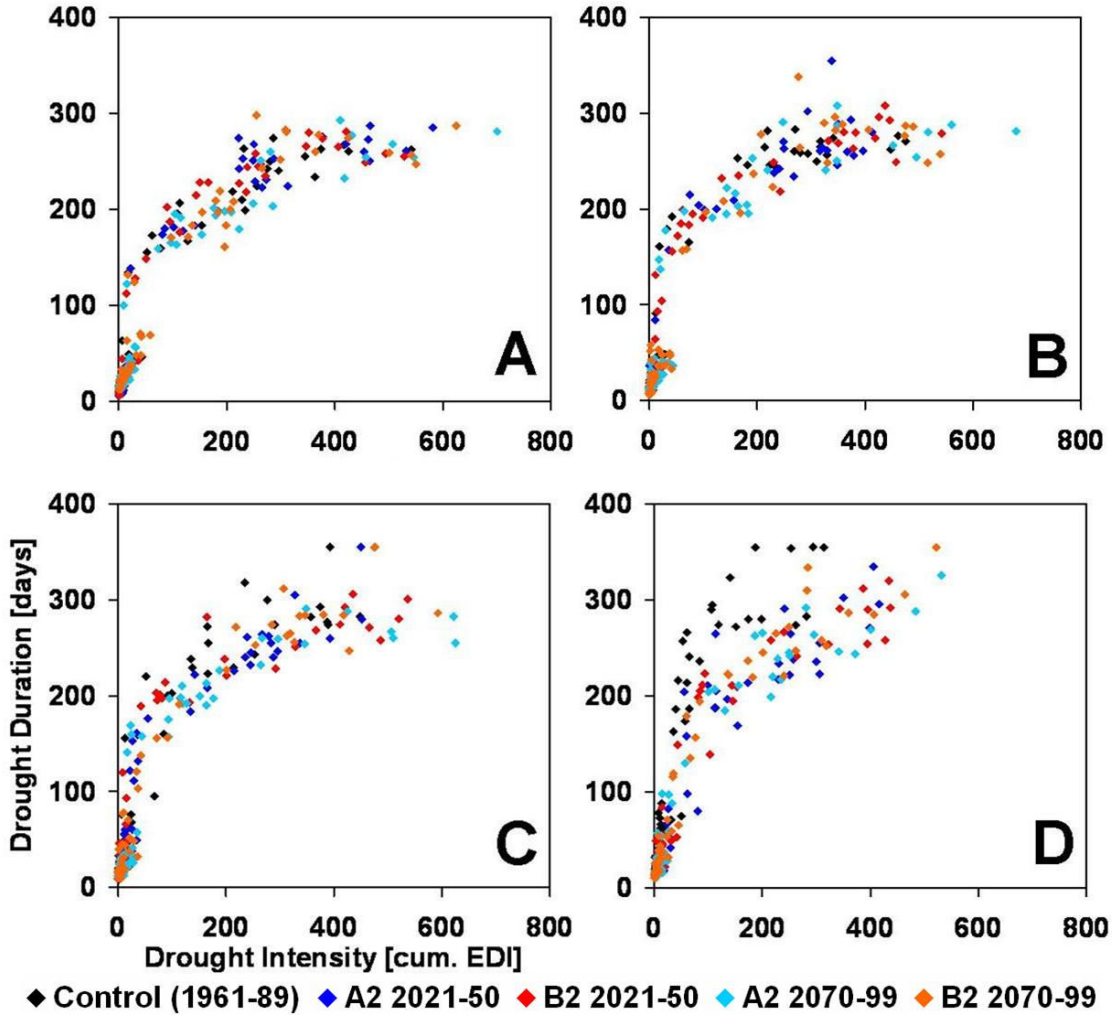

Figure VII-12: Drought duration and drought intensities for the regions A – D

Changes in precipitation can be summarized as follows:

- Changes in precipitation are almost everywhere over the region negative with a little exception at the Egyptian coast where little increases can be seen
- Negative changes are higher in the far than the near future indicating a continuous negative trend in both scenarios
- Decreases in scenario B2 are higher than in scenario A2 for the near future, but smaller in the far future.
- While in the more humid north absolute decrease is more extreme, in the south relative decrease is higher accompanied with an increased variability.

- Intensity of droughts is likely to increase all over the region, while in the south variability with more extreme dry and wet events rises.

VII.3 Climate Change Impact on Terrestrial Hydrology

Analysis of the regional climate simulations in chapter VII.2 shows steadily increasing temperatures and especially for the northern parts including the basin of the Upper Jordan high reduction in precipitation amounts in the future. In this chapter it is investigated how these changes influence the water balance of the UJC by analyzing the output of the joint climate-hydrology simulations. Besides the main components of the water balance, namely precipitation (P), evapotranspiration (ET) and discharge (Q), snow cover as a seasonal storage is investigated. The snow cover is of major importance for the water balance in the UJC in the elevated areas of Mount Hermon as snow melts account for up to 30 % of the discharge in late spring and early summer (GILAD and BONNE, 1990). Therefore, a decrease in snow storage due to raised temperatures during the rainy period could alter discharge behavior considerably.

Analysis of the considered variables includes first examination of the time slices for the near and far future in comparison to the control period including the test of climate change signal based on SN ratio. In a second step time series of annual means are investigated and tested for linear trends. Finally, uncertainties of the simulation results due to emission scenarios (and - if available - due to observations) are illustrated by displaying monthly means and daily frequencies.

VII.3.1 Time Slice Analysis

For the time slice analysis absolute values, standard deviations, coefficients of variance, absolute and relative future changes as well as the signal to noise ratios for different variables are given in Table VII-6. Additionally, absolute and relative changes are shown in Figure VII-14 and Figure VII-17, respectively. The spatial distribution of the changes in the future in the UJC can be seen at Figure VII-16 in comparison to the values of the control run (Figure VII-15).

Precipitation in the UJC shows recession in the near future ranging between 12 % (scenario A2) and 19 % (scenario B2). Although this sounds like a denotative change the signal to noise ratio remains with values of 0.4 (A2) and 0.65 (B2) considerably < 1 indicating that changes reside within recent natural climate variability. Another situation

is noticed for the far future were decrease of annual precipitation exceeds 32 % in both scenarios and SN ratios of 1.08 (A2) and 1.11 (B2) are calculated. In both scenarios and both future time slices decreases in precipitation are higher in the northern and northwestern parts of the UJC.

Potential evapotranspiration (ETP) strongly depends on available energy and therefore amounts are highest in the warmer, exposed deep elevations in the Hula Valley in the south of the UJC. In contrast, real evapotranspiration (ETR) depends on water availability. Therefore, the simulated real evapotranspiration shows a clear dependency on the soil type: Maximum ETR is calculated in the southeastern parts of the UJC where relatively impermeable soils hamper percolation and offer higher water content near the surface to evaporate.

Potential evapotranspiration increases due to steadily increasing temperatures in the near future of about 5 % (A2) to 6.5 % (B2), in the far future 17.4 % and 12.4 %, respectively. Only for the scenario A2 in the near future this signal is not significant (SN = 0.82), while for the far future considerable values of 2.8 (A2) 2 (B2) in the SN ratio are obtained. Relative changes are higher in the northern parts of the UJC than in the southern part, where ETP values are already considerable high. In general, ETP does not show high interannual variability due to its relation to temperature.

The same can be seen for ETR: Variability of annual amounts is very low, although it is highly dependent on available water at the surface and within the upper soil layer, and therefore on precipitation. However, although precipitation amounts drop down in the future, ETR remains almost unchanged. That means that the decline in precipitation gets compensated by the surplus in ETP resulting in unchanged annual ETR amounts as well for the near as for the far future.

As a consequence another component has to decrease maintaining the equation of the water balance. This is confirmed when investigating the discharge. Due to its big karstic groundwater reservoir, variability of the discharge in the UJC is lower than of precipitation, but annual discharge magnitudes are directly dependent on precipitation amounts. Since annual ETR remains unchanged the decrease in precipitation results in an emphasized signal of runoff reduction. For the near future discharge shrinkage of 16 – 23 % is simulated with SN ratios of 0.62 (A2) and 0.88 (B2). For the far future reductions in discharge exceed 40 % with RN ratios of 1.65 (A2) and 1.71 (B2) indicating

a clear significant change signal. Highest reductions in discharge generation are seen in the southeastern parts of the UJC.

Table VII-6: Means, standard deviations (STDV), coefficient of variance (CV), change and signal to noise ratio (SN) of water balance components for control run and near and far future

PERIOD	VARIABLE	Precipitation		Discharge		Potential ET		Real ET		Snowmelt	
	SCENARIO	A2	B2	A2	B2	A2	B2	A2	B2	A2	B2
1961 - 1989	MEAN [mm]	923.3		585.1		1206.4		398.8		206.5	
	STDV [mm]	274.1		155.4		74.8		19.4		143.4	
	CV [%]	29.7		26.6		6.2		4.9		69.4	
2021 - 2050	MEAN [mm]	813.8	745	488.3	448.6	1268	1285	394.6	398.7	95	79.5
	STDV [mm]	250.9	269.1	111.8	148.9	66.6	71.2	27.7	31.2	67.3	78.9
	CV [%]	30.8	36.1	22.9	33.2	5.2	5.5	7	7.8	70.8	99.3
	Δ abs [mm]	-110	-178	-96,8	-136.5	61.4	78.1	-4.2	-0.1	-112	-127
	Δ rel [%]	-11.9	-19.3	-16.5	-23.3	5.1	6.5	-1.1	0	-54	-61.5
	SN [-]	0.4	0.65	0.62	0.88	0.82	1.04	0.22	0.01	0.78	0.89
2070 - 2099	MEAN [mm]	626	620.2	329	319.7	1416	1356	402.3	397.7	24.9	29.2
	STDV [mm]	165.8	164	84.8	67.8	65	64	32.9	25.9	19.9	30.2
	CV [%]	26.5	26.4	25.8	21.2	4.6	4.7	8.2	6.5	79.9	103.5
	Δ abs [mm]	-297	-303	-256.1	-265.4	209.9	149.8	3.5	-1.1	-182	-177
	Δ rel [%]	-32.2	-32.8	-43.8	-45.4	17.4	12.4	0.9	-0.3	-87.9	-85.9
	SN [-]	1.08	1.11	1.65	1.71	2.81	2	0.18	0.06	1.27	1.24

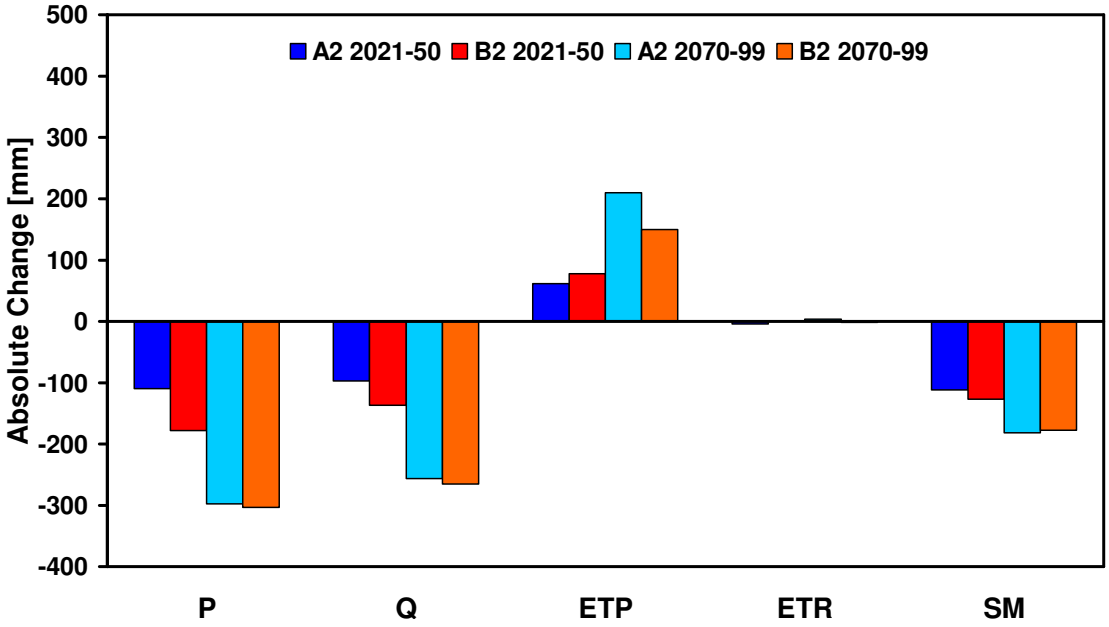

Figure VII-13: Absolute change of water balance components (precipitation P, discharge Q, potential evapotranspiration ETP, real evapotranspiration ETR, and snow melt SM) in the near and far future in comparison to the control period (1961 - 1989)

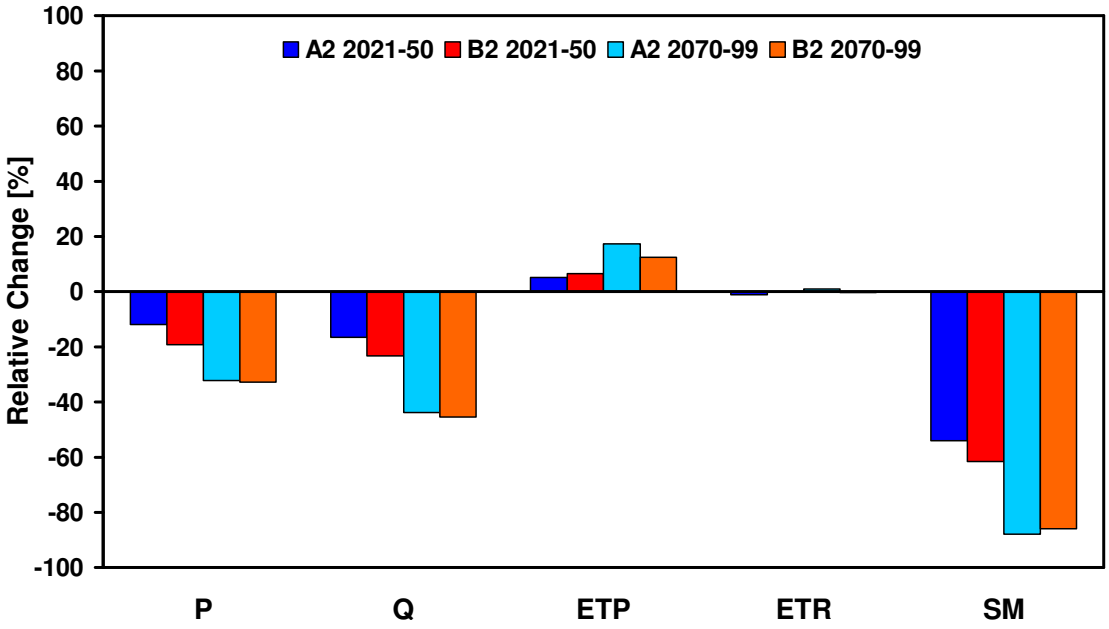

Figure VII-14: Relative change of water balance components (precipitation P, discharge Q, potential evapotranspiration ETP, real evapotranspiration ETR, and snow melt SM) in the near and far future in comparison to the control period (1961 - 1989)

Biggest reductions occur for snowmelt: In the near future amounts of less than 54 % (A2) and 61.5 % (B2) in comparison to the control period are simulated, while for the far future reductions of 87.9 % (A2) and 85.9 % (B2) are found. As interannual variability is very high with amounts of almost 70 % in the recent climate, for the near future no significant climate signal is calculated (0.78 and 0.89 for the scenarios A2 and B2, respectively). Only for the far future the signal is > 1 with values of 1.27 (A2) and 1.25 (B2). This means that one important storage component within the UJC, that enables a temporal shift of discharge from the rainy to the dry season impends to drop out for the future. Relative decreases are highest at lower elevations. For the future snow cover decreases dramatically. The missing values in the very south indicate that in this region never snowfall is simulated and thus no changes can occur.

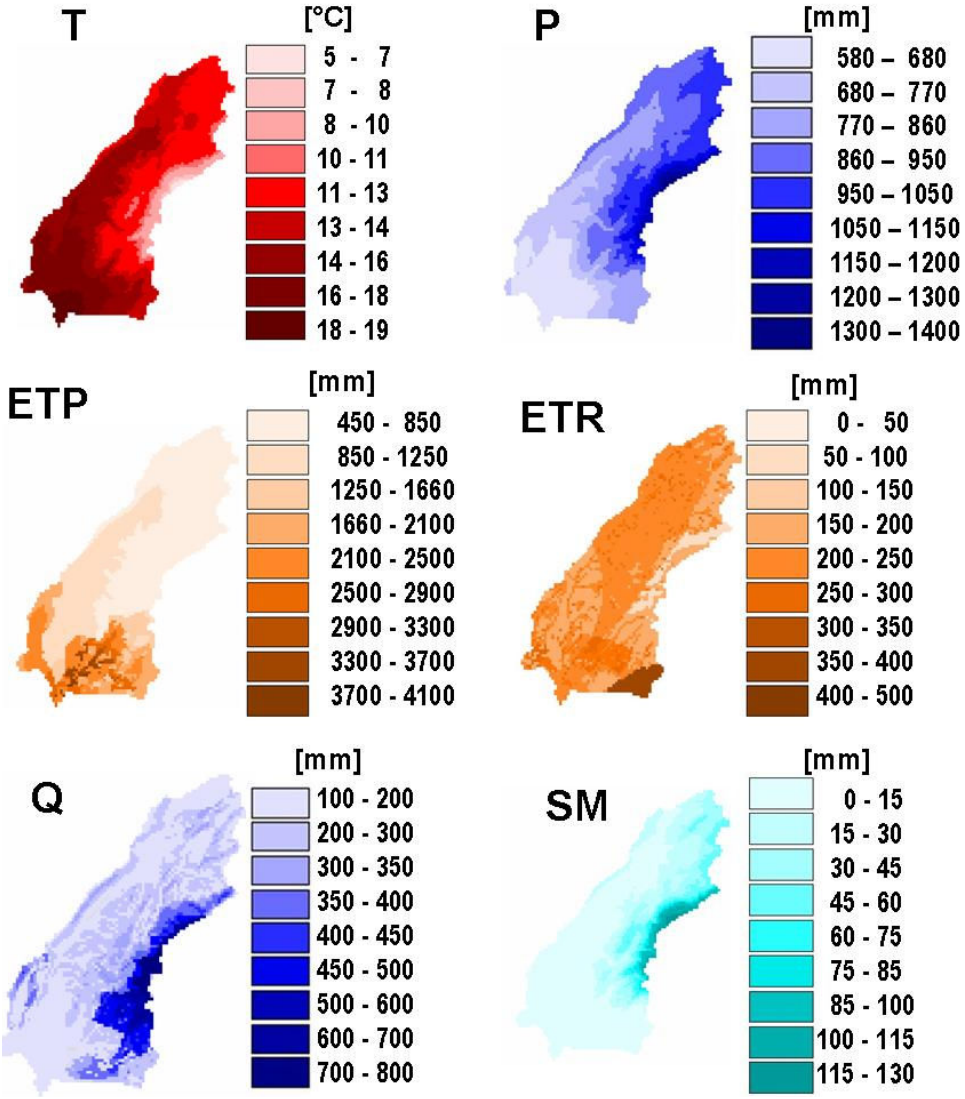

Figure VII-15: Annual means in the control run (1961 - 1989) for temperature (T), precipitation (P), potential evapotranspiration (ETP), real evapotranspiration (ETR), discharge (Q), and snow melt (SM)

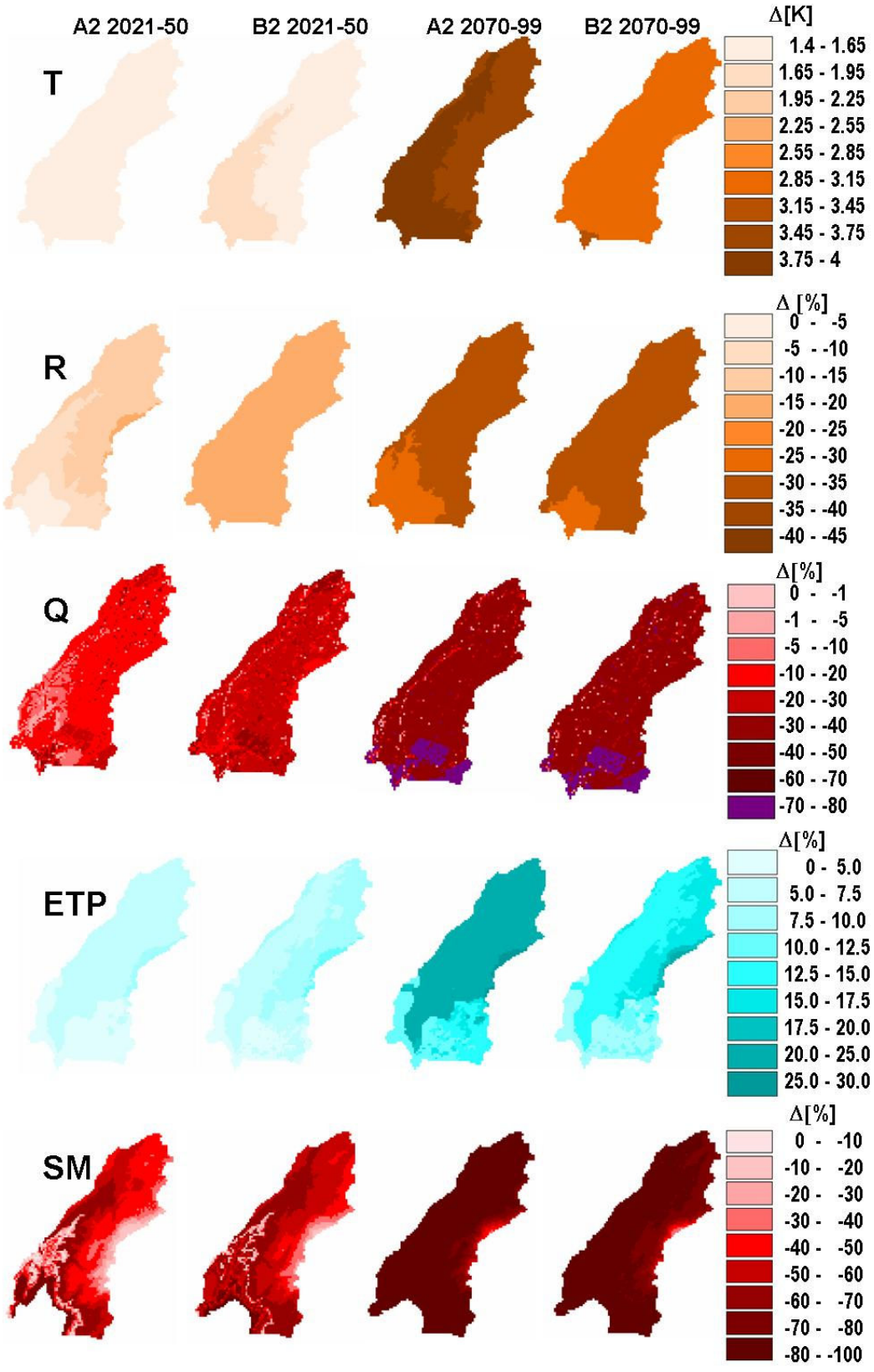

Figure VII-16: Future changes in temperature (T), precipitation (P), discharge (Q), potential evapotranspiration (ETP), and snow melt (SM) in comparison to the control period (1961 - 1989)

VII.3.2 Time Series Analysis

Time series of annual values for the considered variables are illustrated in Figure VII-17, while results of time series analysis including linear trend test are given in Table VII-7.

Precipitation shows until the end of the century decreasing annual amounts accompanied with a decline in interannual variability for both scenarios. Until the middle of the century a linear trend is only significant for the scenario B2, but for the time series ending 2099 significance for a decreasing trend is seen for both scenarios. In contrast to the precipitation the trend in discharge reduction is already significant for A2 until 2050 and even more for B2 and the time series to 2099.

Again the contrarian development of the two scenarios within the UJC is conspicuous, that is already seen in the analysis of the time slices: The more optimistic scenario B2 offers until 2050 higher increase in temperature and therefore ETP accompanied with higher reduction in precipitation than the scenario A2. This is reversed until the end of the century, where in the scenario A2 temperature increase is much higher than in B2 causing higher ETP. However, level of precipitation amounts is comparable in the far future between the scenarios.

ETP is steadily increasing parallel to temperature (compare Figure VII-4) with significance in the linear trend for both scenarios and both time series. In contrast, ETR does not show any trend at all. Snowmelt has a very strong decreasing trend. In Figure VII-17 a very high variability of about 70 % can be seen (Table VII-6). Afterwards amounts diminish, but still in some years considerable snow masses occur, while years with almost no snow storage become more frequent. However, from about 2050 on mean temperatures during the rainy season seem to reach at a level, where no snow accumulation in considerable amounts is able to be built.

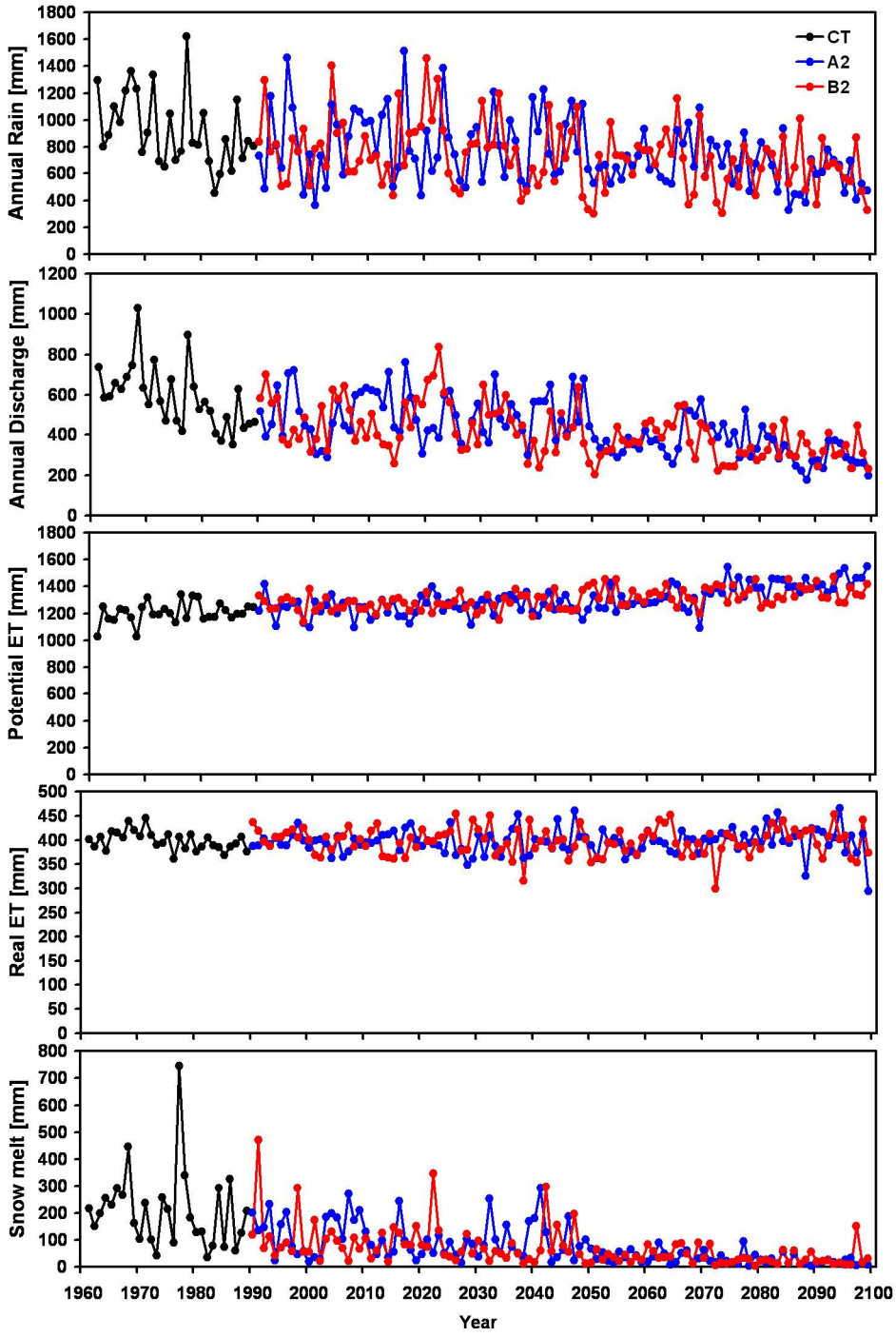

Figure VII-17: Time series of water balance components

Table VII-7: Future trends for water balance components

Time Series 1961 - 2050						
VARIABLE	**SCENARIO**	**MEAN [mm]**	**STDV [mm]**	**CV [%]**	**SIGNI *)**	**Change [mm/10y]**
Precipitation	**A2**	858.1	273.4	31.9		-19.4
	B2	826.6	272.7	33	**	-32.5
Discharge	**A2**	526.3	138.9	26.4	**	-14.6
	B2	500.7	152	30.4	***	-26.2
Potential evapotranspiration	**A2**	1235	76.3	6.2	**	62
	B2	1253	73.6	5.9	***	59
Real Evapotranspiration	**A2**	397.1	21.6	5.4		-0.8
	B2	398.8	24.6	6.2		-0.8
Snow Melt	**A2**	138.4	110.5	79.8	***	-14.5
	B2	129.1	118.4	91.7	***	-16.2
Time Series 1961 – 2099						
VARIABLE	**SCENARIO**	**MEAN [mm]**	**STDV [mm]**	**CV [%]**	**SIGNI *)**	**Change [mm/10y]**
Precipitation	**A2**	787.5	259.5	33	***	-24.4
	B2	770.9	257.9	33.5	***	-23.1
Discharge	**A2**	463.5	150.2	32.4	***	-22.3
	B2	448.1	149.6	33.4	***	-21.4
Potential Evapotranspiration	**A2**	1281	104.3	8.1	***	81
	B2	1285	83.3	6.5	***	65
Real Evapotranspiration	**A2**	397.3	24.3	6.1		0.2
	B2	398.3	26.3	6.6		-0.2
Snow melt	**A2**	100.2	103.6	103.4	***	-12.1
	B2	96.3	106.4	110.4	***	-10.1

*) trends at significance levels $\alpha = 0.001$: ***, $\alpha = 0.01$: ** , $\alpha = 0.05$: *, $\alpha = 0.1$:

VII.3.3 Uncertainties of Model Chain in Comparison to Climate Change

Figure VII-18 to Figure VII-27 show monthly means and frequencies of different variables for the control run and uncertainty bounds due to the two different future scenarios A2 and B2 for the near and far future. Additionally, simulated values based on station data (referred to as “reference simulated”, see VI.5) and – in case of discharge – observed values (referred to as reference observed) are presented. No direct observations can be used for other variables as they are simulation results (e.g. evapotranspiration) or at least interpolated (precipitation and temperature). In this way the uncertainties of the model chain can be quantitatively compared to climate change: While the differences between the control run and the future scenarios represent the climate change signal, the difference between the control run and the simulated reference shows the uncertainties of the model chain consisting of the GCM, the RCM and the

hydrological model. Additionally, the distinction between the observed and simulated reference denotes the uncertainty of solely the hydrological model.

In case of monthly means in precipitation no observed values are given in Figure VII-18, as simulations results are bias corrected (see chapter VI.3) and hence the control run is adjusted to the interpolated rainfall observations. Precipitation does not show any seasonal change in the future, only the decrease of precipitation in January for both scenarios is mentionable. Differences between the scenarios are bigger in February and March, while they are quite homogeneous during the rest of the wet season.

Rainfall intensities do not show any significant changes in the future as the normalized frequency distribution of daily rainfall amounts in Figure VII-19 and Figure VII-20 demonstrate. Extreme events are not more frequent within the UJC in the future. However, it must be mentioned that a comparison to reference simulation based on station data show that the modeling approach is not able to reproduce the very extreme events of > 100 mm/d. This is due to the resolution of 18 x 18 km² of the RCM MM5, which is still too coarse to be directly comparable to stations observations.

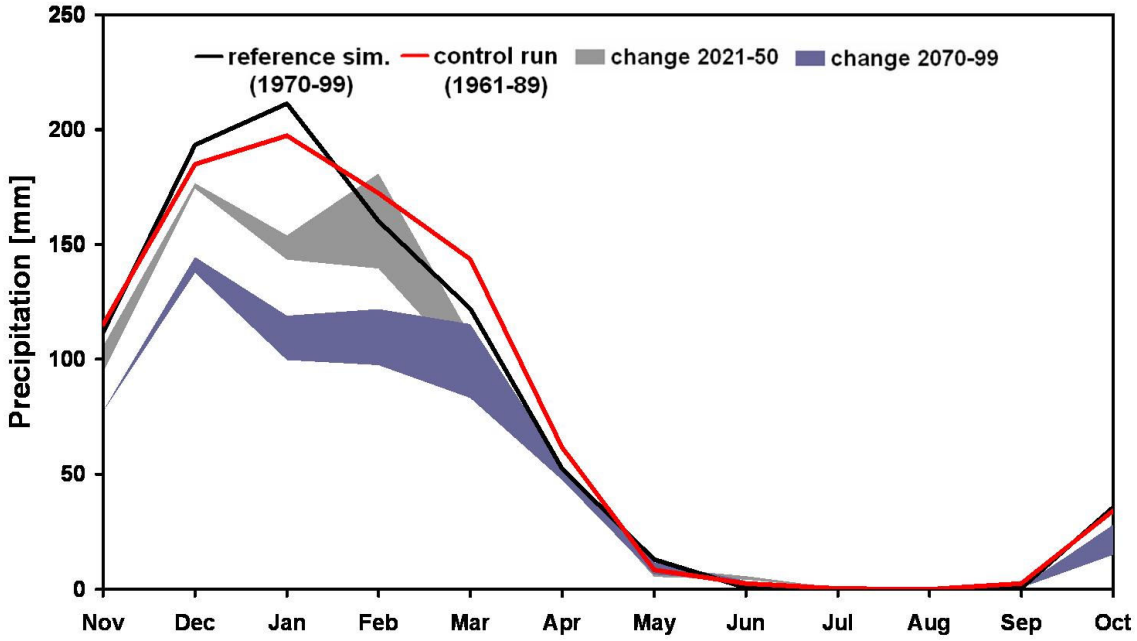

Figure VII-18: Change in monthly means of precipitation

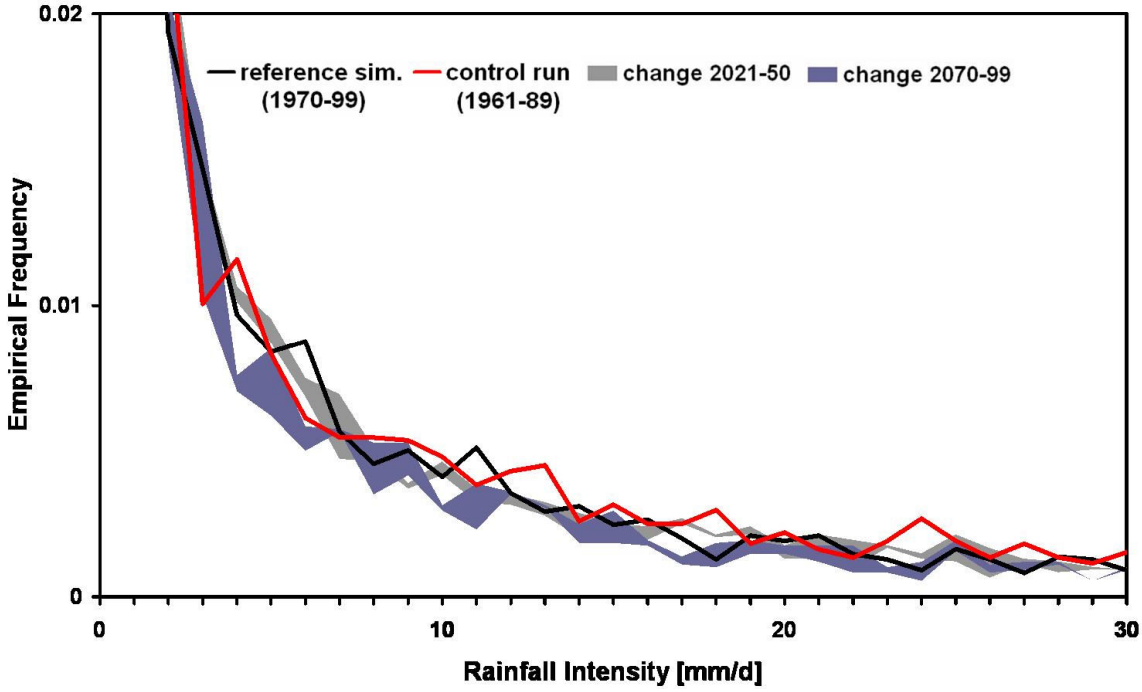

Figure VII-19: Change in normalized frequency distribution of daily rainfall 1 – 30 mm (class width 1 mm)

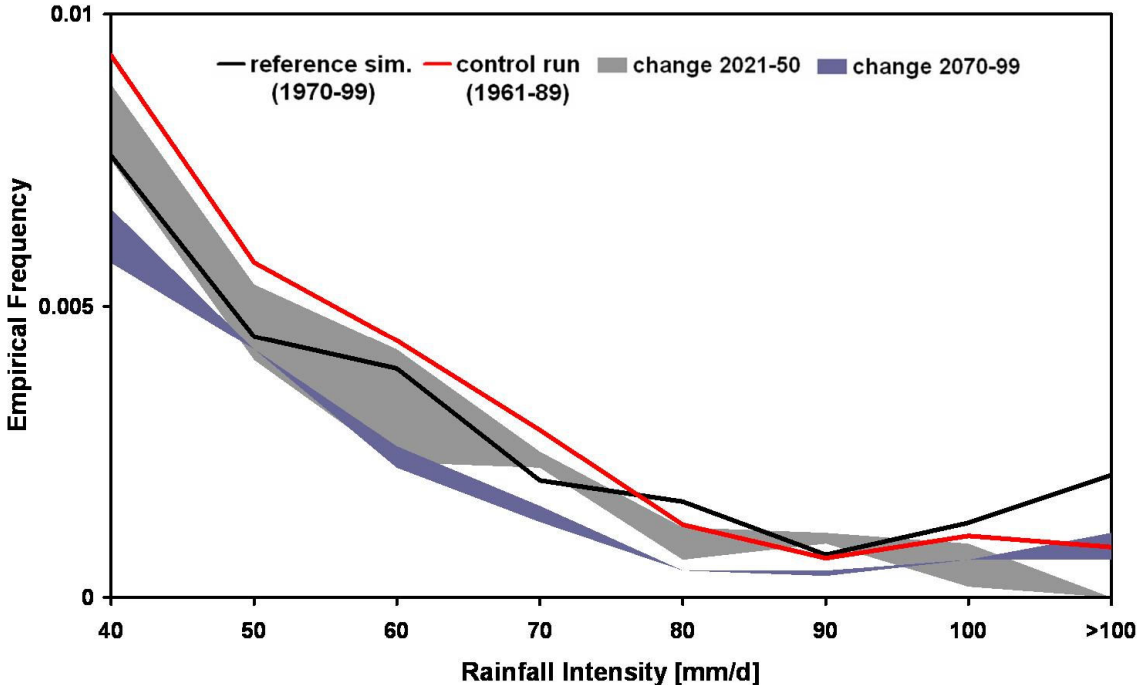

Figure VII-20: Change in normalized frequency distribution of daily rainfall >30 mm (class width 10 mm)

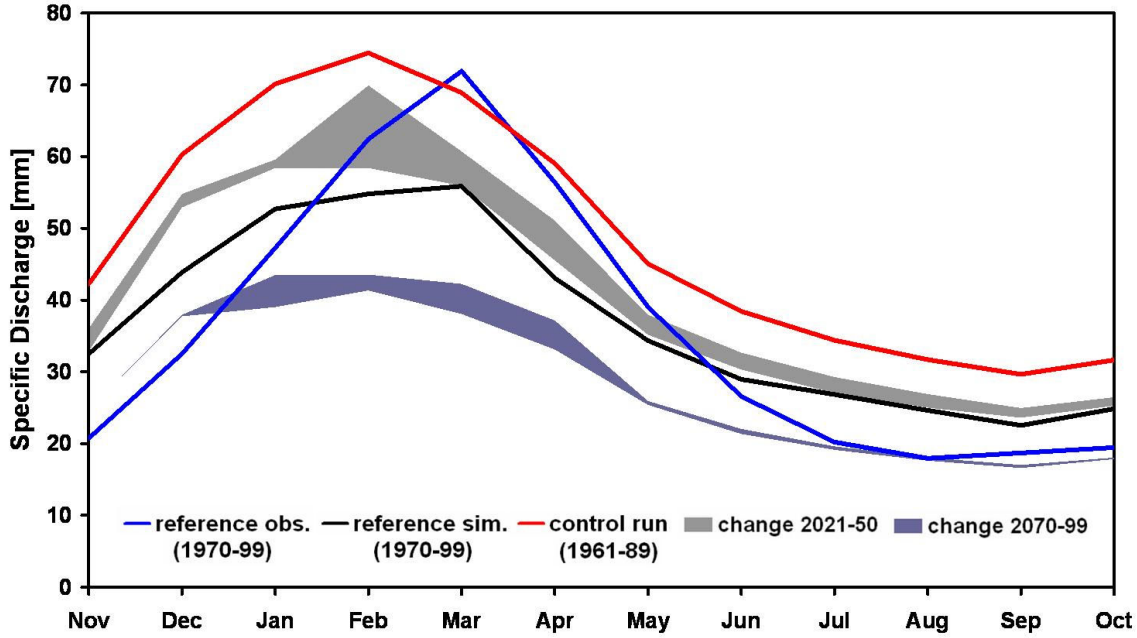

Figure VII-21: Change in monthly means of discharge

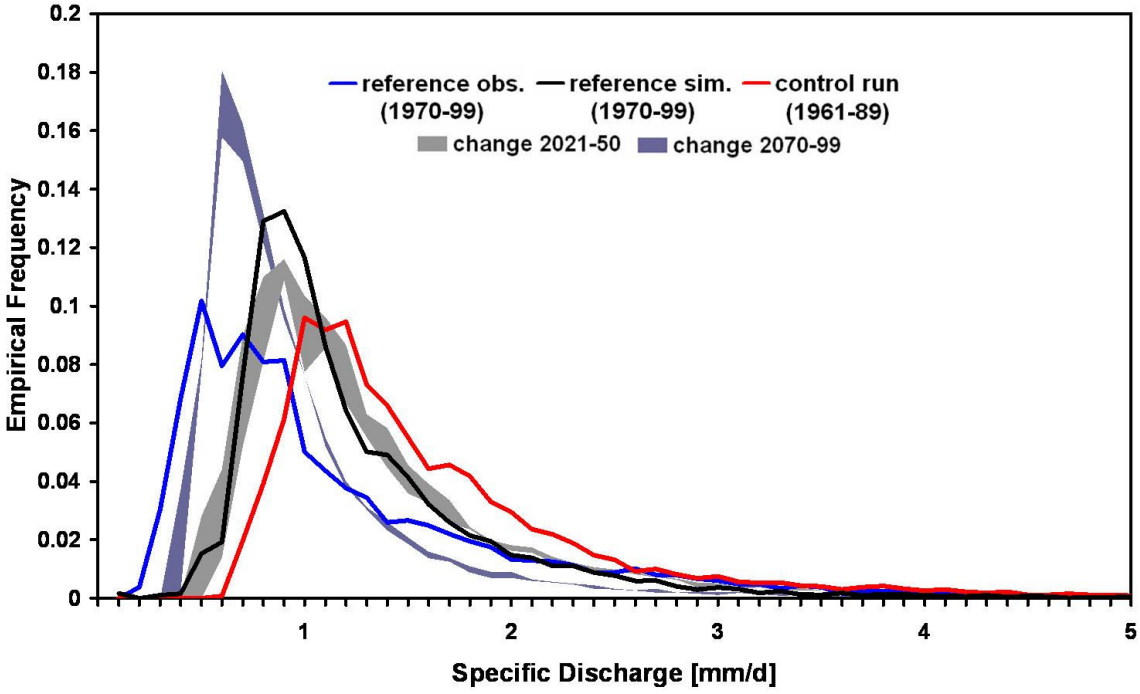

Figure VII-22: Change in normalized frequency distribution of daily discharge 0 – 5 mm (class width 0.1 mm)

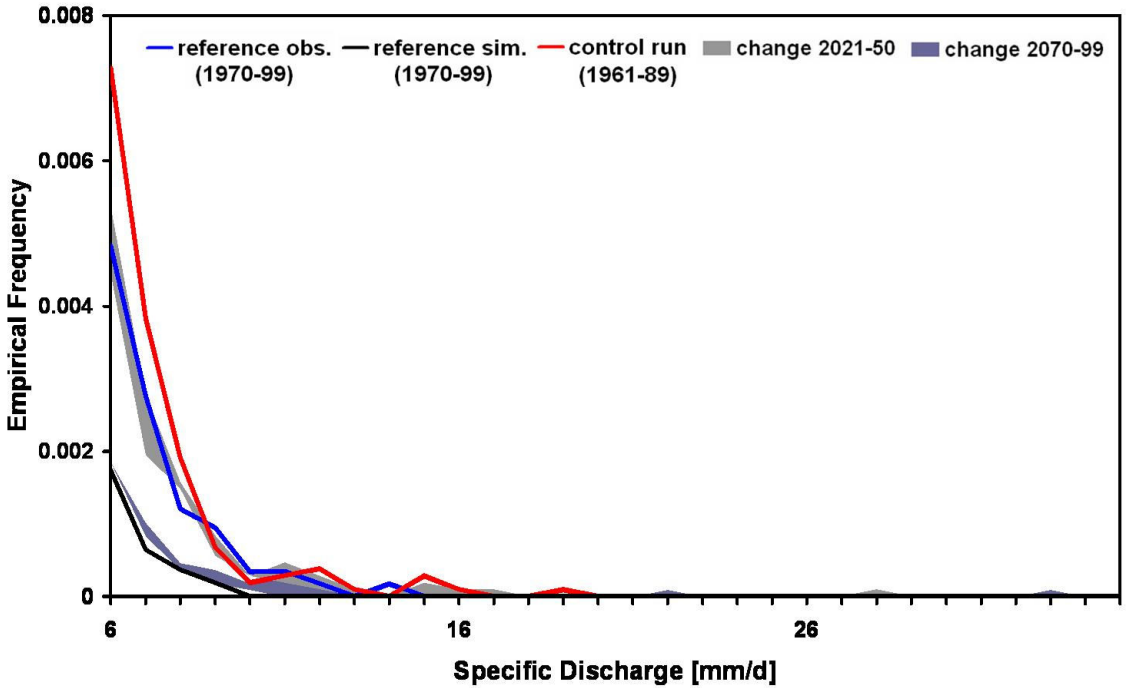

Figure VII-23: Change in normalized frequency distribution of daily discharge >5 mm (class width 1 mm)

Discharge over a mean hydrological year is overestimated in the control period in comparison to observations especially during summer and autumn. This is due to unknown consumption of the river included in the observation data and shortcomings of the modeling system. These inaccuracies were discussed before in the chapters VI.5 and VI.6. The changes in discharge for the near future range between the simulated values of the control run, the simulation based on station data, and the observation data. Thus they are uncertain. In contrast, discharge in the far future is well below this uncertainty range. Differences between the scenarios are much lower than uncertainties between simulations and observations. Deviations of A2 and B2 are highest between January and April, when maximum in discharge occurs.

The normalized frequency distribution of daily discharge (Figure VII-22 and Figure VII-23) shows for little discharge amounts a wide range of uncertainties, where future changes range between the control run, the simulated and the observed values. Like for the rainfall intensities in Figure VII-19 a change in the scale of daily specific discharge has to be considered. According to higher discharge events, a reduction in the future is simulated.

Changes in the monthly means of temperatures in the UJC (Figure VII-24) are more pronounced during summer. Differences between the scenarios are more accentuated for the far than for the near future. The higher temperatures in the simulated values based on station data compared to the control run can be explained by inaccuracies in the interpolation like described in VI.5.

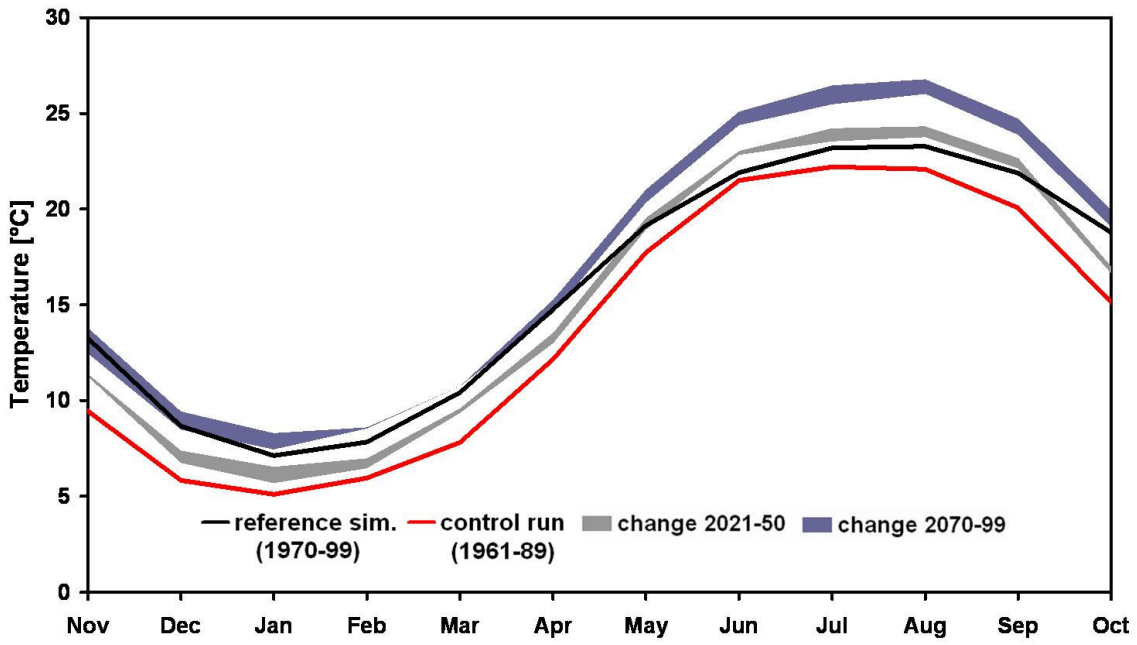

Figure VII-24: Change in monthly means of temperature

The normalized frequency distribution of daily temperature (Figure VII-25) shows a clear shift to warmer temperatures without significant change of the distribution itself. This means that extreme cold days with mean temperatures below 0°C are getting more improbable, while on the same time new extreme hot temperatures are getting reached. Differences between the scenarios are bigger in the far future than for the near future. Again warmer values in the station based simulations are likely to be produced by lacking interpolation performance.

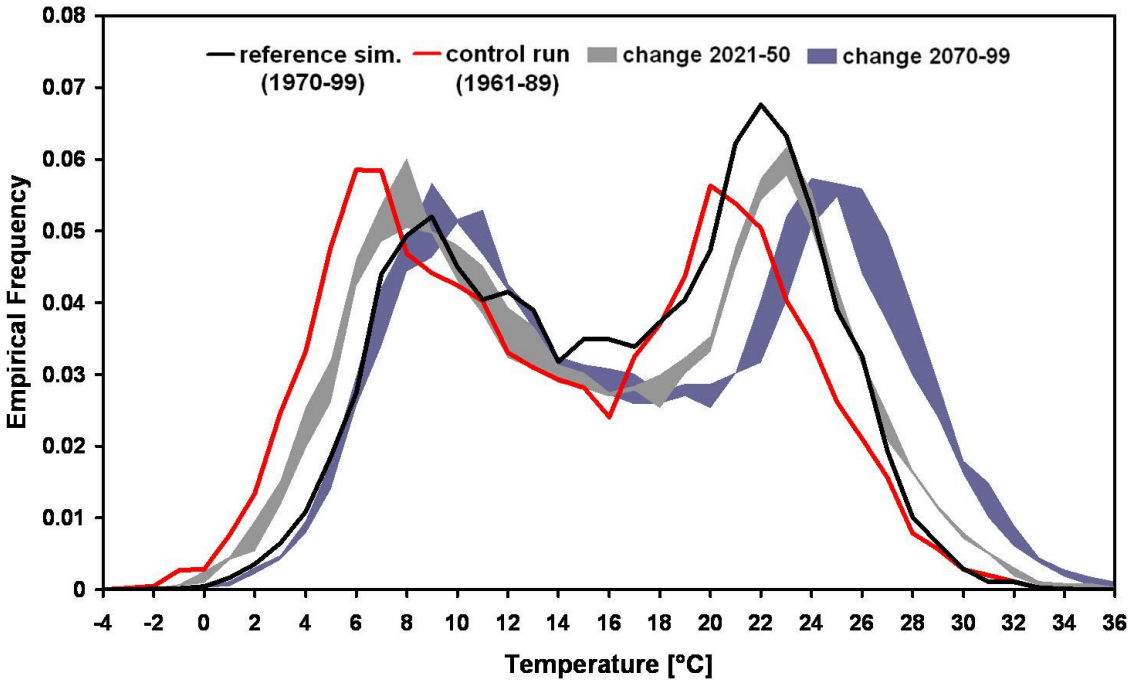

Figure VII-25: Change in normalized frequency distribution of daily temperature

Maximum in ET is reached in April where already raised temperatures are accompanied with high soil moisture owing to the expiring rainy season (Figure VII-26). In contrast, higher ET amounts are inhibited during summer because of low soil moisture, during winter due to low temperatures. Amounts of ET are only little changed in the future as analysis of annual values has shown before.

However, the illustration of monthly means in Figure VII-26 shows a change in the ET's seasonality, especially for the far future. While the maximum of ET remains in April, amounts in summertime decrease, while they increase during winter. This is due to the increasing temperatures all over the year. In the rainy season during winter now more energy for evapotranspiration is available, while drying-out of the soils is reached earlier in summer inhibiting higher ET.

The change of snow storage is demonstrated in Figure VII-27. Differences between the emissions scenarios turn out to be very small. Already for the near future a massive reduction of snow storage is given, while for the far future snow amounts are negligible. Also a seasonal change is distinct: On the one hand begin of the snow accumulation is more and more delayed, on the other hand snow melt ends earlier. For the far future average snow accumulation starts with end of December one month later than for the control run. End of the snow melt is reached in the control run on average in June,

while in the near and far future it is already in May and April, respectively. Again, comparison to the station based simulations is hampered due to the too warm temperatures at higher elevations.

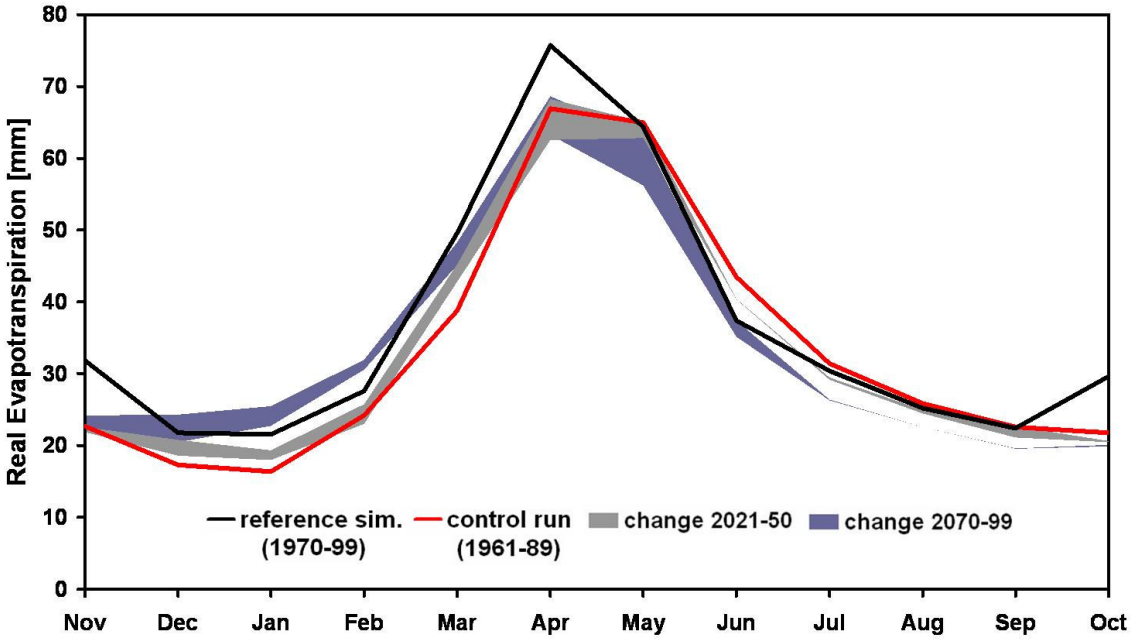

Figure VII-26: Change in monthly means of real evapotranspiration

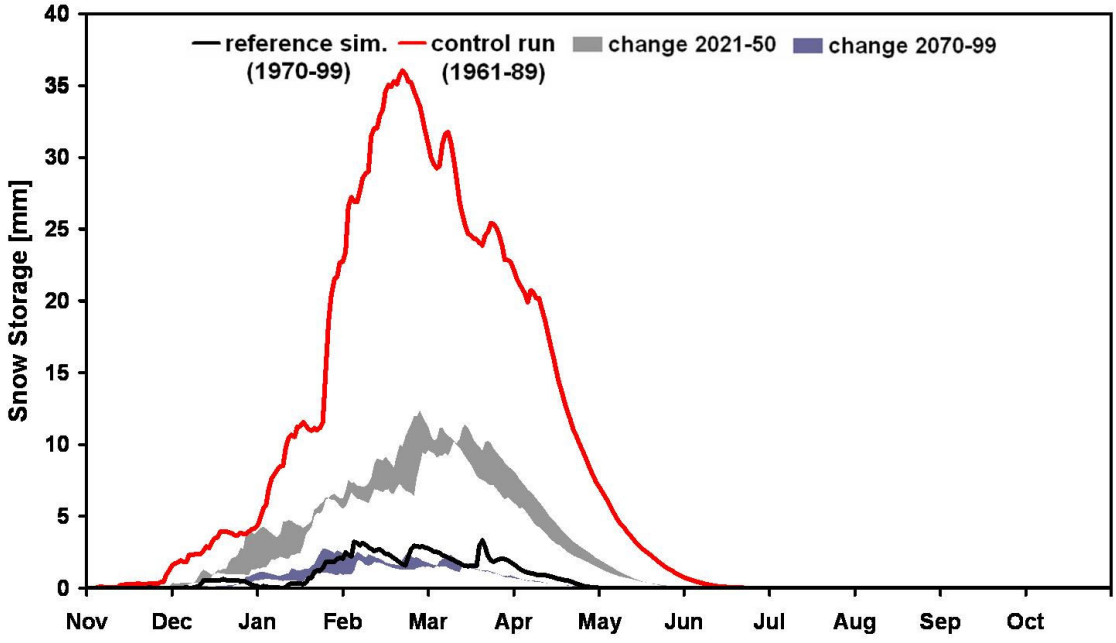

Figure VII-27: Change in snow storage

VII.4 Discussion of Simulated Future Climate and Terrestrial Hydrology

Simulated future changes of meteorological and hydrological variables have to be considered within the framework of different sources of uncertainties and natural climate variability.

One source of uncertainties is the modeling system with the chain of subsequent models. They were discussed in detail already in chapter VI.6.

The approach of dynamical downscaling with MM5 enables the simulation of changes in the dynamical regime as far as the responsible processes are reproduced properly. Additionally, a high resolution allows for detection of regionally distributed changes in contrast to statistical approaches of downscaling that are based on station data. In this study, for the Jordan River region mainly decreasing precipitation amounts are simulated for the future, but in the southwestern parts of the region at the Egyptian coast increases are seen, which are out of the ordinary picture. One possible explanation could be continuation of a recent trend in a rise in the occurrence of RST described by ALPERT ET AL. (2004b). It causes already in the present a decrease in precipitation in the northern and central parts of Israel as it replaces occurrence of Cypress Lows. At the same time rainfall increases in the southern parts in case of active RST. To prove this theory further analysis of the RCM output due to circulation pattern would be necessary, which is not object of the thesis.

With WaSiM a distributed water balance model with mainly physically based approaches describing the different processes of terrestrial hydrology is chosen. This is due to the set demand of the hydrological model to a high degree of transferability to different climate conditions. It turned out that subsurface processes can not be described properly in WaSiM. With the concept of an artificial bypass describing the karstic system good simulation results can be achieved. The model proved its ability to simulate hydrological response to changing meteorological conditions as it is shown in chapter VII.3 e.g. for evapotranspiration and snow. The changes in the amount and seasonal dynamics of snow accumulation, snow melt, and evapotranspiration simulated by WaSiM are seasonable.

The investigation of uncertainty due to unknown future anthropogenic greenhouse gas emissions is considered by the use of two different IPCC emissions scenarios (A2 and

B2). Based on the transient simulations a continuous analysis of time series is enabled. Therein temperature shows for all seasons all over the region increasing trends. With respect to the different emissions scenarios a striking phenomenon can be mentioned representing well the non-linear character of the climate system: A2 is the more pessimistic scenario with higher increasing green house gas concentrations in the future. Concentrations are diverging considerable until the end of the century, while differences at the beginning are not that high. However, concentrations in A2 are always higher than in B2 (see Figure III-2). As a consequence the A2 scenario causes also considerably higher temperatures in the far future until the end of the century. In the near future temperature increase in scenario B2 exceeds A2 showing that the regional changes in temperature do not necessarily follow the global green house gas concentrations. Responsible processes for this development can be manifold; ascription to one would be speculative.

To detect climate change signals exceeding present day climate variability the signal to noise ratio is calculated. Most considered variables show significant changes with values > 1. An exception is precipitation since recent variability is very high. However, the decrease in rainfall is considered as significant. The reason for this assumption is that future variability also decreases, which is not considered in the calculation of SN. This offers the limitations of the SN ratio that can not identify an in some cases obvious climate change signal where a clearly significant linear trend in the time series is seen.

In contrast to precipitation, trends in temperature are very distinct and significant with high values in the SN ratio. Seasonal changes in precipitation within the UJC in the joint simulations have to be seen with caution since they are influenced by the bias correction, which is not only performed for the control period (1961 - 89), but also fur the future simulations (see chapter VI.3). Changes in discharge are very high of amount and show also a clear negative signal. However, since uncertainty due to shortcomings of observation data and model performance is very high, predictions at least for the near future until 2050 have to be taken with caution.

In summary, the changing signals in the regional climate simulations with increasing temperatures accompanied with decreasing precipitation amounts denote in general a clear aggravation in the future situation of water availability within the Eastern Mediterranean and the Jordan River region. The Upper Jordan River is one of the most important easy accessible water resources for Israel. The joint climate – hydrology simula-

tions for this area show a highly sensitive and nonlinear response to modified atmospheric conditions in the future with negative changes gaining critical dimensions. The snow accumulation in winter as a considerable storage for spring and early summer discharge is imminent to be lost. It is unlikely that under future climate conditions with warmer temperatures all around the year and diminished precipitation during the rainy season discharge in summer into the Lake Kinneret is stopped as it is controlled by the groundwater and the karstic springs serving as a natural reservoir. Nevertheless, adaptation to reduced water availability out of the lake in the future has to be considered for a sustainable water resources management.

VIII Summary and Conclusions

The Near East is a region with long-lasting political conflicts. At the same time it is one of the regions with the lowest water availability per capita in the world. This gives the Jordan River as a transboundary water resource a political relevance. Global climate change could aggravate the situation considerably. To enable sustainable water management within the affected countries scientific sound information about expected future climate change in the Eastern Mediterranean and its effects on the water availability is needed.

For this purpose in this thesis joint regional climate-hydrology simulations are performed for the Eastern Mediterranean with a special focus on the hydrology on the Upper Jordan River basin. ECHAM4 data with the two SRES emission scenarios A2 and B2 are dynamically downscaled with the RCM MM5 transient for the period 1961 - 2099 and offline coupled to the mainly physically based distributed hydrological model WaSiM that was set up, calibrated, and validated for the Upper Jordan River.

It was demonstrated that high resolution climate simulations with MM5 are able to reproduce the sharp transition of climate zones. The wetter conditions in the north and the coastal areas in contrast to the extremely dry area in the south and eastern areas as well as temperatures are simulated in sufficient accuracy. However, a seasonal bias in precipitation was investigated originating from the driving data of ECHAM4 and NCEP reanalysis that turned out to be serious, especially when the aim is to use the simulations for further impact analysis in terrestrial hydrology. Therefore, a bias correction with monthly scaling factors was performed in the forefront of the joint climate-hydrology simulations.

The hydrological model WaSiM was successfully applied for the UJC including the innovative concept of representing the karst aquifer by a 2D-groundwater model for porous aquifers accompanied by an artificial bypass simulating the Dan spring. With this approach the water balance of the Upper Jordan River could be simulated satisfactorily. Thus, WaSiM turned out to be suitable for the UJC and showed plausible sensitive reactions on changes in the meteorological driving conditions based on climate simulations.

These simulated future climate conditions based on the two scenarios have to be considered as being two of an endless number of possible future climate scenarios. Additionally the mentioned uncertainties of the modeling system itself have to be respected.

As two extreme emission scenarios have been used, it is possible to draw conclusions out of the simulation result's analysis that can be of importance for future water management planning. With the signal to noise ratio it was tried to filter out natural recent climate variability for detection of climate change signals. With the use of two different emission scenarios another source of uncertainty, namely the unknown future anthropogenic greenhouse gas emissions, was tried to consider. Thus, an uncertainty margin of future climate conditions due to different green house gas concentrations could be determined.

In general it could be shown that global increase in greenhouse gas concentrations has a distinct impact to the region of the Jordan River. Simulation results show steadily rising temperatures in all seasons and all over the considered area while at the same time precipitation amounts are decreasing almost over the whole Jordan River region with one exception at the Egyptian coast at the southwestern part of the investigated area where small increasing rainfall amounts occur. The non-linearity of the reaction of regional climate in the Eastern Mediterranean to global greenhouse gas concentrations can be seen when comparing the two scenarios: While the CO_2 - concentrations of the more pessimistic scenario A2 exceed the concentrations of B2 during the whole 21st century, increase in temperature and decrease in rainfall is higher in B2 than for A2 in the 30 year period 2021 - 2050. This situation reverses at the end of the century when for A2 much higher emissions are assumed than for B2.

Trend analysis of temperature assigns significant increase and calculation of signal to noise ratio shows a clear change signal with a warming until 2050 of 1.3 – 1.7 K and until the end of the century of 3 K (scenario B2) and 3.7 K (scenario A2). Precipitation trends are until the middle of the century insignificant, although decreases of up to 20 % occur. This is due to the high variability of annual rainfall amounts in this region. For the end of the century reduction in rainfall ranging in most of the areas between 20 and >40 % is simulated. Trend tests for annual precipitation are highly significant for the period until 2099, while SN ratio still only sporadically exceeds a value of 1. However, a climate change signal is distinct as also variability decreases, which is not considered in the calculation of SN ratio. The joint climate – hydrology simulations show a

highly sensitive response to these modified atmospheric conditions. As actual evapotranspiration remains almost unchanged, simulated discharge in the UJC decreases until 2050 16.5 - 23.3 %, until the end of the century more than 40 %. Due to increased temperatures snow cover is likely to be lost as storage for spring and early summer discharge. Results of the joint climate – hydrology simulations let draw the conclusion that it is unlikely that changed climate conditions with warmer temperatures all over the year and reduced precipitation amounts resulting in significant reduction in annual discharge will stop discharge during summer since the karstic conditions serve as a big reservoir. However, water resources management faces most probably strongly reduced water availability out of the Lake Kinneret fed by the Upper Jordan River.

Outlook:

Several sources of uncertainties that are discussed and analyzed in this thesis can be reduced in the future enabling more reasonable estimates of future climate change and hydrological impact within the Eastern Mediterranean and the UJC.

First, the full analysis of uncertainties of regional climate simulations (at least 2 GCM, 2 RCM and two emission scenarios) can be done within the framework of GLOWA Jordan River as additionally to this work the RCM RegCM2 and the scenario A1B based on the GCMs ECHAM5 and HadCM3 are used.

Furthermore, the development of models will decrease sources of uncertainties consisting of neglected processes and inaccuracies evolved by model coupling. Neglected processes are e.g. the consideration of land-use changes and dust aerosols as an important factor of the region. These processes can be implemented in a RCM or in case of land use change in a distributed hydrological model. Feedback mechanisms of the atmosphere with the Mediterranean Sea on a regional scale could be considered by coupling a regional ocean model to a RCM.

An inaccuracy evolved by model coupling in the used approach is the fact, that terrestrial hydrology is simulated twice in two different models (RCM and hydrological model). Two approaches could increase consistency: On the one hand a 2-way coupling of a hydrological model to the atmospheric part of MM5 can be developed. On the other hand the extension of a RCM to more hydrological processes (like e.g. discharge

routing) accompanied with a high spatial resolution could make coupling to a hydrological model dispensable.

Bibliography

Ahmed, S., de Marsily, G. 1987. Comparison of geostatistical methods for estimating transmissivity using data on transmissivity and specific capacity. Water Resources Research, 23(9), 1717–1737.

Alpert, P., Baldi, M., Ilani, R., Price, C., Rodó, X., Saaroni, H, Ziv, B. Kishcha, P., Barkan, J., Mariotti, A., Xoplaki, E. 2006. Relations between climate variability in the Mediterranean Region and the tropics: ENSO, South Asian and African monsoons, hurricans and Saharan dust. In: Lionello, P., Malanotti-Rizoli, P., Boscolo, R. (Eds.), Mediterranean Climate Varibility, Elsevier, Amsterdam, pp. 149-177.

Alpert, P., Ben-Gai, T., Baharad, A., Benjamini, Y., Yekutieli, D., Colacino, M., Diodato, L., Ramis, C., Homar, V., Romero, R., Michaelides, S., and Manes, A. 2002. The paradoxial increase of Mediterranean extreme daily rainfall in spite of decrease in total values, Geophysical Research Letters, 29, 11, 31-1–31-4, (June issue).

Alpert, P., Kishcha, P., Svtivelman, A., Krichak, S. O., Joseph, J. H. 2004a. Vertical distribution of Saharan dust based on 2.5-year model predictions. Atmospheric Research, 70, 109-130.

Alpert, P., Neeman, B. U., Shay-El, Y. 1990. Climatological analysis of Mediterranean cyclones using ECMWF data. Tellus Series A: Dynamic Meteorology and Oceanography, 42, 65–77.

Alpert, P., Osetinsky, I., Ziv, B., Shafir, H. 2004b. Semi-objective classification for daily synoptic systems: application to the eastern Mediterranean climate change. International Journal of Climatology, 24, 1001–1011.

Alpert, P., Price, C., Krichak, S. O., Ziv, B., Saaroni, H., Osetinsky, I., Kishcha, P. 2005. Tropical tele-conections to the Mediterranean climate and weather. Advances in Geosciences, 2, 157-160.

Alpert P, Ziv B. 1989. The Sharav cyclone - observations and some theoretical considerations. Journal of Geophysical Research, 94, 18 495–18 514.

Amery, H.A., Wolf, A.T., 2000. Water Resources and the Geography of Peace in the Middle East: An Introduction. In Amery, H. A. and A. T. Wolf (eds.) Water in the Middle East: A Geography of Peace. Austin: University of Texas Press. 1-18.

Anderson, E.A. 1973. National Weather Service river forecast system - snow accumulation and ablation model. National Oceanographic and Atmospheric Administration (NOAA), Tech. Mem., NWS- HYDRO-17, U.S. Department of Commerce, Silver Spring, MD.

Arnell, N.W. 1998. Climate change and water resources in Britain. Climatic Change, 39, 83–110.

Atkinson, T. C. 1977. Diffuse and conduit flow in limestone terrain in the Medip Hills, Somerset (Great Britain). Journal of Hydrology, 35, 93-110.

Barnston A., Livezey, R. E. 1987. Classification, seasonality and persistence of low-frequency circulation patterns. Monthly Weather Review, 115, 1083–1126.

Bastidas, L. A., Gupta, H. V.,Sorooshian, S. 2002. Mathematical Models of Large Watershed Hydrology. Water Resources Publications, LLC.

Baumgartner, A., Liebscher, H. J. 1990. Lehrbuch der Hydrologie. Bd1: Allgemeine Hydrologie – Quantitative Hydrologie. Berlin/Stuttgart.

Ben-Gai, T., Bitan, A., Manes, A., Alpert, P., Kushnir, Y. 2001. Temperature and surface pressure anomalies in Israel and North Atlantic Oscillation. Theoretical and Applied Climatology, 69, 171-177.

Ben-Gai, T., Bitan, A., Manes, A., Alpert, P., Rubin, S.1998. Spatial and temporalchanges in annual Rainfall frequency distribution patterns in Israel. Theoretical and . Applied Climatology, 61, 207-215.

Ben-Gai, T., Bitan A., Manes A., Alpert P., Rubin R.1999. Temporal and spatial trends of temperature patterns in Israel. Theoretical and Applied Climatology, 64, 163-177.

Bengtsson, L. 2003. Climate modelling and prediction -Achievements and challanges. (www.clivar.org).

Beran, M. A., Rodier, J. A. 1985. Hydrological aspects of Drought. WMO-UNESCO. Panel Report. Studies and Reports in Hydrology. UNESCO Press, Paris.

Berger, D. 2001. Estimating the natural flow in the upper catchment of the Jordan River. WaterShed Unit, Mekorot, Sapir Site, Israel

Beven, K. 1989. Changing ideas in hydrology - the case of physically-based models. Journal of Hydrology, 105, 157–172.

Beven, K. J., Kirkby, M. J. 1979. A physically based variable contributing area model of basin hydro logy. Hydrological Science. Bulletin, 24 (1), 43-69.

Bougeault, P. 1983. A non-reflective upper boundary condition for limited-height hydrostatic models. Monthly Weather Review, 111, 420–429.

Bozkurt, D., Sen, O. L., Turuncoglu, U. U., Karaca, M., Dalfes, H. N. 2008. Regional climate change projections for the Eastern Mediterranean: Preliminary results. Poster presentation at the 1st ESF/MedClivar Summer School, Rhodes, 17-27 September 2008.

Braun, L.N. 1985. Simulation of snowmelt-runoff in lowland and lower alpine regions of Switzerland. Zürcher Geographische Schriften, ETH Zürich, 21.

Brutsaert, W. 1982. Evaporation into the Atmosphere. Kluwer Academic Publishers. Dordrecht.

Brielmann, H. 2008. Recharge and discharge mechanism and dynamics in the mountainous northern Upper Jordan River Catchment, Israel. . Ph.D. thesis, university of Muncih, Germany. Available at http://edoc.ub.uni-muenchen.de/9972/.

Byun, H.-R., Wilhite, D. A. 1999. Objective quantification of drought severity and duration. Journal of Climate, 12, 2747-2756.

Christensen, J.H., Carter, T.R., Giorgi, F. 2002. PRUDENCE employs new methods to assess European climate change. EOS, Transactions American Geophysical Union, 83 (13), 147.

Christensen, J. H., Christensen, O. B. 2003. Climate modeling: severe summertime flooding in Europe. Nature, 421, 805–806.

Christensen, J. H., Hewiston, B. 2007. Chapter 11, Regional climate projections. Fourth Assessment Report of the Intergovernmental Panel on Climate Change. IPCC.

Conte, M., Giufridda, S., Tedesco, S. 1989. The Mediterranean oscillation: impact on recipitation and hydrology in Italy. Proceedings of the conference on climate and water, Publications of the Academy of Finland, Helsinki, 1, 121-137.

Cullen, H. M., A. Kaplan, P. Arkin, and P. B. deMenocal. 2002. Impact of the North Atlantic Oscillation on Middle Eastern climate and streamflow. Climatic Change, 55, 315–338.

Dan,Y., Yaalon, D., Koymdjisky, H., Raz, Z. 1977. The Soils of Israel. The Volcanic Institute of Agricultural Research, Beit Dagan.

Déqué, M. 2007. Frequency of precipitation and temperature extremes over France in an anthropogenic scenario: Model results and statistical correction according to observed values. Global and Planetary Change, 57, 16-26.

Dershowitz, W. S., La Pointe, P. R., Doe, T. W. 2004. Advances in discretefracture network modelling. Proceedings of the U.S. EPA/ NGWA Fractured Rock Conference, 882-894. Portland.

DKRZ 1993. The ECHAM4 Atmospheric General Circulation Model. techreport No. 6; Deutsches Klimarechenzentrum.

Dudhia, J., Gill, D., Manning, K., Wang, W., Bruyere, C., Wilson, J.,Kelly, S. 2003. PSU/NCAR Mesoscale Modelling System Tutorial Class Notes and User's Guide, MM5 Modeling System Version 3.

Dünkeloh, A., Jacobeit, J. 2003. Circulation dynamics of Mediterranean Precipitation Variability 1948-1998. International Journal of Climatology, 20, 853-863.

Dyck, S., Peschke, G. 1995. Grundlagen der Hydrologie. Teil2: Der Wasserhaushalt der Flussgebiete. Verlag für Bauwesen, Berlin.

Eshel, G., Farrell, B. F. 2000. Mechanisms of Eastern Mediterranean rainfall variability. Journal of Atmospheric Sciences, 57, 3219-3232.

Farr, T. G., et al. (2007), The Shuttle Radar Topography Mission, Review of Geophysics, 45, RG2004, doi:10.1029/2005RG000183.

Ford, D. C., Williams, P.W. 1989. Karst Geomorphology and Hydrology. London.

Forkel, R., Knoche, H.-R. 2006. Regional climate change and its impact on photooxidant concentrations in southern Germany: Simulations with a coupled regional climatechemistry model; Journal of Geophysical Research, 111, No.D12, D12302, doi:10.1029/2005JD006748.

Frei, C., Christensen, J. H., Déqué, M., Jacob, D., Jones, R. G., Vidale, P. L. 2003. Daily precipitation statistics in regional climate models: Evaluation and intercomparison for the European Alps, Journal of Geophysical Research, 108(D3), 4142, doi:10.1029/2002JD002287.

Freiwan, M., Kadioglu, M. 2008. Climate variability in Jordan. International Journal of Climatology, 28, 69-89.

Gao, X., Pal, J. S., Giorgi, F. 2006. Projected changes in mean and extreme precipitation over the Mediterranean region from high resolution double nested RCM simulations. Geophysical Research Letters, 33, L03706.

Gellens, D., Roulin, E. 1998. Streamflow response of Belgian catchments to IPCC climate change scenarios. Journal of Hydrology, 210, 242–258.

Genuchten, M. T. Van. 1976. A closed-form equation for predicting the hydraulic conductivity of unsaturated soils. American Journal of Soil Sciences, 44(5), 892–898.

Gilad, D., Bonne, J. 1990. Snowmelt of Mt. Hermon and its contribution to the sources of the Jordan River. Journal of Hydrology, 114, 1-15.

Gilad, D., Schwartz, S. 1978. Hydrogeology of the Jordan sources aquifers. Israeli Hydrological Service Report Hydro/5/78, 58pp. (in Hebrew).

Giorgi, F. 2002. Variability and trends of sub-continental scale surface climate in the twentieth century. Part I: Observations. Climate Dynamics, 18, 675–691.

Giorgi, F. 2006. Climate change hot-spots, Geophysical Research Letters, 33, L08707, doi:10.1029/2006GL025734.

Giorgi, F., Bi, X., Pal, J. S. 2004a. Mean, interannual variability and trends in a regional climate change experiment over Europe. I: present day climate (1961–1990). Climate Dynamics, 22, 733–756.

Giorgi, F., Bi, X., Pal, J. S. 2004b. Mean, interannual variability and trends in a regional climate change experiment over Europe. II: climate change scenarios (2071-2100). Climate Dynamics, 23, 839-858.

Giorgi, F., Francisco, R. 2000. Evaluating Uncertainties in the Prediction of Regional Climate Change. Geophysical Research Letters, 27(9), 1295–1298.

Giorgi, F., Hewitson, B., Christensen, J., Hulme, M., Storch, H. V., Whetton, P., Jones, R., Mearns, L., Fu, C. 2001. Regional climate information - evaluation and projections. In: Climate Change 2001: The scientific basis.

Girorgi, F., Lionello, P. 2008. Climate change projections for the Mediterranean region. Global and Planetary Change, 63, 90-104.

Goldreich, Y., Mozes, H., D., 2004. Radar analysis of cloud systems and their rainfall yield in Israel. Israel Journal of Earth Sciences, 53, 63-76.

Gonzàlez-Ruoco, J. F., Heyen, H., Zorita, E., Valero, F. 2000. Agreement between observed rainfall trends and climate change simulations in the southwest of Europe. Journal of Climate, 13, 3057-3065.

Graham, L. P., Andréasson, J., Carlson, B. 2007. Assessing climate change impacts on hydrology from an ensemble of regional climate models, model scales and linking methods – a case study on the Lule River basin. Climate Change, 81, 293-307.

Grell, G. A., Dudhia, J., & Stauffer, D. R. 1995. A description of the Fifth-Generation Penn State/NCAR Mesoscale Model (MM5). Technical report.

Grell, G. A., Emeis, S., Stockwell, W. R., Schönemeyer, T., Forkel, R., Michalakes, J., Knoche, R., Seidl, W. 2000. Application of a multiscale, coupled MM5/chemistry model to the complex terrain of the VOTALP valley campaign. Atmospheric Environment, 34, 1435–1453.

Grell, G. A., Kuo, Y.-H. 1991. Semiprognostic tests of cumulus parameterization schemes in the middle latitudes. Monthly Weather Review, 119(1), 5–31.

Gur, D., Bar-Matthews, M., Sass, E. 2003. Hydrochemistry of the main Jordan River sources: Dan, Banias, and Kezinim springs, north Hula Valley, Israel. Israel Journal of Earth Sciences 52: 155-178.

Hartmann, A., Rimmer, A., Lange, J. 2008. Hymke_dual: Modelling of the Mt. Hermon hydrological system based on karst specific processes. Poster presentation at the GLOWA Jordan River status conference, Aqaba, Jordan, 25-27 June 2008.

Hay, L.E., Clark, M.P., 2003. Use of statistically and dynamically downscaled atmospheric model output for hydrologic simulations in three mountainous basins in the western United States. Journal of Hydrology, 282, 56–75.

Hay, L. E., Wilby, R. L., Leavesley, G. H. 2000. A comparison of delta change and downscaling GCM scenarios for three mountainous basins in the United States. Journal of the American Water Resources Association, 36, 387-398.

Hertig, E., Jacobeit, J. 2008a Assessments of Mediterranean precipitation changes for the 21st century using statistical downscaling techniques. International Journal of Climatology, 28, 1025-1045.

Hertig, E., Jacobeit, J. 2008b. Downscaling future climate change: Temperature scenarios for the Mediterranean area. Global and Planetary Change, 63, 127-131.

Hong, S.-Y., Pan, H. L. 1996. Nonlocal boundary layer vertical diffusion in a mediumrange forecast model. Monthly Weather Review, 124, 2322–2339.

Horowitz, A., 1973. Development of the Hula basin, Israel. Israeli Journal of Earth Sciences, 22, 107.

IPCC, 2007. Summary for Policymakers. In: Solomon, S., Qin, D., Manning, M., Chen, Z., Marquis, M., Averyt, K.B., Tignor, M., Miller, H.L. (Eds.), Climate Change 2007: The Physical Science Basis. Contribution of Working Group I to the Fourth Assessment Report of the Intergovernmental Panel on Climate Change. Cambridge University Press, Cambridge, United Kingdom and New York, NY, USA.

Jacobeit, J. 1987. Variations of trough position and precipitation patterns in the Mediterranean Area. Journal of Climatology, 7, 453–476.

Jacobeit, J. 2000. Rezente Klimaentwicklung im Mittelmeerraum. Pettermanns Geographische Mitteilungen, 144/6, 22-35.

Jacobeit, J., Dünkeloh, A., Hertig, E. 2004. Die Niederschlagsentwicklung im mediterranen Raum und ihre Ursachen. In: Lozán, J., Graßl, H., Hupfer, P., Menzel, L., Schönwiese, C.-D (Eds.), Warnsignal Klima: Genug Wasser für alle?, Hamburg, pp. 192-196.

Jansson, P.E., Karlberg, L. 2001. Coupled heat and mass transfer model for soil-plant-atmosphere system. Division of Land & Water Resources, Department of Civil and Environmental Engineering, Royal Institute of Technology, Stockholm.

Jasper, K., Calanca, P., Gyalistras, D., Fuhrer, J. 2004. Differential impacts of climate change on the hydrology of two alpine river basins. Climate. Research, 26 113-129.

Jasper, K., Gurtz, J., Lang, H. 2002. Advanced flood forecasting in Alpine watersheds by coupling meteorological observations and forecasts with a distributed hydrological model. Journal of Hydrology, 267, 40-52.

Jung, G. 2006: Regional climate change and the impact on hydrology in the Volta basin of West Africa. Ph.D. thesis, university of Augsburg, Germany.

Jung, G., Kunstmann, H. 2007a. High-resolution regional climate modeling for the Volta region of West Africa. Journal of Geophysical Research, 112, D23108, doi:10.1029/2006JD007951.

Jung G., Kunstmann, H. 2007b. Modelling regional climate change and the impact on surface and sub-surface hydrology in the Volta Basin (West Africa), IAHS Publ. 313.

Jones, R. G., Murphy, J. M., Noguer, M. 1995. Simulation of climate change over Europe using a nested regional-climate model. Part I: Assessment of control climate, including sensitivity to location of lateral boundaries. Quarterly Journal of the Royal Meteorological Society, 121, 1413–1449.

Kafri, U., Lang, B. 1987. New data on the Late Quaternary fill of the Hula Basin. Israel Journal of Earth Sciences, 36, 73-81.

Kalnay, E. 2003. Atmospheric Modeling, Data Assimilation and Predictability. Cambridge University Press, Cambridge.

Kalnay, E., Kanamitsu, M., Kistler, R., Collins,W., Deaven, D., Gandin, L., Iredell, M., Saha, S., White, G.,Woollen, J., Zhu, Y., Chelliah, M., Ebisuzaki,W., Higgins,W., Janowiak, J., Mo, K.C., Ropelewski, C., Wang, J., Leetmaa, A., Reynolds, R., Jenne, R., Joseph, D. 1996. The NCEP/NCAR 40-year reanalysis project. Bulletin of the American Meteorological Society, 77, 437–471.

Karas, S., Zangvil, A. 1999. A preliminary analysis of disturbance tracks over the Mediterranean Basin. Theoretical and Applied Climatology, 64, 239-248.

Karmon, Y. (1983): Israel: Eine geographische Landeskunde. – Wissenschaftliche Buchgesellschaft, Darmstadt.

Kessler, A. 1999. Hydrologic model of Dan Spring monthly flow using a conic linear reservoir, Submitted to the Israeli Water Commission.

Kirlay, L. 2002. Karstification and groundwater flow. Proceedings of the conference on evolution of karst: From prekarst to cessation, 155-190.

Klaer, W. (1962): Eine Landnutzungskarte von Libanon. Heidelberger Geographische Arbeiten, 10, Heidelberg.

Klemp, J. B., Durran, D. R. 1983. An upper boundary condition permitting internal gravity wave radiation in numerical mesoscale models. Monthly Weather Review, 111, 430–444.

Kistler, R., Kalnay, E., Collins, W., Saha, S., White, G., Woollen, J., Chelliah, M., Ebisuzaki, W., Kanamitsu, M., Kousky, V., van den Dool, H., Jenne, R., Fiorino, M. 2001. The NCEP/NCAR 50-year ranalysis. Bulletin of the American Meteorological Society, 82, 247-268.

Klemp, J. B., Wilhelmson, R. B. 1978. The simulation of three-dimensional convective storm dynamics. Journal of the Atmospheric Sciences; 35, 1070–1096.

Köppen, W. and Geiger, R. 1936. Handbuch der Klimatologie, 5 Vols., Berlin. Karas, S., Zangvil, A. 1999. A preliminary analysis of disturbance tracks over the Mediterranean Basin. Theoretical and Applied Climatology, 64, 239-248.

Kotlarski, S., Block, A., Boehm, U., Jacob, D., Keuler, K., Knoche, R., Rechid, D., Walter, A. 2005. Regional climate model simulations as input for hydrological applications: Evaluation of uncertainties. Advances in Geosciences, 5, 119-125.

Krichak, S. O., Alpert, P. 2005. Signatures of the NAO in the atmospheric ciculation during wet winter months over the Mediterranean region. Theoretical and Applied Climatology, 82, 27-39.

Krichak, S., Alpert, P., Krishnamurti, T. 1997. Red Sea trough/cyclone development numerical investigation. Meteorology and Atmospheric Physics, 63, 159–170.

Krichak, S., Alpert, P., Kunin, P. 2009. Projections of climate change over non-boreal east-Europe during first half of the twenty-first century according to results of a transient RCM simulation. In: Groisman, P.Y., Ivanov, S. I. (Eds.), Regional Aspects of Climate-Terrestial-Hydrologic Interactions in Non-boreal Eastern Europe., Springer Science + Business Media B.V, pp. 55-62.

Krichak, S. O., Kishcha, P., Alpert, P. 2002. Decadal trends of the main Eurasian osciallations and the Eastern Mediterranean precipitation. Theoretical and Applied Climatology, 72, 209-220.

Kunstmann, H., Krause, J., Mayr, S. 2005. Inverse distributed hydrological modeling of alpine catchments. Hydrology and Earth System Sciences Discussions, 2, 1–43.

Kunstmann H., Schneider K., Forkel R., Knoche R. 2004. Impact analysis of climate change for an Alpine catchment using high resolution dynamic downscaling of ECHAM4 time slices. Hydrology and Earth System Sciences, 8(6), 1030–1043.

Kunstmann, H., Stadler, C. 2005. High resolution distributed atmospheric-hydrological modeling for Alpine catchments. Journal of Hydrology, 314, 105-124.

Krause, P., Boyle, D. P., Bäse, F. 2005. Comparison of different efficiency criteria for hydrological model assessment. Advances in Geosciences, 5, 89–97.

Kutiel, H., Maheras, P., Türkes, M., Paz, S. 2002. North Sea – Caspian pattern (NCP) – an upper level atmospheric teleconnection affecting the Eastern Mediterranean - implications on the regional climate. Theoretical and Applied Climatology, 72, 173-192.

Laux, P., Wagner, S., Wagner, A., Jacobeit, J., Bárdossy, A, Kunstmann, H., 2009. Moedlling daily precipitation features in the Volta Basin of West Africa. International Journal of Climatology, 29, 937-954.

Lenderink, G., Buishand, T.A., van Deursen, W., 2007. Estimates of future discharges of the river Rhine using two scenario methodologies: direct versus delta approach. Hydrology and Earth System Sciences 11, 1145–1159.

Liedl, R., Sauter, M., Hückinghaus, D., Clemens, T, Teutsch, G. 2003. Simulation of the development of karst aquifers using a coupledcontinuum pipe flow model. Water Ressources Research, 39 (1), 1057, doi:10.1029/2001WR01206.

Luterbacher, J., Xoplaki, E., Casty, C., Wanner, H., Pauling, A., Küttel, M., Rutishauser, T, Brönnimann, S., Fischer, E., Fleitmann, D., González-Rouco, F. J., García-Herrera, R., Barriendos, M., Rodrigo, F., Gonzalez-Hidalgo J. C., Angel Saz, M., Gimeno, L., Ribera, P., Brunet, M, Paeth, H., Rimbu, N., Felis, T., Jacobeit, J., Dünkeloh, A., Zorita, E., Guiot, J., Türkes, M., Alcoforado, M. J., Trigo, R.,Wheeler, D., Tett, S., Mann, M. E., Touchan, R., Shindell, D. T., Silenzi, S., Montagna, P., Camuffo, D, Mariotti, A., Nanni, T., Brunetti, M., Maugeri, M., Zerefos, C., De Zolt, S., Lionello, P., Nunes, M. F., Rath, V., Beltrami, H., Garnier, E., Le Roy Ladurie, E. 2006. Mediterranean climate variability over the last centuries: a review. In: Lionello, P., Malanotti-Rizzoli, P., Boscolo, R. (Eds.), Mediterranean Climate Varibility. Elsevier, Amsterdam, pp. 27-148.

Machenhauer, B., et al.. 1998. Validation and analysis of regional present-day climate and climate change simulations over Europe. MPI Report No, 275. MPI, Hamburg, Germany.

Mangin, A. 1975. Contribution a l'etude hydrodynamique des aquiferes karstiques. These, Institut des Sciences de la Terre de l'Universite de Dijon.

Marx, A., Mast, M., Knoche, R., Kunstmann, H. 2008. Global climate change and regional impact on the water balance - Case study in the German alpine area. Wasserwirtschaft, 98 (9, 12-16.

Marx, A. 2007. Einsatz gekoppelter Modelle und Wetterradar zur Abschätzung von Niederschlagsintensitäten und zur Abflussvorhersage. Ph.D. Thesis, University of Stuttgart.

Medzini, A., Wolf, A., 2004. Towards a Middle East at peace: hidden issues in Arab-Israeli hydropolitics. Water Resources Development, 20, 193-204.

Menzel, L., Bürger, G. 2002. Climate change scenarios and runoff response in the Mulde catchment (Southern Elbe, Germany). Journal of Hydrology, 267, 53–64.

Michelson, H., 1975. Geohydrology of the enclave and the southeastern flanks of Mount Hermon. TAHAL Report 01/75/05.

Middelkoop, H., Daamen, K., Gellens, D., Grabs, W., Kwadijk, J. C. J., Lang, H., Parmet BWAH, Schädler, B., Schulla, J., Wilke, K. 2001. Impact of climate change on hydrological regimes and water resources management in the Rhine Basin. Climate Change,49,105–128.

Mitchell, T. D., Carter, T. R., Jones, P. D., Hulme, M., New, M. 2004. A comprehensive set of high-resolution grids of monthly climate for Europe and the globe: The observed record (1901 – 2000) and 16 scenarios (2001 – 2100), Tech. Rep. Tyndall Centre Working Paper 55, Tyndall Centre, Norwich, U. K.

Mitchell, T. D., Jones, P. D. 2005. An improved method of constructing a database of monthly climate observations and associated high resolution grids. International Journal of Climatology, 26, 693– 712.

Monteith, J. L. 1975. Vegetation and the atmosphere, vol. 1: Principles. Academic Press.

Morin, Y., Michaeli, A., Agassi, M., Atzmon, B., Rozentzveig, D. 1979. The Rainfall-Runoff–Erosion relations in the Lake Kinneret Basin. Research report R-42, the Erosion Research Station in Rupin Collage (Israel).

Nakicenovic, N., Swart, R. (Eds.) 2001. Special Report on Emissions Scenarios (SRES). Special Report of the Intergovernmental Panel on Climate Change. Cambridge.

Neumann, R., Jung, G., Laux, P. Kunstmann, H. 2006. Climate trends of temperature, precipitation and river discharge in the Volta Basin of West Africa. International Journal of River Management, 5,1,17 – 30.

New, M., Hulme, M., Jones, P.D., 1999. Representing twentieth century space-time climate variability. Part 1: development of a 1961-90 mean monthly terrestrial climatology. Journal of Climate 12, 829-856.

Oberhuber, J. M. 1993. Simulation of the Atlantic circulation with a coupled sea icemixed layer-isopycnal general circulation model. Part I: Model description; Journal of Physical Oceanography; 23, 808–829.

Osetinsky, I., Aplpert, P. 2004. Evaluation of GCM/RCM by the classified synoptic systems' approach. 17th Conference on Probability and Statistics in the Atmospheric Sciences, 15/1/2004, Seattle, USA.

Palmer, W. C. 1965. Meteorological drought. Research Paper No. 45. U.S. Department.

of Commerce Weather Bureau, Washington, D.C.

Pardè, M. 1964. Fleuves et rivières. Paris.

Parrish, D. F., Derber, J. C. 1992. The National Meteorological Center's spectral statistical interpolation analysis system. Monthly Weather review, 120, 1747-1763.

Picard, L. 1965. The geological evolution of the Quaternary in the central-northern Jordan Graben, Israel. The Geological Society of America, Special Paper 84, 337-366.

Ponce, V. M. 1989. Engineering Hydrology – Principles and Practices. Prentice-Hall, Englewood Cliffs, New Jersey.

Price, C., Stone, L., Rajagopalan, B., and Alpert, P. 1998. A possible link between El Nino and precipitation in Israel, Geophysical Research Letters,25, 3963–3966.

Ramage, C.S. 1983. Teleconnections and the siege of time. Journal of Climatology, 3, 223–231.

Randall, D.A., Wood, R. A. 2007. Chapter 8, Climate models and their evolution. Fourth Assessment Report of the Intergovernmental Panel on Climate Change. IPCC.

Reisner, J., Rasmussen, R. M., Bruintjes, R. T. 1998. Explicit forecasting of supercooled liquid water in winter storms using the MM5 mesoscale model. Quarterly Journal of the Royal Meteorological Society, 124, 1071–1107.

Richards, L. 1931. Capillary Conduction of liquids through porous medium. Physics, 1, 318–333.

Rimmer, A., Salinger, Y. 2006. Modelling precipitation-streamflow processes in karst basin: The case of the Jordan River sources, Israel. Journal of Hydrology, 331, 524-542.

Röckner, E., Bengtsson L., Feichter, J. 1999. Transient climate change simulations with a coupled atmosphere-ocean GCM including the tropospheric sulfur cycle; Journal of Climate; 12, 3004–3032.

Rom, M. 1994. Creating synthetic time series of available water for Lake Kinneret. WaterShed Unit, Mekorot, Sapir Site, Israel

Rosbjerg, D., Madsen, H. 2005. Concepts of Hydrologic Modeling. Encyclopedia of Hydrological Sciences. John Wiley and Sons, Ltd.

Samuels, R., Rimmer, A., Alpert, P. 2009. Effect of extreme rainfall events on the water resources of the Jordqan River. Journal of Hydrology, 375, 513-523.

Samuels, R., Rimmer, A., Hartmann, A., Krichak, S., Alpert, P. 2010: Climate Change Impacts on Jordan River Flow: Downscaling Application from a Regional Climate Model. Journal of Hydrometeorology, 11, 860–879.

Saaroni, H., Halfon, N., Ziv, B., Alpert, P., Kutiel, H. 2009. Links between the rainfall regime in Israel and location and intensity of Cyprus lows. International Journal of Climatology, DOI: 10.1002/joc.1912.

Saaroni, H., Ziv, B., Alpert, P. 2003. Long-term variations in the summer temperatures over the Eastern Mediterranean. Geophysical Research Letters, 30 (18), 1946, doi:10.1029/2003GLO17742.

Saaroni H, Ziv B, Bitan A, Alpert P. 1998. Easterly wind storms over Israel. Theoretical and Applied Climatology, 59, 61–77.

Salmi, T., Määttä, A., Anttila, P., Ruoho-Airola, T., Amnell, T. 2002. Detecting trends of annual values of atmospheric pollutants by the Mann-Kendall test and Sen's slope estimates – the excel template application MAKESENS. Publications on Air Quality, 32, Finish Meteorological Institute, Helsinki.

Samuels, R., Rimmer, A., Alpert, P. 2009. Effect of extreme rainfall events on the water resources of the Jordan River. Journal of Hydrology, 375, 513-523.

Scheffer, F., Schachtschabel, P. 1998. Lehrbuch der Bodenkunde. Stuttgart.

Schneider, U., Fuchs, T., Meyer-Christoffer, A., Rudolf, B. 2008. Global Precipitation Analysis Products of the GPCC. Global Precipitation Climatology Centre (GPCC), DWD, internet publication at http://www.dwd.de.

Schulla, 1997. Hydrologische Modellierung von Flussgebieten zur Abschätzung der Folgen von Klimaänderungen. Ph.D. thesis, university of ETH-Zürich, Switzerland.

Schulla J., Jasper, K. 2007. Model Description WASIM-ETH (Water Balance Simulation Model ETH), ETH-Zurich, Zurich.

Semmler, T., Jacob, D., 2004. Modeling extreme precipitation events — a climate change simulation for Europe. Global and Planetary Change, 44, 119-127.

Seubert, S., 2010. Telekonnektionen des Niederschlags im Mittelmeerraum zur Zirkultion in den Tropen. Ph. D. Thesis at University of Augsburg.

Shabalova, M. V., van Deursen, W. P. A., Buishand, T. A. 2003. Assessing future discharge of the river Rhine using regional climate model integrations and a hydrological model. Climate Research, 23, 233–246.

Skamarok, W. C., Klemp, J. B. 1994. The stability of time-split numerical methods for the hydrostatic and nonhydrostatic elastic equations. Monthly Weather Review; 120, 2109–2127.

Sharon, D., Kutiel, H., 1986. The distribution of rainfall intensity in Israel, its regional and seasonal variations and its climatological evaluation. International Journal of Climatology, 6, 277-291.

Shay-El, Y., Alpert ,P. 1991. A diagnostic study of winter diabatic heating in the Mediterranean in relation with cyclones. Quarterly. Journal of the Royal Meteorological Society, 117, 715–747.

Shentsis, I., Ben Tzvi A. 1994. Updated model to predict the available water for Lake Kinneret. Israeli Hydrological Service, Report 94/2.

Simpson, B., Carmi, I. 1983. The hydrology of the Jordan River tributaries (Israel): Hydrographic and isotopic investigation. Journal of Hydrology, 62, 225-242.

Singh, V. P., Frevert, D. K. 2002. Mathematical Models of Large Watershed Hydrology. Water Resources Publications, LLC.

Sivapalan, M., Ruprecht, J.K., Viney, N.R. 1996. Water and salt balance modeling to predict the effects of land-use changes in forested catchments. 1. Small catchment water balance model. Hydrological Processes, 10, 393–411.

Stroeve, J., Holland, M. M., Meier, W., Scambos, T., Serreze, M. 2007. Arctic sea ice decline: Faster than forecast. *Geophysical Research Letters* 34, L09501, doi:10.1029/2007GL029703.

Teutsch, G. 1988. Grundwassermodelle im Karst: Praktische Ansätze am Beispiel zweier Einzugsgebiete im tiefen und seichten Malmkarst der Schwäbischen Alb. Ph.D. thesis, University of Tübingen.

Trigo, I. F., Bigg, G. R., Davies, T.D. 2002. Cliimatology of cyclogenesis mechanisms in the Mediterranean. Monthly Weather Review, 130, 549-569.

Trigo, I. F., Davies, T. D., Bigg, G. R. 1999. Objective climatology of cyclones in the Mediterranean region. Journal.of Climate, 12, 1685–1696.

Trigo, R. M., Palutikof, J. P. 2001. Precipitation scenarios over Iberia: a comparison between direct GCM output and different downscaling techniques. Journal of Climate, 14, 4422-4446.

Trigo, R., Xoplaki, E., Zorita, E., Luterbacher, J., Krichak, S.O., Alpert, P., Jacobeit, J., Sáenz, J., Fernaández, J., González-Rouco, F., Garcia-Herrera, R., Rodo, X. Brunetti, M., Nanni, T., Maugeri, M., Türkes, M., Gimeno, L., Ribera, P., Brunet, M., Trigo, I. F., Crepon, M., Mariotti, A. 2006. Relations between variability in the Mediterranean and Mid-Latitude variablity. In: Lionello, P., Malanotti-Rizzoli, P., Boscolo, R. (Eds.), Mediterranean Climate Varibility. Elsevier, Amsterdam, pp. 179-226.

Troen, I., Mahrt, L. 1986. A simple model of the atmospheric boundary layer; sensitivity to surface evaporation. Boundary Layer Meteorology, 37, 129-148.

Ulbrich, U, May, W., Li, L., Lionello, P., Pinto, J. G., Somot, S. 2006. The Mediterranean climate change under global warming. In: Lionello, P., Malanotte-Rizzoli, P., Boscolo, R. (Eds.), Mediterranean Climate Variability. Elsevier, Amsterdam, pp. 398–415.

Wagner, S., Kunstmann, H., Bárdossy, A., Conrad, C., Colditz, R. 2008. Water balance estimation of a poorly gauged catchment in West Africa using dynamically downscaled meteorological fields and remote sensing information. Physics and Chemistry of the Earth, 34, 225-235.

Wang, Y., Leung, L. R., McGregor, J. L., Lee, D.-K., Wang, W.-C., Ding, Y., Kimura, F. 2004. Regional climate modeling: Progress, challenges and prospects. Journal of the Meteorological Society of Japan, 82(6), 1599–1628.

Watershed Unit of Mekorot, 1991. Estimations of available water in Lake Kinneret for the years 1991/2 as palnning tool for pumping from the lake. Watershed Unit of Mekorot, Sapir Site, Israel.

WBGU (Wissenschaftlicher Beirat der Bundesregierung, globale Umweltveränderungen) 1997. Wege zu einem nachhaltigen Umgang mit Süßwasser, www.wbgu.de.

Wilby, R. L., Hay, L. E., Gutowski Jr., W. J., Arrit, R. W., Takle, E. S., Pan, Z., Leavesley, G. H., Clark, M. P. 2000. Hydrological responses to dynamically and statistically downscaled climate model output. Geophysical research Letters, 27(8), 1199-1202.

Wolfart, R. (1967): Geologie von Syrien und dem Libanon. Beiträge zur Regionalen Geologie der Erde, 6,Gebrüder Borntraeger, Berlin.

Xoplaki, E. 2002. Climate variability over the Mediterranean. Ph.D. thesis, university of Bern, Switzerland. Available at http://sinus.unibe.ch/klimet/docs/phd_xoplaki.pdf.

Xoplaki, E. González-Rouco, J. F., Luterbacher, J., Wanner, H. 2004. Wet season Mediterranean precipitation variability: influence of large-scale dynamics and trends. Climate dynamics, 23, 63-78.

Zhang, Y., Klein, S. A Liu, C., Tian, B., Marchand, R., Haynes, J., McCoy, R., Zhang, Y., Ackerman, T. P. 2008. On the diurnal cycle of deep convection, high clouds and the upper troposphere water vapor in the Multi-scale Modeling Framework. Journal of Geophysical Research, Atmospheres, 113, D16105, doi:10.1029/2008JD009905.

Zangvil, A., Karas, S., Sasson, A. 2003. Connection between Eastern Mediterranean seasonal mean 500 hPa height and sea-level pressure patterns and the spatial rainfall distribution over Israel. International Journal of Climatology, 23 (13), 1567-1576.

Ziv, B. Dayan, U., Kushnir, Y., Roth, C., Enzel, Y. 2006. Regional and global atmospheric patterns governing rainfall in the southern Levant. International Journal of Climatology, 26, 55-73.

Ziv, B., Saaroni, H., and Alpert, P. 2004. The factors governing the summer regime of the eastern Mediterranean. International. Journal of Climatology, 24, 1859–1871.

Appendix

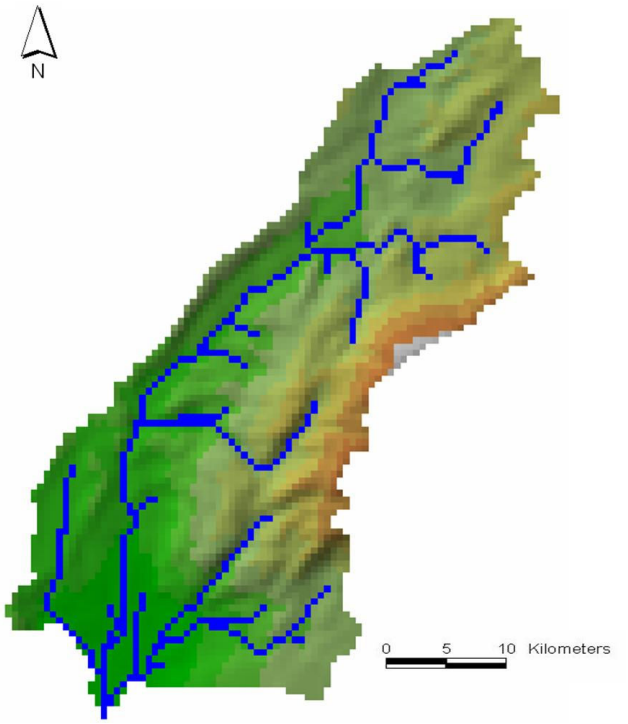

Figure 0-1: River network of the UJC derived by TANALYS

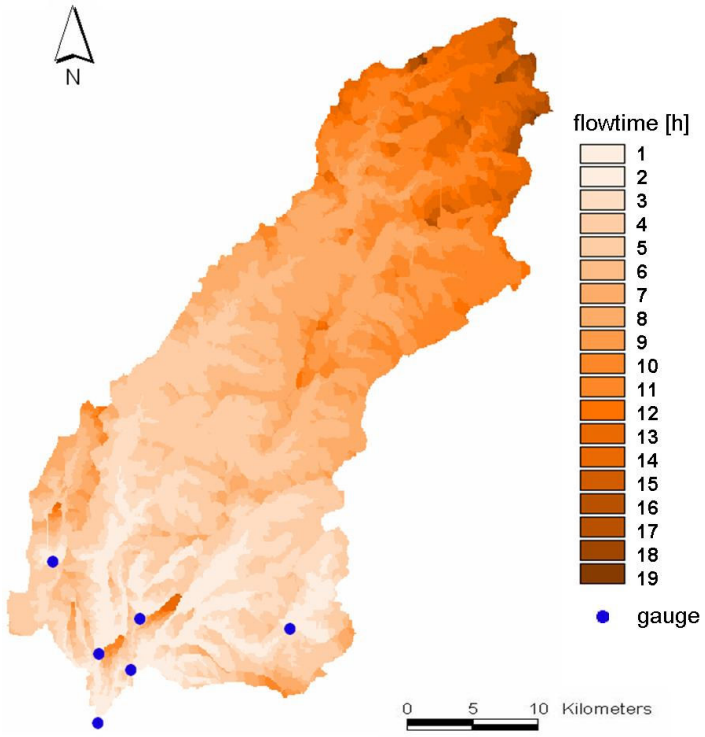

Figure 0-2: Flowtimes to the subbasin outlets derived by TANALYS

Table 0-1: Assignment of the soil types to the soil textures in WaSiM

CODE	**FAO-Classification**	**WaSiM**	CODE
Bk	Calcic Cambisol	Loamy Sand	2
Bv	Vertic Cambisol	Clay Loam	11
Vc	Vertisols	Silty Clay	7
Lc	chromic Luvisols	Sandy Loam	3
Xk	calcic Xerosols	Sandy Loam	3
Be	Chromic Cambisols	Loamy Sand	2
CODE	**Soil types (after DAN et al., 1977)**	**WaSiM**	CODE
a	Terra rossas, brown rendzinas and pale rendzinas	Silty Clay Loam	13
b	Brown rendzinas and pale rendzinas	Silty Clay Loam	13
c	Pale rendzinas	Clay Loam	11
d	Basaltic protogrumusols, basaltic brown grumusols and pale rendzinas	Clay Loam	11
e	Hamra soils	Loam	5
f	Basaltic brown mediterranean soils and basaltic lithsols	Loamy Sand	2
h	Grumusols	Silty Clay	7

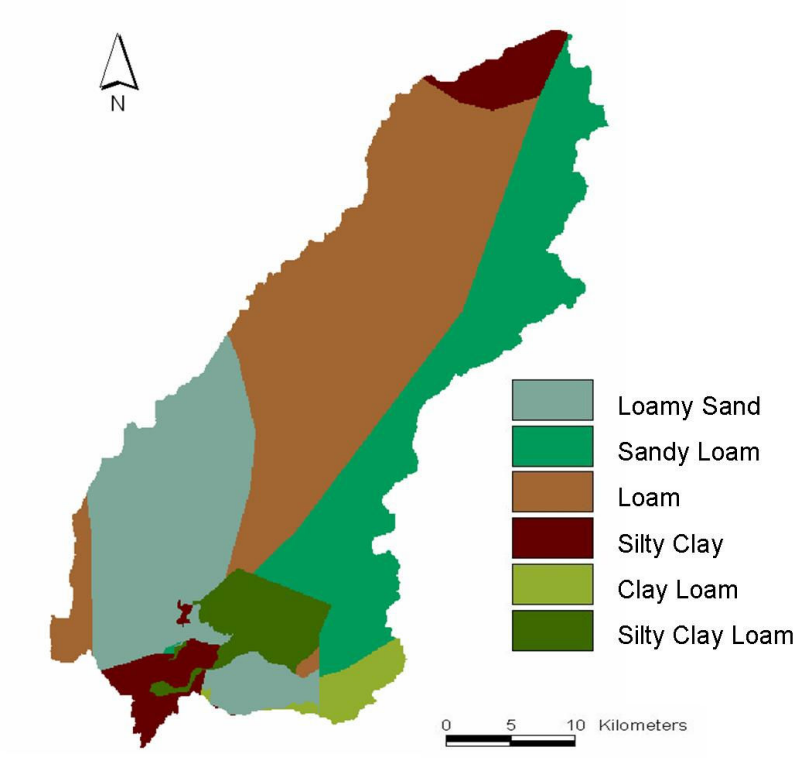

Figure 0-3: Soil textures in the UJC

Table 0-2: Assignment to the land use classes in WaSiM

Landuse Classes			
Code	**KLL**	**Code**	**WaSiM-ETH**
1	fallow land	7	grass
2	cultivated	6	agriculture
3	village	2	settlements
4	0	6	agriculture
5	water body	1	water
6	sport ground	7	grass
7	fruet orchards	19	horticulture
8	shrubs	8	bushes
9	open ground	7	grass
10	vinyards	6	agriculture
11	rocky land and vegetation	7	grass
12	thin natural grove	8	bushes
13	rocky land	15	rock
14	natural grove	8	bushes
15	unknown	7	grass
17	forest - planted	5	mixed forest
18	grove - planted	5	mixed forest
19	citrus orchards	19	horticulture
20	built area - densed	2	settlements
22	disturbed soil	6	agriculture
Code	**MODIS**	**Code**	**WaSiM-ETH**
1	settlements	2	settlements
2	dryland	7	grass
7	grassland		
10	savanna		
16	water	1	water

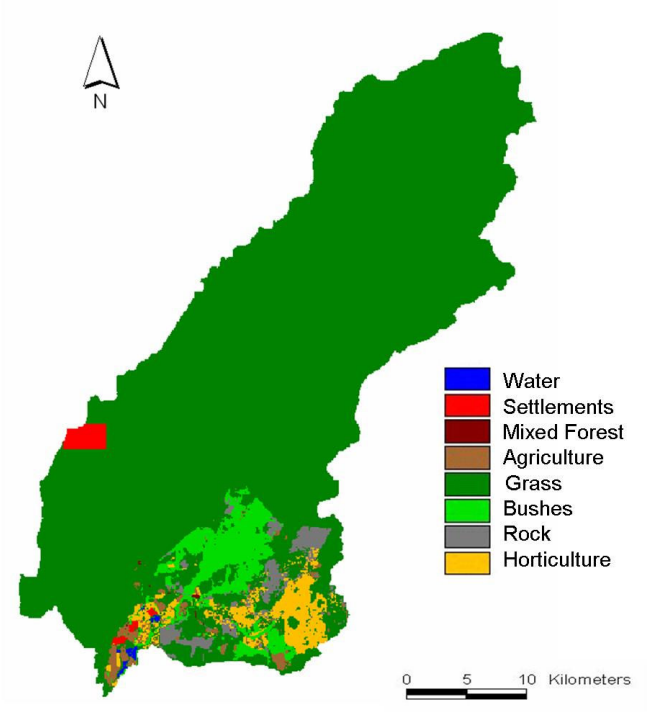

Figure 0-4: Land use in the UJC